UNIVERSITY OF CALIFORNIA, SAN DIEGO

An Experimental and Numerical Study of Wind Turbine Seismic Behavior

A dissertation submitted in partial satisfaction of the
requirements for the degree
Doctor of Philosophy

in

Structural Engineering

by

Ian Prowell

Committee in charge:

Professor Ahmed Elgamal, Chair
Professor Joel P. Conte
Professor Raymound de Callafon
Professor William Hodgkiss
Professor J. Enrique Luco
Professor Chia-Ming Uang

2011

The dissertation of Ian Prowell is approved, and it is acceptable in quality and form for publication on microfilm and electronically:

_____

_____

_____

_____

_____

_____
Chair

University of California, San Diego

2011

DEDICATION

To my grandfather whose inspiration provided the energy to make this work possible. To my father who allowed me to open my mind. To my wife whose love and support never failed.

EPIGRAPH

Imagination is more

important than knowledge.

—Albert Einstein

TABLE OF CONTENTS

LIST OF FIGURES

LIST OF TABLES

ACKNOWLEDGEMENTS

I would like to thank my advisor, Professor Ahmed Elgamal, for his tireless dedication to supporting my Ph.D. research at the University of California, San Diego. His persistence and encouragement have challenged me to grow beyond what I thought possible. For his support I express my most sincere gratitude and deepest appreciation.

I would also like to thank my committee members, Professor Joel P. Conte, Professor Raymond A. de Callafon, Professor William Hodgkiss, Professor J. Enrique Luco and Professor Chia-Ming Uang, for the contribution of their time, guidance, and experience in my research efforts.

I am in debt to Professor José Restrepo and Professor Mark Veletzos who conducted a pioneering shake table test of a 65-kW wind turbine in 2004. The results from this test provided a solid foundation from which I was able to conduct research. The fundamental insights their work provided was extremely valuable for the research presented in this dissertation.

Professor Chia-Ming Uang's leadership was essential in planning and execution of the 2010 shake table tests. His extensive testing experience and keen insight increased the value of the test program enabling the presented analysis. As Principal Investigator of the UCSD NEES equipment site, Professor J. Enrique Luco facilitated and enabled the successful test program. His feedback was also essential in interpreting most of my experimental work. Professor Joel P. Conte was a primary source of support with regards to my work on system identification. His guidance

and suggestions were always appreciated and valued.

Through communications undertaken by Professor Elgamal, the support rendered by Hal Romanowitz and J. Edward Duggan of Oak Creek Energy Systems (OCES) is gratefully acknowledged. OCES generously donated the 65-kW turbine used to conduct the shake tests and assisted in the construction of the turbine on the shake table. Field testing was made possible by OCES's willingness to allow in-situ testing at their active wind farm near Mojave, California. In addition, the staff at OCES generously participated in the field work. The research team was granted full access to two large modern turbines with power ratings of 900-kW and 1.5-MW. The continued support from Oak Creek Energy Systems (including Michael Burns, J. Edward Duggan, Vaughn Johnson, Hal Romanowitz, and many others) has been fundamental to advancing this important area of research.

I am in debt to Dr. Paul Veers for his direction during my time at the Sandia National Laboratories in the Wind Energy Technology Department. Dr. Veers selflessly invited me to study as an intern thereby greatly increasing my understanding of the wind industry. His continued support, time, and guidance have been essential to increase the relevance of my research.

The cooperation and support of Dr. Jason Jonkman, of the National Renewable Energy Laboratory is deeply appreciated. Dr. Jonkman's feedback was integral to the extension of the FAST code that support base shaking as a loading source. His review of my simulation efforts served as an expert opinion that could not be replaced.

I would like to thank the NEEShub Project Warehouse team for all their assis-

tance in archiving and documenting the experimental data collected. Their effort has greatly increased the value of the collected data by ensuring effective documentation and ensuring availability for inspection by other researchers.

Special thanks are given to all of my colleagues and friends who helped me make the completion of this dissertation possible.

In-situ instrumentation would not have been possible without the oversight of Dr. Robert Nigbor of UCLA and the hard work of the NEES@UCLA team (Ben Ferrero, Steve Kang, Steve Keowen, and Dr. Alberto Salamanca). Shake table testing would not have been possible without the oversight of Mr. Andrew Gunthardt of UCSD and the hard work of the NEES@UCSD team headed by Dan Radulescu (including Robert Beckley, Lawrence Berman, Michael Dyson, Paul Greco, Dr. Chris Latham, Darren McKay, Lawton Rodriguez, Alex Sherman, and Richard Whalen), Professor Lanhui Guo who provided assistance for planning and execution of the 2010 shake table tests, Professor Ziyad Duron and students from Harvey Mudd College. I would like to thank the Sandia National Laboratories Wind Energy Technology Department including Dr. Tom Ashwill and Dr. Todd Griffith. And additional thanks to the following individuals: Barbara Chang, Professor ZhiQiang Chen, Dr. Michael Fraser, Dr. Xianfei He, Dr. Michael Le, Geoff Lloyd, Dr. Jinchi Lu, Professor Jerry Lynch, Professor Lance Manuel, Professor Babak Moaveni, Dr. Hyoung-Bo Sim, Tim Schmidt, Richard Wargo, Dr. Pat Wilson, and Dr. Andy Zimmerman.

Chapter 1 of this dissertation contains material from the report published by Sandia National Laboratories under the title “Assessment of Wind Turbine Seismic Risk: Existing Literature and Simple Study of Tower Moment Demand,” with authors

Ian Prowell and Paul Veers (2009). The dissertation author is the first author of this paper.

Chapter 2 of this dissertation is based on material published by the Journal of Earthquake Engineering titled "Experimental and Numerical Seismic Response of a 65 kW Wind Turbine," with authors, Ian Prowell, Mark Veletzos, Ahmed Elgamal, and José Restrepo (2009). The dissertation author is the first author of this paper.

Chapter 3 of this dissertation contains material from the following two papers under preparation for publication: (1) tentatively titled "Shake Table Testing of a Utility Scale Wind Turbine," with a preliminary author list of Ian Prowell, Chia-Ming Uang, Ahmed Elgamal, Lanhui Guo, and J. Enrique Luco (2011) and (2) tentatively titled "Shake Table Testing of a Utility Scale Wind Turbine Including Operational Effects," with a preliminary author list of Ian Prowell, Ahmed Elgamal, Chia-Ming Uang, J. Enrique Luco, Hal Romanowitz, and Ed Duggan (2011). The dissertation author is the first author of these papers.

Chapter 4 of this dissertation is based on material from a manuscript submitted for publication, tentatively titled "In-situ Ambient Vibration Study of a 900-kW Wind Turbine," with an author list of Ian Prowell, Ahmed Elgamal, J. Enrique Luco, and Joel P. Conte (2011). The dissertation author is the first author of this paper.

Chapter 5 of this dissertation is based on material from a manuscript under preparation for publication, tentatively titled "In-situ Ambient Vibration Study of a 1.5-MW Wind Turbine," with a preliminary author list of Ian Prowell, Ahmed Elgamal, Joel P. Conte, Hal Romanowitz, and J. Edward Duggan (2011). The dissertation author is the first author of this paper.

Chapter 6 of this dissertation is an extended version of the material published in the proceedings of the following two conferences (1) 17th International Conference on Soil Mechanics & Geotechnical Engineering, Alexandria, Egypt, titled "Modal properties of a modern wind turbine including SSI," with authors Ian Prowell, Ahmed Elgamal, Jinchi Lu, and J. Enrique Luco (2009) and (2) 5th International Conference on Recent Advances in Geotechnical Earthquake Engineering and Soil Dynamics in Honor of Professor I.M. Idriss, San Diego, California, USA, titled "Modeling the Influence of Soil Structure Interaction on the Seismic Response of a 5 MW Wind Turbine," authored by Ian Prowell, Ahmed Elgamal, and Jinchi Lu (2010). The dissertation author is the first author of these papers.

Chapter 7 of this dissertation is an extended version of material published in the following three National Renewable Energy Laboratory reports and a manuscript under preparation for publication as a journal article: (1) "FAST Simulation of Wind Turbine Seismic Response," authored by Ian Prowell, Ahmed Elgamal, and Jason Jonkman (2010), (2) "Estimation of Seismic Load Demand for a Wind Turbine in the Time Domain," with authors Ian Prowell, Ahmed Elgamal, Jason Jonkman, and Chia-Ming Uang (2010), (3) "Earthquake Response Modeling for a Parked and Operating Megawatt-Scale Wind Turbine," with authors Ian Prowell, Ahmed Elgamal, Harold Romanowitz, J. Edward Duggan, and Jason Jonkman (2010), and (4) tentatively titled "Shake Table Testing of a Utility Scale Wind Turbine Including Operational Effects," with a preliminary author list of Ian Prowell, Ahmed Elgamal, Chia-Ming Uang, J. Enrique Luco, Hal Romanowitz, and Ed Duggan (2011). The dissertation author is the first author of these papers.

Chapter 8 of this dissertation is an extended version of a manuscript in preparation for publication tentatively titled "Understanding Trends in Seismic Demand for the Current Inventory of Wind Turbines," with a preliminary author list of Ian Prowell, Ahmed Elgamal, Chia-Ming Uang, and Jason Jonkman (2011). The dissertation author is the first author of this paper.

Support for this research was provided by the U.S. National Science Foundation under George E. Brown Jr. NEES Research project (NSF NEESR-II grant No. CMMI 0830422). This support is gratefully acknowledged.

VITA AND PUBLICATIONS

1999	B.S. in Engineering, Harvey Mudd College, Claremont
2006	Graduate Teaching Assistant, UCSD
2007	Master of Science in Structural Engineering, UCSD
2007-2008	Graduate Research Assistant, UCSD
2008	Graduate Professional Intern, Sandia National Laboratories
2008-2010	Graduate Research Assistant, UCSD
2011	Doctor of Philosophy, UCSD

Journal Publications

Prowell, I., Veletzos, M., Elgamal, A., and Restrepo, J., (2009). "Experimental and Numerical Seismic Response of a 65 kW Wind Turbine." *Journal of Earthquake Engineering*, 13(8), pp. 1172-1190.

Shoele, K., Prowell, I., Zhu, Q., and Elgamal, A., (2011). "Dynamic and Structural Modeling of a Floating Wind Turbine." *International Journal of Offshore and Polar Engineering*, (in press).

Prowell, I., Elgamal, A., Luco, J.E., and Conte, J.P., (2011). "In-situ Ambient Vibration Study of a 900-kW Wind Turbine." *Journal of Earthquake Engineering and Structural Dynamics*, (under review for publication).

Prowell, I., Uang, C.-M., Elgamal, A., Luco, J.E., and Guo, L., (2011). "Shake Table Testing of a Utility Scale Wind Turbine." (under review for publication).

Prowell, I., Elgamal, A., Uang, C.-M., Luco, J.E., Romanowitz, H., and Duggan, E. (2011). "Shake Table Testing of a Utility Scale Wind Turbine Including Operational Effects." (under preparation for publication).

Prowell, I., Elgamal, A., Uang, C.-M., and Jonmkan, J. (2011). "Understanding Trends in Seismic Demand for the Current Inventory of Wind Turbines." (under preparation for publication).

National Laboratory Reports

Prowell, I. and Veers, P. (2009). *Assessment of Wind Turbine Seismic Risk: Existing Literature and Simple Study of Tower Moment Demand*, Sandia National Laboratories, SAND2009-1100, Albuquerque, New Mexico, USA.

Prowell, I., Elgamal, A., and Jonkman, J. (2010). *FAST Simulation of Wind Turbine Seismic Response*, National Renewable Energy Laboratory, NREL/CP-500-46225, Golden, Colorado, USA. Also published at: *2009 ANCER Workshop*, Urbana, Illinois, USA.

Prowell, I., Elgamal, A., Jonkman, J., and Uang, C.M. (2010). *Estimation of Seismic Load Demand for a Wind Turbine in the Time Domain*, National Renewable Energy Laboratory, NREL/CP-500-47536, Golden, Colorado, USA. Also published in: *2010 Proceedings of the European Wind Energy Conference and Exhibition*, Warsaw, Poland.

Prowell, I., Elgamal, A., Romanowitz, H., Duggan, J.E., and Jonkman, J. (2010). *Earthquake Response Modeling for a Parked and Operating Megawatt-Scale Wind Turbine*, National Renewable Energy Laboratory, NREL/TP-5000-48242, Golden, Colorado, USA. Also published in: *2010 Proceedings of the American Wind Energy Association WINDPOWER Conference and Exposition*, Huston, Texas, USA.

Conference Publications

Prowell, I., Veletsos, M., and Elgamal, A., (2008). "Full Scale Testing for Investigation of Wind Turbine Seismic Response." *Proceedings of the 7^{th} World Wind Energy Conference*, Kingston, Ontario, Canada.

Prowell, I. and Elgamal, A., (2008). "Highway Bridge Testbed: Internet Accessibility of Data and Video in Real Time." *Proceedings of the International Conference on Engineering Education*, Pécs, Hungary.

Prowell, I., Veletsos, M., Elgamal, A., and Restrepo, J., (2008). "Shake Table Test of a 65 kW Wind Turbine and Computational Simulation.", *Proceedings of the 14^{th} World Conference on Earthquake Engineering*, Beijing, China.

Elgamal, A., Prowell, I., Conte, J., Luco, J.E., Uang, C.M., Duron, Z. (2009). "NEESR-II: A Seismic Study of Wind Turbines for Renewable Energy." *NSF CMMI Research and Innovations Conference*, Honolulu, Hawaii, USA.

Prowell, I., Elgamal, A., Lu, J., and, Luco, J. E. (2009). "Modal properties of a modern wind turbine including SSI." *17^{th} International Conference on Soil Mechanics & Geotechnical Engineering*, Alexandria, Egypt.

Prowell, I., Elgamal, A., and, Lu, J. (2010). "Modeling The Influence of Soil Structure Interaction on the Seismic Response of a 5 MW Wind Turbine." *5^{th} International Conference on Recent Advances in Geotechnical Earthquake Engineering and Soil Dynamics in Honor of Professor I.M. Idriss*, San Diego, California, USA.

Prowell, I., Elgamal, A., and Jonkman, J., (2010). "Seismic Response of a 5-MW Wind Turbine: The Shakeout Scenario." *9^{th} US National and 10^{th} Canadian Conference on Earthquake Engineering*, Toronto, Ontario, Canada.

Prowell, I., Elgamal, A., Uang, C.-M., Luco, J.E., and Conte, J. (2011). "Recent Advances in Understanding the Seismic Response of Wind Turbines." *NSF CMMI Research and Innovations Conference*, Atlanta, Georgia, USA.

Prowell, I., Schmidt, T., Elgamal, A., Uang, C.-M., Romanowitz, and H., Duggan, J.E. (2011). "Measuring Global Response of a Wind Turbine to Earthquake Shaking Assisted by Point Tracking Videogrammetry." *52nd AIAA/ASME/ASCE/ASC Structures, Structural Dynamics and Materials Conference*, Denver, Colorado, USA.

ABSTRACT OF THE DISSERTATION

An Experimental and Numerical Study of Wind Turbine Seismic Behavior

by

Ian Prowell

Doctor of Philosophy in Structural Engineering

University of California, San Diego, 2011

Professor Ahmed Elgamal, Chair

This dissertation presents an experimental and numerical investigation into the seismic response of modern wind turbines. Currently, no consensus exists in the industry and there is significant interest in improving prediction of the behavior of wind turbines simultaneously subjected to wind, earthquake, and operational excitation.

To this end, an experimental program was planned in order to evaluate seismic loading of wind turbines. In 2004, a preliminary shake table test of a 65-kW utility

scale wind turbine was conducted that provided an experimental basis to begin the work discussed herein. A monitoring campaign was performed at Oak Creek Energy Systems in Mojave, California to assess variability of in-situ dynamic characteristics of two modern wind turbines (900-kW and 1.5-MW rated power) under different operational states and wind conditions. A second shake table experiment with a more extensive test program and improved instrumentation was executed, in which orientation of shaking and operational state were found to significantly influence response.

Using the finite element program OpenSees, beam-column models of the tested specimens were constructed and calibrated. Collected data provided a basis to show that such a model could reproduce salient characteristics including natural frequencies, mode shapes, and dynamic response time histories for a parked turbine. In-situ results were used to guide construction of full turbine-foundation-soil models that provided insight into soil-structure interaction phenomena.

An existing tool to simulate turbine dynamics, the FAST code, was extended to include seismic loading to allow simulation of operational turbines subjected to base shaking and validated based on shake table results. Using a calibrated model of the tested 900-kW turbine it is shown that neglecting aerodynamics results in significant over estimation of the tower bending demand. An investigation of turbines ranging from 65-kW to 5-MW concluded that consideration of aerodynamics and operational state becomes increasingly important with size.

The updated FAST code was demonstrated to accurately reproduce observed dynamics of operating turbines, providing a validated tool for seismic design of tur-

bines. These contributions clarify that operational state and orientation of shaking are important considerations and enable the development of a new generation of turbines that appropriately consider seismic loads.

Chapter 1

Introduction

The last two decades have seen significant growth in use of wind power throughout the United States (AWEA, 2007). With this growth, the wind turbine is starting to play a critical role in the United States power infrastructure. It is imperative that wind farms remain in operation immediately following an earthquake to provide power for rescue and recovery efforts. In contrast to a city comprised of many different structures, a wind farm consists of few types of unique structures. This homogeneity raises the problem that an earthquake with unfavorable characteristics may damage most of the turbines at a given wind farm. Survival of wind turbines through earthquake events will mitigate major financial loss due to disruption and the need for replacement. Turbines capable of surviving an earthquake without damage provide lifeline infrastructure for recovery, as well as being a needed component of sustainable communities, requiring minimal post-disaster repair. Reliable methods for understanding seismically induced load on wind turbines will increase the likelihood of surviving seismic events without being over conservative.

In this chapter, an introduction to wind energy is provided. Existing literature on seismic loads for turbines is discussed. The objectives and scope of this research is then explained. Finally, the organization of this dissertation is presented.

1.1 Introduction to Producing Electricity from the Wind

Wind energy has been used for centuries with historical uses including pumping water and grinding grain. These applications are the source of the term "windmill" which implies a mill used to grind grain. Starting in the 20^{th} century numerous research projects explored the possibility of extracting electricity from the wind (Hau, 2006). The birth of utility scale production of electricity from the wind is frequently placed in the early 1980s. In this era, the term "wind turbine" became popular for describing a machine used to convert kinetic energy in the wind into electrical power. Early turbines explored many different design alternatives, including vertical axis turbines (VAWTs). Gradually, as the industry matured, most design concepts standardized on horizontal axis wind turbines (HAWTs) with one, two, or three blades. Figure 1.1 shows a typical wind farm used to generate electricity from the wind locate in Palm Springs, California, USA.

1.1.1 Modern Wind Turbine Configurations

The HAWT consists of three major components, a tower, a nacelle, and a rotor (Figure 1.2). The tower supports the rest of the machine and elevates the rotor to

Figure 1.1: White Water Wind Farm located near Palm Springs, California, USA

the desired height. The nacelle, houses the generator, gear box and other mechanical components of the turbine required to support the rotor. The turbine hub provides a mechanical connection between the blades and the drive shaft which connects the hub to the nacelle. The hub and blades collectively are referred to as the turbine rotor.

Various design approaches have been explored for the turbine tower, with the primary design alternatives being a truss and a tube tower. Many early turbines use truss towers as they were similar to other existing designs, such as electrical transmission towers. Tube towers made of steel are constructed by rolling flat steel plates to the desired diameter and welding to join. Some turbines use a relatively slender tower, with guy wires to provide additional stiffness and lateral resistance, but this is uncommon in large production scale machines. Recent designs have explored the possible use of concrete as an alternative material for tube tower construction.

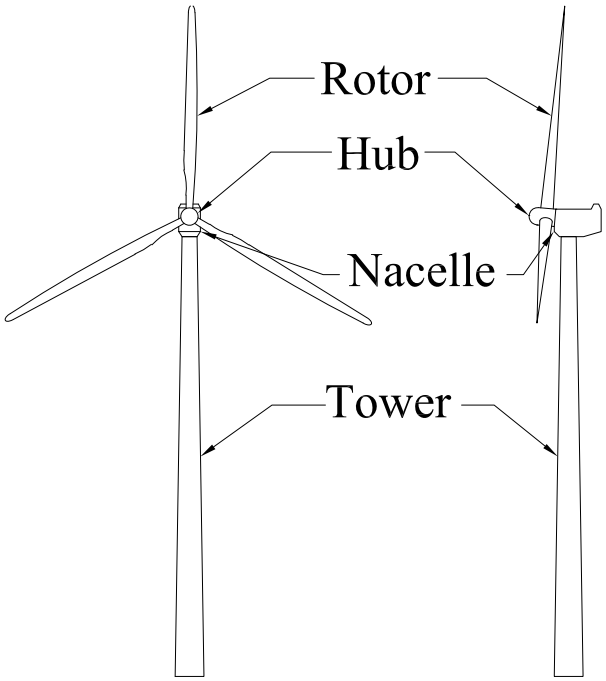

Figure 1.2: Components of a modern wind turbine

The steel tube tower is currently the most common tower used in utility scale HAWTs.

HAWTs require a mechanism to appropriately orient the turbine rotor (known as yaw) relative to the wind for optimal production of energy. Two primary methods of yaw exist, passive and active. A passive machine relies on a force generated by the wind to rotate the nacelle. This is commonly achieved by extending a tail behind the rotor which catches the wind. In contrast, an active yaw machine relies on a control mechanism to mechanically rotate the nacelle. By converting a dynamic degree of freedom to a control parameter, active yaw turbines have simpler dynamic properties. To simplify design, most modern turbines capitalize on active yaw to create a machine with fewer degrees of freedom. Machines that orient the rotor in front of the nacelle are known as upwind machines, and are more common in large turbines.

Almost all modern turbines are lift machines, which implies that the turbine

blades have airfoil shaped cross-sections capable of generating lift that supplies the torque needed to spin the rotor and generator. This design concept is in contrast to early turbines, which rely on blades that resemble flat plates and use drag on the plates to spin the rotor. A lift turbine is capable of extracting a greater portion of the kinetic energy from the wind (Hau, 2006).

Since a lift turbine is capable of moving faster than the wind, a method to regulate the rotor speed is needed. Simpler turbines rely on the blades entering a stall when a specified rotational speed is exceeded. Upon initiation of a stall, the blades no longer generates significant lift and the rotor is prevented from accelerating further. As a safety measure, such machines normally have aerodynamic tip brakes, which can be deployed to assist in slowing the rotor. Like a variable pitch airplane propeller, an active pitch turbine can rotate the blades to adjust the amount of lift generated from the passing wind. The blade pitch is continuously adjusted in an active pitch machine to keep the rotor speed in an acceptable range. Like the aerodynamic brakes at the tips of stall regulated machines, most active machines can fully pitch the blades to slow the rotor. In addition to stall regulation, tip brakes, and active pitch, all large turbines have a mechanical break capable of providing resistance to rotation of the rotor.

This dissertation focuses on three bladed, horizontal axis, active yaw, upwind power generation wind turbines with tubular steel towers. Both stall regulated and variable pitch machines are considered.

1.1.2 Wind Turbine Operational States

Unlike conventional civil structures, which have a single state, stationary, wind turbines have multiple dynamic states which may influence earthquake response. This dissertation divides these states into three broad load cases: non-operational, operational, and emergency shutdown.

The non-operational state is divided into two conditions, parked and idling. For fixed pitch turbines, such as smaller, older machines, a mechanical break is used to park the rotor, preventing it from spinning in the wind. Instead of applying a mechanical break, active pitch turbines, including most larger, modern turbines, can idle by feathering the blades such that they do not generate sufficient torque to spin the rotor. The operational case is the the standard state of the turbine while it is generating electricity. Emergency shutdown scenarios are conducted differently for fixed pitch and active pitch machines. For fixed pitch turbines, shutdown can be initiated by deployment of aerodynamic breaks located at the tip of each blade, followed by application of the high speed shaft (HSS) break. For active pitch turbines, emergency shutdown can be achieved by feathering the turbine blades to reduce torque on the rotor. By reducing rotor torque the blades slow and the turbine transitions to the idling state.

1.2 Literature Review

Seismic loading of wind turbines is being actively addressed in current literature. Guidelines for wind turbine design include earthquake considerations. Numer-

ous models have been published to investigate seismic loading of turbines. Results from specific investigations have been published providing preliminary conclusions regarding seismic loading on turbines.

1.2.1 Existing Codes and Standards

Three main standards or guidelines provide direct guidance for seismic loading of wind turbines: Guidelines for Design of Wind Turbines (Risø, 2001); Guideline for the Certification of Wind Turbines (GL, 2003); and IEC 61400-1 Ed.3: Wind turbines - Part 1: Design requirements (IEC, 2005). Outside of these, building codes, such as the 2006 IBC (ICC, 2006), can be used to inform about earthquake analysis, but do not directly address wind turbines. All three turbine guidelines suggest that there are few regions throughout the world where seismic loads may be design driving. However, over one quarter of the turbines installed in 2007 were erected in the United States (US), India, and China (DOE, 2008), all with large regions of high seismic hazard. In all three guidelines, seismic analysis is only required in regions of high seismic hazard or as required by local authorities.

Of the three guidelines mentioned, Guidelines for Design of Wind Turbines (Risø, 2001) provides the most general suggestions. The Risø guidelines function as a basic introduction to the concerns associated with seismic loading. This is consistent with the general intent of the publication to serve as a detailed introduction to all engineering wind turbine subjects. A model for seismic analysis is proposed that accounts for the nacelle, rotor, and 1/4 of the tower mass with a lumped mass at the top of the tower. It is suggested that the resulting period be used to select a

spectral response acceleration from a design response spectrum that will be used to determine the seismic loads on the tower. This is a single degree of freedom (SDOF) frequency domain analysis because of the simple model used (without any time domain simulations). The procedure is similar to simplified procedures used in building codes. No recommendation is provided for the appropriate level of damping. An assumed level of damping will be embedded in the design response spectrum used in analysis, which is typically 5% (ICC, 2006). No guidance is provided in translating the resulting spectral response acceleration into design loads. In the absence of specific guidance, it is assumed that appropriate building code procedures will be employed.

In contrast to the Risø guidelines, the Germanischer Lloyd (GL) guidelines (GL, 2003) provide little introduction to the specific details of earthquake engineering. These guidelines are more prescriptive and provide detailed guidance on particular aspects of seismic risk, which is consistent with the intent of the publication as a set of requirements for certification. The guidelines first suggest that either local building codes should be applied or the American Petroleum Institute (API, 2000) recommendations are to be applied in consultation with GL Wind. The guidelines then prescribe details of the required seismic analysis. A return period of 475 years is prescribed as the design level earthquake. The resulting earthquake load is to be combined with all normal external conditions with a safety factor of 1.0 for the earthquake load. Consideration of at least 3 modes is required for both time domain and frequency domain analyses. For time domain analyses at least 6 simulations must be performed per load case. Finally, it is prescribed that the tower is to behave

elastically unless the tower has characteristics that allow ductile response, such as a lattice tower. As with the Risø guidelines (Risø, 2001), no guidance is provided regarding the level of viscous damping.

In a similar fashion to the GL guidelines (GL, 2003) the IEC guidelines (IEC, 2005) focus on prescribing requirements for analysis of seismic loads. The design level earthquake is prescribed as a 475 year return period event and the resulting loads must be superimposed with the greater of the lifetime averaged operating loads or the emergency shutdown loads. Consistent with building code (ICC, 2006) the GL guidelines required safety factor for the earthquake load is 1.0 (GL, 2003). The analysis may be conducted through time domain or frequency domain methods, but either method must use consecutive modes with a total modal mass of 85% of the total mass of the turbine. A simplified procedure is provided in Annex C, which is intended to be a conservative estimate of seismic loads. The procedure suggests the use of a design response spectrum from local building code adjusted to a damping of 1% to establish the design response acceleration based on the first tower mode. The force required to accelerate a mass equal to the combination of the rotor, nacelle, and half of the tower mass by the design response acceleration is applied at the tower top to determine a design base shear and moment. This value is then combined with the loads calculated for an emergency shutdown at the rated wind speed.

1.2.2 Turbine Modeling Methods

Existing literature regarding modeling wind turbines for seismic loading is divided between two types of models; models that focus on the tower by accounting

for the mass of the nacelle and rotor as a point mass at the top of the tower; and models that describe the full turbine including the nacelle and rotor with some level of detail. Simplified models are attractive as they remove the complexity of modeling the rotor. The simplified approach casts the turbine as a SDOF system and may be unreliable for modeling behavior that arises from modes other than the first tower mode.

In contrast, full system models increase complexity of interpreting the results. The additional overhead is rewarded by model flexibility. Existing full system models attempt to incorporate all possible factors to seismic risk including aerodynamic loads, rotor dynamics, soil-structure interaction, electrical system dynamics, and other sources. A full system model further has the benefit of prediction of component loads instead of only tower loads. Since there is no systematically documented experience of seismically induced failure in wind turbines, designers cannot be certain how a turbine might fail in a seismic event. It is generally assumed that the tower and foundation are the critical components for seismic loading. Full systems models can help evaluate component loads not included in a simple tower based model.

Simple Models

As previously discussed, both Risø National Laboratory (Risø, 2001) and the IEC Annex C (IEC, 2005) provide simplified procedures for estimating seismic loading of a wind turbine. The difference between these two procedures is subtle. The Risø procedure uses a simplified model to determine the first tower natural period that could prove useful for estimation during design iterations. The IEC assumes that

the first natural period is known based on existing analysis. Both procedures then use this first natural period to extract the design response acceleration from a design response spectrum. The Risø procedure then leaves the designer free to select an appropriate method to translate the design response acceleration into seismic loads where the IEC procedure prescribes that this acceleration be translated into a base shear and moment as described in section 1.2.1.

Full System Models

Proper aerodynamic analysis of wind turbines requires a full system model. This has led to mature and widely used full system models in the wind energy industry. Two notable modeling tools specific to the wind industry are GH Bladed (Bossanyi, 2000) which is produced by Garrad Hassan (GH) and the FAST code (Jonkman and Buhl Jr., 2005) which is maintained by the United States National Renewable Energy Laboratory (NREL). Both GH Bladed and the FAST code have been validated by Germanischer Lloyd for calculating operational loads associated with typical load cases. Other high quality models are also used in the wind industry, such as the FLEX5 code (Hansen et al., 2005), and several others.

GH added a seismic module to GH Bladed in response to demand for estimation of loading at seismically active sites (Bossanyi, 2000). GH Bladed does not model the turbine using a finite element method due to computational complexity, but instead uses a limited-degree-of-freedom modal model. Modal calculations are conducted in the time domain for the major components of the turbine. The resulting forces for each mode are then calculated at the component interfaces. GH Bladed

has two methods for simulating seismic loading. The first method is to use recorded acceleration time histories. The second method uses an iterative procedure to produce a synthetic acceleration time history with an elastic response spectrum that closely resembles a specified design response spectrum. To further increase flexibility, the user is able to specify a foundation stiffness to account for soil and foundation influences on the structural response. The end result is a comprehensive package that is able to simulate seismic response of a turbine in the time domain with any specified level of damping in combination with other load sources. This approach allows the designer to explore numerous loading scenarios and obtain a detailed understanding of the resulting structural loads.

The FAST code (Jonkman and Buhl Jr., 2005) uses a combined modal and multibody dynamics formulation to simulate the dynamic behavior of a turbine. The equations of motion are solved using standard multibody dynamics formulations for elements whose flexibility is determined by the summation of mode shapes provided by the user. Prior to work presented in this dissertation, the FAST code did not directly provide a facility to simulate seismic loading. Instead, a generic framework was provided that allows the user to provide a custom-developed loading routine to be imposed at the base of the turbine. This dissertation details appropriate additions to the FAST code so that it is capable of providing a full system model for seismic loading.

Another software package, FLEX5, may be used to model seismic loading of wind turbines (Ritschel et al., 2003). FLEX5 was developed by Stig Oye from the Department of Fluid Mechanics at the Technical University of Denmark (Larwood

and Zuteck, 2006). The implementation of FLEX5 is based on a modal formulation with selected degrees of freedom (Hansen et al., 2005). Simulations are conducted in the time domain and produce records of component loads and deflections.

Efforts have been made to use a hybrid multibody system (MBS) (Zhao and Maißer, 2006; Zhao et al., 2007) to develop a full system model for wind turbines. This approach casts the turbine as a series of rigid bodies connected by flexible elements. A set of analytical governing equations can be derived for the turbine using this approach and Lagrange's equations of the second kind. This approach, though more mathematically rigorous, does not require external calculation of component mode shapes.

1.2.3 Existing Results

The growth of wind power has led to an interest in addressing seismic loading of wind turbines. Early publications (Bazeos et al., 2002; Lavassas et al., 2003) considering seismic loading of wind turbines focused on loading of the tower based on simplified models that lumped the nacelle and rotor as a point mass. Gradually interest shifted from these simple models to more refined models that also consider loads for turbine components other than the tower (Ritschel et al., 2003; Witcher, 2005; Häenler et al., 2006; Zhao and Maißer, 2006).

Somewhat unique, but worthy of note, is a 1984 publication considering seismic loads in combination with wind loads for a wind turbine rotor (Hong, 1984). This work develops a set of analytical equations describing the statistical distribution of blade response parameters. Seismic input motion is considered as white-noise, filtered

to approximate the shaking transmitted by the tower, in each of three orthogonal directions at the hub. The effects and interaction with tower vibrations are neglected in this study. Based on the proposed formulation, it is concluded that turbulence is a larger contributor to fatigue for wind turbine blades than earthquake loads.

In 2002, another attempt to quantify the dynamics of wind turbines due to seismic loading was published (Bazeos et al., 2002). This publication presented extensive finite element modeling of a prototype 450-kW turbine with a 38 meter tall steel tower designed for installation in Greece. The tower was modeled in detail using shell elements as well as by a simpler model that used beam-column elements. Both models addressed the rotor and nacelle by adding a point mass at the top of the tower and used a viscous damping of 0.5%. Time history analyses of the two models were conducted and compared. The results from the two models showed good agreement, but the more detailed model was required for buckling analysis. Soil structure interaction (SSI) was investigated using springs, dampers, and added mass. The main outcome of the SSI analysis was to show a significant decrease in the frequencies at which the second and third tower bending modes occurred due to base fixity. The analysis concluded that seismic loading did not produce design driving loads.

An early publication considering both earthquake and wind loads was published by Kiyomiya et al. (2002). First the relative probabilities of wind speed and earthquake acceleration is examined. Based on appropriate probability distributions for each, it is concluded that likelihood of concurrent extrema is small enough to be neglected. In the case of a large and rare earthquake it is found that the highest likely wind speed is the mean wind speed. A simplified beam-column model with a

lumped mass for the nacelle and rotor mass at the hub height with an assumed equivalent viscous damping of 2% is used to simulate the turbine structure. The wind is applied as a static point load at the hub height. Additionally, a FE mesh is used to model the soil and foundation. Simulations are conducted using a recording of the Hyougoken-Nanbu earthquake obtained at a depth of 82 m below Port Island. A resulting tower base demand of 1.5 times the demand from a storm condition is found for the simulated earthquake, but is found to be below the capacity of the simulated tower. It is concluded that the turbine has sufficient strength to resist the earthquake without damage. Suggestions for further research support the work presented in this dissertation to allow consideration of dynamic wind loads in parallel with earthquake loads.

In 2003, a detailed finite element investigation was published of 1-MW turbine with a 44 m tall steel tower and 52 m rotor diameter designed for installation in Greece (Lavassas et al., 2003). The seismic loading in this investigation was based on a multimode linear analysis which used a design response spectrum from Eurocode 3 for a site in seismic zone II with rocky soil. The authors concluded seismic stresses were 60 percent lower compared to those developed by extreme wind loads for this level of seismicity. Again the rotor and nacelle were simplified to a point mass at the top of the tower. The authors speculate that seismic design could become critical in regions with higher seismic hazard and less favorable soil conditions.

Windrad Engineering published an analysis that considers seismic loads for components other than the turbine tower (Ritschel et al., 2003). The publication first looks at the seismic loads produced by a modal analysis of a simple distributed

mass cantilever beam model of a 2.5-MW Nordex N80 wind turbine with an 80 m rotor diameter and 60 m hub height. This modal approach produced seismic loads that closely matched the contemporary IEC approach (IEC, 1999) based on a synthetic input time history with a peak ground acceleration (PGA) of 0.3 g. Realizing that such a model was incapable of properly addressing component loads, a full system model with 28 degrees of freedom was developed using FLEX5 by mapping ground acceleration through a coordinate transformation into effective external nodal forces. The FLEX5 model produced lower moment demand at the base of the tower compared to both the IEC approach and the modal approach using the same synthetic earthquake time history. The loads approached parity toward the top of the tower. At the top of the tower the seismic load from FLEX5 slightly exceeded both the IEC approach and the modal approach. The difference was not significant and it was concluded that the existing design loads were sufficient. The vertical seismic excitation caused higher bearing loads than those from extreme wind conditions. Vertical excitation was also found to induce tilt vibration in the nacelle. This investigation concluded that seismic loads in the blades were about 70% lower than those caused by the 50-year wind loads.

Witcher (2005) presents an overview of the GH Bladed seismic module in conjunction with some preliminary results for loading of a 2-MW upwind machine with an 80 m diameter rotor and a 60 m tower. The results show the response in three load cases: continuous operation throughout the earthquake; emergency shutdown initiated during the earthquake; and parked throughout the earthquake. The difference in the resulting maximum moment demand at the base of the tower

for the three load cases was compared for a time and frequency domain calculation. Only a 2.9% increase in the maximum moment demand was observed in the time domain compared to the demand from the frequency domain. A fourth load case considered the turbine parked while subjected to an earthquake in combination with high winds. This case resulted in a 79% increase in moment demand for a time domain simulation from that calculated using a modal simulation. This result is used to highlight the importance of time domain simulations to account for aeroelastic interaction.

Windrad Engineering presented initial results of their new software, Simulation of Wind Energy Converters (SIWEC), for simulation of wind turbine dynamics including seismic loading at the 2006 European Wind Energy Conference (Häenler et al., 2006). This paper shows how SIWEC will be capable of addressing wind industry requirements (IEC, 2005) as well as requirements introduced from Eurocode 8. Results are shown for simulation that subjects a turbine with an 80 m rotor diameter and 60 m hub height operating in 13 m/s wind to an earthquake with a 0.3 g PGA. The simulation also includes the dynamics associated with shutdown of the turbine. The full system model predicts modes at frequencies in the region of maximum spectral response acceleration for typical design response spectra. The results focus on the relative increase in higher mode response. It is noted that for normal wind loading 80% of the tower energy is associated with the first mode. During the earthquake simulation the energy in the first mode is reduced to only 54% percent of the tower energy. The analysis concludes that higher tower modes are more important for earthquake loading than typical wind loading.

In collaboration with Peter Maißer and Jingyan Wu, Xueyong Zhao presents what was termed a hybrid MBS for modeling turbine dynamics (Zhao and Maißer, 2006; Zhao et al., 2007). The technique is detailed in the 2007 publication (Zhao et al., 2007) by providing the theoretical development, showing resulting mode shapes, and variation in natural frequencies as a function of rotor speed for a 600-kW turbine with a 43 m diameter rotor and a 52 m tower. This introduction is followed by an extension of the technique to include seismic loading and soil structure interaction (Zhao and Maißer, 2006). The rotor, which was initially modeled with three flexible blades, was simplified to a rigid disk when considering seismic loading. The soil structure interaction was addressed by connecting the turbine base to a rigid support with translational and rotational springs and dampers whose properties were derived based on assumed soil properties. The response of a 1.5-MW turbine subjected to turbulent wind with a mean velocity of 10.16 m/s and an earthquake acceleration time history with a maximum acceleration of 0.06 g is calculated using this model. The low PGA is consistent with a minor or very distant earthquake. Negligible impact was observed for the tower base shear and bending moment. In contrast, oscillation in the lateral reaction force of the main bearing was significantly increased. This observation is similar to that of Ritschel et al. (2003) regarding vertical loads in the main bearing.

Ishihara and Sawar (2008) completed a study on seismic demands for two different sizes of wind turbines (400-kW and 2-MW). Initially two modeling techniques are explored: one that places the rotor and nacelle mass into a single lumped mass; and a second that included mass and stiffness distribution of the nacelle and rotor.

It is concluded that for first mode response both models provide good representations, but when the second and higher modes are considered the lumped mass model diverges from the more representative model. Presented results show that, for the 2-MW turbine, second mode and higher responses are important and contribute significantly. Based on calculated demand, a semi-analytical approach to estimate shear and moment demand is proposed. It is shown that for the two studied turbines, moment is well modeled by the approach, but greater disagreement exists for the shear results. It is concluded that since moment generally governs design of the turbine tower that the approach is a useful tool for understanding seismic loads for wind turbines.

More recently, an extensive investigation into the seismic response of a 1.65-MW Vestas turbines was constructed (Nuta, 2010). In this work a full shell model of the turbine tower was constructed using the modeling package ANSYS (2007). Effects such as mesh refinement and connection detail modeling were explored. In the model the rotor and nacelle are lumped as two point masses near the top of the tower. The mass representing the rotor was offset to account for eccentricity. Consistent with this approach, aerodynamics are not considered and only the parked state of the turbine is simulated. Modeling procedures were validated against experimental results from the 2004 shake table test conducted at UCSD on a 65-kW Nordtank turbine and showed good general agreement in lower frequency response, but lacked some of the higher frequency content that was experimentally recorded (Prowell et al., 2009). Once the modeling procedure and the mesh of the 1.65-MW Vestals turbine were validated, an incremental dynamic analysis (IDA) was conducted using 20 records composed of 2

horizontal components from 10 earthquakes. Using the IDA results fragility curves were developed for the magnification factor, peak ground velocity (PGV), and PGA intensity measures (IM). Finally, the procedure is applied for two specific sites, one in Western and one in Eastern Canada.

Experimental and numerical investigations of damping due to aerodynamic effects show a wide range of damping for turbines (Riziotis et al., 2004; Hansen et al., 2006). Theoretical predictions show that some turbines can exhibit negative damping depending on the wind speed (Riziotis et al., 2004). It appears that newer pitch controlled machines exhibit higher damping in the tower at the first natural frequency than older stall regulated machines (Riziotis et al., 2004). Existing publications show that in all cases aeroelastic effects lead to directional damping that is higher for fore-aft (in the direction of the wind) vibration than for side-to-side (horizontally normal to the wind) vibration. This predicted and observed directivity in damping suggests that seismic loading should be considered in both directions to ascertain if the decreased damping in the side-to-side direction will increase the resulting design loads despite not being directly additive with other loads.

1.2.4 Perceived and Actual Risk

Few strong earthquakes have occurred in the vicinity of utility scale wind farms. Two events of interest for seismic loading of wind turbines are the 1986 North Palm Springs Earthquake and 1992 Northridge Earthquake. Ground motion recordings from the vicinity of wind farms are available for both earthquakes. The North Palm Springs Earthquake occurred very near wind turbine installations situated to

the northwest of Palm Springs. California Strong Motion Instrumentation Program (CSMIP) station 12149 was approximately 5 km from these wind farms. The 1992 Northridge earthquake occurred about 80 km from wind farms located in Tehachapi, California and was recorded by the CSMIP station 34237. This station is within 1 km of Tehachapi wind farms.

The Northridge Earthquake had a moment magnitude of 6.7 whereas the North Palm Springs Earthquake was weaker with a moment magnitude of 6.2. Monetary damage from for the Northridge Earthquake was greater, mainly due the proximity of the epicenter to a densely populated area. This supports the perception that the Northridge earthquake presented a higher risk to wind turbines than the North Palm Springs earthquake. The recorded earthquake records do not support this conclusion. The recording near the Tehachapi wind farms (Northridge) shows a peak ground acceleration of 0.06 g, which is similar to that investigated by Zhao and Maißer (2006) that showed minimal impact on resulting loads. Verbal reports indicate no damage to turbines in the area in agreement with published findings. In contrast the PGA recorded near the Palm Springs wind farms from the North Palm Springs Earthquake was 0.33 g, which represents a much more significant event in the range shown by numerical investigation to produce structural demand near design loads (Ritschel et al., 2003). This level of ground acceleration represents a much higher chance of damage to civil structures, including the wind turbines that were in the area. News reports from the 1986 North Palm Springs Earthquake do not detail any wind turbine damage, but document significant damage to buildings in the vicinity. Proximity to the earthquake epicenter is a primary factor for PGA experienced at a

site and should be considered in site specific assessments of seismic loads for wind turbines.

1.2.5 Current Practice

A picture of the state of practice early in the decade for site specific seismic analysis of turbines was presented at the 2002 annual convention of the Structural Engineering Association of California (Agbayani, 2002). The publication details seismic loading based on the 1997 Uniform Building Code (ICBO, 1997). Design response spectra are scaled from 5% viscous damping to 2% using FEMA-273 (FEMA, 1997). The article notes that in contrast to past turbines, some newer units with increased size and weight are governed by seismic loads instead of wind loads in regions of high seismic hazard due to provisions limiting the minimum base shear considered for long period structures.

1.3 Objectives and Scope

Wind energy is growing and turbines are regularly installed in regions with seismic hazard. Due diligence requires consideration of seismic loads for turbines and as indicated by the literature reviewed above, interest exists in both the corporate and academic communities in improving prediction of seismic loads for wind turbines. Further, regulations and certification guidelines require certification of load cases where wind turbines are simultaneously subjected to wind and earthquake loads.

Current research has been numerical and little experimental work exists. The

experimental work that does exist is focuses on experimental modal identification to characterize turbine dynamic properties. The majority of specimens previously studied were vertical axis wind turbines, which are not currently predominant in wind energy production. Some publications document dynamic characteristics of HAWTs (James III et al., 1992), but little data is publically available which addresses large megawatt or greater scale turbines (Molinari et al., 2010). Further characterization of large turbines is valuable for understanding seismic response.

Currently, numerical approaches have been documented and tools exist for simulation of seismic loads for turbines. Most of these tools are not readily available for peer review and customization (Witcher, 2005; Zhao and Maißer, 2006; Hansen et al., 2005; Häenler et al., 2006). A common platform where researchers can assess seismic loads for turbines will assist in improving the understanding and simulation of earthquake influence on turbine design.

Of particular importance is understanding appropriate consideration of combined wind and earthquake loads. Most current procedures for combining loads use a simple method of adding the two loads, usually direct linear combination. This is appropriate where the loads sources do not interact, but in the case of wind turbines non-linear interaction exists between these two load sources.

The research program presented in this dissertation attempts to directly address current opportunities for improving understanding of seismic loads for turbines by addressing the following factors:

1. Existing data from the 2004 shake table test of a 65-kW Nordtank turbine will

be used to provide a preliminary basis for seismic loading of wind turbines. With this data, modal properties such as natural frequencies, damping and mode shapes under strong earthquake excitation will be clarified.

2. Models similar to those currently used in the wind industry for seismic loads are developed. Using these models, experimental and simulated results are compared to assess the suitability of these approaches and the ability of conventional FE programs to predict the observed dynamics.

3. Implications of various values of viscous damping currently used to assess turbine dynamics are explored with the resulting, calibrated models.

4. Based on insights gleaned from the preliminary test a more extensive shake table test of the 65-kW Nordtank turbine is planned and executed. This second test collects valuable data regarding the implication of the orientation of shaking and the operational state of the turbine.

5. Strong earthquake shaking conducted on the 65-kW Nordtank turbine is used to illuminate turbine damage mechanisms. Appropriate instrumentation is used to segregate damage into damage of the super-structure and the attachment of the turbine to the table platen.

6. In-situ modal identification is conducted on two large, modern wind turbines to extend the set of publically available results for dynamic properties of HAWTs. In addition to parked state dynamics, the operational state is analyzed. It is shown that existing modal analysis techniques, with proper guidance, can

successfully identify modal properties in the presence of operational forcing. Operational results are used to show variation in mode shape, natural frequency, and damping as they depend on state of the turbine.

7. The in-situ results are used to guide numerical approaches for consideration of soil-structure interaction effects for large turbines. The created model is used to explore the implications of soil stiffness on resulting dynamic properties and seismic demand.

8. The FAST code is extended to include base shaking as a load source for turbines allowing simultaneous consideration of wind and earthquake loads.

9. Models of the 65-kW Nordtank turbine developed using OpenSees and the FAST code are compared to validate that code modifications produce expected dynamic time histories and demand parameters.

10. Results from the 2010 shake table test are used as a basis to show that the influence of operational state on seismic response is properly simulated by the FAST code.

11. Using the validated modifications to the FAST code, simulations were conducted to show the extent that aerodynamic forces impact the response of a megawatt scale turbine to earthquake loads.

12. FAST code models of four different turbines are subjected to a large suite of earthquake time histories for three different load cases: non-operating, operating, and emergency shutdown. The predictive capability of intensity measures

are assessed by exploring their relation to resulting demand parameters.

13. Existing techniques for combining operational and seismic loads are assessed and compared to simulation results to understand accuracy. A new generalized method of combining loads is proposed.

1.4 Organization

This dissertation is arranged as follows:

This chapter of the dissertation presents the objectives, scope and organization of the dissertation. General information regarding the loads experienced by wind turbines and the operational states of turbines is presented. A literature review is conducted that describes existing codes and standards, turbine modeling methods, other pertinent research, turbine performance in historic earthquakes, and the current practice of estimation of seismic loads.

Chapter 2 presents the results of a full scale test of an actual 65-kW wind turbine subjected to base excitation using the Network for Earthquake Engineering Simulation (NEES) Large High Performance Outdoor Shake Table (LHPOST). Two simple finite element (FE) models are discussed which were calibrated with the results of the test. The chapter then presents an assessment of the influence of equivalent viscous damping on the predicted turbine response conducted by subjecting the FE models to a suite of California earthquake records.

A second test of the 65-kW turbine is presented in Chapter 3. This experiment investigated the relative orientation of the rotor and earthquake loads, level of

shaking, and higher resolution characterization of structural response. Shaking was imparted both parallel and perpendicular to the axis of rotation of the rotor. The test preparation and pertinent associated details are presented. Enabled by more extensive instrumentation, improved characterization of dynamic properties including clarification of higher modes is documented. The results of the test regimen for the parked configuration are analyzed to evaluate (a) the observed dynamic characteristics, (b) the implications of orientation and intensity of shaking, (c) the effectiveness of spectral acceleration as an indicator of maximum displacement demand, and (d) the relation between displacement and shear demand at various levels of shaking. Overall trends and important results are discussed with consideration of modern turbines.

Chapters 4 and 5 describe a set of dynamic tests performed on a 900-kW and a 1.5-MW HAWT located at Oak Creek Energy Systems near Mojave, California. The tests monitored structural vibrations using an array of up to 81 force balanced accelerometers installed at stations in the turbine tower, on the foundation, and in the surrounding soil. The chapters present modal identification results obtained using an output-only system identification method applied to the observed vibration. The results of Chapter 4 are used to calibrate a representative finite element (FE) model for the 900-kW turbine using the experimental modal analysis results. The experimental results are compared with those obtained numerically and implications of these results for seismic loading of wind turbines are discussed.

Expanding on previous investigations, Chapter 6 presents the influence of SSI on the seismic response of a hypothetical 5-MW reference turbine. First, a detailed FE model of the turbine is created and validated by comparison with published properties

of the turbine, and extended to include a full three-dimensional soil mesh. The soil-turbine system is then modified to simulate 3 different 15-meter thick soil profiles and subjected to a 1994 Northridge Earthquake record. Using these models, simulations are conducted to further assess the influence of SSI on the relative distribution of tower moment and shear demand.

Chapter 7 introduces modifications to the FAST code (Jonkman and Buhl Jr., 2005), which enable a base shaking time history to be applied in conjunction with other load sources for wind turbines. First, the FAST code is described with pertinent details of modifications required for consideration of seismic input. A model of th 65-kW Nordtank turbine used in shake table test at UCSD is constructed for the FAST code and compared to a conventional FE model for simulations of while the turbine is parked without consideration of aerodynamics. Next the results presented in Chapter 3 where the turbine was operating while earthquake like input was imparted are used to validate that salient changes in dynamics are numerically reproduced. Lastly, a FAST model of the 900-kW developed in Chapter 4 is used to illustrate the importance of considering aerodynamic forces on a turbine when assessing seismic loads.

Chapter 8 presents an extensive study of seismic loading in conjunction with the non-operating, operating, and emergency shutdown operational states. The 65-kW and 900-kW turbines, developed in Chapter 7, are considered in conjunction with two standard models for a 1.5-MW and 5-MW turbine. This range provides insight into the majority of turbines currently deployed in operational roles. Simulation results are used to evaluate the efficiency of various earthquake intensity measures to predict resulting structural demand. Finally, simplified methods of estimating this

combined load case are compared to simulation results.

Chapter 9 finishes this dissertation with concluding remarks that highlight the contributions presented here. Further, recommendations are provided for future research to improve the scientific understanding and modeling capabilities of seismically induced loads for wind turbines.

Appendix A contains additional plots from the preliminary shake table test conducted in 2004 not presented in Chapter 2.

Appendix B contains a brief methodology for estimation of a turbines fundamental period based on the preliminary shake table test discussed in Chapter 2.

Appendix C details the instrumentation layout and other pertinent details of the in-situ field test at Oak Creek Energy Systems.

Appendix D provides detailed information rebarding the 2010 shake table test of the 65-kW Nordtank turbine.

All experimental data presented in this dissertation may be obtained through the NEEShub Project Warehouse (http://nees.org/warehouse) for analysis in future studies.

1.5 Summary

The topic of seismic loads for wind turbines has received significant attention and is the focus of numerous research articles in recent years. Many numerical approaches have been explored and presented by others, which motivates the experimental and numerical work presented here.

An in-depth review of existing literature on the topic is presented in this chapter. Further, the objectives and scope of the research effort are clarified with an outline of this dissertation provided.

1.6 Acknowledgements

This text is reproduced verbatim as it appears in the acknowledgments section on page xvii per the UCSD Office of Graduate Studies Formatting Requirements.

Chapter 1 of this dissertation contains material from the report published by Sandia National Laboratories under the title "Assessment of Wind Turbine Seismic Risk: Existing Literature and Simple Study of Tower Moment Demand" with authors Ian Prowell and Paul Veers (2009). The dissertation author is the first author of this paper.

Bibliography

Agbayani, N. A. (2002). "Design challenges in international wind power projects: From foreign codes to computer coding in a small office setting." *71st Annual Structural Engineers Association of California (SEAOC) Convention*, Santa Barbara, California, USA. 117–132.

ANSYS (2007). *Release 11.0 Documentation for ANSYS*. ANSYS, Inc., Canonsburg, Pennsylvania, USA.

API (2000). *Recommended Practice for Design and Construction of Fixed Offshore Platform, PR2A, Chapter 2.3.6: Earthquake*. American Petroleum Institute, Washington, District of Columbia, USA.

AWEA (2007). *Wind Power Outlook 2007*. American Wind Energy Association, Washington, District of Columbia, USA.

Bazeos, N., Hatzigeorgiou, G. D., Hondros, I. D., Karamaneas, H., Karabalis, D. L., and Beskos, D. E. (2002). "Static, seismic and stability analyses of a prototype wind turbine steel tower." *Engineering Structures*, 24(8), 1015–1025.

Bossanyi, E. A. (2000). *Bladed for Windows User Manual*. Garrad Hassan and Partners, Bristol, UK.

DOE (2008). "20% wind energy by 2030: Increasing wind energy's contribution to U.S. electricity supply." *Report No. DOE/GO-102008-2567*, Department of Energy.

FEMA (1997). "NEHRP guidelines for the seismic rehabilitation of buildings." *Report No. FEMA-273*, Federal Emergency Management Agency.

GL (2003). *Guidelines for the Certification of Wind Turbines*. Germanischer Lloyd, Hamburg, Germany.

Häenler, M., Ritschel, U., and Warnke, I. (2006). "Systematic modelling of wind turbine dynamics and earthquake loads on wind turbines." *European Wind Energy Conference and Exhibition*, Athens, Greece. European Wind Energy Association, 1–6.

Hansen, M. H., Hansen, A., Larsen, T. J., Oye, S., Sorensen, P., and Fuglsang, P. (2005). "Control design for a pitch-regulated, variable speed wind turbine." *Report No. Riso-R-1500(EN)*, Risø National Laboratory.

Hansen, M. H., Thomsen, K., Fuglsang, P., and Knudsen, T. (2006). "Two methods for estimating aeroelastic damping of operational wind turbine modes from experiments." *Wind Energy*, 9(1-2), 171–191.

Hau, E. (2006). *Wind Turbines*. Springer, Berlin, Germany.

Hong, R. C.-Y. (1984). "Response of a wind turbine blade to seismic and turbulent wind excitations," PhD thesis, University of Illinois at Urbana-Champaign.

ICBO (1997). *Uniform Building Code 1997. Volume 2*. International Conference of Building Officials, Washington, District of Columbia, USA.

ICC (2006). *International Building Code 2006*. International Code Council, Country Club Hills, Illinois, USA.

IEC (1999). *IEC 61400-1 Ed. 2: Wind turbine generator systems - Part 1: Safety requirements*. International Electrotechnical Commission, Geneva, Switzerland.

IEC (2005). *IEC 61400-1 Ed. 3: Wind Turbines - Part 1: Design Requirements*. International Electrotechnical Commission, Geneva, Switzerland.

Ishihara, T. and Sawar, M. W. (2008). "Numerical and theoretical study on seismic response of wind turbines." *European Wind Energy Conference and Exhibition*, Brussels, Belgium. European Wind Energy Association, 1–5.

James III, G. H., Carne, T. G., and Lauffer, J. P. (1992). "The natural excitation technique (NExT) for modal parameter extraction from operating wind turbines." *Report No. SAND92-1666, UC-261*, Sandia National Laboratories.

Jonkman, J. M. and Buhl Jr., M. L. (2005). "FAST user's guide." *Report No. NREL/EL-500-38230*, National Renewable Energy Laboratory.

Kiyomiya, O., Rikiji, T., and van Gelder, P. H. A. J. M. (2002). "Dynamic response analysis of onshore wind energy power units during earthquakes and wind." *Proceedings of The Twelfth (2002) International Offshore and Polar Engineering Conference*, Kitakyushu, Japan. The International Society of Offshore and Polar Engineers, 520–526.

Larwood, S. and Zuteck, M. (2006). "Swept wind turbine blade aeroelastic modeling for loads and dynamic behavior." *Windpower*, Pittsburgh, Pennsylvania, USA.

Lavassas, I., Nikolaidis, G., Zervas, P., Efthimiou, E., Doudoumis, I. N., and Baniotopoulos, C. C. (2003). "Analysis and design of the prototype of a steel 1-MW wind turbine tower." *Engineering Structures*, 25(8), 1097–1106.

Molinari, M., Pozzi, M., Zonta, D., and Battisti, L. (2010). "In-field testing of a steel wind turbine tower." *Proceedings of the IMAC-XXVIII*, Bethel, Connecticut, USA. Society for Experimental Mechanics Inc., 1–10.

Nuta, E. (2010). "Seismic analysis of steel wind turbine towers in the canadian environment. Master's thesis, University of Toronto, Toronto, Ontario, Canada.

Prowell, I., Veletzos, M., Elgamal, A., and Restrepo, J. (2009). "Experimental and numerical seismic response of a 65kW wind turbine." *Journal of Earthquake Engineering*, 13(8), 1172–1190.

Risø (2001). *Guidelines for Design of Wind Turbines*. Wind Energy Department of Risø National Laboratory and Det Norske Veritas, Copenhagen, Denmark.

Ritschel, U., Warnke, I., Kirchner, J., and Meussen, B. (2003). "Wind turbines and earthquakes." *2nd World Wind Energy Conference*, Cape Town, South Africa. World Wind Energy Association, 1–8.

Riziotis, V. A., Voutsinas, S. G., Politis, E. S., and Chaviaropoulos, P. K. (2004). "Aeroelastic stability of wind turbines: the problem, the methods and the issues." *Wind Energy*, 7(4), 373–392.

Witcher, D. (2005). "Seismic analysis of wind turbines in the time domain." *Wind Energy*, 8(1), 81–91.

Zhao, X. and Maißer, P. (2006). "Seismic response analysis of wind turbine towers including soil-structure interaction." *Proceedings of the Institution of Mechanical Engineers, Part K: Journal of Multi-body Dynamics*, 220(1), 53–61.

Zhao, X., Maißer, P., and Jingyan, W. (2007). "A new multibody modeling methodology for wind turbine structures using a cardanic joint beam element." *Renewable Energy*, 32(3), 532–546.

Chapter 2

Experimental and Numerical Seismic Response of a 65-kW Wind Turbine

2.1 Introduction

Recognizing that experimental validation is currently scarce, a full-scale test was planned and conducted at the University of California, San Diego (UCSD) by Professors A. Elgamal, J. Restrepo, and M. Veletzos. An actual 65-kW wind turbine was subjected to base excitation using the Network for Earthquake Engineering Simulation (NEES) Large High Performance Outdoor Shake Table (LHPOST). This experiment provided a baseline for seismic behavior of a parked turbine in low winds. In this chapter, analysis of the experimental results was conducted to infer natural frequencies, mode shapes, and equivalent viscous damping. These results were then

employed to calibrate two simple finite element (FE) models that may be of use for conducting practical analyses (Agbayani, 2002; Bazeos et al., 2002; Lavassas et al., 2003; Jonkman and Buhl Jr., 2005; Witcher, 2005; Häenler et al., 2006).

The numerically derived modal properties were compared to those observed experimentally. Following calibration, the simple model that explicitly represented the rotor blades was used to conduct numerical simulations. For that purpose, a suite of California earthquake records was employed as base input excitation. The influence of viscous damping on the predicted turbine response was assessed. Finally, the reported results were used to motivate future research into the dynamics of wind turbines under earthquake loading conditions.

2.2 Shake Table Experiment

A full-scale test was conducted at UCSD to explore the response of a parked turbine due to base excitation. For that purpose, Hal Romanowitz and J. Edward Duggan of Oak-Creek Energy Systems in Mojave, California donated a 65-kW turbine that was erected on site and mounted on the shake table platform (Figure 2.2).

2.2.1 Turbine Description

The tested 65-kW turbine (Figure 2.2) was manufactured in Denmark by Nordtank. In the early 1980s, this Nordtank turbine and its contemporaries were installed in large numbers for utility scale power generation in California (Hau, 2006). By 1985, Danish machines accounted for approximately 40% (Hau, 2006) of the turbines

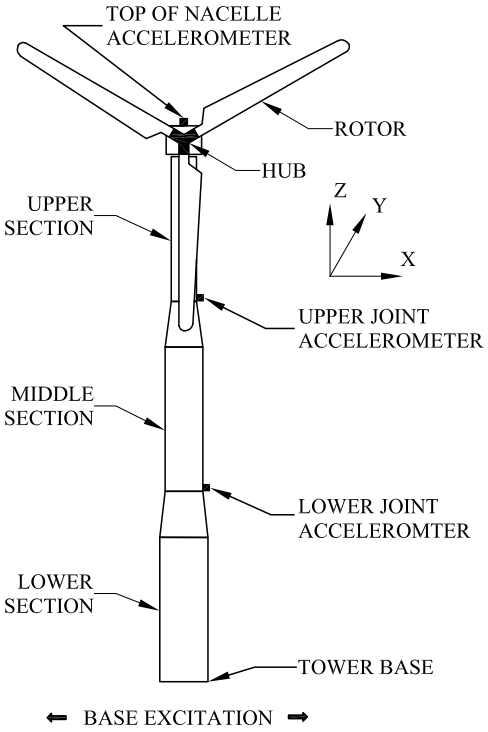

Figure 2.1: Wind turbine configuration and location of accelerometers

Figure 2.2: Wind turbine mounted on the outdoor UCSD shake table

installed throughout California (Figure 2.3).

These early turbines are often employed beyond the original design life, with retired machines frequently sold on the secondhand market (Burns, 2009). In comparison to modern Megawatt-level machines, the tested unit is relatively small, but represents the canonical configuration (Figure 2.1) of a tubular steel tower topped with a nacelle that actively yaws to orient the rotor into the wind. A summary of the pertinent engineering properties of the test turbine is presented in Table 2.1.

2.2.2 Shake Table Facility

The Large High Performance Outdoor Shake Table (LHPOST) (Restrepo et al., 2005) was built to impart uni-axial horizontal excitation, with a platform of 7.6

Figure 2.3: Field installation at Oak Creek Energy Systems in Tehachapi, California, USA

Table 2.1: Properties of the 65-kW wind turbine

Property	Value
Rated power	65-kW
Rated wind speed	43 km/H (21 MPH)
Rotor diameter	16 m (628 inches)
Tower height	21.9 m (864 inches)
Lower section length	8.0 m (313 inches)
Lower section diameter	2.0 m (79.5 inches)
Middle section length	7.9 m (312 inches)
Middle section diameter	1.6 m (62.1 inches)
Top section length	6.0 m (238 inches)
Top section diameter	1.2 m (47.2 inches)
Tower wall thickness	6.0 mm (0.21 inches)
Rotor hub height	22.6 m (888 inches)
Tower mass	6400 kg (14.1 kips)
Nacelle mass	2400 kg (5.2 kips)
Rotor mass (with hub)	1860 kg (4.1 kips)

m by 12.2 m in size (Figure 2.2) and a stroke of ±0.75 m. Salient features include a peak horizontal velocity of 1.8 m/s, a horizontal force capacity of 6.8 MN, and a vertical peak payload capacity of 20 MN. The overturning moment capacity is 50 MN-m (for a nominal specimen configuration with mass = 200 metric tons at an effective height of 10 m, and acceleration = 2.5 g). Motions containing frequencies up to 33 Hz can be simulated. These characteristics make the LHPOST the largest seismic shake table worldwide in terms of load capacity and the first outdoor facility of its kind. The LHPOST is a significant U.S. testing facility, with no overhead space and lifting constraints, essential considerations for full-scale wind turbine experimentation.

2.2.3 Experimental Test Program

For all test motions, the rotor was parked with one blade oriented downward, parallel to the tower (Figure 2.2). The uni-axial horizontal base motion was imparted in the side-to-side direction of the turbine, perpendicular to the rotor's axis of rotation (Figure 2.2). To capture this side-to-side response, uni-axial DC-coupled accelerometers were installed as indicated in Figure 2.1. One accelerometer was located on top of the shake table. Four others were located on the tower, at the base, the lower joint, the upper joint, and at the top of the nacelle (Figure 2.1).

Excitation for the tests was derived from the east-west component (0.15 g PGA) of the June 28th, 1992 strike-slip Landers Earthquake (moment magnitude $M_w = 7.3$) recorded at Desert Hot Springs (DHS). DHS is a California Strong Motion Instrumentation Program station situated on deep alluvium, 23 km from the fault trace of the Landers Earthquake. With a shear wave velocity profile to a depth of 30

m (V_{s30}) of 345 m/s (CSMIP, 2006), the ground profile is classified as stiff soil, site class D (ASCE, 2005).

To remove any superfluous DC offset as well as high frequency noise, the original earthquake record was filtered with a pass band of 0.05 to 25 Hz. The record was then scaled to approximately 100%, 150%, and 200% of the original amplitude for the tests. Figures 2.4 and 2.5 present the recorded data for the 100% and 200% level tests, respectively. Additional events are reproduced in Appendix A. The above experimentation program constitutes the first full-scale base excitation test of a wind turbine and to date is the tallest structure tested on a shake table.

2.2.4 Experimentally Observed Modal Properties

Natural frequencies and mode shapes were extracted from the experimentally observed data. As mentioned earlier, the deployed accelerometers (Figure 2.1) only record the side-to-side component (in the direction of base shaking) of dynamic response. Figure 2.6 shows the estimates of the frequency response of the transfer function (base to top of the nacelle) calculated using Welch's averaged periodogram method (Welch, 1967) from the recorded acceleration for each of the base shaking tests. The results show good agreement (Figures 2.6 and 2.7) with a consistent first natural frequency of about 1.7 Hz (T = 0.6 s), indicating an essentially linear response. A band of higher resonance appears around 11.7 to 12.3 Hz (T = 0.08 to 0.09 s), with agreement between the tests appearing to be somewhat lower (Figure 2.6).

For each accelerometer location (Figure 2.1), an average of the amplitude and phase of the estimate of the frequency response of the transfer function was used to

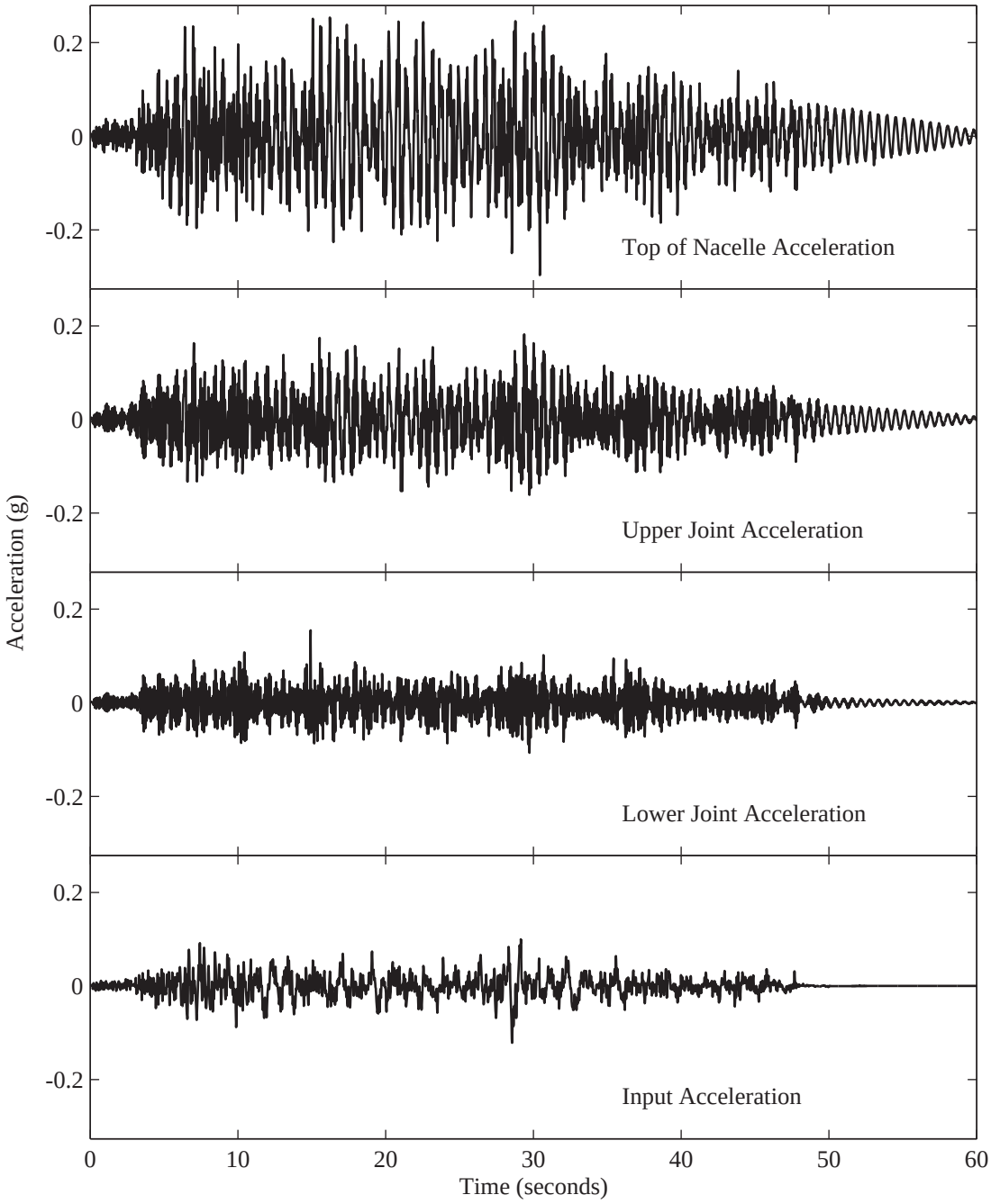

Figure 2.4: Recorded acceleration for Landers 100% level test

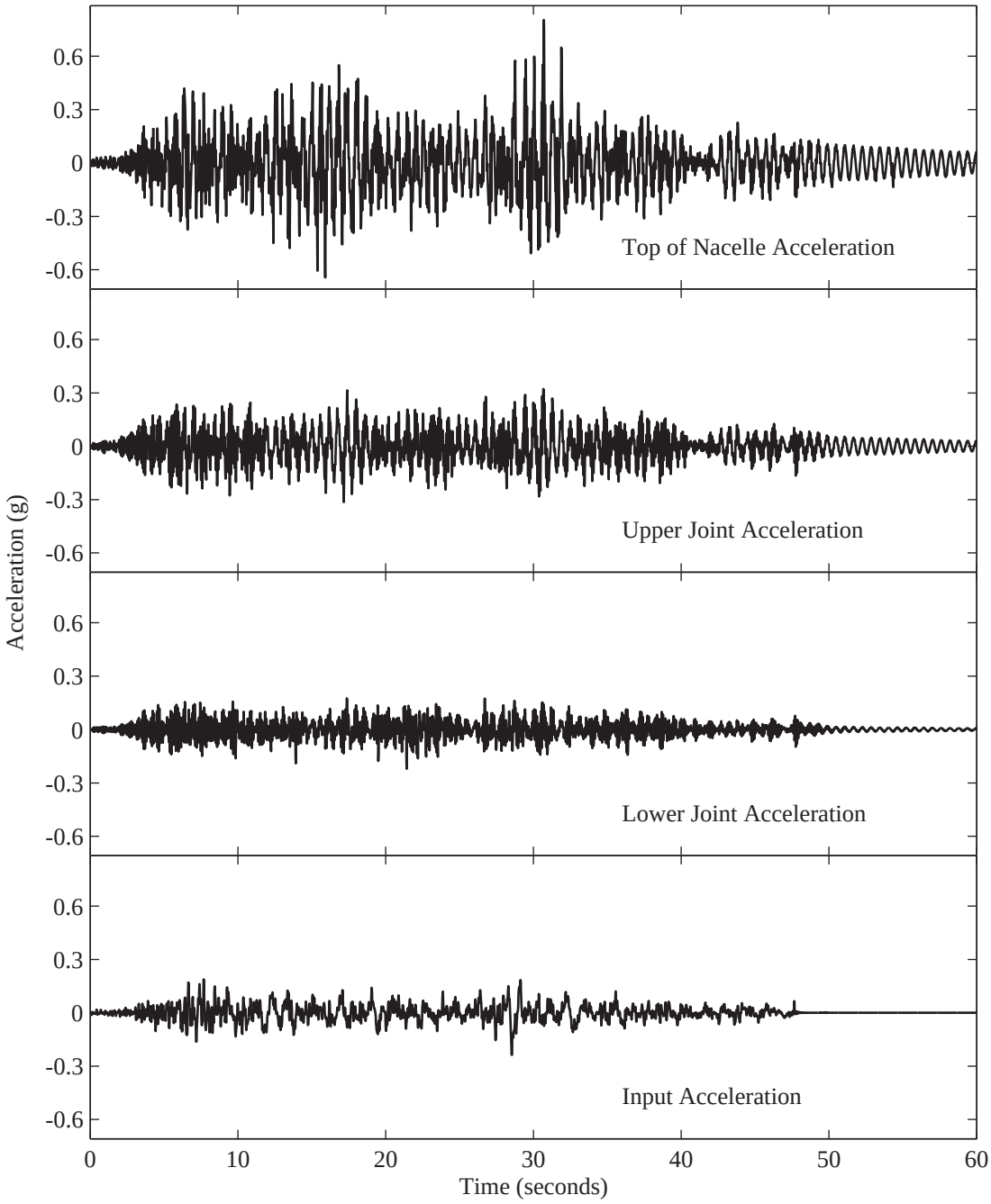

Figure 2.5: Recorded acceleration for Landers 200% level test

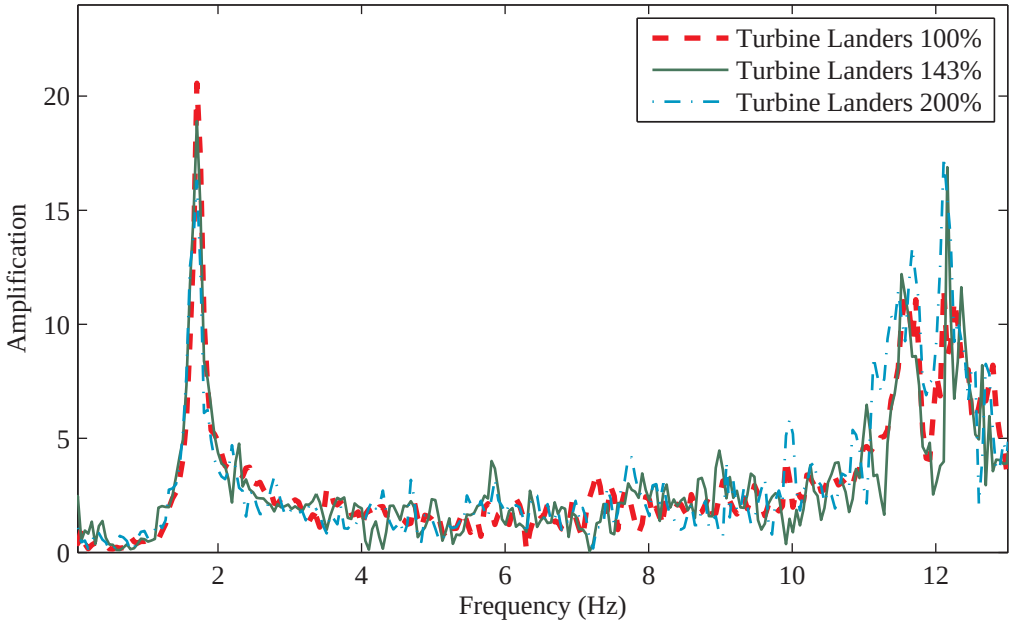

Figure 2.6: Estimates of the frequency response of the transfer function

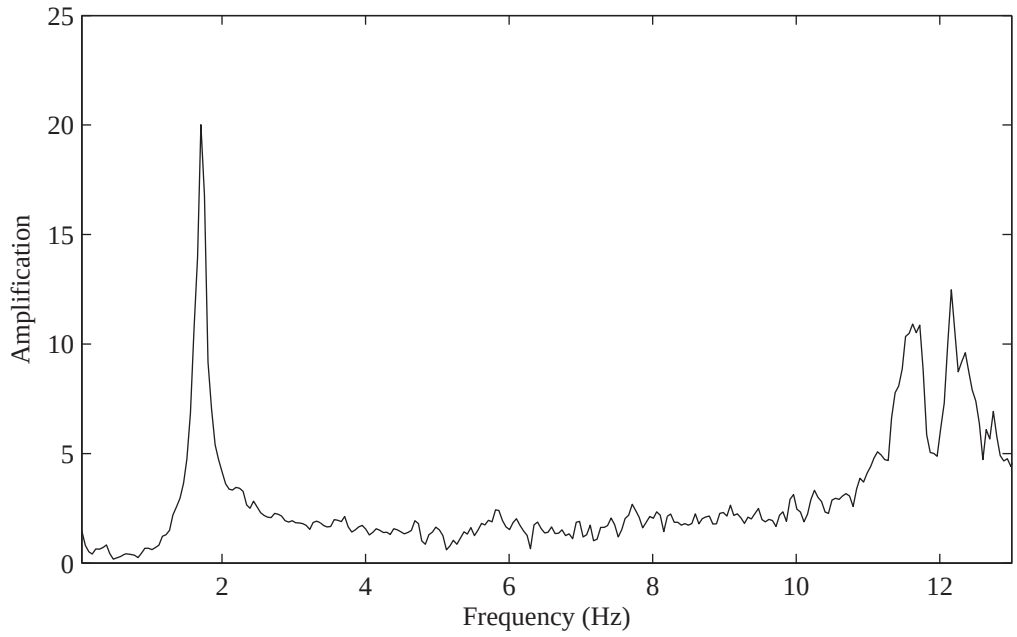

Figure 2.7: Average of the frequency response of the transfer function estimates

construct mode shapes at the observed resonances. The fundamental mode shape (Figure 2.8(a)) and that of a higher mode (Figure 2.8(b)) are seen to resemble the bending modes of a cantilever beam with a point mass (Laura et al., 1974).

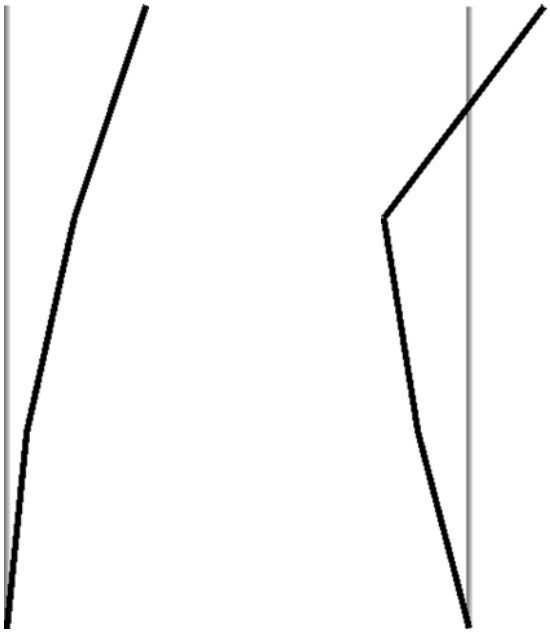

(a) 1.7 Hz (b) 11.7 - 12.3 Hz

Figure 2.8: Experimentally observed side-to-side modes

Equivalent viscous damping during dynamic excitation is also a property of interest. Using the recorded time histories, the log decrement method (Chopra, 2006) was used to estimate damping at the first natural frequency. After the shaking phase, the higher resonances quickly decay, resulting in an essentially first mode free vibration response (48 to 60 s in Figures 2.4 and 2.5).

On this basis, damping was estimated to be less than 1 percent (Table 2.2) at the first natural frequency. With quiescent winds and a parked rotor, damping within the turbine structure has likely dominated these observed low values (Table 2.2). It should be noted that in-situ values may in certain cases be higher, due to

considerations such as energy radiation through the foundation (Kramer, 1996) and aeroelastic damping in both horizontal directions for an operating turbine (Riziotis et al., 2004).

Table 2.2: Observed damping for Landers motion (log decrement method)

Approximate scaling	Average damping
100%	0.86%
150%	0.43%
200%	0.41%

2.3 Finite Element Modeling

Earlier results suggest that a beam-column model provides results that are consistent with more detailed shell models for towers (Bazeos et al., 2002) as well as turbine blades (Malcolm and Laird, 2003). On this basis, two simple FE models were studied herein. The first (Model I) consisted of a cantilever beam with distributed tower mass and an additional lumped mass at the top to represent the nacelle and rotor (Bazeos et al., 2002; Lavassas et al., 2003). The second (Model II), explicitly represented the turbines geometric configuration and mass distribution by adding beam-column elements to emulate the nacelle and the rotor (Witcher, 2005; Häenler et al., 2006). Currently, these simple modeling configurations correspond to the two main approaches for simulation of seismic loading on wind turbines.

The above FE models were implemented using the open source computational platform OpenSees (Mazzoni et al., 2006). In both cases, the tower (Figure 2.1) was divided into 30 beam-column elements with a flexural stiffness based on the cross

section at the center of each element. Model II was developed with 12 beam-column elements per blade to represent the mass and stiffness of the rotor (Figure 2.1 and Figure 2.2). A hinge condition was added to allow for the free rotation of the rotor. Finer meshes for the tower and blade were investigated, but the results were not significantly impacted by such refinement. The blade mass and stiffness distribution was approximated by scaling reported values for a similar unit (Jonkman and Buhl Jr., 2005) to match the Nordtank blade geometry. Unlike the tower where bending stiffness at the base is only 8 times that of the upper section, the blade is over 3,000 times stiffer at the root compared to the tip.

2.4 Finite Element Modal Properties

Based on the engineering properties (Table 2.1) and Youngs Modulus for steel = 200 GPa, Model I (bending beam with a point mass) closely matched the experimentally observed first natural frequency (1.7 Hz) and mode shape (Figure 2.9(a)). The second cantilever type mode occurred at 11.8 Hz, in the neighborhood of the higher experimentally observed resonance (Figure 2.9(b)). At a much higher frequency (34.1 Hz), a third bending mode was predicted (Figure 2.9(c)).

Model II with the explicit rotor representation also matched the first natural frequency and mode shape (Figure 2.10). Due to the involved rotor eccentricity, Model II showed an additional fore-aft bending mode parallel to the rotors axis rotation at 1.7 Hz (Figure 2.11) and a first torsional mode at 9.2 Hz (Figure 2.12). The next mode, a second cantilever type fore-aft mode, was observed at 9.7 Hz (Figure 2.13). A

(a) 1.7 Hz (b) 11.8 Hz (c) 34.1 Hz

Figure 2.9: Model I OpenSees side-to-side modes

second cantilever type side-to-side mode was then observed at 12.1 Hz (Figure 2.14), within the range of the higher observed resonance. The third fore-aft bending mode in Model II was predicted at 21.5 Hz (Figure 2.15), which is a much lower frequency than the prediction for Model I.

As such, both models showed reasonable results for the first and second observed side-to-side bending modes. This reasonable agreement reinforces earlier observations as to the viability of simple models for predicting seismic response (for the tested turbine). While outside the range of seismic excitation, Models I and II predicted significantly different resonant frequencies for the third tower bending mode (Figures 2.9(c) and 2.15). For modern large turbines, such higher bending modes may well fall within the seismic range of interest (Häenler et al., 2006), possibly highlighting the need for further modeling refinements.

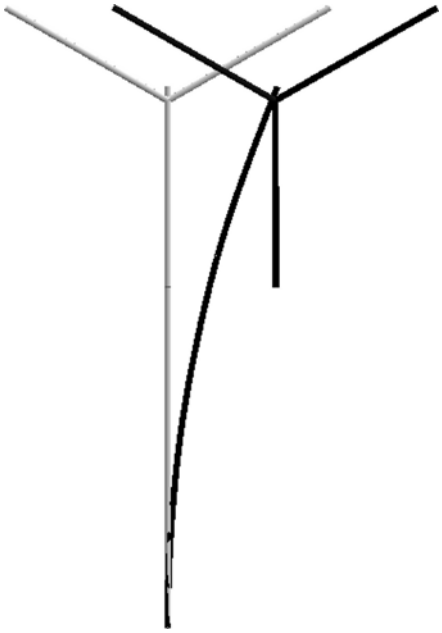

Figure 2.10: OpenSees Model II 1st side-to-side mode (1.7 Hz)

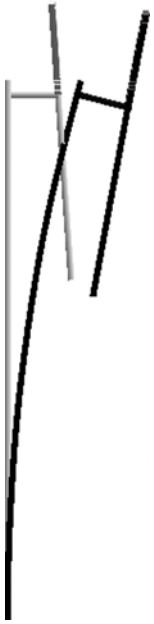

Figure 2.11: OpenSees Model II 1st fore-aft mode (1.7 Hz)

2.5 Numerical Simulation of Recorded Response

Model II with the explicit rotor representation, was used to conduct dynamic base excitation simulations. Based on the recorded response and industry guidelines (IEC, 2005), damping was set to 1% for the first mode. At the higher resonance band (near 12 Hz), a value of 3.5% was needed for a better match with the recorded response (specified in the form of Rayleigh damping). Figures 2.16 and 2.17 show a comparison of the recorded and simulated time histories (100% and 200%, respectively) for the calibrated model. Further comparisons are contained in A. This reasonable agreement between observed and computed response, was found to hold for any first mode damping within the experimentally observed range of approximately 0.5 to 1.0% (Table 2.2).

Figure 2.12: OpenSees Model II 1st torsional mode (9.2 Hz)

Figure 2.13: OpenSees Model II 2nd fore-aft mode (9.7 Hz)

2.6 Numerical Modeling of Seismic Response

After calibration, Model II simulations were conducted using a set of ground motions from California earthquakes (Table 2.3). These motions were all recorded at ground level in relatively stiff structures (one or two story buildings). For reference, an IBC design spectrum (ICC 2006) for Desert Hot Springs (DHS), a location near the White Water Wind Farm in Palm Springs, California, is seen to be an envelope around the selected motion spectra (Figure 2.18).

Table 2.3: Earthquake data

Earthquake	Moment Mag. (M_w)	Station	PGA (g)
1940 El Centro 180°	6.9	Array Station 9	0.35
1979 Coyote Lake 230°	5.7	Gilroy Array Station 6	0.42
1981 Westmorland 180°	5.9	Fire Station	0.50
1986 Palm Springs 0°	6.2	New Fire Station	0.33
2000 Yountville 90°	5.0	Fire Station No. 3	0.41

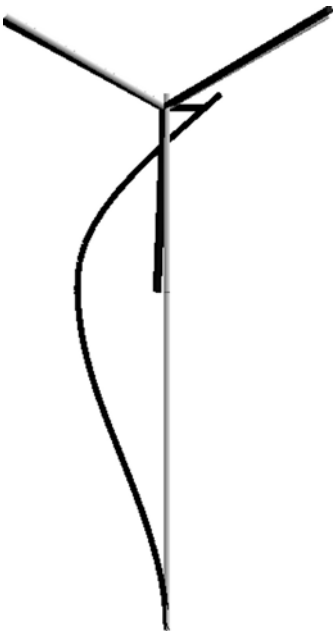

Figure 2.14: OpenSees Model II 2nd side-to-side mode (12.1 Hz)

Figure 2.15: OpenSees Model II 3rd fore-aft mode (21.5 Hz)

As in the shake table test, excitation was imparted laterally (side-to-side). In light of certification guidelines (GL, 2003; IEC, 2005) and the observed behavior, linear response was studied without consideration of potential shell buckling or other nonlinear phenomena (which should be carefully analyzed if deemed necessary).

Influence of damping on seismic response was investigated. For that purpose, base excitation (Figure 2.19) was simulated using 0.5% (Bazeos et al., 2002), 1% (IEC, 2005), 2% (Agbayani, 2002), and 5% (ICC, 2006) of critical damping at the first resonance. At the higher resonance range damping was kept constant at 3.5%. As seen in Table 2.4, damping was of relatively little influence on peak acceleration in most cases. In contrast, the Palm Springs record showed a difference of about 100%. Figure 2.19 shows a comparison of the acceleration time histories at the top of the nacelle for the 0.5% and 5.0% damped scenarios. A clear difference may be seen

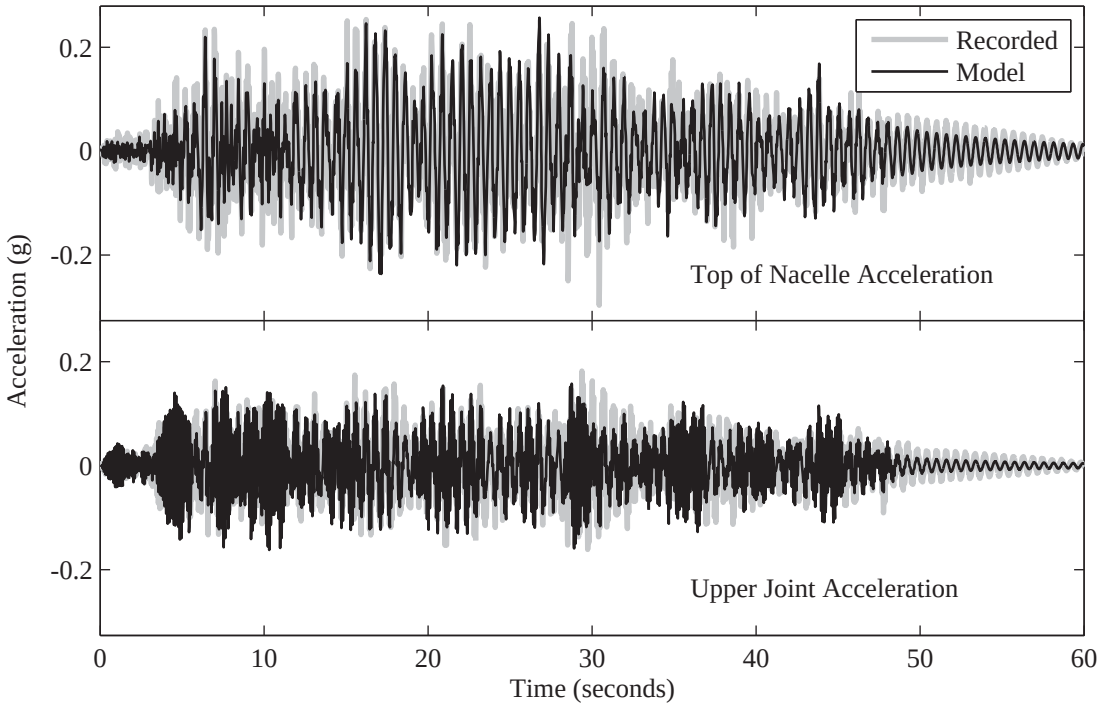

Figure 2.16: Model II acceleration for Landers 100% level simulation (see Figure 2.4 on page 39 for presentation of recorded data alone)

(Figure 2.19) in terms of the especially long duration of cyclic response for the 0.5% damping case (following the earthquake strong shaking phase).

Table 2.4: Peak response at top of nacelle for different damping levels

Earthquake	Response at Top of Nacelle (g)			
	5%	2%	1%	0.5%
1940 El Centro 180°	1.2	1.4	1.4	1.5
1979 Coyote Lake 230°	1.1	1.1	1.2	1.2
1986 Palm Springs 0°	0.8	1.1	1.3	1.6
2000 Yountville 90°	1.4	1.5	1.6	1.6

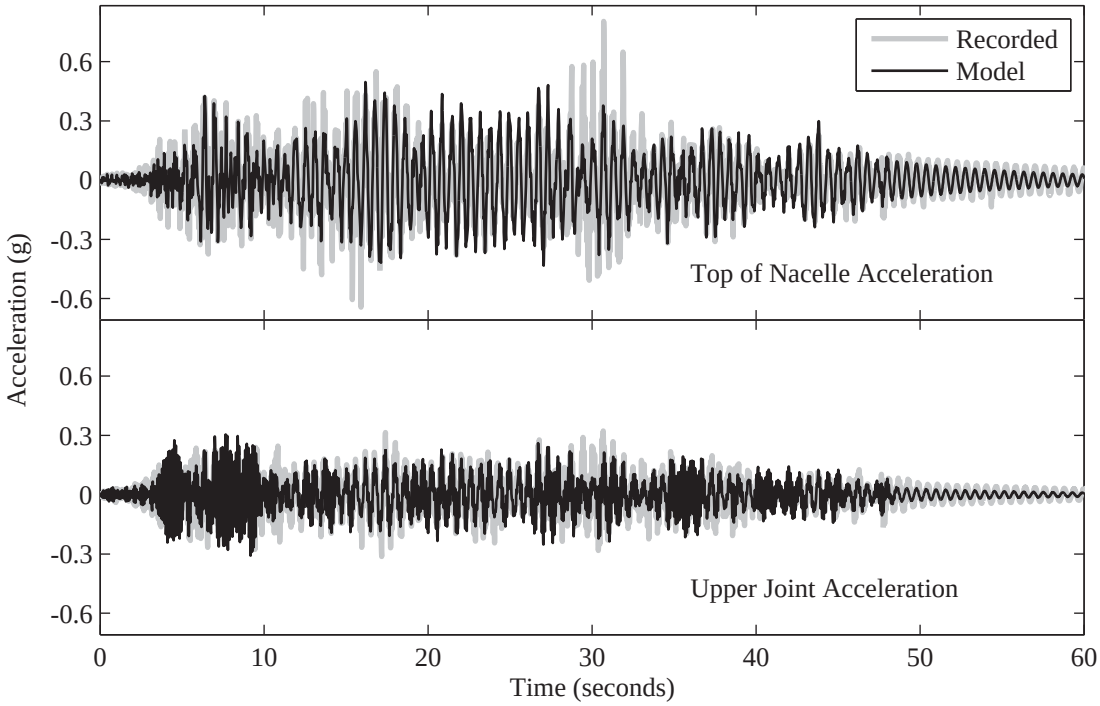

Figure 2.17: Model II acceleration for Landers 200% level simulation (see Figure 2.5 on page 40 for presentation of recorded data alone)

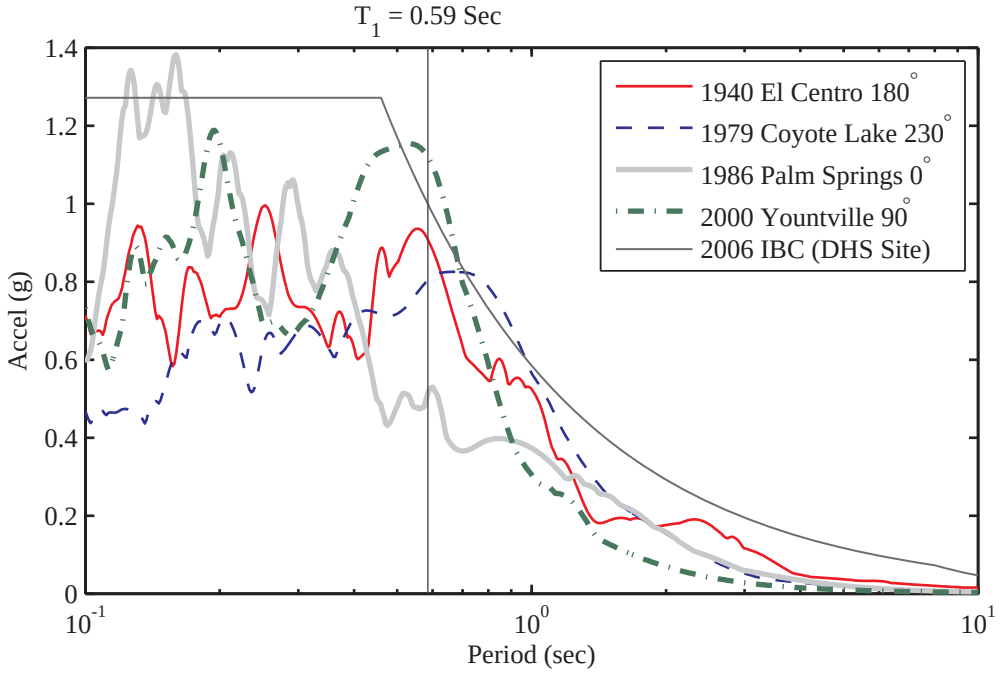

Figure 2.18: Comparison of 2006 IBC design spectrum to 5% damped elastic response spectrum at DHS (T_1 is the first natural period of the turbine)

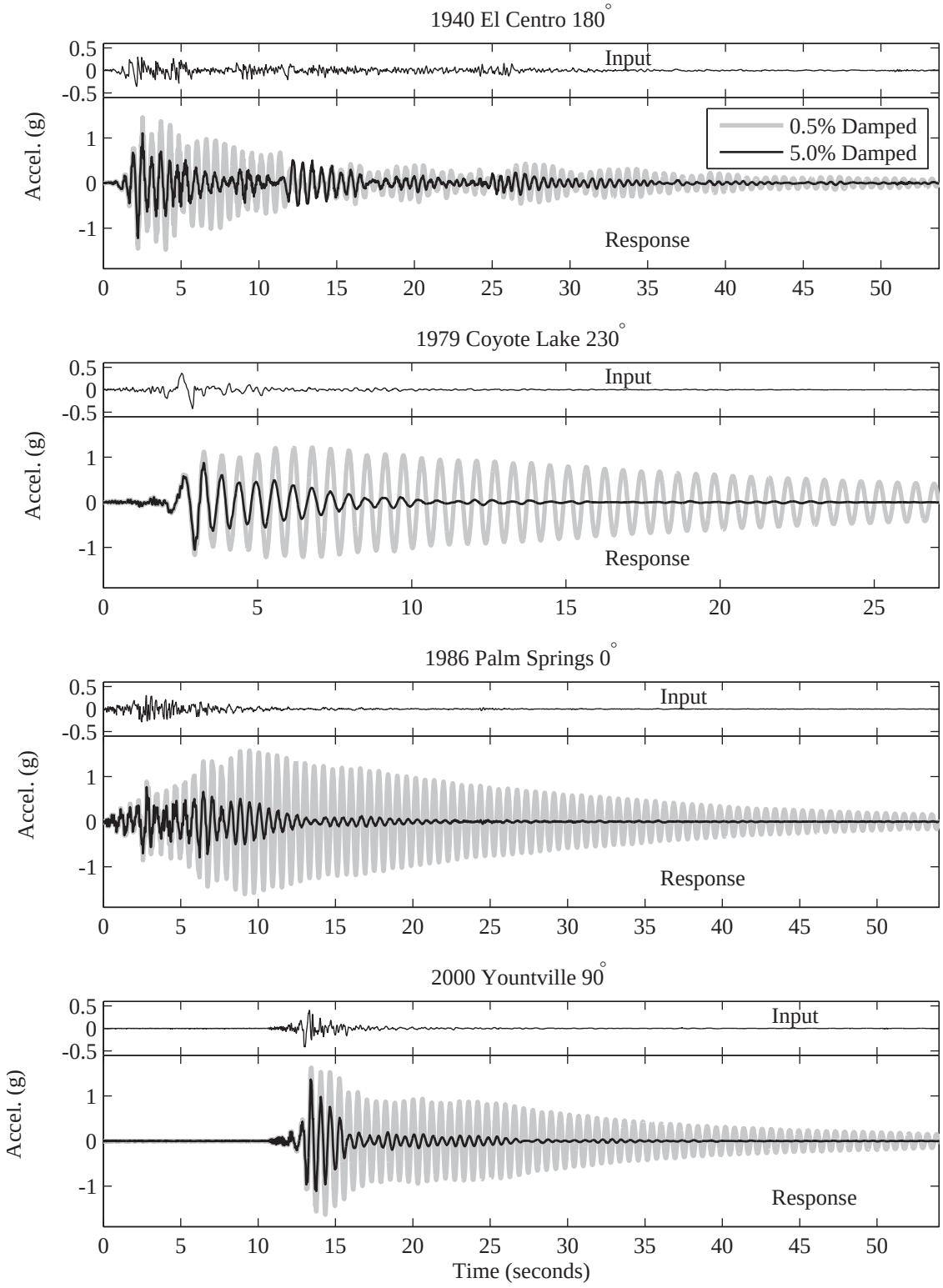

Figure 2.19: Input time history of ground motions and response at top of nacelle

2.7 First Mode and Response Spectrum Seismic Response

Using modal analysis (Chopra, 2006), the following single-degree-of-freedom solution describes the turbines first mode seismic response:

$$u = \phi_1 q_1 \tag{2.1}$$

$$\ddot{q}_1 + 2\zeta_1\omega_1\dot{q}_1 + \omega_2^2 q_1 = -\beta_1\ddot{u}_g \tag{2.2}$$

where u is the turbine displacement relative to the ground, the 1 subscript denotes first mode response, ϕ the mode shape, q the generalized coordinate, ω the resonant frequency in radians/second, ζ the viscous damping ratio, β the modal participation factor, and $\ddot{u}_g$ is time history of the input seismic base acceleration.

With the parameters derived from Model II, the above equations were used to compute the turbines seismic response to the input earthquake records of Table 2.4. In all cases, the results were quite close to those reported earlier using the FE beam-column Model II (Figure 2.19). As such, the turbines response at the nacelle level may be conveniently calculated using equations 2.1 and 2.2, where $\beta_1 = 1.2$ for a normalized modal value of 1.0 at this location. For units similar to the tested turbine, this simple approach may prove useful, in conjunction with the existing tools for estimation of wind turbine mode shapes (Bir, 2005).

Alternatively, an estimate of peak acceleration, a_{max}, at the nacelle may be

obtained from the response spectrum of an earthquake record, that being equal to $1.2S_a$ (where S_a is pseudo spectral acceleration at the fundamental period). The maximum moment may be estimated (Annex C of IEC, 2005) as $M_{max} = h_t \cdot a_{max} \cdot m_{eff}$ where m_{eff}, the effective mass, is equal to the mass of rotor, nacelle, and 1/2 the tower and h_t is the tower height. The moment at any height, h, along the tower can be approximated as $M(h) = (h_t - h) \cdot a_{max} m_{eff}$ assuming linear variation. This implies a constant shear of $a_{max} \cdot m_{eff}$ throughout the tower.

2.8 Discussion of Results

The experimental and numerical results presented above suggest the following observations:

1. For estimating the fundamental period, both employed FE models resulted in reliable predictions. Using the hub height plus 2/3 of the blade length, the 2006 IBC code estimate (see Appendix B) closely agrees with both models and observation.

2. For units similar to the tested turbine, the results show seismic response to be governed primarily by the first mode. For such systems, a Rayleigh-Ritz approach based on the first mode shape yields a satisfactorily estimate of the system response.

3. Agreement between observations and numerical prediction was somewhat lower for the high frequency second side-to-side bending mode (around 10 Hz). How-

ever, as discussed earlier, this issue had no appreciable impact on the conducted simulation results.

4. Seismic excitation records with especially high frequency content, may provoke higher mode behavior for the tested 65-kW turbine (e.g., the 1988 Saguenay earthquake record; (Somerville et al., 1990)). For the new taller turbines, such higher modes will fall in the more typical frequency range of interest for earthquake loading (Häenler et al., 2006). Similar to most ground motion records in California, the employed test motion was relatively poor in high frequency energy. Future tests should be designed to include complementary shaking scenarios with low and high frequency content.

5. Model II showed an offset in frequency between the second bending modes in the two horizontal directions as predicted earlier by Zhao et al. (2007). Further tests with a denser configuration of multi-axial accelerometers are needed to more comprehensively document this type of higher frequency behavior.

6. Free vibration results show that a low level of damping (less than 1%) is not over conservative for modeling at the first natural frequency. This level is appropriate for the tested parked turbine scenario. Depending on the underlying ground properties, SSI may increase overall damping due to energy radiation (Kramer, 1996). In addition, effective damping, for an operational turbine may be strongly influenced by wind speed (Riziotis et al., 2004).

2.9 Summary and Conclusions

Experimental results from the first full-scale shake table test of a wind turbine were presented. The salient resonant response characteristics were identified. First mode damping was estimated to be below 1% for the tested parked-turbine configuration. Beam-column computational models were calibrated, and found to be a valuable tool for assessment of seismic response. For small utility scale turbines, a first mode response was shown to provide a reasonable approximation. As such, the response spectrum approach may provide a convenient approach for estimating the seismically induced peak shear force and moment.

For larger modern turbines, higher modes may play a prominent role in the overall seismic response. Higher fidelity modeling may be necessary for such situations (Häenler et al., 2006). Additional experimental data related to damping, and soil structure interaction effects would be also most worthwhile.

2.10 Acknowledgements

The text below is reproduced verbatim as it appears in the acknowledgments section on page xvii per the UCSD Office of Graduate Studies Formatting Requirements.

Chapter 2 of this dissertation is based on material published by the Journal of Earthquake Engineering titled “Experimental and Numerical Seismic Response of a 65 kW Wind Turbine” with authors, Ian Prowell, Mark Veletzos, Ahmed Elgamal, and José Restrepo (2009). The dissertation author is the first author of this paper.

Bibliography

Agbayani, N. A. (2002). "Design challenges in international wind power projects: From foreign codes to computer coding in a small office setting." *71st Annual Structural Engineers Association of California (SEAOC) Convention*, Santa Barbara, California, USA. 117–132.

ASCE (2005). *Minimum Design Loads for Buildings And Other Structures*. American Society of Civil Engineers, New York, New York, USA.

Bazeos, N., Hatzigeorgiou, G. D., Hondros, I. D., Karamaneas, H., Karabalis, D. L., and Beskos, D. E. (2002). "Static, seismic and stability analyses of a prototype wind turbine steel tower." *Engineering Structures*, 24(8), 1015–1025.

Bir, G. S. (2005). "Users guide to bmodes; software for computing rotating beam coupled modes." *Report No. NREL TP-500-38976*, National Renewable Energy Laboratory.

Burns, M. (2009). Personal Communication, Oak Creek Energy Systems, Mojave, California, USA.

Chopra, A. K. (2006). *Dynamics of Structures: Theory and Application to Earthquake Engineering*. Prentice-Hall, Upper Saddle River, New Jersey, USA.

CSMIP (2006). "GR12149.htm: Station selected." accessed on Feb. 4, 2009 at http://www.quake.ca.gov/cisn-edc/GrndResponsePages/GR12149.HTM.

GL (2003). *Guidelines for the Certification of Wind Turbines*. Germanischer Lloyd, Hamburg, Germany.

Häenler, M., Ritschel, U., and Warnke, I. (2006). "Systematic modelling of wind turbine dynamics and earthquake loads on wind turbines." *European Wind Energy Conference and Exhibition*, Athens, Greece. European Wind Energy Association, 1–6.

Hau, E. (2006). *Wind Turbines*. Springer, Berlin, Germany.

ICC (2006). *International Building Code 2006*. International Code Council, Country Club Hills, Illinois, USA.

IEC (2005). *IEC 61400-1 Ed. 3: Wind Turbines - Part 1: Design Requirements*. International Electrotechnical Commission, Geneva, Switzerland.

Jonkman, J. M. and Buhl Jr., M. L. (2005). "FAST user's guide." *Report No. NREL/EL-500-38230*, National Renewable Energy Laboratory.

Kramer, S. L. (1996). *Geotechnical Earthquake Engineering*. Prentice-Hall, Upper Saddle River, New Jersey, USA.

Laura, P. A. A., Pombo, J. L., and Susemihl, E. A. (1974). "A note on the vibrations of a clamped-free beam with a mass at the free end." *Journal of Sound and Vibration*, 37(2), 161–168.

Lavassas, I., Nikolaidis, G., Zervas, P., Efthimiou, E., Doudoumis, I. N., and Baniotopoulos, C. C. (2003). "Analysis and design of the prototype of a steel 1-MW wind turbine tower." *Engineering Structures*, 25(8), 1097–1106.

Malcolm, D. J. and Laird, D. L. (2003). "Modeling of blades as equivalent beams for aeroelastic analysis." *2003 ASME Wind Energy Symposium AIAA/ASME*, Reno, Nevada, USA. 293–303.

Mazzoni, S., McKenna, F., and Fenves, G. L. (2006). *Open System for Earthquake Engineering Simulation User Manual*. Pacific Earthquake Engineering Research Center, Berkeley, California, USA.

Restrepo, J. I., Conte, J. P., Luco, J. E., Seible, F., and Van Den Einde, L. (2005). "The NEES@UCSD large high performance outdoor shake table earthquake engineering and soil dynamics (gsp 133)." *Proc. Geo-Frontiers 2005, Sessions of the Geo-Frontiers 2005 Congress*, R. W. Boulanger, M. Dewoolker, N. Gucunski, C. H. Juang, M. E. Kalinski, S. L. Kramer, M. Manzari, and J. Pauschke, eds., Austin, Texas, USA.

Riziotis, V. A., Voutsinas, S. G., Politis, E. S., and Chaviaropoulos, P. K. (2004). "Aeroelastic stability of wind turbines: the problem, the methods and the issues." *Wind Energy*, 7(4), 373–392.

Somerville, P. G., McLaren, J. P., Saikia, C. K., and Helmberger, D. V. (1990). "The 25 november 1988 saguenay, quebec, earthquake: Source parameters and the attenuation of strong ground motion." *Bulletin of the Seismological Society of America*, 8(5), 1118–1143.

Welch, P. (1967). "The use of fast Fourier transform for the estimation of power spectra: a method based on time averaging over short, modified periodograms." *IEEE transactions on audio and electroacoustics*, 15(2), 70–73.

Witcher, D. (2005). "Seismic analysis of wind turbines in the time domain." *Wind Energy*, 8(1), 81–91.

Zhao, X., Maißer, P., and Jingyan, W. (2007). "A new multibody modeling methodology for wind turbine structures using a cardanic joint beam element." *Renewable Energy*, 32(3), 532–546.

Chapter 3

Expanded Full-Scale Shake Table Test

3.1 Introduction

Encouraged by the successful shake table testing of a full-size utility-scale wind turbine, a second testing phase was planned and executed at UCSD in 2010 (as part of this dissertation). The earlier experimental results provided a basis and the investigation were expanded to include the relative orientation of the rotor and earthquake loads, level of shaking, parked and operational states, and higher resolution characterization of structural response. Dense instrumentation was deployed to measure in-plane and out-of-plane response of the turbine tower.

Shaking was imparted both parallel (configuration 1, Figure 3.1(a)) and perpendicular (configuration 2, Figure 3.1(b)) to the axis of rotation of the rotor. Following extensive low level tests in both configurations, a final series of progressively

stronger simulated earthquake tests were performed in configuration 1 in an attempt to evaluate the damage limit states. Between every earthquake test run, a baseline motion consisting of band limited white noise motion (0.25 to 25 Hz) with a root mean square (RMS) amplitude of 0.05 g was imparted to provide a controlled excitation to infer natural frequencies, mode shapes, and equivalent viscous damping.

(a) Configuration 1 (b) Configuration 2

Figure 3.1: Wind turbine on the LHPOST (arrows indicate direction of shaking)

The test preparation and pertinent associated details are presented herein. Enabled by more extensive instrumentation, improved characterization of dynamic properties including clarification of higher modes is documented. The results of the test regimen for the parked configuration are analyzed to evaluate; (a) the observed dynamic characteristics, (b) the implications of orientation and intensity of shaking, (c) the effectiveness of spectral acceleration as an indicator of maximum displacement

demand, (d) the relation between displacement and shear demand at various levels of shaking, and (e) the sources of reduction in system stiffness. Overall trends and important results are discussed with consideration of modern turbine configurations.

3.2 Testing Program

3.2.1 Description of Test Wind Turbine

Having sustained no identifiable damage from earlier testing, the previously used 65-kW turbine, donated by Oak Creek Energy Systems of Mojave, California, was employed as a representative turbine for testing (Figure 3.1). The tested 65-kW turbine was manufactured in Denmark by Nordtank. In the early 1980s, this Nordtank turbine and its contemporaries were installed in large numbers for utility scale power generation in California. By 1985, Danish machines accounted for approximately 40% of the turbines installed throughout California (Hau, 2006). A 65-kW turbine is near the lowest power rating used in 1980s era utility scale wind farms. Though no longer desirable for utility scale applications, this size unit is still appropriate for distributed power applications. In comparison to modern megawatt-level machines, the tested unit is relatively small, but represents the canonical configuration of a tubular steel tower topped with a nacelle that actively yaws to orient the rotor into the wind (Figure 3.2).

In this test, the turbine tower is the primary structural system under investigation. The tower consists of three discrete hollow cylindrical sections that are constructed by welding large 6-mm thick metal plates curved to the desired diameter.

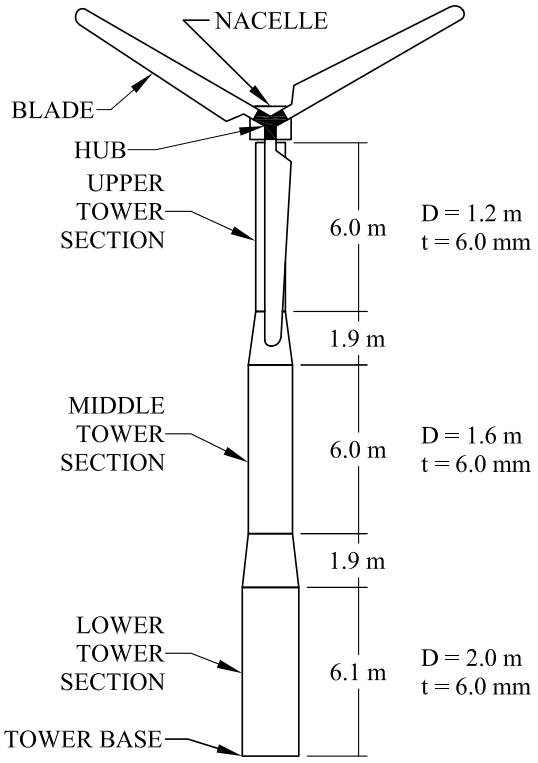

Figure 3.2: Wind turbine configuration (D indicates tower outside diameter and t represents tower wall thickness)

Following welding, the tower sections are hot dip galvanized to prevent corrosion. The outside diameter of each successive piece of the tower is reduced in relation to the bending demand, to use material efficiently. The transition in diameter is accommodated by 1.9-m long tapered segments in the lower two sections. Each section is joined by securely bolting steel flanges, welded to the ends of each tower section. Bolt size and torque details for joining each sub component of the turbine are shown in Table 3.1. Coupon tests showed that the steel possessed a yield stress of 270 GPa and an ultimate stress of 350 GPa. Based on response in the linear range of the coupon tests, the Young's Modulus of the steel was 191,000 GPa. As a slender tubular structure, with a diameter thickness ratio ranging from approximately 200 to 333, the ultimate

moment capacity of 3,200 kN-m is governed by local buckling according to the AISC Specification (AISC, 2005). A summary of other pertinent engineering properties of the tested turbine was presented earlier in Table 2.1.

Table 3.1: Bolt specifications for connections

Connection	Bolts		Torque
	Size	Number	(N-m)
Blade/rotor flange connection	M20 × 130*	3 × 24+	400
Nacelle/tower, main bearing	M12 × 35*	22	110
Tower flange connection, top section	M20 × 80*	30	400
Tower flange connection, bottom section	M24 × 90*	30	700
Tower base flange nuts	M30*	30	1200

*First number indicates bolt diameter and second number indicates bolt length in millimeters
+3 sets of 24 bolts per blade

3.3 Test Preparation

Pre test modeling was conducted with guidance from previous results (Prowell et al., 2009b) to provide input to selection of actual table motions, understanding probable structural response, and placement of instrumentation.

3.3.1 Model Description

A FE model, similar to Model II (Prowell et al., 2009b), was developed using SAP2000 (CSI, 2005) to facilitate dynamic simulation of the turbine while parked. The tower (Figure 3.2) was divided into 31 beam-column elements with a flexural stiffness based on the corresponding cross section at the center of each element. Each blade was modeled using 12 beam-column elements to represent the mass and stiffness

of the rotor. The nacelle was modeled with rigid elements to connect the top of the tower to the rotor. The FE model predicted the first side - to - side and fore - aft bending modes at 1.68 Hz, and the second bending modes at 10.8 Hz in the side-to-side direction and 10.9 Hz in the fore aft direction. Previous full-scale shake table tests of this parked 65-kW turbine validated this model, with good agreement between predicted and observed modal properties (Prowell et al., 2009b).

3.3.2 Selection and Scaling of Motions

Earthquake records recommended by FEMA-P695 were considered as input motions for experimental testing (ATC, 2009). Digitized versions of the records utilized are available from the Pacific Earthquake Engineering Research Center (PEER) Strong Motion Database at http://peer.berkeley.edu/smcat/. The library of candidate records consists of 50 events, each with 2 horizontal components. In all, 100 uni-directional ground acceleration records were evaluated.

A design spectrum for a site with high seismic demand, typical of southern California (Figure 3.3), from the International Building Code (IBC) served as a basis for scaling records to ensure shaking levels in the range of interest (ICC, 2006). In the IBC, the Maximum Considered Earthquake (MCE) is set by an event with a 2% probability of exceedance in 50 years (2500 year return period). The 5% damped elastic response spectrum (ERS), to be consistent with the level of damping used by the IBC, was calculated for each of the 100 acceleration time histories and used to derive a scale factor required to match the code spectral value of 1.5 g at a period of 0.59 seconds (frequency of 1.7 Hz), the first period of the turbine (Prowell et al.,

2009b). By scaling in this manner, differences in structural response are driven by motion characteristics other than intensity (first period spectral acceleration).

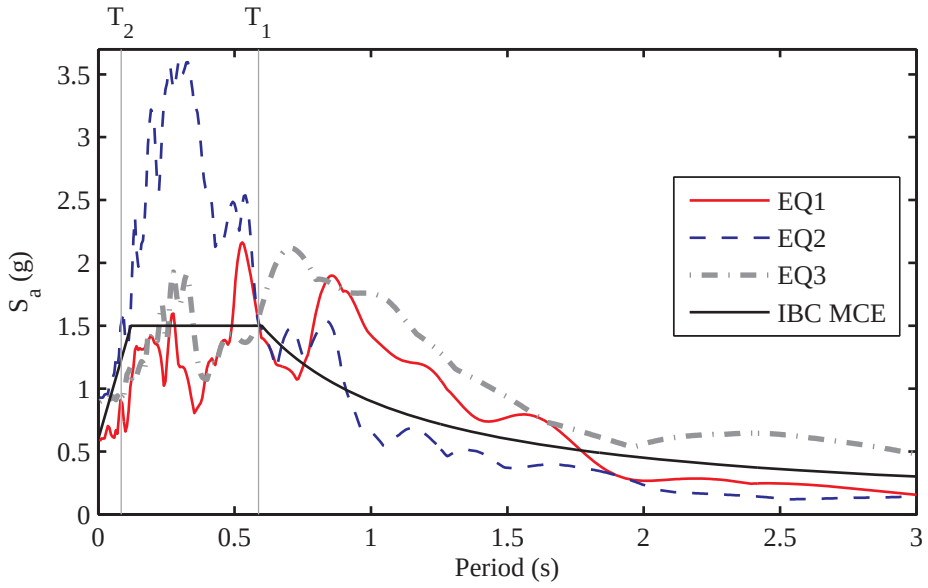

Figure 3.3: 5% damped ERS of scaled motions (Table 3.2) and IBC MCE design spectrum (T_1 and T_2 represent the first and second natural period of the turbine, respectively)

Table 3.2: Selected earthquake ground motion records

ID	Earthquake	Moment Mag (M_w)	Station and Component	Epicentral Distance (km)
EQ1	1994 Northridge	6.7	14145 Mulholland Dr. - 009	13.4
EQ2	1992 Landers	7.3	Coolwater - LN	82.1
EQ3	1979 Imperial Valley	6.5	El Centro Array #7 - 140	27.6

Being a pre-existing structure, the tested turbine was not designed such that the MCE in this test program would have driven the design. Instead, this level was selected to represent a relatively high level of hazard comparable to that expected in wind regions such as Palm Springs, California (Prowell and Veers, 2009). The turbine ultimate loads would likely be controlled by extreme wind conditions as it has a fixed

blade pitch and is designed to survive in winds up to 53.6 m/s.

To allow rational selection of a reduced set of test motions, the response of the turbine was then simulated using the SAP2000 model for all 100 scaled records. Consistent with past findings and certification guidelines (Prowell et al., 2009b; IEC, 2005), an equivalent viscous damping at 1% of critical was considered for all simulations. Candidate motions were evaluated on: duration of shaking, similarity of 5% damped response spectrum to the code design spectrum, amplitude of relative displacement response at the top of the nacelle, and scale factor required to match the code spectrum at the first period of the turbine. Events were first ranked by the amplitude of tower top relative displacement and duration of strong shaking, with a preference toward a smaller scale factor. Events with relatively lower response, short shaking durations, or large scale factors were eliminated. Originally five motions were selected and used in configuration 2 (Figure 3.1(b)). From analysis of the results, it was found that three of the five motions (Figure 3.3) were sufficient to demonstrate the results reported herein. The characteristics of these three motions are presented in Table 3.2. The 5% damped ERS for the motions scaled to the MCE level is compared to the code design spectrum in Figure 3.3. Considering multiple motions allows general trends independent of motion characteristics to be discerned from behavior specific to a particular input.

All motions were scaled for testing such that the spectral acceleration at the first period of the turbine was 25% of the Design Basis Earthquake (DBE) value. In the IBC, the DBE is defined as 2/3 of the MCE (ICC, 2006). This level of shaking was selected so that the response of the turbine could be evaluated for different mo-

tion characteristics, orientations of shaking, and operational states without incurring damage in the tower or other turbine components. Further, EQ1 was scaled to intensities of 50%, 100%, 150%, 200%, and 250% of the DBE level to illustrate the effect of shaking intensity on the turbines structural response. The sequence of reported test runs is shown in the first four columns of Table 3.3. For the parked tests, wind speeds varied but were generally low, approximately 2 to 4 m/s (Prowell et al., 2011b).

Table 3.3: Test sequence (see Table D.1 on page 262 for full test sequence)

Index	Motion	Configuration	State	Level (% of DBE)
1	EQ3	2	Parked	25
2	EQ3	2	Operating	25
3	EQ1	2	Parked	25
4	EQ1	2	Operating	25
5	EQ2	2	Parked	25
6	EQ2	2	Operating	25
7	WN*	2	Operating+	-
8	EQ1	1	Parked	25
9	EQ1	1	Operating	25
10	EQ2	1	Parked	25
11	EQ2	1	Operating	25
12	WN*	1	Operating+	-
13	EQ3	1	Parked	25
14	EQ3	1	Operating	25
15	EQ1	1	Parked	50
16	EQ1	1	Parked	100 (DBE)
17	EQ1	1	Parked	150 (MCE)
18	EQ1	1	Parked	200
19	EQ1	1	Parked	250

*Indicates white noise motion as described in Section 3.1 on page 58
+In addition, a test run with white noise as the input motion in the parked state was conducted between each test

Prior to installation of the turbine on the shake table, standard tuning/training protocol of the shake table was followed for each motion at every desired level of shaking to improve reproduction of the target earthquake motions (Luco et al., 2010).

The obtained table motions with the turbine installed on the shake table platen for EQ1, EQ2, and EQ3 for the 25% DBE level are shown in Figure 3.4. Post-test analysis showed, particularly for the low level tests (25% DBE), that the LHPOST characteristics produced higher than desired response in the 10 to 11 Hz frequency range due to the oil column frequency of the table. For EQ2 and EQ3, the discrepancy resulted in considerably greater excitation in this range compared to that of EQ1. The discrepancy decreased with increasing intensity of shaking, resulting in a better agreement between the desired and realized response spectrum for higher intensity motions.

For reference, pertinent intensity measures for each of the tests are reported in Table 3.4. A measure of the difference between the target and measured table motions with the turbine installed on the table can be obtained from the results listed in Table 3.4. The error between the target and measured values of S_a (f=1.7 Hz and 5% damping) for EQ1 at different levels ranged from -14.3% to -3.5% with an average of -10.7%.

3.4 Turbine Installation

To connect a specimen, the LHPOST platen (Restrepo et al., 2005) has a grid of tie down holes spaced at 0.61 m on center. A 50-mm thick square adapter plate was fabricated with a corresponding hole pattern, which allowed 21 DYWIDAG threadbars (35-mm nominal bar size) to attach the plate to the platen ensuring a rigid connection. To attach the turbine tower base to the adapter plate, thirty 30-mm

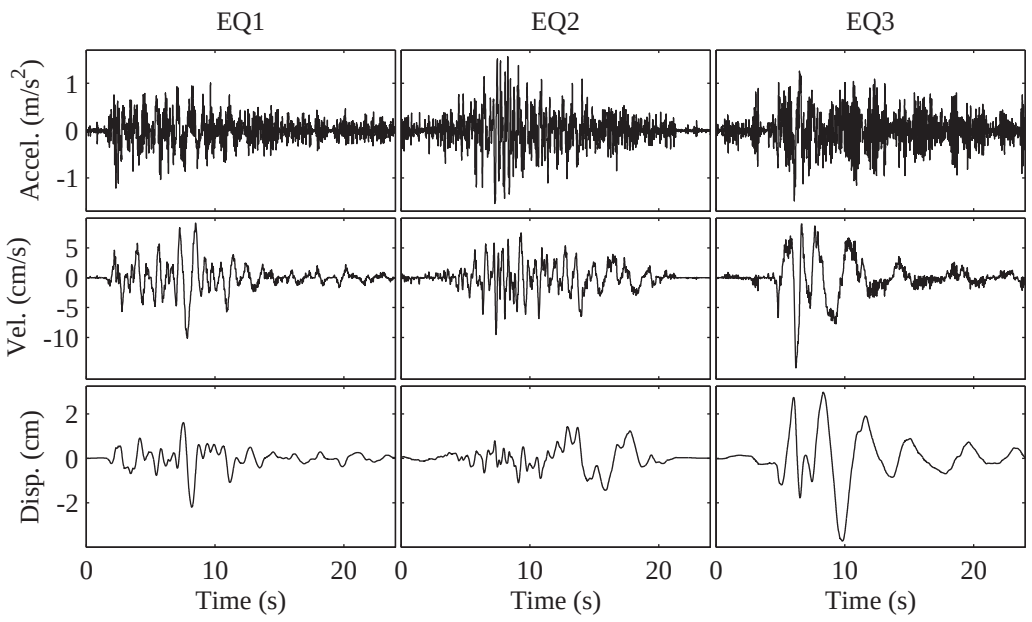

Figure 3.4: Recorded table response for motions scaled to 25% DBE level (From test indices 1 (EQ3), 2 (EQ1), and 3 (EQ3))

diameter threaded studs were welded to the adapter plate to match the hole pattern in the bottom flange of the base tower section. These studs mimic rods used in field installations that would extend into the foundation. The base tower section was installed and leveled approximately 50 mm above the adapter plate with the access door facing east (Figure 3.12). To simulate as - built field conditions and provide full support under the base flange, grout was used to fill the gap between the adapter plate and the tower flange. Figure 3.5 illustrates the connection detail between the tower and the shake table platen. The turbine was assembled and installed by a commercial wind turbine contractor familiar with the 65-kW Nordtank turbines.

Table 3.4: Test intensity measures and wind data (further information on wind speed can be found in Table D.2 on page 264)

Index	PGD	PGV	PGA	S_a at f = 1.7 Hz Damping		Wind Speed	Wind Direction
				1%	5%		
	(cm)	(cm/s)	(m/s^2)	(m/s^2)	(m/s^2)	(m/s)	(deg)
1	3.7	15.1	1.5	2.7	2.2 (2.45)*	2.5	209
2	3.7	14.7	1.4	2.7	2.2 (2.45)*	2.7	195
3	2.2	10.2	1.2	3.7	2.0 (2.45)*	2.4	203
4	2.2	10.4	1.1	3.7	2.0 (2.45)*	2.0	211
5	1.4	9.5	1.6	2.8	2.2 (2.45)*	3.3	262
6	1.5	9.8	1.7	2.8	2.2 (2.45)*	3.1	268
7	-	-	-	-	-	3.8	264
8	2.0	9.5	1.2	4.0	2.1 (2.45)*	3.5	197
9	2.0	9.8	1.3	4.0	2.1 (2.45)*	3.9	198
10	1.5	9.3	1.6	2.8	2.2 (2.45)*	4.5	203
11	1.5	9.8	1.8	2.8	2.2 (2.45)*	4.5	203
12	-	-	-	-	-	4.9	203
13	3.2	15.3	1.8	2.9	2.4 (2.45)*	5.1	207
14	3.2	15.0	1.5	2.9	2.4 (2.45)*	4.5	204
15	4.1	19.4	1.8	8.0	4.2 (4.90)*	3.8	284
16	8.3	36.7	3.6	16.3	8.5 (9.81)*	3.9	265
17	12.4	55.2	5.1	26.6	14.2 (14.71)*	2.0	256
18	16.6	73.2	7.0	33.3	17.6 (19.61)*	2.4	259
19	21.9	96.3	8.9	42.7	22.2 (25.52)*	3.2	255

*Target value

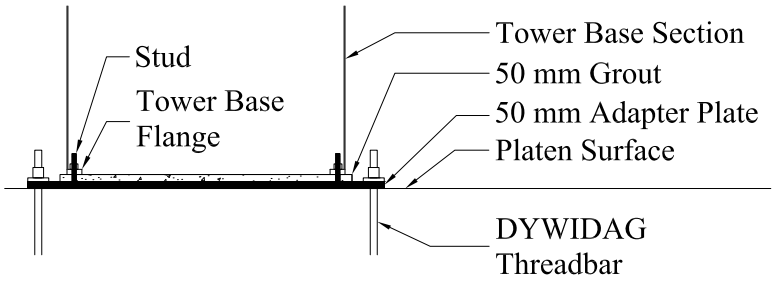

Figure 3.5: Connection detail between tower base and table platen

3.5 Instrumentation

The turbine was instrumented with accelerometers and strain gauges prior to installation on the platen. In all, 59 uni-axial accelerometers (MEAS model 4000A) were installed to monitor vibration response during testing. In the turbine tower, the accelerometers were placed at 14 approximately evenly distributed elevations with an additional level located in the nacelle to provide high spatial resolution with a minimum of 2 accelerometers at each elevation (oriented to capture in-plane and out-of-plane vibration, Figures 3.6 through 3.11). Seven rosette and eight uni-axial strain gauges were installed at 6 elevations (2 elevations per tower section, Figures 3.12 through 3.14). At the tower base, linear variable differential transformers (LVDTs) were used to capture base rocking and sliding relative to the table platen (Figure 3.15). Displacement of the tower was measured through string potentiometers attached from the top of each tower section to a fixed instrumentation tower (Figures 3.16 and 3.17). Prowell et al. (2011b) contains full details regarding instrumentation of the test specimen. All data analyzed here will be publically available on the NEES data archive at http://www.nees.org.

A standard Cartesian coordinate system originating at the center of the tower base was used to describe instrument location and orientation. The X axis was parallel to the direction of shaking with positive values to the east. Normal to the table surface, the Z axis values increased with elevation. Oriented to the north, the Y axis completed a right handed coordinate system.

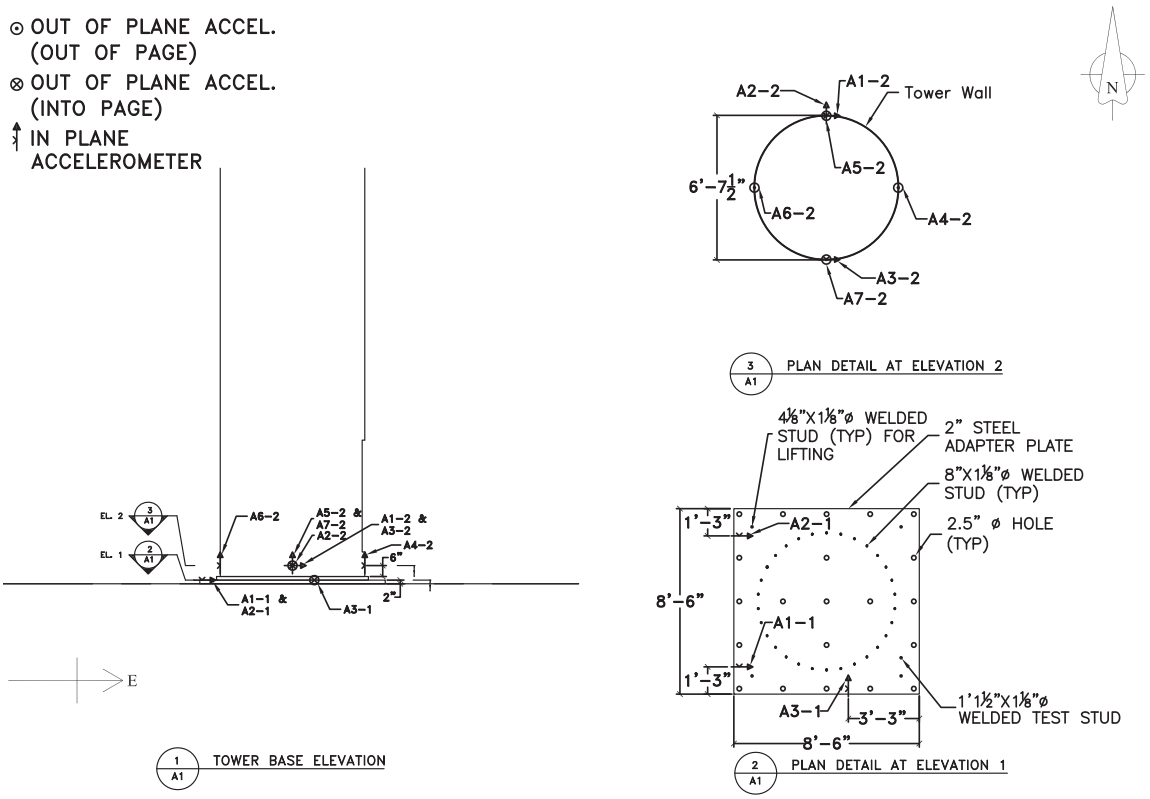

Figure 3.6: A1: Tower Base Accelerometer Detail

3.5.1 Video Photogrammetry Measurement

In a noble gesture, Tim Schmidt of Trilion Quality Systems donated his time to participated in the test and capture video photogrammetry measurements of displacement using recordings from two synchronized cameras (Prowell et al., 2011a). Visual targets (Figure 3.1(a)) were placed on the tower and all three blades to serve as fixed reference points. Cameras were placed on tripods approximately 9 m away from each other, and approximately 41 m away from the tower of the wind turbine, resulting in a camera angle of about 13 degrees. Sunlight provided adequate illumination for all tests despite variations from time of day and cloud cover. The accuracy of the photogrammetry system depends on the size of the field of view and the num-

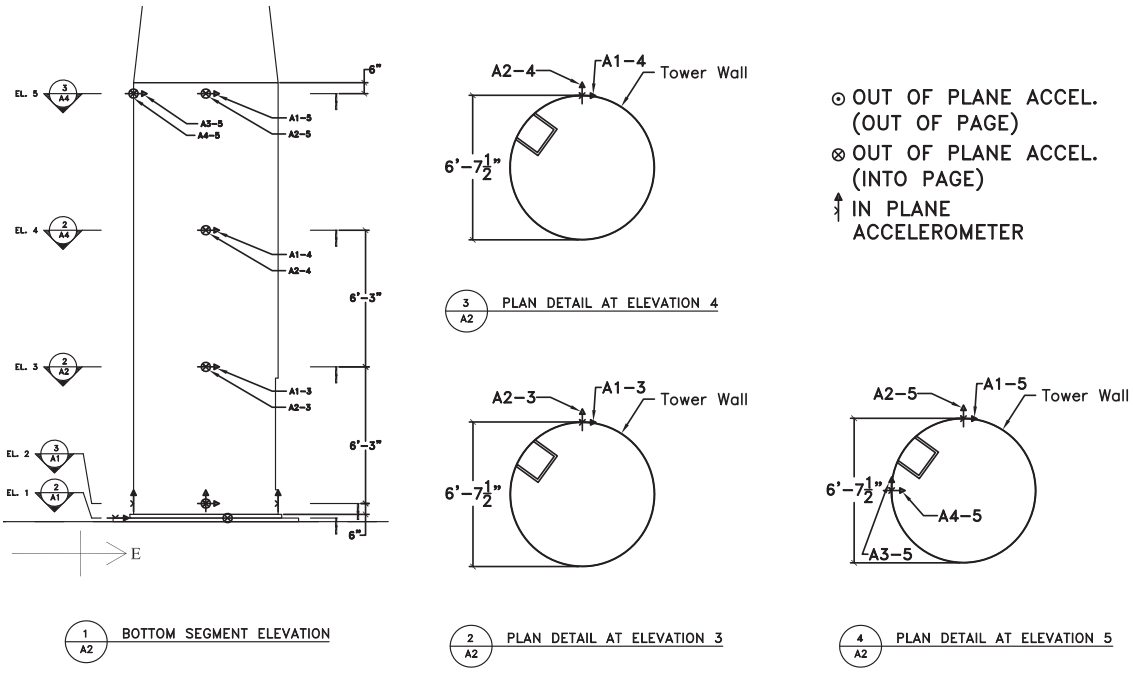

Figure 3.7: A2: Bottom Segment Accelerometer Detail

ber of pixels on the cameras. The targets had a diameter of 178 mm in order to meet or exceed the 10 pixel diameter requirement for accurate determination of the center-point coordinates. After targets were attached they were laminated for moisture protection. Lamination did not detrimentally influence target identification and facilitated survival in outdoor conditions for the entire testing testing program (over 1 month). In this setup, with a 18 m field of view and 2,450 pixels across that width, the nominal accuracy is expected to be $\pm$ 1 mm for the out-of-plane measurements (nominally parallel to the Y axis) and $\pm$ 0.33 mm for the in-plane measurements.

Due to logistical constraints it was not possible to capture video and other measurements using the same clock, thus post processing is required to synchronize

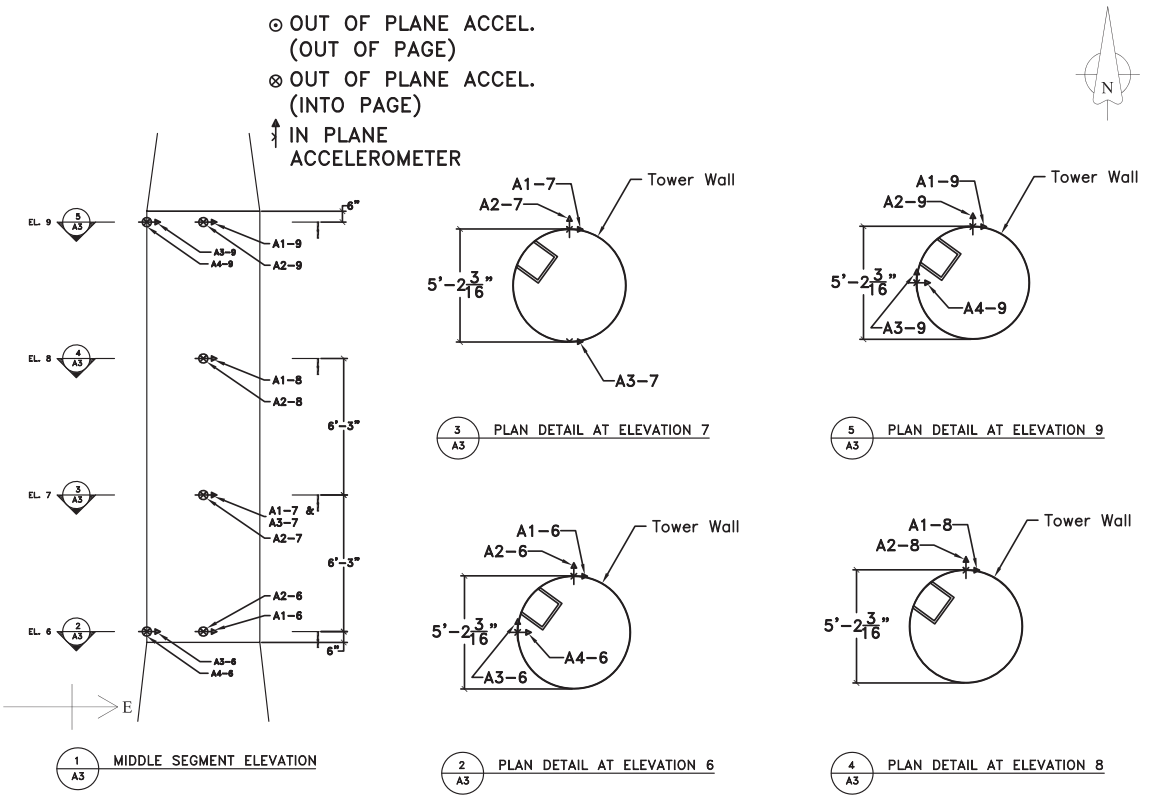

Figure 3.8: A3: Middle Segment Accelerometer Detail

the signals. Of particular interest to this approach is an optical target located at the top of the tower, which coincides with the point of attachment for the upper most string potentiometer. Using the known initial geometry of the string potentiometer and known horizontal displacement of the turbine base a corrected horizontal displacement can be calculated from the inclined measurement. Since this measurement coincides with the optical measurement the time shift between the two measurements is determined by minimizing the norm of the error between the two signals. Figure 3.18 shows a comparison of absolute horizontal displacement captured using a traditional string potentiometer and the video photogrammetry. A very high level of agreement between the two methods is apparent with the optical results showing

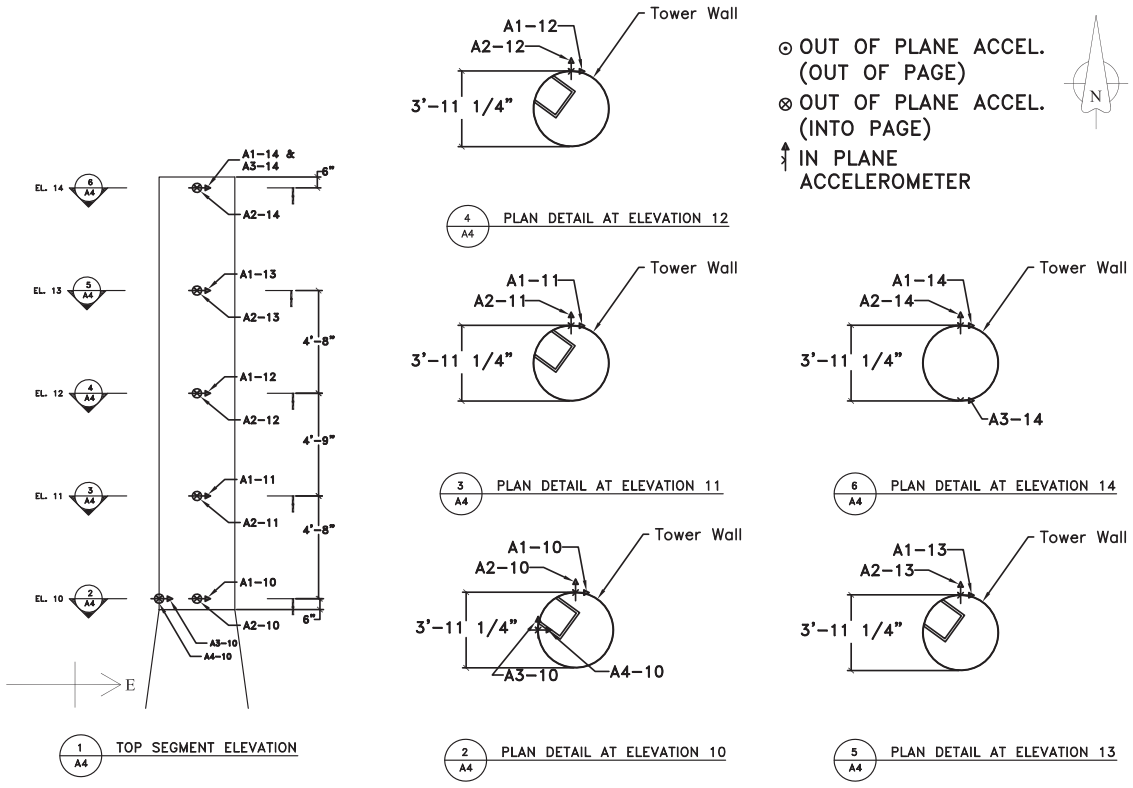

Figure 3.9: A4: Top Segment Accelerometer Detail

resolution of higher frequencies not transmitted through the long cable of the string potentiometer.

By placing optical targets throughout each of the blades and at the top of the turbine tower, the conventional instrumentation was augmented to provide valuable information about the turbine rotor when subjected to earthquake shaking. As shown in Figure 3.19, the point tracking videogrammetry system was capable of capturing displacement in three orthogonal directions for each instrumented point. By using simultaneous optical results (Figure 3.19(a)) from two synchronized cameras the target location can be captured in 3 dimensions at every time step, allowing reconstruction of the position and deformed geometry of the rotor (Figure 3.19(b)). This informa-

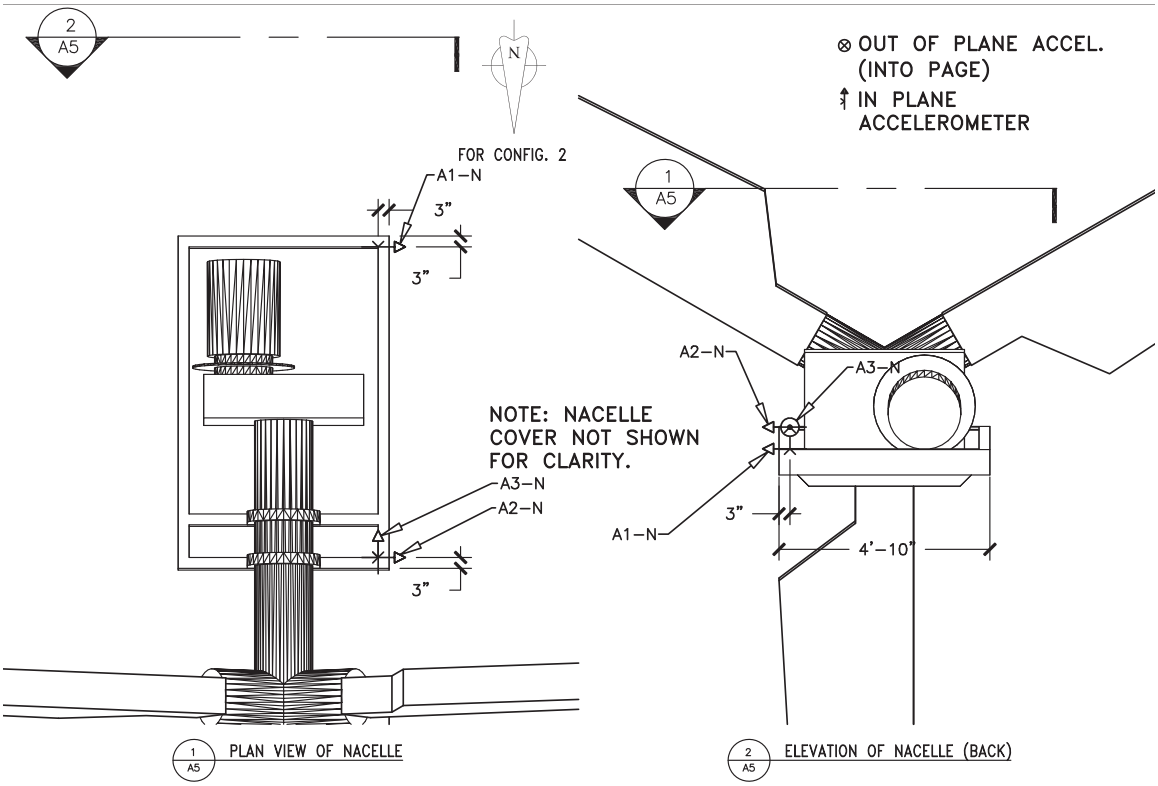

Figure 3.10: A5: Nacelle Accelerometer Detail

tion can be used directly to understand displacement of the rotor for parked and operational states when subjected to the simulated earthquakes. With displacement measurements of the rotor blades the influence of earthquake shaking on key demand parameters, such as blade root bending moment can be more fully understood.

3.6 Estimation of Wind Speed and Direction

Wind speed and direction were estimated using data reported from four local weather stations. The four stations geographically surrounded the site and were located within a 3 km radius. Following averaging of data from the stations, wind speeds were corrected from the reported 10-m elevation (U_{10}) to a hub height of

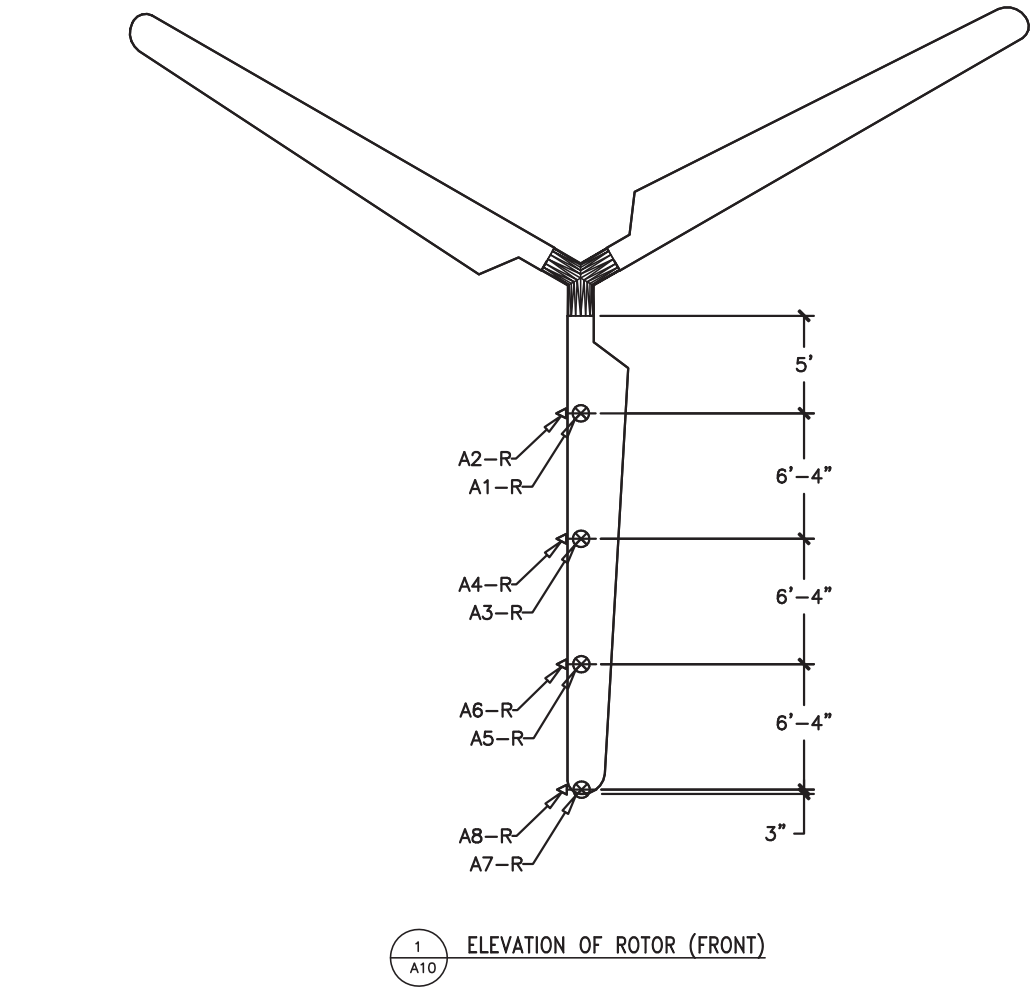

Figure 3.11: A6: Rotor Accelerometer Detail

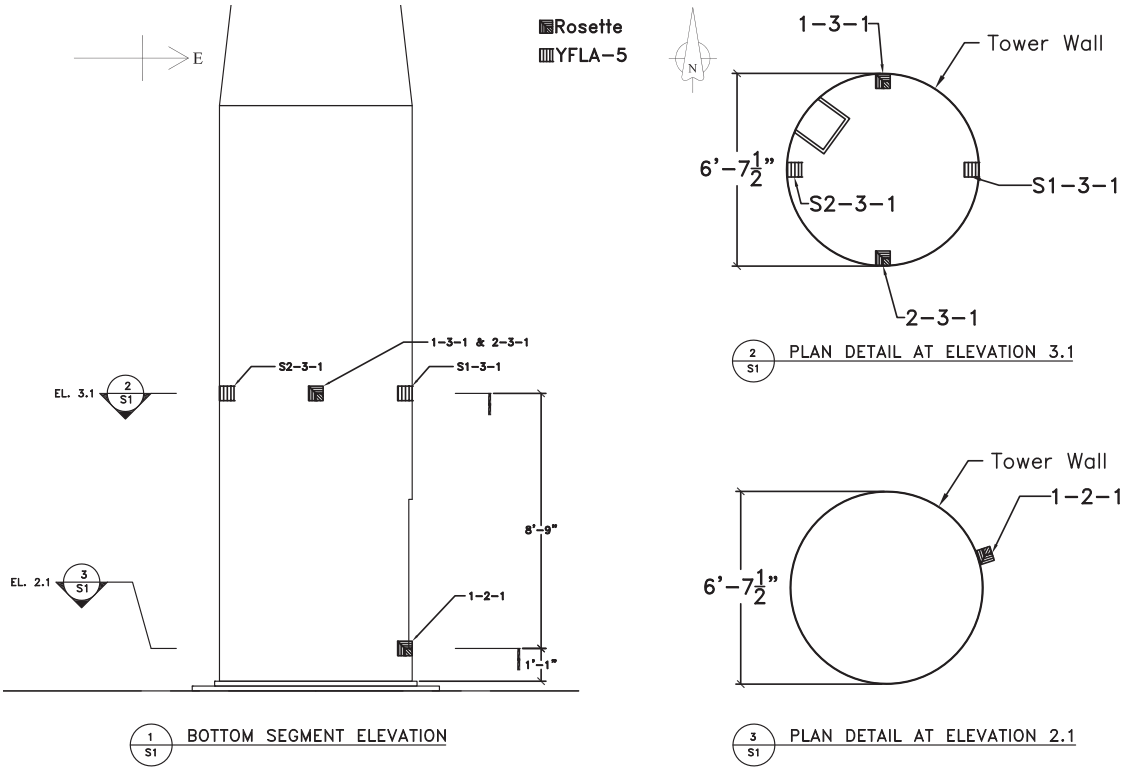

Figure 3.12: S1: Bottom Segment Strain Detail

$z = 22.6$ m (U_z) using (Jonkman, 2009; Prowell et al., 2011b):

$$U_z = \frac{U_{10}}{(10/z)^{1/5}} \tag{3.1}$$

The resulting estimates of the hub height wind speed are reported in Table 3.4. The reported values should be viewed as informative, instead of exact quantitative measurements of wind speed and direction given the associated uncertainty and variability. For reference, the rotor was facing 270 degrees from north in configuration 1 (Figure 3.1(a)) and 0 degrees from north in configuration 2 (Figure 3.1(b)).

Similar to temperature at the site, wind speed is a parameter largely outside of the control of the researchers. Recorded values fell below the rated wind speed,

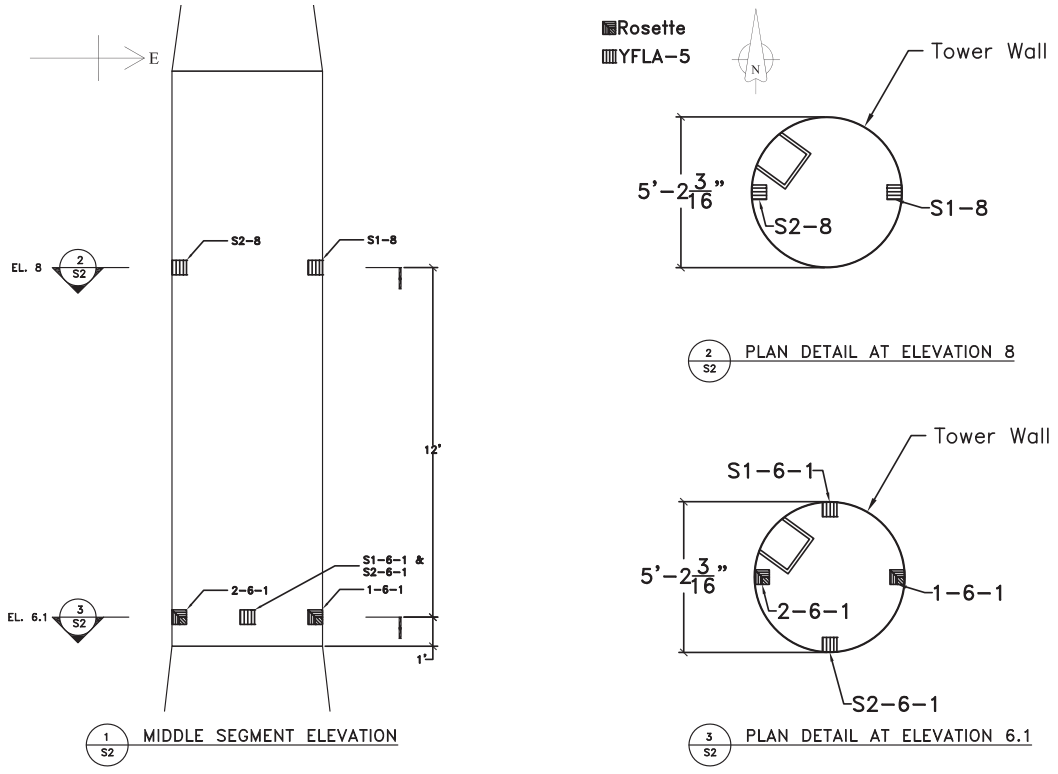

Figure 3.13: S2: Middle Segment Strain Detail

but in most cases were sufficient to initiate rotation at the rated rotor speed of 55 revolutions per minute (RPM). In the few cases where sufficient wind was unavailable, power (from an external electric generator) was applied to the generator to spin the rotor to approximatly the rated speed.

3.7 Dynamic Characterization

3.7.1 System Modal Properties at Low Excitation Level

Data from the white noise motions that were run before and after each imparted 25% earthquake ground motion provided the basis to estimate natural fre-

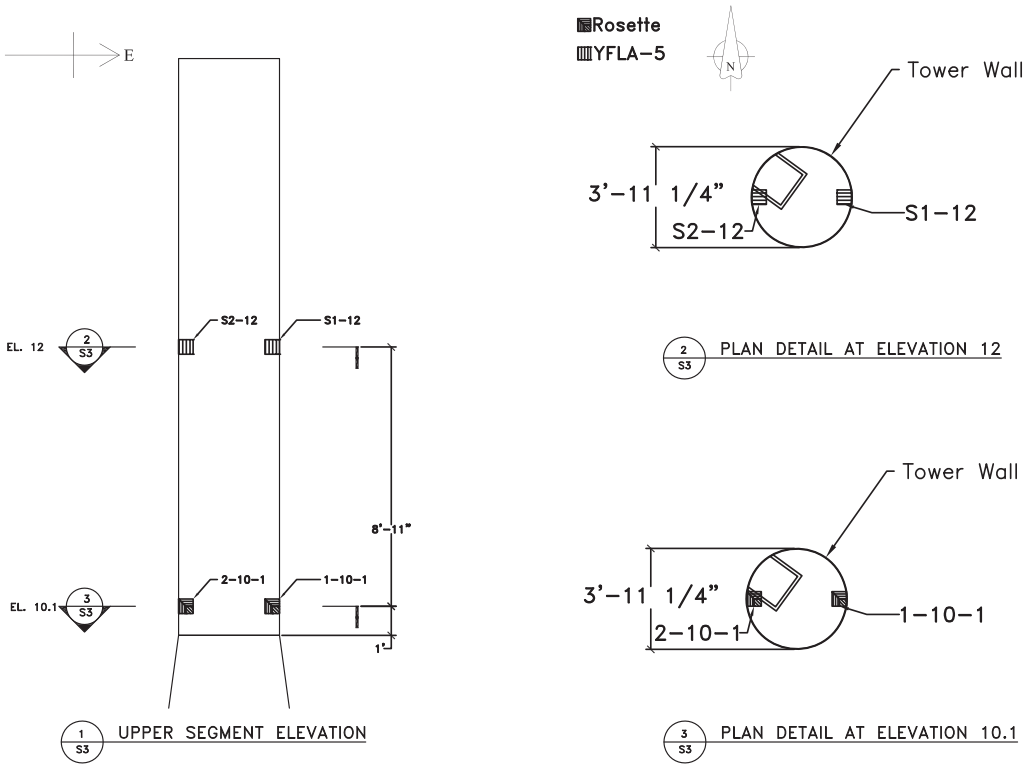

Figure 3.14: S3: Top Segment Strain Detail

quencies and mode shapes of the turbine. Assuming linear response, the estimate of the frequency response of the transfer function between the measured input acceleration and other response acceleromters was used as a basis for approximation of modal parameters through peak picking and half-power bandwidth (Chopra, 2006). Results from configuration 1 serve to estimate the fore-aft modes (Figure 3.20(a) and Figure 3.21(b)), while the side-to-side modes (Figure 3.20(b) and Figure 3.21(c)) were derived from data collected in configuration 2. One coupled mode was also observed in configurations 1 and 2 (Figure 3.21(a)). A summary of the natural frequencies and damping of the identified modes is presented in Table 3.5. Analysis of earthquake events showed very similar results for natural frequencies, damping, and mode shapes.

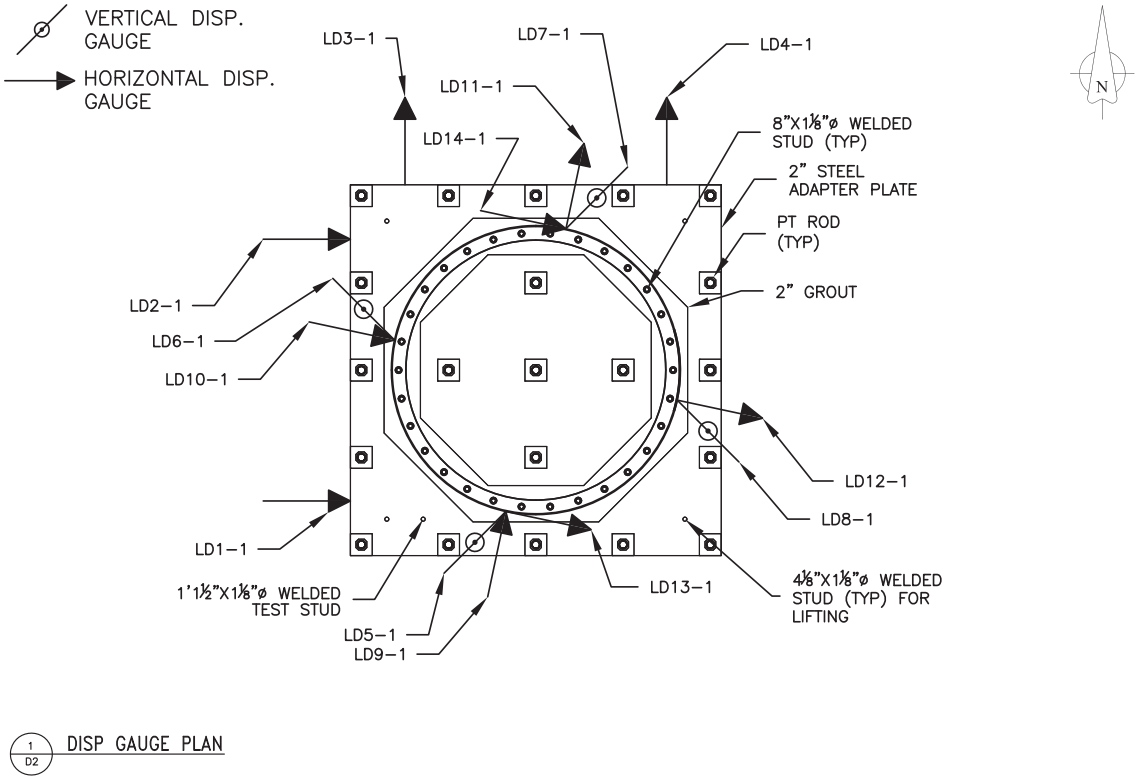

Figure 3.15: D1: Tower Base LVDT Detail

Table 3.5: Summary of modal properties while parked (25% DBE)

Mode Type	Orientation	Illustration	Frequency (Hz)		Damping (%)	
			Mean	Range	Mean	Range
1st Bending	Fore-aft	Figure 3.20(a)	1.70	1.70-1.70	1.0	0.9-1.0
	Side-to-side	Figure 3.20(b)	1.71	1.71-1.72	1.1	0.9-1.4
2nd Bending	Coupled	Figure 3.21(a)	11.3	11.2-11.3	1.5	1.2-1.8
	Fore-aft	Figure 3.21(b)	11.9	11.8-12.0	1.5	1.2-1.9
	Side-to-side	Figure 3.21(c)	12.4	12.3-12.6	2.2	1.7-2.8

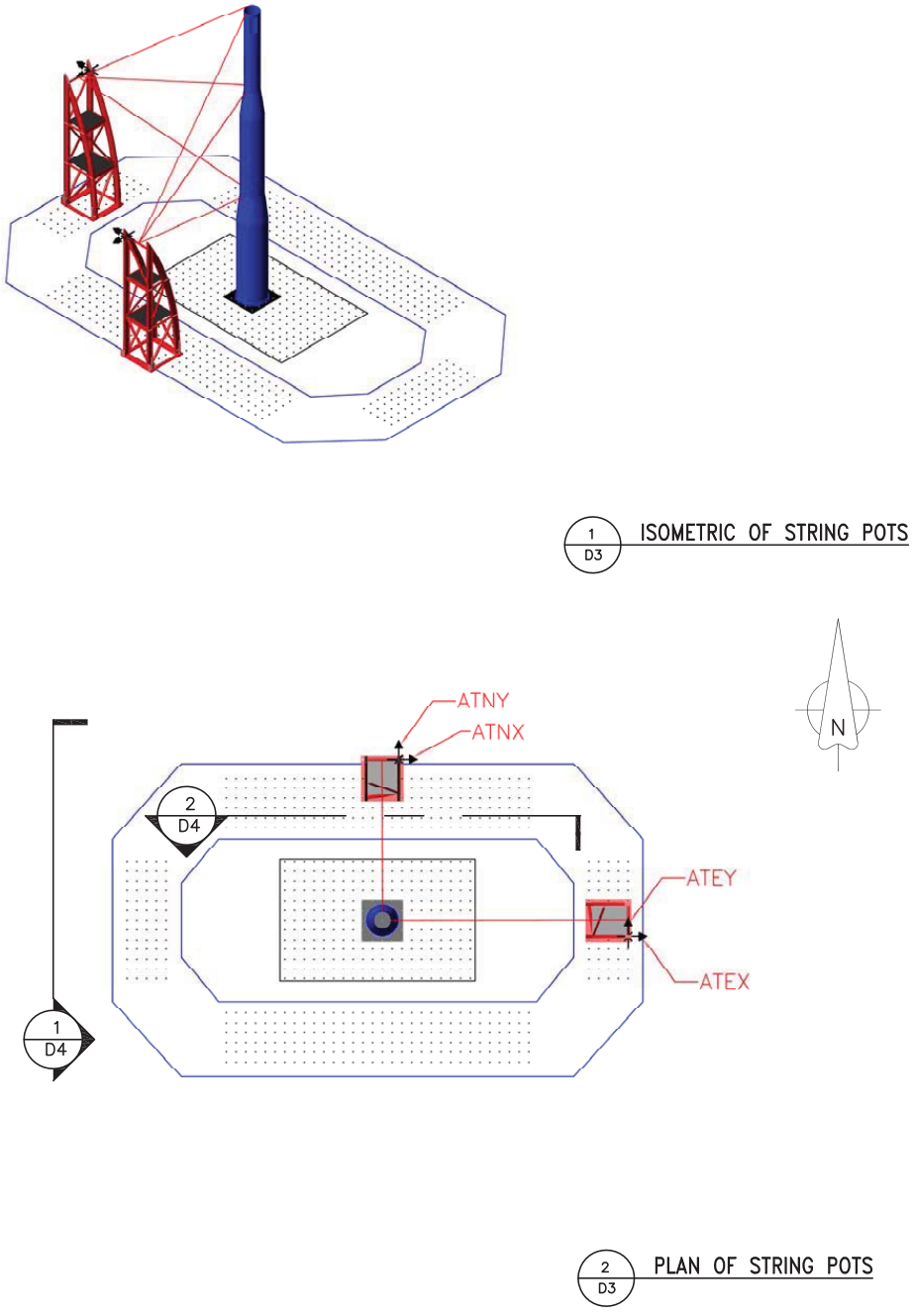

Figure 3.16: D2: Tower String Pot Plan and Isometric Detail

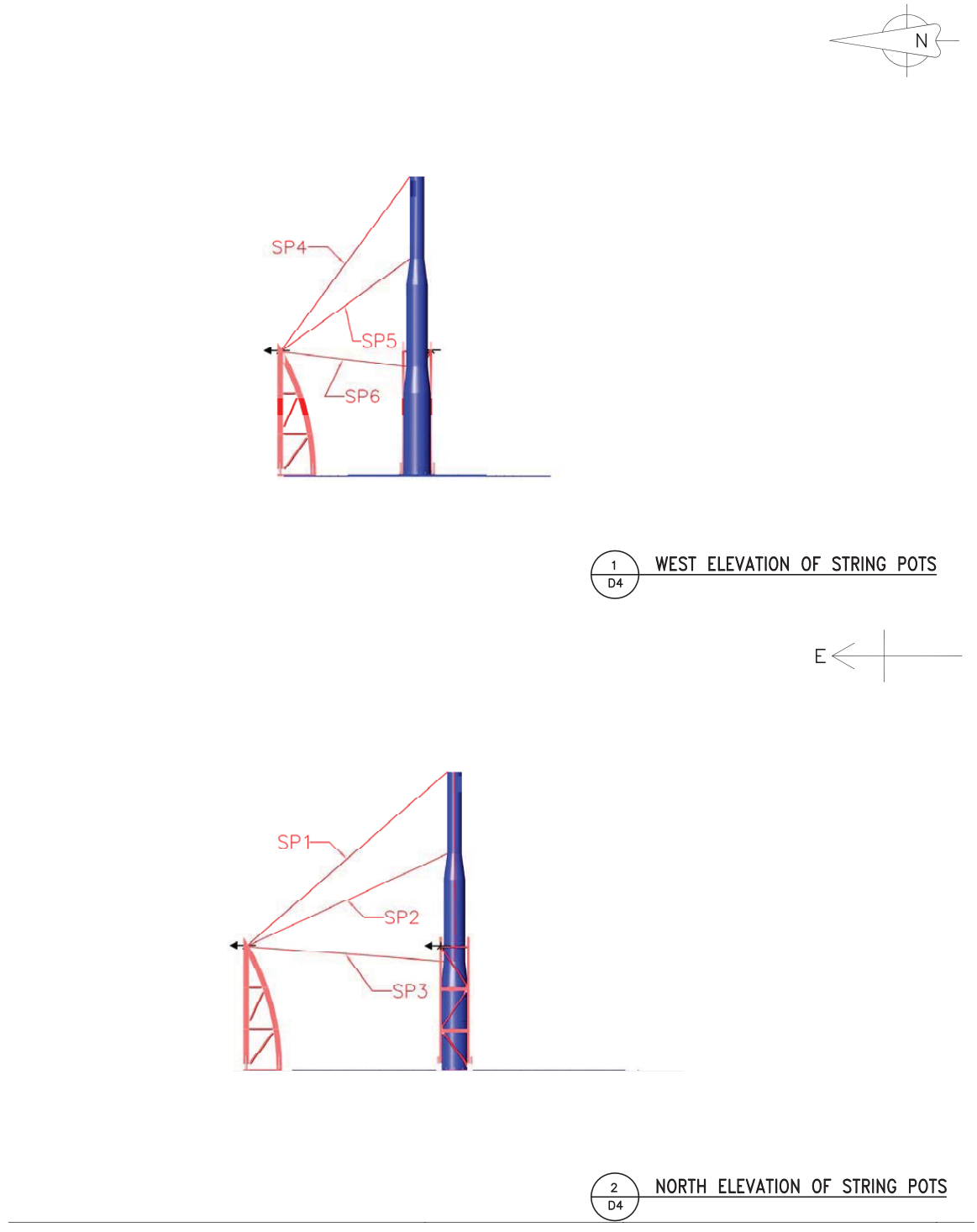

Figure 3.17: D3: Tower String Pot Elevation Detail

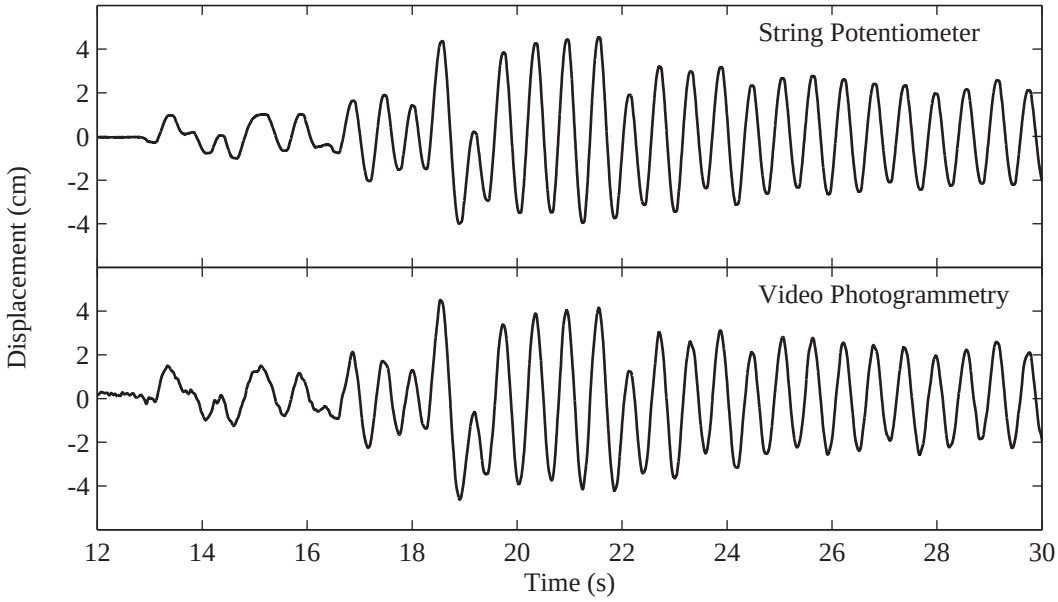

Figure 3.18: Comparison of absolute horizontal tower top displacement from string potentiometer and video photogrammetry

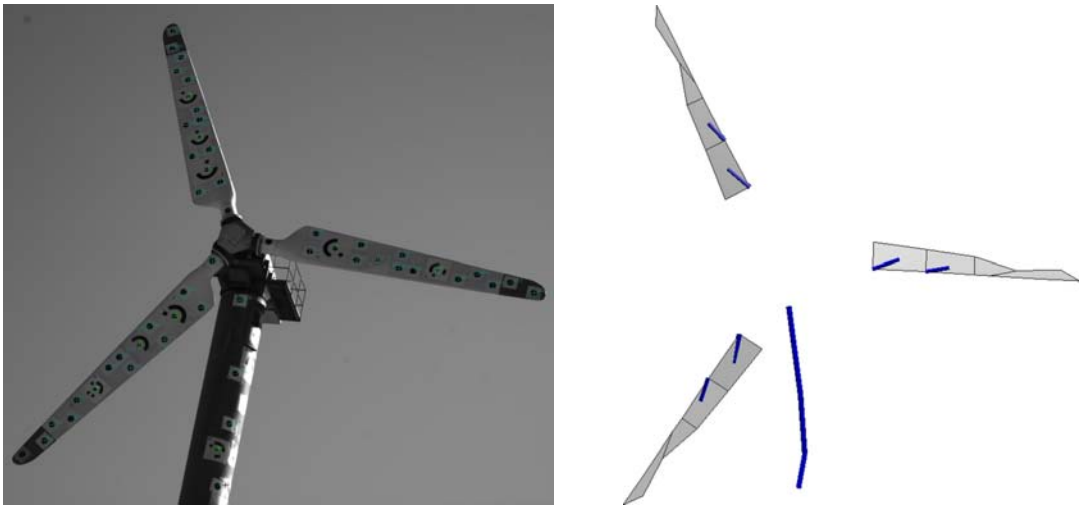

(a) Layout of optical targets (b) Conversion into 3 dimensional model

Figure 3.19: Full representation of rotor position at each time step in 3 dimensional space

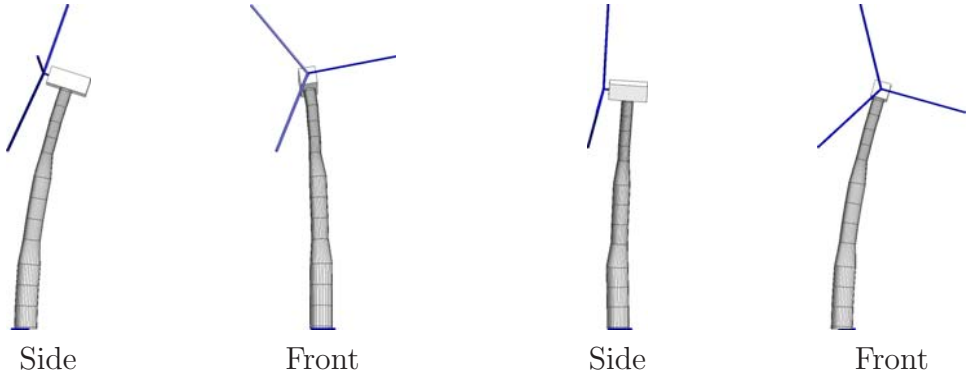

(a) Fore-aft at 1.70 Hz (b) Side-to-side at 1.71 Hz

Figure 3.20: Observed 1st tower bending modes from white noise input during 25% DBE earthquake tests

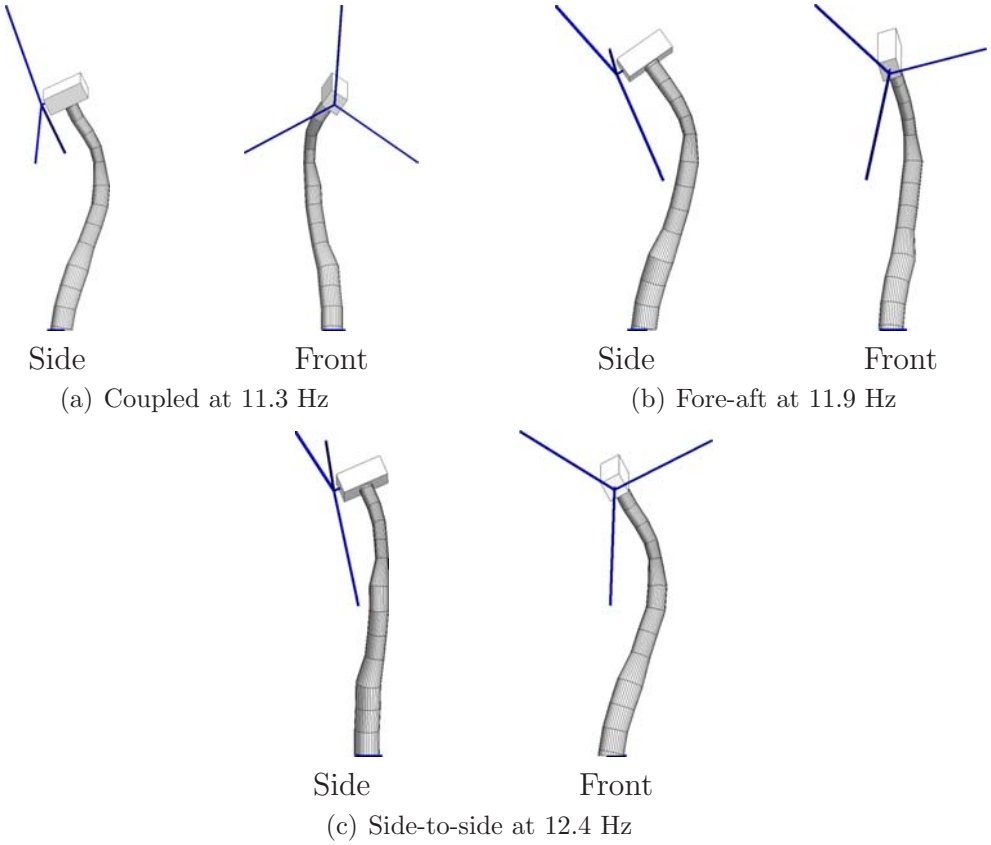

(a) Coupled at 11.3 Hz (b) Fore-aft at 11.9 Hz

(c) Side-to-side at 12.4 Hz

Figure 3.21: Observed 2nd tower bending modes from white noise input during 25% DBE earthquake tests

In addition to the parked tests, the white noise excitation was used for one test in each configuration while the turbine was operating with a rotational velocity of approximately 55 RPM. Analysis of the results shows only a slight change in modal properties (Table 3.6). Only a single test was used for reported results, thus an observed range is not noted. The frequencies of all modes for the operational configuration (Table 3.6) fell within the ranges for the modes of the turbine while parked (Table 3.5). While the turbine was operating observed damping was also similar to the values estimated while parked. The first fore-aft mode is an exception to this observation with damping increasing to approximatly 2% while operating as compared to 1% while parked.

Table 3.6: Summary of modal properties while operating

Mode Type	Orientation	Frequency (Hz)	Damping (%)
1st Bending	Fore-aft	1.70	2.0
	Side-to-side	1.71	0.8
2nd Bending	Coupled	11.3	2.3
	Fore-aft	11.9	1.6
	Side-to-side	12.5	2.0

In the case of the first fore aft mode equivalent viscous damping was approximately twice the highest value observed while the turbine was parked (Figure 3.22). This additional observed damping in the first fore aft mode is expected and predicted by aerodynamic theory. While in operation, a blade generates additional energy dissipation for flap vibration (vibration in the direction of the wind) due to increased aerodynamic damping (James III et al., 1992). The first fore-aft tower mode is coupled with blade flapping (Zhao et al., 2007), thus leading to additional damping when the turbine is operating. Further, gyroscopic forces from the rotation of the rotor may

also contribute to observed changes in dynamics while the turbine is operating.

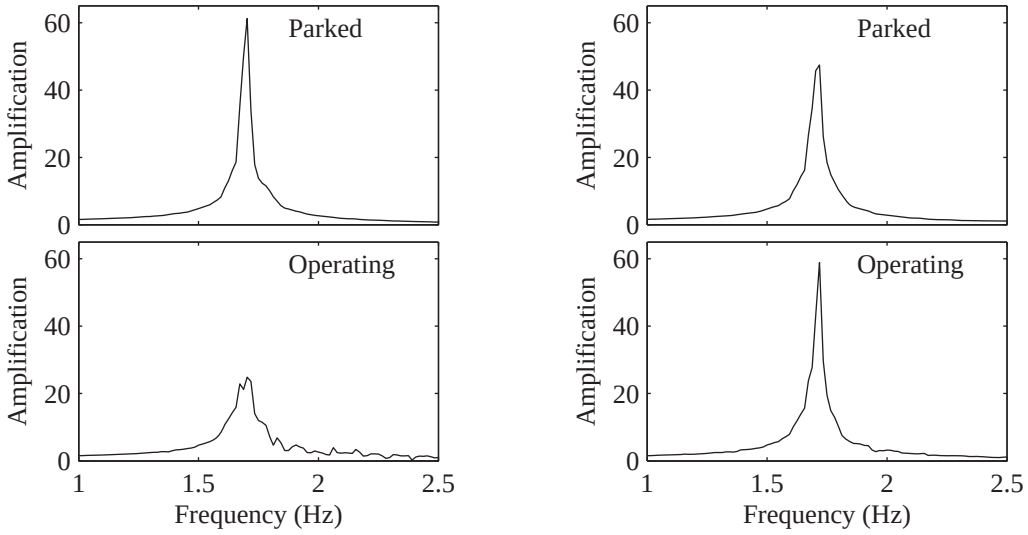

(a) Configuration 1 (b) Configuration 2

Figure 3.22: Observed acceleration amplification from table to top of tower for white noise motions (Configuration 1 from Test 14 Trial 4 and Test 15 Trial 1. Configuration 2 from Test 11 Trial 4 and Test 11 Trail 5. See Table D.1 on page 262 for full information)

Repeated testing with the same motion allowed identification of variability in system parameters. For the primary bending modes, almost no variation was observed in natural frequency or damping (Table 3.5). Higher modes showed more variability, but still remained relatively constant. This consistency in modal parameters suggests that, as expected, the 25% DBE level shaking did not cause damage to the turbine.

3.7.2 Degradation of Structural and Support Properties

Once stronger shaking events were being imparted, the small amplitude white noise tests between seismic tests of increasing amplitude showed a reduction of the apparent frequency of the system. Methods developed to isolate the effects of soil-

structure interaction in structural response (Luco, 1980; Luco et al., 1987) were used to investigate whether the change in apparent system frequency was due to loss of stiffness in the turbine structure, degradation of the tower base connection, or both. The basic relation is (Luco, 1980):

$$\frac{1}{\tilde{\omega_1}^2} \approx \frac{1}{\omega_1^2} + \frac{1}{\omega_R^2} \tag{3.2}$$

where $\tilde{\omega_1}$ is the observed system frequency, ω_1 is the fixed-base fundamental frequency of the turbine, and ω_R is the rocking frequency associated with flexibility of the base. To determine ω_1 and ω_R from the observed data, a second relation involving a ratio of the bending deformation at the top of the tower (U_b), the base rocking angle (θ_s) and the tower height (H) is used (Luco, 1980):

$$\frac{U_b}{H\theta_s} \approx \frac{\beta_1 H_1}{H} \left(\frac{\omega_R}{\omega_1}\right)^2 \tag{3.3}$$

The terms β_1 and H_1 are given by:

$$\beta_1 = \frac{\{\Psi_1\}^T [M] \{1\}}{\{\Psi_1\}^T [M] \{\Psi_1\}} \tag{3.4}$$

$$H_1 = \frac{\{\Psi_1\}^T [M] \{h\}}{\{\Psi_1\}^T [M] \{1\}} \tag{3.5}$$

where $\{\Psi_1\}$ is the first mode shape, $[M]$ is the mass matrix, $\{h\}$ is a column vector of the heights, and $\{1\}$ is a column vector of ones. For the turbine under study, $\beta_1 =$ 1.2, $H_1 = 20.3$ m, and H = 22.0 m. By rearranging Eqs. 3.2 and 3.3 it can be shown

that the fixed base and rocking frequencies can be written as (Luco, 1980):

$$\frac{\omega_1}{\tilde{\omega_1}} = \left[1 + \frac{\beta_1 H_1}{H}\frac{H\theta_s}{U_b}\right]^{1/2} \tag{3.6}$$

$$\frac{\omega_R}{\tilde{\omega_1}} = \left[1 + \frac{H}{\beta_1 H_1}\frac{U_b}{H\theta_s}\right]^{1/2} \tag{3.7}$$

which involve known or measured quantities ($\tilde{\omega_1}$, β_1, H_1, U_b, and θ_s). From the low-level tests in configuration 1 (test indices 8 through 14 in Table 3.3) the undamaged mean frequencies are estimated at: $\tilde{\omega_1} = 10.7$ rad/sec (1.70 Hz) the observed system frequency, $\omega_1 = 11.1$ rad/sec (1.77 Hz) for the fixed base frequency, and $\omega_R = 40.2$ rad/sec (6.40 Hz) for the rocking frequency.

Following estimates for the undamaged structure during low-level tests, results from the white noise motions imparted between stronger motions indicated a progressive loss in fixed base and rocking frequencies starting with test No. 16 3.3. Tracking the progression of the parameters $\tilde{\omega_1}$, ω_1, and and ω_R as a percentage of the undamaged mean frequencies (Figure 3.23), it is apparent that there is a 14% reduction of the final fixed-base frequency which translates into a 26% reduction of the fixed-base tower stiffness. Inspection following test No. 19 showed that torque in 4 to 6 of the connecting bolts at each splice joint was below specified levels (Table 3.1), which likely accounts for the observed loss in tower stiffness. The rocking frequency degrades by 40%, which implies a 64% reduction of the rocking stiffness. For higher level tests (Test No. 17), rocking resulted in separation of the flange at the tower base from the grout and subsequent impact. The observed reduction in rock-

ing stiffness can be explained by the spalling and deterioration of the grout caused by this pounding. Further, an increase in observed damping up to a final value of approximately 1.5% was noted at the first apparent system frequency ($\tilde{\omega}_1$).

In production configurations, bolt torque is maintained by a second nut and inspection routines normally specify verification of bolt torque to prevent a similar loss in stiffness. However, the softening due to deterioration of the grout reinforces the importance of proper connection detailing for the tower base. Repairing the foundation would be more expensive and difficult than re-torquing connecting bolts.

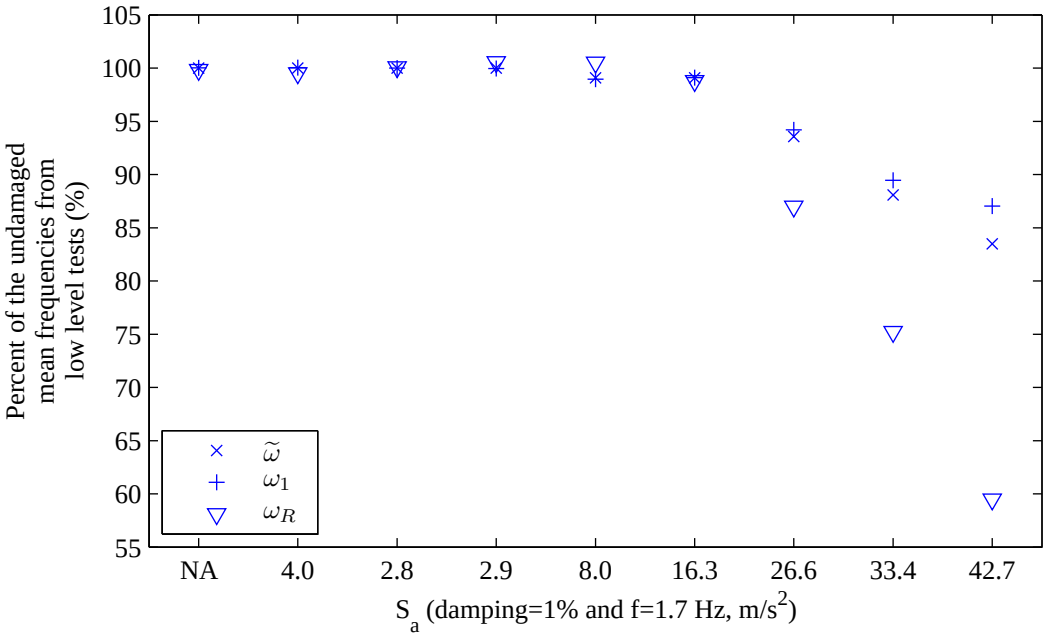

Figure 3.23: Variation in observed, fixed base, and rocking frequency for configuration 1 tests (calculated S_a shown from test before white noise excitation)

3.8 Characterization of Turbine Rotor

Following testing, the rotor was placed horizontally and instrumented with 8 MEAS accelerometers. Two accelerometers were placed at each of the quarter points along the length of the blade with one oriented to capture flap bending and the other edge to capture edge bending. To provide estimates of modal parameters for the blades, the blades were impacted at various locations and the resulting free vibration records were analyzed using the Eigensystem Realization Algorithm (Juang and Pappa, 1985). The resulting estimates of modal parameters for the blades are presented in Table 3.7.

Table 3.7: Summary of measured blade modal properties

Mode Type	Orientation	Frequency (Hz)	Damping (%)
1st Bending	Flap	3.47	0.8
	Edge	5.79	1.0
2nd Bending	Flap	11.0	0.8
	Edge	14.4	1.0
3rd Bending	Flap	21.7	0.5

When the rotor was disassembled each individual blade was measured to determine the mass. Table 3.8 shows the resulting mass for each blade. The observed imbalance created an addition source of vibration for tests where the turbine was operating.

Table 3.8: Measured Blade Mass

Blade Number	Mass (kg)
1	303
2	308
3	333

3.9 Results of Simulated Earthquake Shaking For Parked Condition

Selected experimental results for the three earthquake motions (EQ1, EQ2, and EQ3) are presented in Figure 3.24 for configuration 1 with configuration 2 results shown in Figure 3.25.

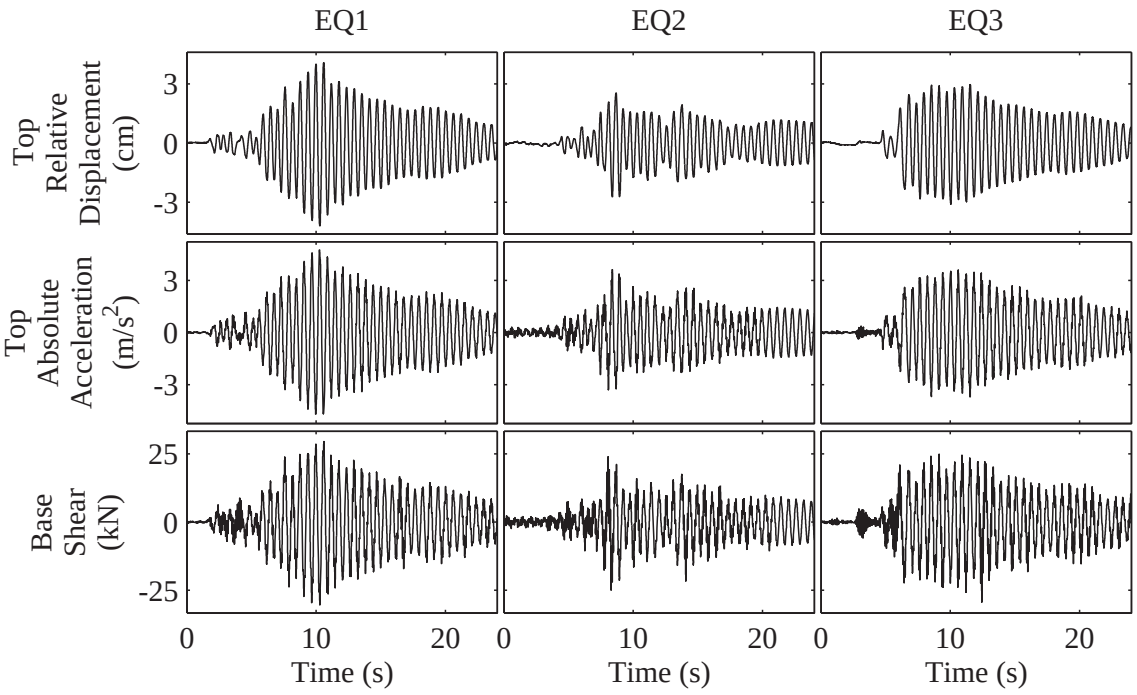

Figure 3.24: Key response parameters for configuration 1 (25% DBE input level)

3.9.1 Apparent Eccentricity

Initial inspection of a wind turbine suggests that the rotor is a large eccentric mass that may cause significant torsional demand for the tower. By careful placement of the generator and gearbox, large portions of the total nacelle mass, the center of

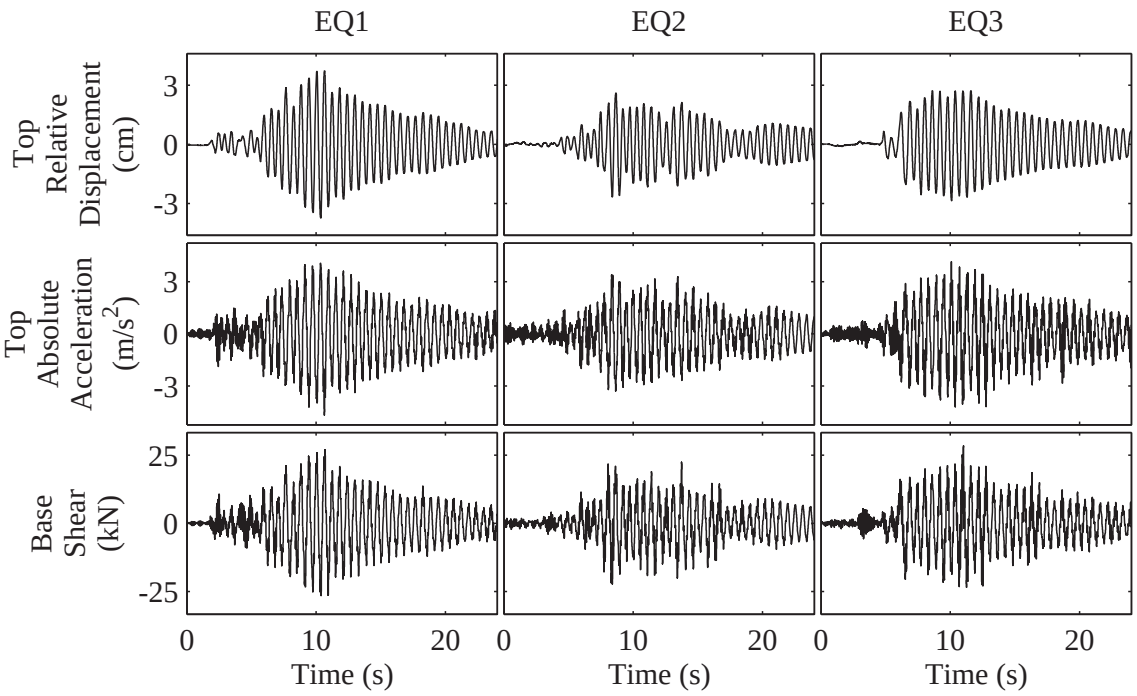

Figure 3.25: Key response parameters for configuration 2 (25% DBE input level)

mass for the nacelle is offset to reduce overall eccentricity of the combined rotor/nacelle system. To verify this simultaneous torque and nacelle acceleration was used to estimate the arm by considering the nacelle as a point mass. It is concluded that the eccentricity is similar for the two tested configurations with a center of mass offset by approximately 0.51 m and 0.46 m for configurations 1 and 2, respectively. In configuration 1, which appears to be symmetric, the eccentricity is likely caused by offset of the generator the centerline and differences in the individual blade weights. Based on this small difference, little eccentric influence is expected or observed between the two configurations.

3.9.2 Implications of Direction of Shaking

To investigate the implications of orientation of shaking, maximum moment demand at the base of the tower is compared for the two configurations. Due to small out of plane displacement in the mode shapes, the maximum is taken as the square root of the sum of the squares (SRSS) of the two horizontal components at each time step. A summary of the maximum moments for the 25% DBE motions is shown in Table 3.9. The observed demand is approximately 15% of the 3,200 kN-m capacity predicted by the AISC Specification using a Load Factor Resistance Design (LRFD) approach (AISC, 2005). Results show variation between earthquakes and orientation, which is due in part to variability in the input motion (Table 3.4). Slight differences in fore - aft and side-to-side modal properties also contribute somewhat to the discrepancies.

Table 3.9: Maximum base moment demand (25% DBE)

Index	Configuration and Motion	In-plane moment (kN-m)	Out-of-plane moment (kN-m)	SRSS moment (kN-m)
8	1 - EQ1	584 at 10.3 sec	103 at 13.6 sec	588 at 10.3 sec
3	2 - EQ1	509 at 10.1 sec	101 at 14.0 sec	509 at 10.1 sec
10	1 - EQ2	445 at 8.4 sec	86 at 15.0 sec	445 at 8.4 sec
5	2 - EQ2	414 at 8.4 sec	65 at 14.7 sec	414 at 8.4 sec
13	1 - EQ3	466 at 11.2 sec	95 at 12.7 sec	469 at 11.2 sec
1	2 - EQ3	491 at 11.0 sec	118 at 10.9 sec	492 at 11.0 sec

As shown in Table 3.9, the out-of-plane maximum moment is delayed from the in-plane maximum moment. Due to this lag, maximum SRSS moment demand was primarily due the contribution from vibration in the direction of shaking. In light of this behavior, it is noted that there little difference in resulting moment demand for

the two orientations of shaking while in the parked state. In actual situations, where shaking may occur in multiple directions in conjunction with additional load sources such as wind and operational vibration, this coupling may be important to accurately estimate structural demand. Models that include coupling between fore-aft and side-to-side modes are likely to represent this observed behavior (Jonkman and Buhl Jr., 2005; Witcher, 2005; Häenler et al., 2006; Zhao and Maißer, 2006).

3.9.3 Response of Observed Modes

The acceleration (Figure 3.26) envelopes are considered to assess the relative contribution of modes to the dynamic response of the turbine. The motions that are richer in higher frequency energy, EQ2 and EQ3 (Figure 3.3), show more second bending mode participation in the acceleration envelope in configuration 1 (Figure 3.26(a)), but only EQ3 shows notable second mode activity in configuration 2 (Figure 3.26(b)). When considered in conjunction with mass distribution, structural demand from the second mode is relatively small, but this is evidence that higher modes are excited by base shaking and can play a role in the seismic response of a turbine, particularly larger modern turbines where the frequencies of these higher modes fall into ranges of significant seismic input energy (Häenler et al., 2006; Ishihara and Sawar, 2008; Prowell et al., 2009b).

3.9.4 Acceleration-Displacement Relationship

Using 1% of critical damping and the natural frequency observed for the first bending mode from the white noise excitation before each test ($\tilde{\omega_1}$), the spectral

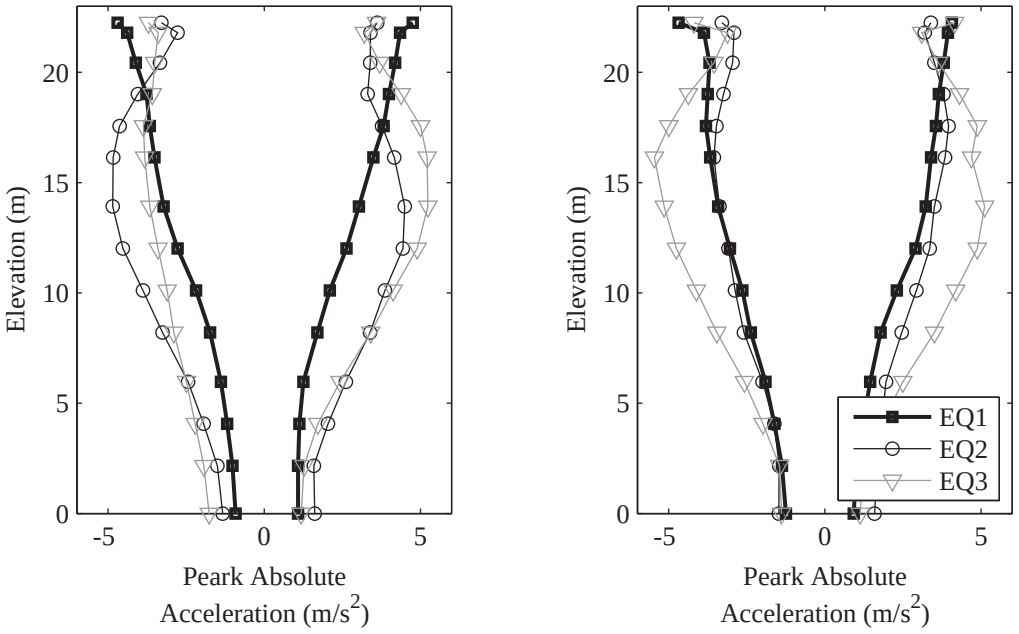

(a) Configuration 1 (b) Configuration 2

Figure 3.26: Peak absolute acceleration envelope for 25% DBE tests (Test indicies 8, 10, and 13 in configuration 1 for EQ1, EQ2, and EQ3, respectively. Test indicies 3, 5, and 1 in configuration 2 for EQ1, EQ2, and EQ3, respectively.)

acceleration for each recording of the platen motion was calculated and compared to the maximum tower top displacement (Figure 3.27). For lower levels of spectral acceleration, up to approximately 1 g, a linear relationship with displacement is observed for both configurations. At the higher levels of shaking, the linear correlation of spectral acceleration and maximum tower top displacement does not appear to be maintained (Figure 3.27(a)), with greater displacement than a linear trend would predict. This deviation can be explained by accounting for the rocking of the tower base in relation to the table platen. As analyzed earlier, the observed rocking is due to deformation and deterioration of the components connecting the tower to the platen. Once the rigid body contribution from base rocking is removed from measured displacement, shown as triangles for each data point, the resulting dis-

placement continues to generally follow the linear trend established by the lower level tests.

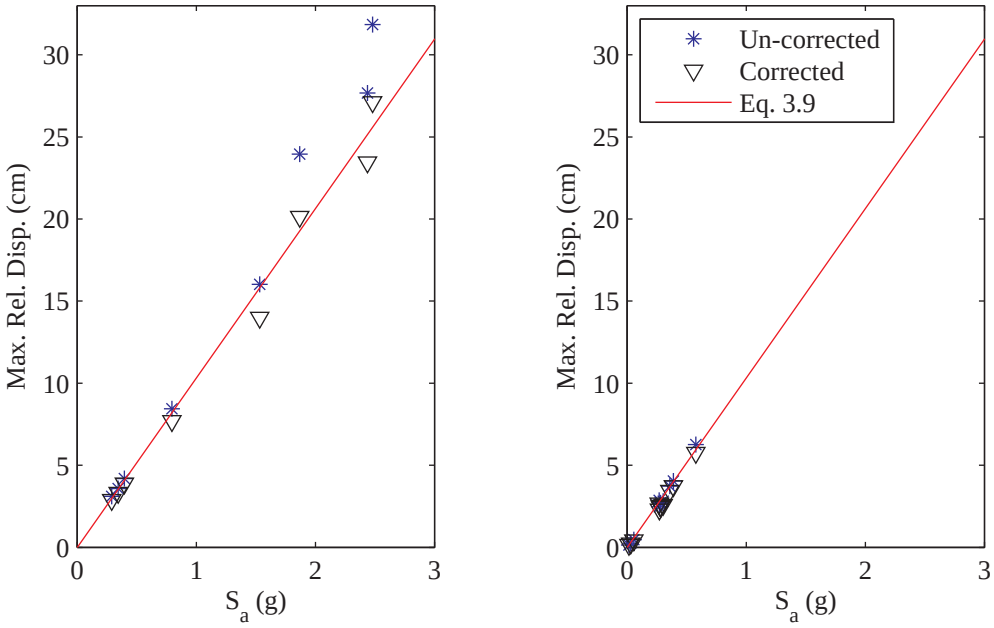

(a) Configuration 1 (b) Configuration 2

Figure 3.27: Maximum tower top relative displacement vs. 1% damped spectral acceleration relationship

The solid line in Figure 3.27 is not simply a best fit line, but instead the relation between spectral acceleration and spectral displacement corrected for the modal participation factor of the turbine (see Section 2.7). The spectral displacement can be related to spectral acceleration as follows (Chopra, 2006).

$$S_d = S_a/\omega^2 = S_a/(2\pi f)^2 \tag{3.8}$$

For the first mode of the tested turbine, it was shown in Eq. 3.4 that the modal participation factor was $\beta_1 = 1.2$ in the fore-aft direction (Prowell et al., 2009b). Therefore, the predicted maximum displacement is:

$$\Delta_{max} = 1.2S_d = 1.2S_a/(2\pi f)^2 \tag{3.9}$$

Observed agreement between Eq. 3.9 and maximum measured displacement corrected for base rocking (Figure 3.27) suggests that such a simple approximation is useful for estimation of seismically induced relative displacement for similar turbines.

3.9.5 Shear-Displacement Relationship

As expected from elastic response, for small tower top displacements (less than 10 cm) a linear trend is observed between tower top relative displacement and base shear (Figure 3.28). In configuration 2 shaking levels were not strong enough to observe any deviation from this trend. For large displacements it appears that base moment demand reduces. However, closer inspection reveals that the fore aft stiffness in the first mode (proportional to the square the first natural frequency, Figure 3.23) was progressively reduced as the deviation from the linear shear versus displacement relation increased. It is expected that, as observed, a decrease in stiffness for a bending structure will lead to greater relative displacement for the same applied moment. These overall linear trends shown in Figure 3.27 and Figure 3.28 indicate that for the tested turbine that 1% damped spectral acceleration may serve as an indicator of the expected level of tower top displacement or, with consideration of lateral stiffness, tower base shear demand.

The relation between base shear and relative displacement at the tower top (Figure 3.28) appears to hold true for the moment envelope throughout the tower

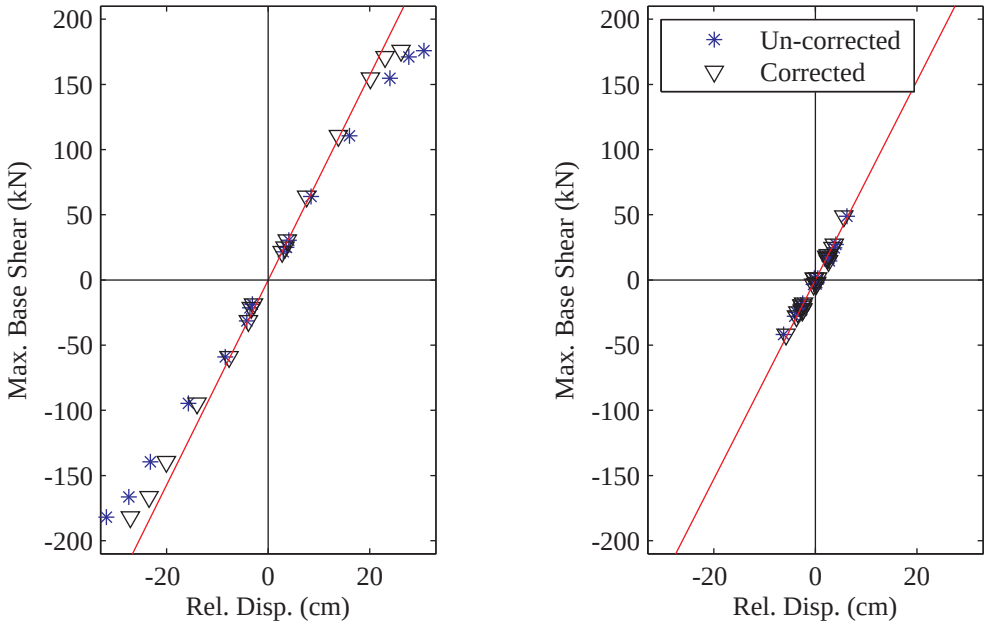

(a) Configuration 1 (b) Configuration 2

Figure 3.28: Maximum base shear versus tower top relative displacement relationship

derived from inertial measurements (Figure 3.29). As in lower level tests, out of plane moment is observed in configuration 1 (Figure 3.1(a)) for the higher levels of shaking. At the highest level of shaking, maximum moment demand at the base, 3,300 kN-m, slightly exceeded the 3,200 kN-m capacity allowed by the AISC Specifications, indicating that buckling of the tower was likely imminent (AISC, 2005). Displacement-moment profiles for the strong shaking also show effectively linear behavior (Figure 3.30). Analysis of shear vs. displacement hysteresis loops suggest that for strong shaking fore-aft damping may be higher than that found from white noise identification, around 2 to 3%. With appropriate consideration of observed bolt loosing and base rocking, the tested turbine performed well, even for very strong earthquake shaking.

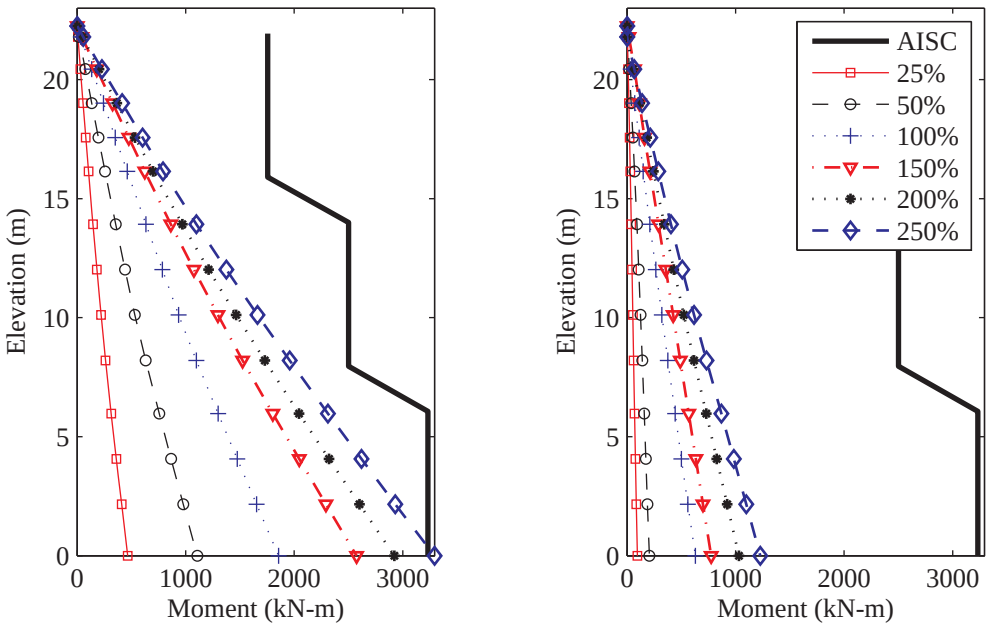

(a) In-plane (b) Out-of-plane

Figure 3.29: Peak moment envelope for EQ1 strong events (Test indicies 8 and 15 through 19)

3.10 Analysis of Response During Operation

The analysis presented here focuses on the response characteristics particular to operational effects. It is expected that the operational state will influence the dynamics and structural response to strong shaking (Witcher, 2005; Prowell et al., 2010a). For earthquake loads, acceleration at the top of the structure is an important indicator of demand. Figure 3.31 compares the absolute acceleration at the tower top for each of the configuration/state combinations for EQ1. Primarily, the absolute acceleration response at the top of the tower is clearly distinct for configuration 1 in the parked and operational states. During operation, the acceleration envelope for configuration 1 has a somewhat lower maximum and significantly faster decay, which directly supports the lower amplification and increased damping observed in dynamic

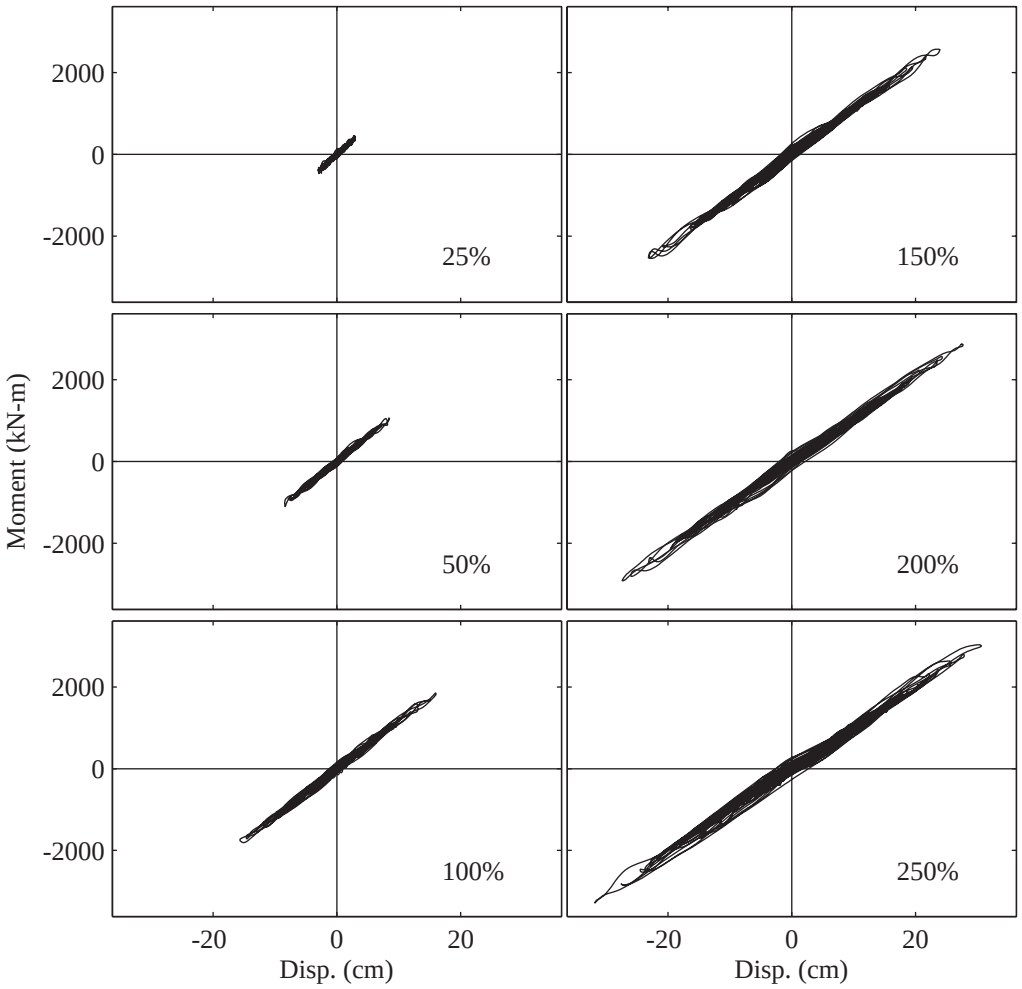

Figure 3.30: Tower top relative displacement-moment relationship for EQ1 tests

characterization (Figure 3.22). Similar trends are observed for EQ2 (Figure 3.32) and EQ3 (Figure 3.33).

The turbine tower is primarily governed by bending, so the moment envelope is compared for each of the states to understand if variations in observed acceleration lead to differences in demand. The data from vertical strain gauges at 5 elevations were used in conjunction with calculated section properties to estimate bending moment demand. Figure 3.34 presents the envelope of the moment at each elevation. Consistent with the observed primary amplification of the first mode (Figure 3.22)

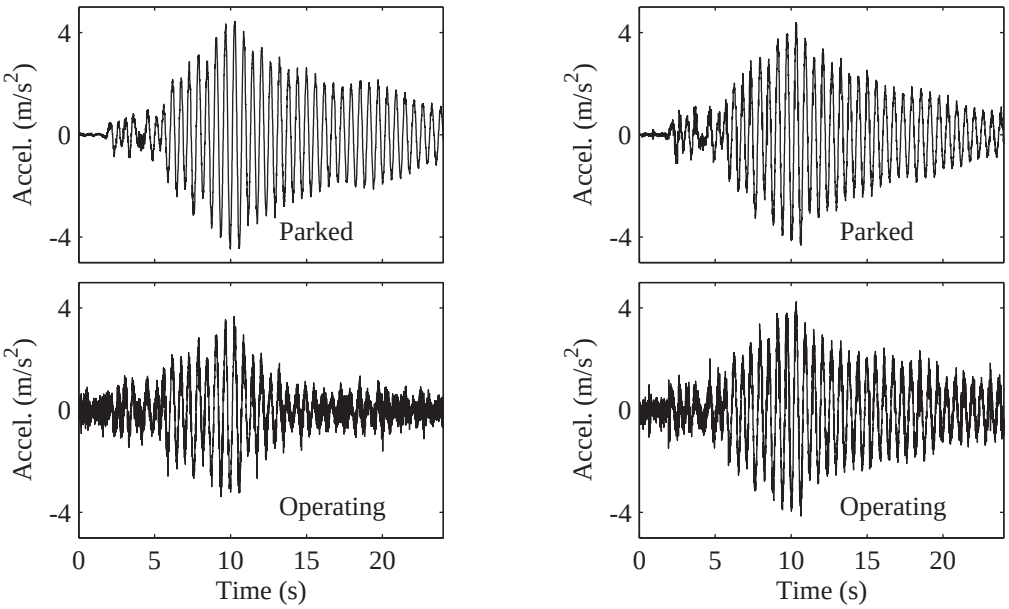

(a) Configuration 1 (b) Configuration 2

Figure 3.31: Observed tower top in-plane absolute acceleration for EQ1 (Test indices 8 and 9 for configuration 1. Test indices 3 and 4 for configuration 2)

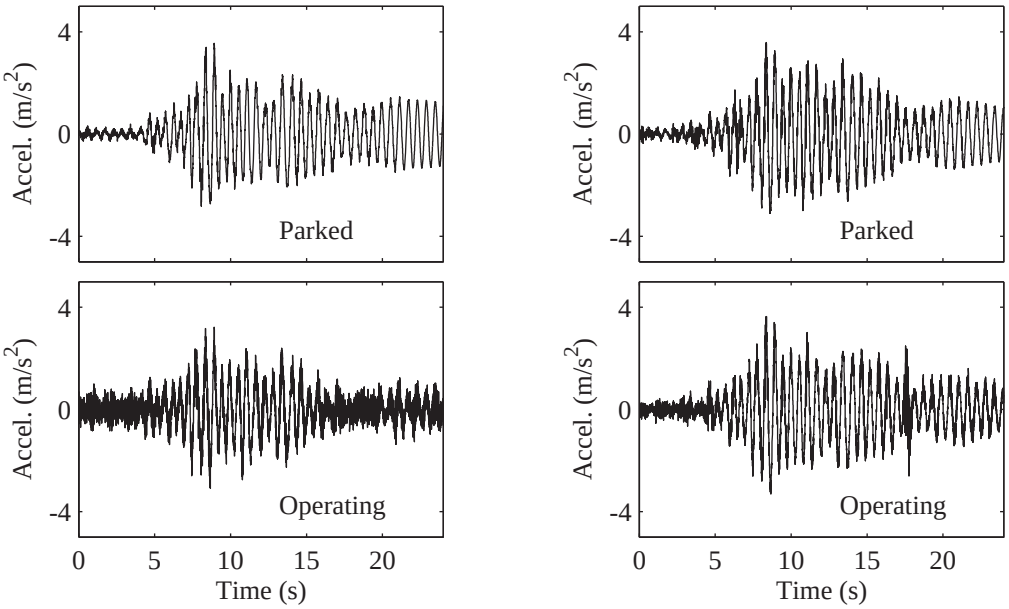

(a) Configuration 1 (b) Configuration 2

Figure 3.32: Observed tower top in-plane absolute acceleration for EQ2 (Test indices 10 and 11 for configuration 1. Test indices 5 and 6 for configuration 2)

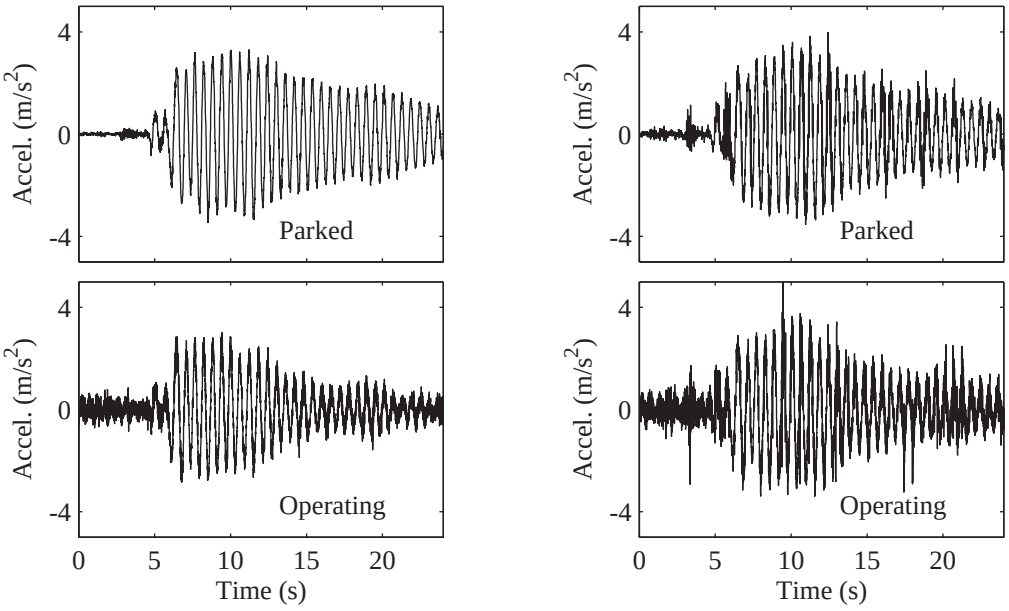

(a) Configuration 1

(b) Configuration 2

Figure 3.33: Observed tower top in-plane absolute acceleration for EQ3 (Test indices 13 and 14 for configuration 1. Test indices 1 and 2 for configuration 2)

and the acceleration responses of Figures 3.31 through 3.33, the moment demand envelope (Figure 8) only shows a reduction in seismic demand for configuration 1 while operating. Configuration 2 does not show a similar reduction in demand when the turbine is operating.

3.10.1 Contribution of Higher Modes While Operating

Though the response of the tested turbine is primarily governed by the first mode response, there is evidence to show that higher mode response is important for estimation of seismically induced loads for large turbines (Häenler et al., 2006; Ishihara and Sawar, 2008). To provide additional insight into the influence of operational state on the contribution of higher modes for seismic shaking, the acceleration envelope is

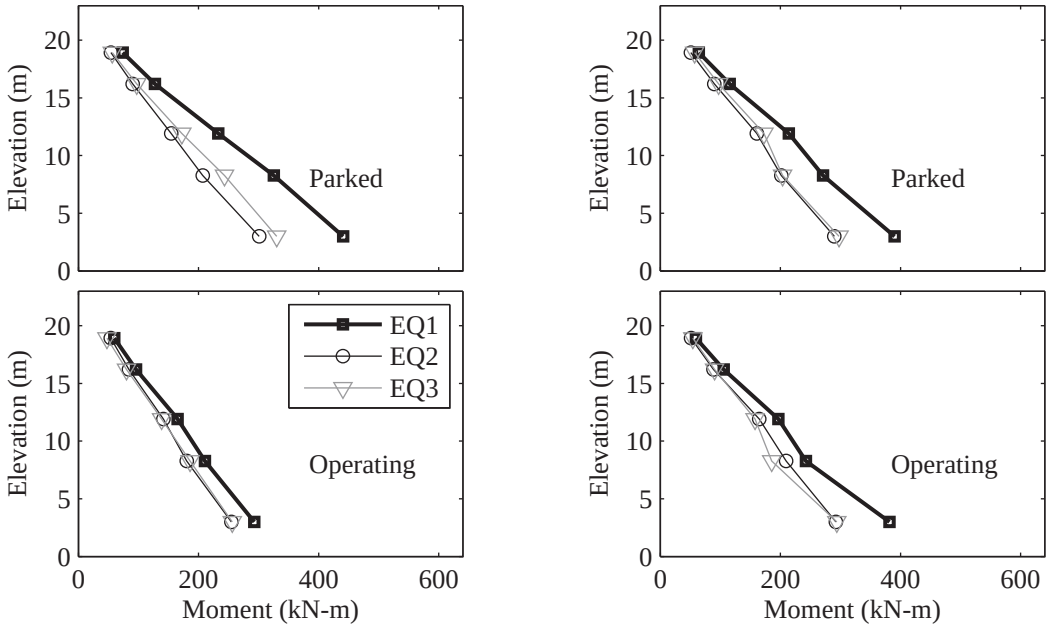

(a) Configuration 1

(b) Configuration 2

Figure 3.34: Observed moment envelope (Test indices 8, 10, and 13 for configuration 1 while parked. Test indices 9, 11, and 14 for configuration 1 while operating. Test indices 3, 5, and 1 for configuration 2 while parked. Test indicies 4, 2, and 6 for configuration 3 while operating)

analyzed (Figure 3.35).

Figure 3.26 shows that for parked conditions, EQ1 exhibited an envelope primarily influenced by the first tower bending mode, while EQ2 and EQ3 showed contributions from second modes. When the turbine in configuration 1 for EQ1 there is a clear reduction, indicated by reduced peak acceleration at the tower top, in the influence of the first mode. For motions EQ2 and EQ3 a similar trend is observed, but not as obvious due to more significant contributions from of the higher tower bending modes. In configuration 2, the trends are less obvious, but there is not a clear reduction in tower top acceleration for any of the motions.

To assess relative contribution of each mode to the tower moment demand

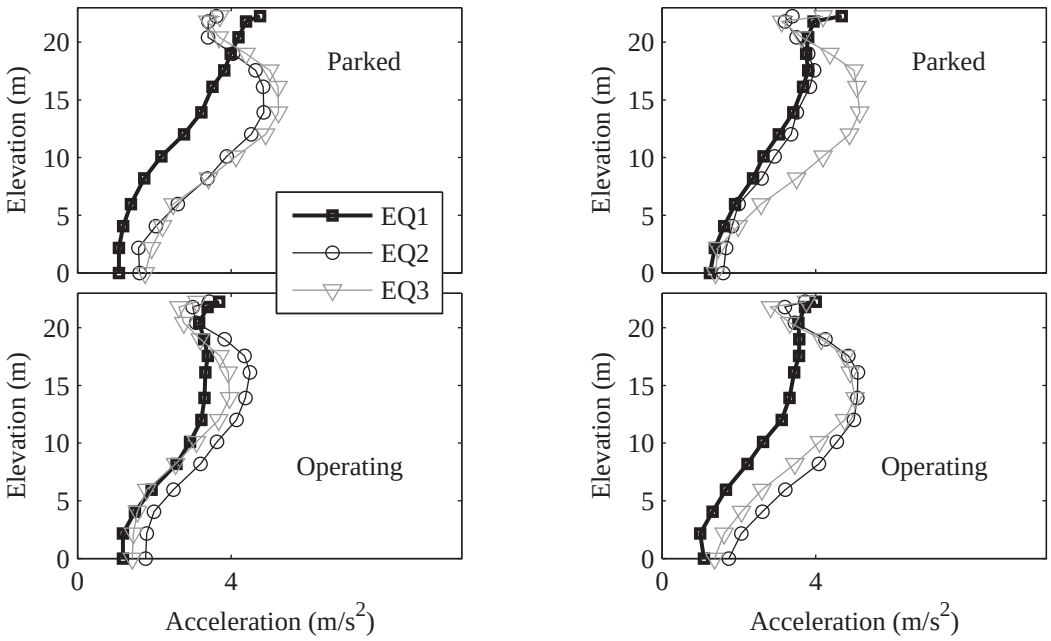

(a) Configuration 1

(b) Configuration 2

Figure 3.35: Observed acceleration envelope (Test indices 8, 10, and 13 for configuration 1 while parked. Test indices 9, 11, and 14 for configuration 1 while operating. Test indices 3, 5, and 1 for configuration 2 while parked. Test indicies 4, 2, and 6 for configuration 3 while operating)

due to in plane vibration the power spectral density (PSD) is presented in Figure 3.36. The moment profile for all experimental tests shows that demand is primarily driven by the response of the turbine in the first mode. As shown by other indicators the relative contribution of the first mode is reduced for configuration 1 while the turbine is operating. While the turbine is operating in configuration 2, an additional peak is noticed at the frequency of rotation of the rotor (1P) which is likely due to a slight difference in the blade weights causing an imbalanced rotor. For higher mode influence there appears to be little difference between the parked and operating conditions.

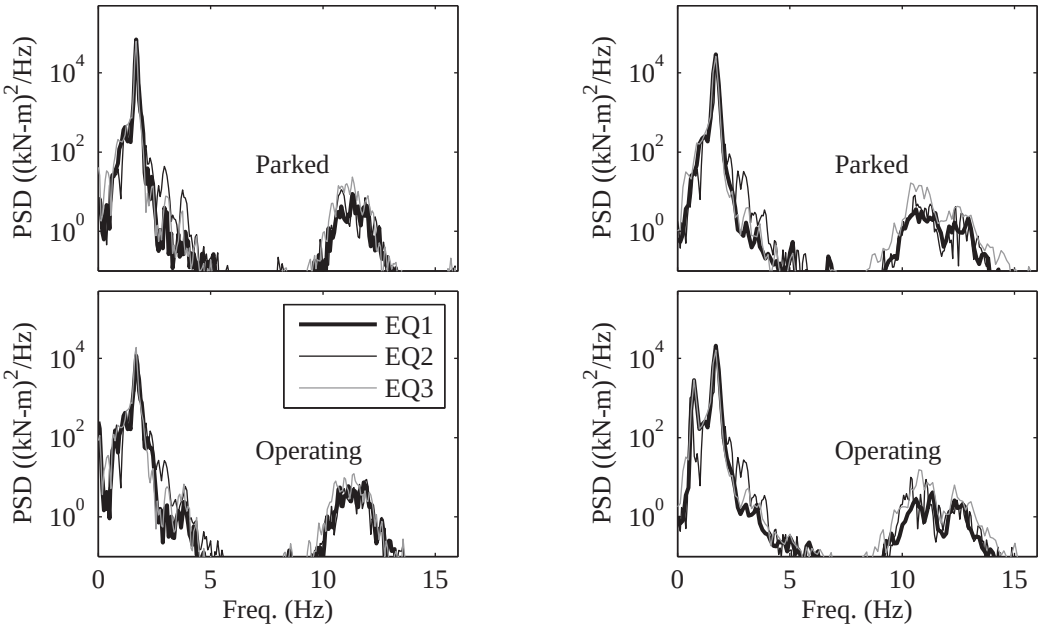

(a) Configuration 1

(b) Configuration 2

Figure 3.36: Observed PSD of in-plane base moment demand (log scale)

3.11 Discussion

The experimental results presented above support the following observations:

1. The experimentally derived first side-to-side frequency, mode shape, and damping estimates reinforce previous test results (Prowell et al., 2009b). More extensive in-plane instrumentation, the addition of out-of-plane instrumentation, and a systematic test program including motions parallel and perpendicular to the rotor's axis of rotation allowed more extensive characterization of the turbine's dynamic properties. Both fore-aft and side-to-side vibration modes were identified. With the higher density and out-of-plane instrumentation, the previously observed band of higher resonance was resolved into three second bending type modes (Figure 3.21): a coupled mode at 11.2 Hz; a fore-aft mode at 11.9 Hz;

and a side-to-side mode at 12.5 Hz.

2. Addition of prolonged white noise shaking between each test run provided a consistent method to identify the system dynamic characteristics (Figure 3.23). Extended record length and augmented high frequency content allowed more accurate estimation and insight into the variability of modal characteristics, such as frequency, mode shapes, and viscous damping. Observed consistency shows that, as expected, the 25% DBE motions did not damage the turbine tower. When the specimen dynamic characteristics changed, this methodology allowed identification and quantification of the extent of structural softening.

3. Observed spalling and deterioration of the grout at the turbine base show that the connection detail between the tower base and the foundation is important to seismic performance. Damage at the level observed in testing would remove the turbine from service and require time consuming repairs to the foundation.

4. Out-of-plane response occurred at a similar level for both orientations of shaking, but did not influence peak moment demand due an offset between maxima. However, in real situations where shaking occurs in multiple directions with the possibility of wind and operational loads, out-of-plane coupling may be important.

5. In agreement with previous findings (Ishihara and Sawar, 2008; Prowell et al., 2009b), the seismic response of smaller turbines is primarily governed by the first mode response. A simple procedure is suggested to estimate maximum relative displacement for a parked turbine similar to the tested unit. However,

the acceleration envelope for motions that were richer in high frequency energy showed excitation of higher modes. For large turbines, where periods of higher modes occur in the range that earthquake excitation typically produces significant spectral response (approximately 0.1 to 0.6 seconds as shown in Figure 3.3), demand parameters may have a more significant higher mode contribution (ICC, 2006; Häenler et al., 2006).

6. Numerical modeling of megawatt scale and larger turbine foundation soil systems, has indicated that soil structure interaction may also be an important consideration for these larger turbines (Prowell et al., 2009a, 2010b). For these reasons, it is important that modeling of modern turbines be able to simulate higher mode effects.

7. The turbine was able to accommodate base motions with S_a (f = 1.7 Hz and 5% damping) of the order of 2.04 g without exceeding the moment capacity of 3,200 kN-m. This level is 36% higher than the assumed MCE level of 1.5 g and exceeds the maximum MCE level in the US considered by the IBC (ICC, 2006) except in the immediate vicinity of known active faults (excluding consideration of modification for local soil conditions where acceleration can be increased by a factor as high as 3.5).

8. For consideration of extreme loads where a turbine is subject to both wind and seismic loads, results show that it is important to consider the orientation of shaking and aerodynamic damping. To ensure conservatism, seismic simulations would need to neglect any contribution of aerodynamic damping and resulting

demand would need to be directly added to loads derived from other sources. Such an approach may lead to overly large design loads for turbines located in seismic regions and add significant pressure to the economic feasibility of wind energy in such areas.

3.12 Conclusion

Experimental results from this full-scale test of a 65-kW turbine are presented and analyzed. The test protocol was designed to augment the results from a previous test and from a callibrated FE model. Key additions were: multiple test motions at multiple levels of shaking, more extensive in-plane and additional out-of-plane instrumentation, and multiple test configurations and operational states.

The results from this set of tests reinforce past experimental and numerical findings. The experimental results were analyzed and presented to show that additional damping appears to only be significant for first mode response to fore-aft shaking (configuration 1). For turbines similar to the tested unit, a simple procedure is suggested to estimate tower top displacement and, with knowledge of lateral stiffness, base shear demand. With a proper consideration of the base rocking, the measured reduction in global stiffness was split into contributions from structural softening and loss of stiffness in the base connection. Degradation of the connection between the tower and foundation was identified as a possible and undesirable damage mechanism. In addition, higher mode response, important for seismic loading of larger turbines, was successfully captured and illustrated. For consideration of com-

bined wind and earthquake loads, it is shown that relative orientation influences the dynamic response of a turbine.

3.13 Acknowledgements

The text below is reproduced verbatim as it appears in the acknowledgments section on page xvii per the UCSD Office of Graduate Studies Formatting Requirements.

Chapter 3 of this dissertation contains material from the following two papers under preparation for publication: (1) tentatively titled "Shake Table Testing of a Utility Scale Wind Turbine" with a preliminary author list of Ian Prowell, Chia-Ming Uang, Ahmed Elgamal, J. Enrique Luco, and Lanhui Guo, (2011) and (2) tentatively titled "Shake Table Testing of a Utility Scale Wind Turbine Including Operational Effects" with a preliminary author list of Ian Prowell, Ahmed Elgamal, Chia-Ming Uang, J. Enrique Luco, Hal Romanowitz, and Ed Duggan (2011). The dissertation author is the first author of these papers.

Bibliography

AISC (2005). *Steel Construction Manual 13th Edition*. American Institute of Steel Construction, Inc., Chicago, Illinois, USA.

ATC (2009). "Quantification of building seismic performance factors." *Report No. FEMA P695*, Federal Emergency Management Agency.

Chopra, A. K. (2006). *Dynamics of Structures: Theory and Application to Earthquake Engineering*. Prentice-Hall, Upper Saddle River, New Jersey, USA.

CSI (2005). *Users Manual, Version 10*. Computers and Structures, Inc., Berkeley, California, USA.

Häenler, M., Ritschel, U., and Warnke, I. (2006). "Systematic modelling of wind turbine dynamics and earthquake loads on wind turbines." *European Wind Energy Conference and Exhibition*, Athens, Greece. European Wind Energy Association, 1–6.

Hau, E. (2006). *Wind Turbines*. Springer, Berlin, Germany.

ICC (2006). *International Building Code 2006*. International Code Council, Country Club Hills, Illinois, USA.

IEC (2005). *IEC 61400-1 Ed. 3: Wind Turbines - Part 1: Design Requirements*. International Electrotechnical Commission, Geneva, Switzerland.

Ishihara, T. and Sawar, M. W. (2008). "Numerical and theoretical study on seismic response of wind turbines." *European Wind Energy Conference and Exhibition*, Brussels, Belgium. European Wind Energy Association, 1–5.

James III, G. H., Carne, T. G., and Lauffer, J. P. (1992). "The natural excitation technique (NExT) for modal parameter extraction from operating wind turbines." *Report No. SAND92-1666, UC-261*, Sandia National Laboratories.

Jonkman, B. J. (2009). "TurbSim user's guide: Version 1.50." *Report No. NREL/TP-500-46198*, National Renewable Energy Laboratory.

Jonkman, J. M. and Buhl Jr., M. L. (2005). "FAST user's guide." *Report No. NREL/EL-500-38230*, National Renewable Energy Laboratory.

Juang, J. N. and Pappa, R. S. (1985). "An eigensystem realization algorithm for modal parameter identification and model reduction." *Journal of Guidance, Control, and Dynamics*, 8(5), 620–627.

Luco, J. E. (1980). "Soil-structure interaction and identification of structural models." *Proceedings of the 2nd ASCE Specialty Conference in Civil Engineering and Nuclear Power*, Knoxville, Tennessee, USA. American Society of Civil Engineers, 10–1–1–10–1–30.

Luco, J. E., Ozcelik, O., and Conte, J. P. (2010). "Acceleration tracking performance of the UCSD-NEES shake table." *Journal of Structural Engineering*, 136(5), 481–490.

Luco, J. E., Trifunac, M. D., and Wong, H. L. (1987). "On the apparent change in dynamic behavior of a nine-story reinforced concrete building." *Bulletin of the Seismological Society of America*, 77(6), 1961–1983.

Prowell, I., Elgamal, A., Jonkman, J., and Uang, C.-M. (2010a). "Estimation of seismic load demand for a wind turbine in the time domain." *Report No. NREL/CP-500-47536*, National Renewable Energy Laboratory.

Prowell, I., Elgamal, A., and Lu, J. (2010b). "Modeling the influence of soil structure interaction on the seismic response of a 5MW wind turbine." *5th International Conference on Recent Advances in Geotechnical Earthquake Engineering and Soil Dynamics*, San Diego, California, USA. 1–8.

Prowell, I., Elgamal, A., Lu, J., and Luco, J. E. (2009a). "Modal properties of a modern wind turbine including SSI." *17th International Conference on Soil Mechanics & Geotechnical Engineering*, Alexandria, Egypt. International Society for Soil Mechanics and Geotechnical Engineering, 1–4.

Prowell, I., Schmidt, T., Elgamal, A., Uang, C.-M., Romanowitz, H., and Duggan, J. E. (2011a). "Measuring global response of a wind turbine to earthquake shaking assisted by point tracking videogrammetry." *52nd AIAA/ASME/ASCE/ASC Structures, Structural Dynamics and Materials Conference*, Denver, Colorado, USA. American Institure of Aeronautics and Astronautics.

Prowell, I., Uang, C. M., and Elgamal, A. (2011b). "Shake table test of a utility-scale wind turbine." *Report No. SSRP-10-06*, Department of Structural Engineering, University of California, San Diego.

Prowell, I. and Veers, P. (2009). "Assessment of wind turbine seismic risk: Existing literature and simple study of tower moment demand." *Report No. SAND2009-1100*, Sandia National Laboratories.

Prowell, I., Veletzos, M., Elgamal, A., and Restrepo, J. (2009b). "Experimental and numerical seismic response of a 65kW wind turbine." *Journal of Earthquake Engineering*, 13(8), 1172–1190.

Restrepo, J. I., Conte, J. P., Luco, J. E., Seible, F., and Van Den Einde, L. (2005). "The NEES@UCSD large high performance outdoor shake table earthquake engineering and soil dynamics (gsp 133)." *Proc. Geo-Frontiers 2005, Sessions of the Geo-Frontiers 2005 Congress*, R. W. Boulanger, M. Dewoolker, N. Gucunski, C. H. Juang, M. E. Kalinski, S. L. Kramer, M. Manzari, and J. Pauschke, eds., Austin, Texas, USA.

Witcher, D. (2005). "Seismic analysis of wind turbines in the time domain." *Wind Energy*, 8(1), 81–91.

Zhao, X. and Maißer, P. (2006). "Seismic response analysis of wind turbine towers including soil-structure interaction." *Proceedings of the Institution of Mechanical Engineers, Part K: Journal of Multi-body Dynamics*, 220(1), 53–61.

Zhao, X., Maißer, P., and Jingyan, W. (2007). "A new multibody modeling methodology for wind turbine structures using a cardanic joint beam element." *Renewable Energy*, 32(3), 532–546.

Chapter 4

In-situ Ambient Vibration Study of a 900-kW Wind Turbine

4.1 Introduction

Field measurement is a reliable approach for determining the dynamic properties of a structure (e.g., natural frequencies, damping ratios, and mode shapes). These dynamic characteristics serve as a basis for validating analytical models so that actual structural properties and in turn structural demand may be numerically reproduced for seismic evaluations (Häenler et al., 2006; Witcher, 2005; Prowell et al., 2010b). Furthermore, vibration-based structural health monitoring relies heavily on the dynamic characteristics extracted from actual measurements (Doebling et al., 1996; Sohn et al., 2002; Rolfes et al., 2007).

Tests of structures may be conducted to monitor ambient vibrations or forced response. Forced vibration tests are directly related to the application of classical

experimental modal analysis (Ewins, 2000), in which the structure is usually excited by an external agent, such as eccentric or linear inertial shakers (Halling et al., 2001; Brownjohn et al., 2003; Yu et al., 2005) or drop weights (Abdel Wahab and Roeck, 1998). Earthquake excitation (when measured) provides a natural source of forced vibration for civil structures (Smyth et al., 2003), but no such recordings are currently available for turbines.

A sudden impact on the structure induces a condition of free vibration. In earlier experimental studies, various techniques have been employed to generate impact type loads in dynamic testing of vertical axis wind turbines (VAWT). For example, in a study by Lauffer et al. (1988), the impulsive force was generated by the sudden release of a tension cable that connected the turbine to a ground anchor. In another study for a VAWT by Carne and Nord (1983), a similar tension cable was used, but developed the tension between the turbine blade and the supporting tower which allowed the impulse to be applied during operation.

In general, forced vibration tests provide more accurate modal identification results than ambient vibration tests, since (a) well-defined input excitations are used, and (b) the excitations can be optimized to enhance the response of the vibration modes of interest. For a small 11-kW horizontal axis wind turbine (HAWT), a good example of this approach was recently presented (Molinari et al., 2010). An instrumented hammer and accelerometers distributed along the tower height provided direct information on the frequency response function (FRF) for a 2-bladed downwind turbine with an 18 m tall tower and 13 m rotor diameter. In the results from Molinari et al. (2010), experimental readings agreed with numerical predictions that, due

to turbine geometry, independent fore-aft and side-to-side modes are often at near identical frequencies (Häenler et al., 2006; Jonkman et al., 2009; Zhao et al., 2007). However, in the case of large turbines with natural frequencies of the fundamental mode in the range 0-1 Hz (Häenler et al., 2006; Witcher, 2005; Jonkman et al., 2009; Bazeos et al., 2002; Lavassas et al., 2003; Ritschel et al., 2003; Prowell and Veers, 2009), it is challenging and costly to provide controlled excitation at an amplitude that would result in a significant level of response.

In contrast, ambient vibration monitoring takes advantage of natural excitation sources such as traffic, wind, micro-tremors, and combinations thereof. Moreover, since ambient vibration tests do not interrupt service of the test structure, they can be used readily for long term continuous structural health monitoring applications (Rolfes et al., 2007) as well as for identifying the dependency of modal properties on operational state. Ambient vibration tests have been successfully applied to a VAWT by Sandia National Laboratories (James III et al., 1992). In this study, system identification based on ambient vibration test data provided accurate estimates of natural frequencies and mode shapes despite the relatively low amplitude of the measured vibrations. Even though modal damping ratios/factors can be satisfactorily identified using ambient vibration data, they may require the use of advanced system identification methods due to the low amplitude and relatively low signal-to-noise ratio of such data. As such, results on identification of modal damping ratios using ambient vibration data are scarce. Also, damping ratios estimated from linear system identification techniques may depend significantly on amplitude of excitation and therefore on the level of structural response.

This chapter describes a set of dynamic tests performed on a 900-kW HAWT (Figure 4.1) located at Oak Creek Energy Systems near Mojave, California (Figure 4.2). The tests monitored structural vibrations using an array of up to 81 force-balanced accelerometer channels from the mobile field laboratory of the George E. Brown, Jr. Network for Earthquake Engineering Simulation (NEES) field testing site at the University of California, Los Angeles (NEES@UCLA). These accelerometers were installed at stations in the turbine tower, on the foundation, and in the surrounding soil. Instead of relocating accelerometers to the different measurement stations with some accelerometers fixed at one or more reference stations (as commonly done for dynamic testing of large structures), acceleration response was recorded simultaneously, including vertical, side-to-side, and fore-aft motion components at each fixed station. For the parked situation, sources of excitation are limited to the wind and vibration transmitted through the ground. In contrast, when the turbine is operating, harmonic narrow band vibration is transmitted throughout the structure from the periodic spinning of the rotor (Figure 4.1(b)) and other rotating components. These dynamic field tests are the first to be presented for such a highly instrumented modern HAWT. Therefore, this test series provides a unique opportunity to determine the dynamic properties of the turbine under in-situ conditions for both parked and operating conditions.

The scope of this chapter is three-fold: (1) describe the dynamic field tests performed on the turbine including the sensor network/array, data acquisition system, and dynamic test procedure; (2) present modal identification results obtained using an output-only system identification method applied to the observed vibration; and

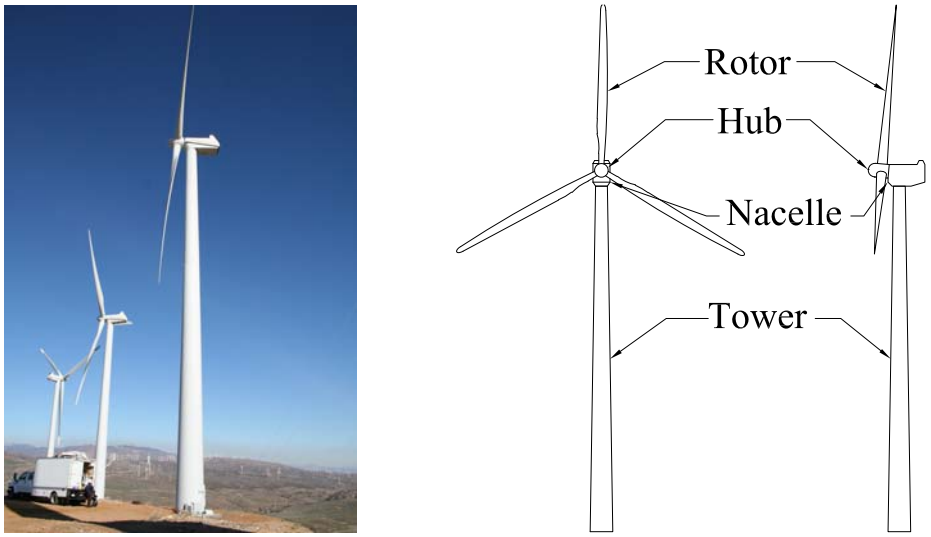

(a) Tested turbine (54m tower) (b) Components of a wind turbine

Figure 4.1: 900-kW wind turbine at Oak Creek Energy Systems

Figure 4.2: Oak Creek Energy Systems location (from Google™ Maps)

(3) calibrate a representative finite element (FE) model using the experimental modal analysis results. In the following, Section 4.2 describes the turbine tested; Section 4.3 describes the sensor layout and data acquisition system used in the dynamic tests; Section 4.4 describes the system identification method used; Section 4.5 presents a summary of the modal identification results obtained; Section 4.6 presents results of vibration tests conducted on one of the rotor blades; Section 4.7 presents a FE model of the tested turbine; Section 4.8 compares the experimental results with those obtained numerically and discusses the implication of these results for seismic loading of wind turbines; and Section 4.9 provides concluding remarks.

4.2 Description of Turbine

A 900-kW turbine (Figure 4.1) installed at Oak Creek Energy Systems (OCES) near Mojave, California, USA, is selected for in-situ measurements. This turbine size (Table 4.1) is characteristic of units installed in the 1990s (Wiser and Bolinger, 2008). The turbine is a fixed pitch machine where the angle of incidence between the blades and the wind is constant while speed is regulated at 14 revolutions per minute (RPM) in low wind conditions and 22 RPM in higher wind speeds by adjusting the generator power draw. Slowing and shutdown of the rotor is assisted by actively controlled tip brakes. In contrast, most multi-megawatt turbines primarily regulate rotor speed through full pitch control of the blades (Jonkman et al., 2009; Malcolm and Hansen, 2006). To follow variation in the wind direction, motors yaw the entire rotor and nacelle to face into the wind.

Table 4.1: 900-kW Wind Turbine Characteristics

Type	Horizontal axis wind turbine
Nominal power	900-kW
Rotor diameter	53.6 m
Tower height	54 m
Hub height	55 m
Operational Speed	14/22 RPM
Mass of nacelle	23,000 kg
Mass of rotor	18,300 kg
Mass of tower	68,700 kg

The tested turbine is installed on a patented foundation, known as the Patrick and Henderson Tensionless Pier (Henderson and Patrick, 1994). The design is a 3.5-m diameter hollow concrete cylinder that extends 9 meters below ground surface, capped on each end by a concrete slab with soil filling the central region in between. Anchoring the turbine to the foundation, are post tensioned steel rods that extend through the concrete to the cylinder base. The foundation is installed in a layered stratum where the upper 2 meters are a sandy soil with a drained friction angle of about 40 degrees, underlain by dense silty sands and clayey sands. Using empirical relations for standard penetrometer test (SPT) results from geotechnical investigations throughout OCES, it is estimated that the shear wave velocity at the site is approximately 300 to 400 m/s near the surface and increases to 400 to 650 m/s at 10 meters below ground surface (Ohta and Goto, 1978).

4.3 Description of Instrumentation and Data Acquisition System

4.3.1 NEES@UCLA Data Acquisition Equipment

Equipment from NEES@UCLA was used to monitor vibrations of the wind turbine. The NEES@UCLA field mobile laboratory deployed for this study consisted of:

1. EpiSensor accelerometers from Kinemetrics Inc. including both EpiSensor ES-U (uni-axial) and EpiSensor ES-T (tri-axial). The EpiSensor force-balanced accelerometers have a wide frequency bandwidth from DC (i.e., 0 Hz) to 200 Hz, a large amplitude range (user selectable at ±0.25 g to ±4.0 g) set at ±4.0 g for these experiments, and a broad dynamic range (140 dB+ for ES-U and 155 dB+ for ES-T). The significant bandwidth allows for the study of motions at higher frequencies while maintaining the very important low frequency and DC response needed in field calibration, in post-processing of the data (e.g., double integration of acceleration records) and in studying the low frequencies predominant in large modern turbines (Häenler et al., 2006; Witcher, 2005; Jonkman et al., 2009; Lavassas et al., 2003).

2. Quanterra Q330 data loggers from Kinemetrics, Inc., to provide signal conditioning, analog to digital conversion, time synchronization across multiple nodes using GPS (i.e., global positioning system), buffering, and IP-network (i.e., Internet Protocol network) communication capabilities via Ethernet for later con-

solidation into a single data file. The nominal performance specifications for the Q330 data loggers include 24-bit analog to digital (A/D) conversion, 135 dB dynamic range, and a time stamp (time synchronization) accuracy of less than 0.1 ms.

3. Kinemetrics Rockhound data acquisition software for monitoring and recording of data. The data concentration point, which consists of a conventional laptop and a network switch, aggregates and stores data from each of the Q330 nodes.

4. Mobile command center containing computing facilities, cellular Internet uplink, and equipment storage. Collectively, the NEES@UCLA field data acquisition system represents the state-of-the-art in vibration monitoring equipment. The accelerometers transmit differential analog voltage signals to the Q330 data loggers where they are digitized, time-stamped, and stored temporarily. From there, the data packets pass to the data concentration point (a laptop). In addition to permanently recording collected data, the laptop computer is also capable of observing the experiment in real-time. Figure 4.3 illustrates the logical topology of the NEES@UCLA field mobile laboratory.

4.3.2 Instrumentation Layout

Due to logistical reasons, two instrumentation configurations were used: one for the parked and another for the operational condition. In both configurations the mobile command center was located a suitable distance (approximately 100 m) from the turbine (Figure 4.1) to reduce the influence on recorded results.

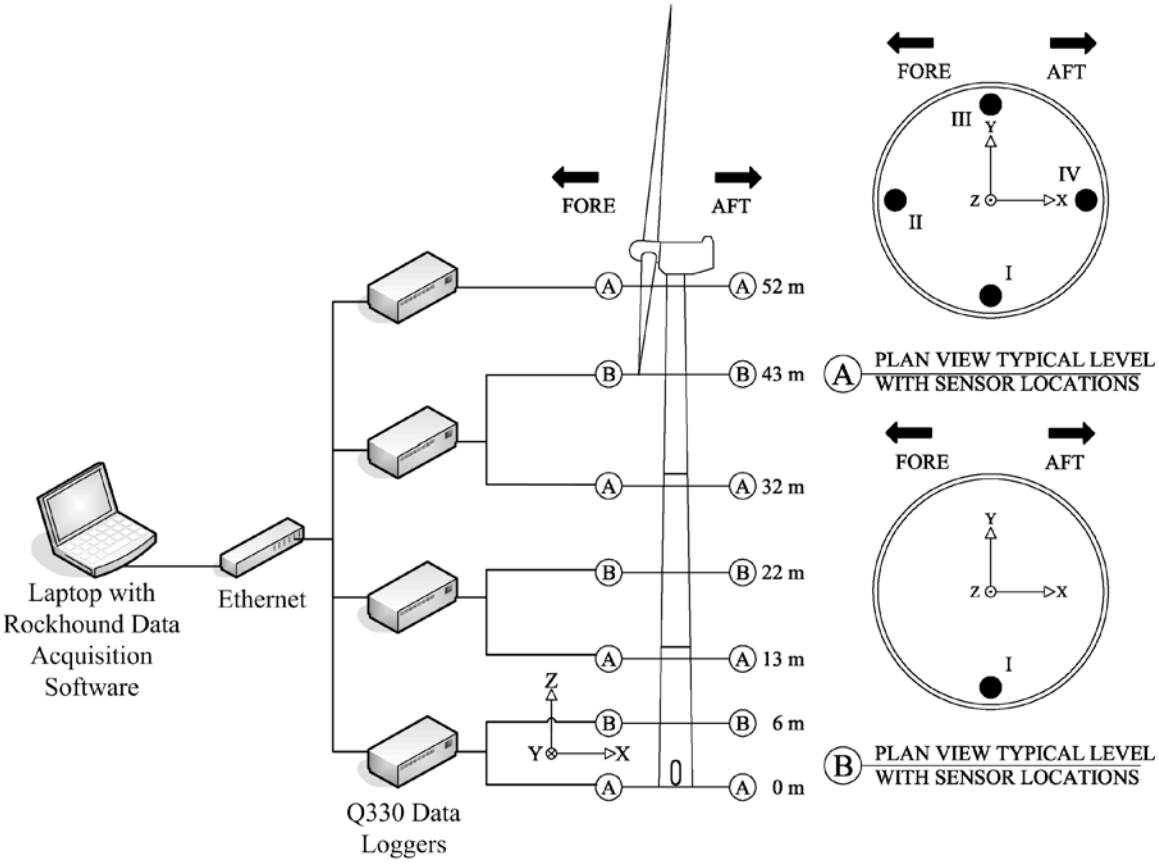

Figure 4.3: Logical diagram of NEES@UCLA data acquisition equipment and layout of accelerometers for 900-kW turbine

For the parked condition, stations were instrumented in six distinct elevations along the turbine tower (Figure 4.1(b)) at 15 locations (Figure 4.3) with either a single EpiSensor ES-T (tri-axial) or three EpiSensor ES-U (uni-axial, Figure 4.4) to measure vertical, side-to-side, and fore-aft vibrations. Each accelerometer was rigidly clamped to the turbine ensuring good coupling. An illustrative segment of the acceleration recorded from the tower stations is displayed in Figure 4.5. In addition to the tower stations, four locations on the surface of the foundation were instrumented with three uni-axial EpiSensor accelerometers (Figure 4.4) to capture translation and rocking of the base of the turbine. Eight stations on the ground, in concentric circles of 6

and 10 meters in diameter, were instrumented with a total of 24 EpiSensor ES-U accelerometers (three uni-axial accelerometers at each of eight stations) to measure the response of the surrounding soil. EpiSensor ES-U units were mounted to a rigid aluminum plate to ensure orthogonality. The soil accelerometers were recessed below the ground surface and covered to reduce extraneous vibration.

Figure 4.4: 3 Epi-Sensor ES-U units mounted to capture three orthogonal axes

Due to operational scheduling logistics, only data from a preliminary reduced set of instrumentation consisting of a total of 10 EpiSensor ES-T accelerometers was available for the operational condition. Tower instrumentation was present at 13 m, 32 m, 43 m, and 52 m. The foundation surface was monitored at 2 stations and an additional 3 stations were located in the surrounding soil in a line parallel to the wind. For the operational condition, Figure 4.6 shows a sample of recorded vibration in the turbine tower. The corresponding auto power spectra (APS) for the parked and operating conditions are shown in Figures 4.7 and 4.8, respectively. The procedure used to calculate cross and auto power spectra will be described in Section 4.4. All data analyzed here will be publically available on the NEES data archive at http://www.nees.org.

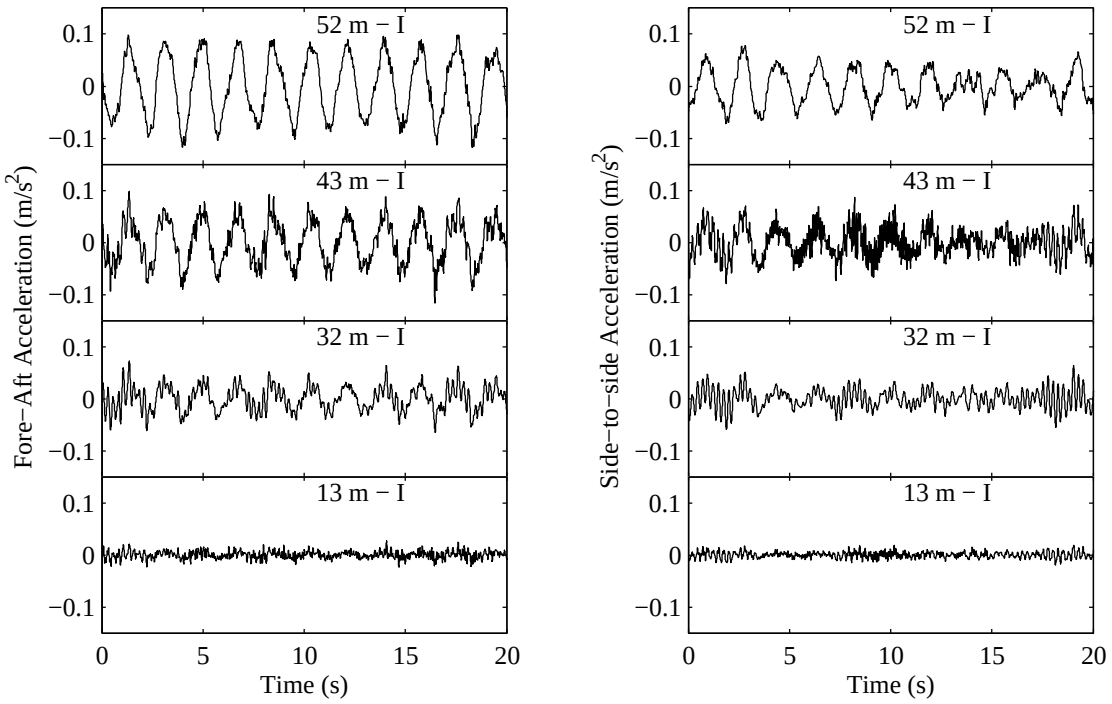

Figure 4.5: Acceleration measured for 900-kW turbine while parked

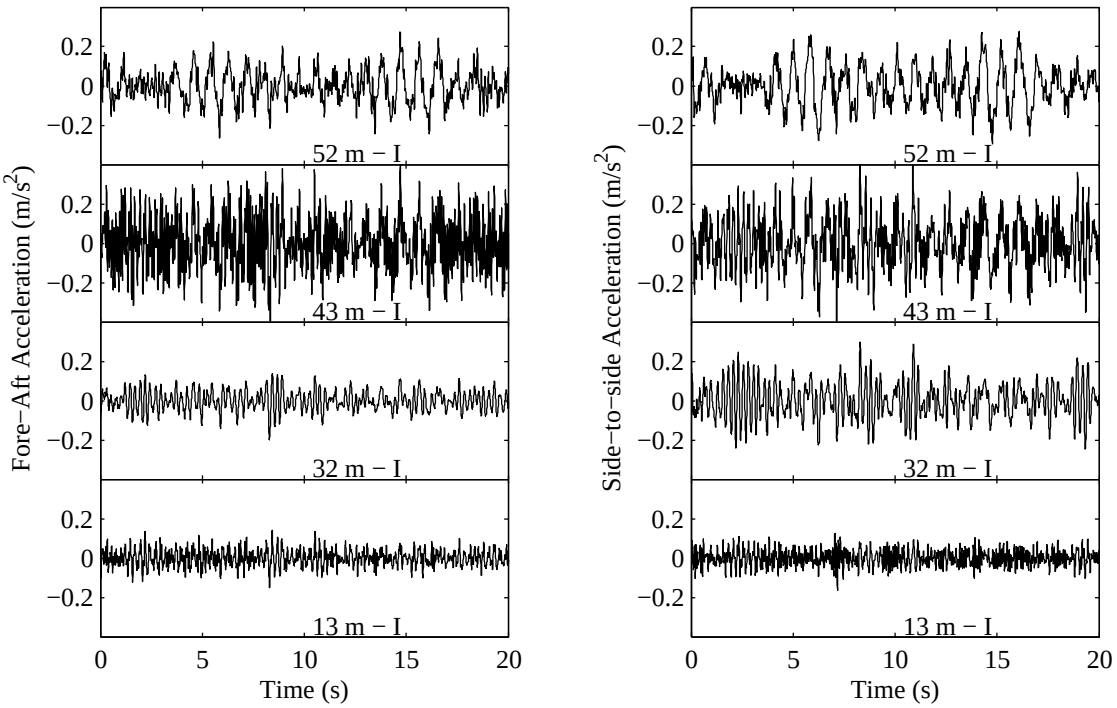

Figure 4.6: Acceleration measured for 900-kW turbine while operating at 22 RPM

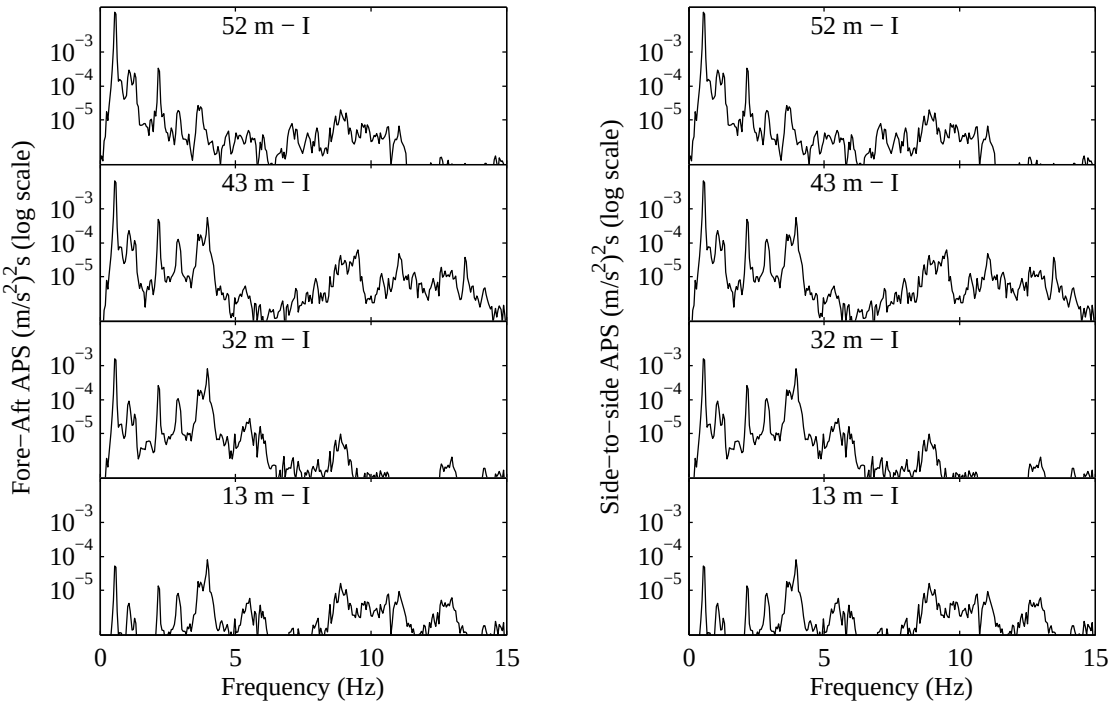

Figure 4.7: Acceleration APS for 900-kW turbine while parked

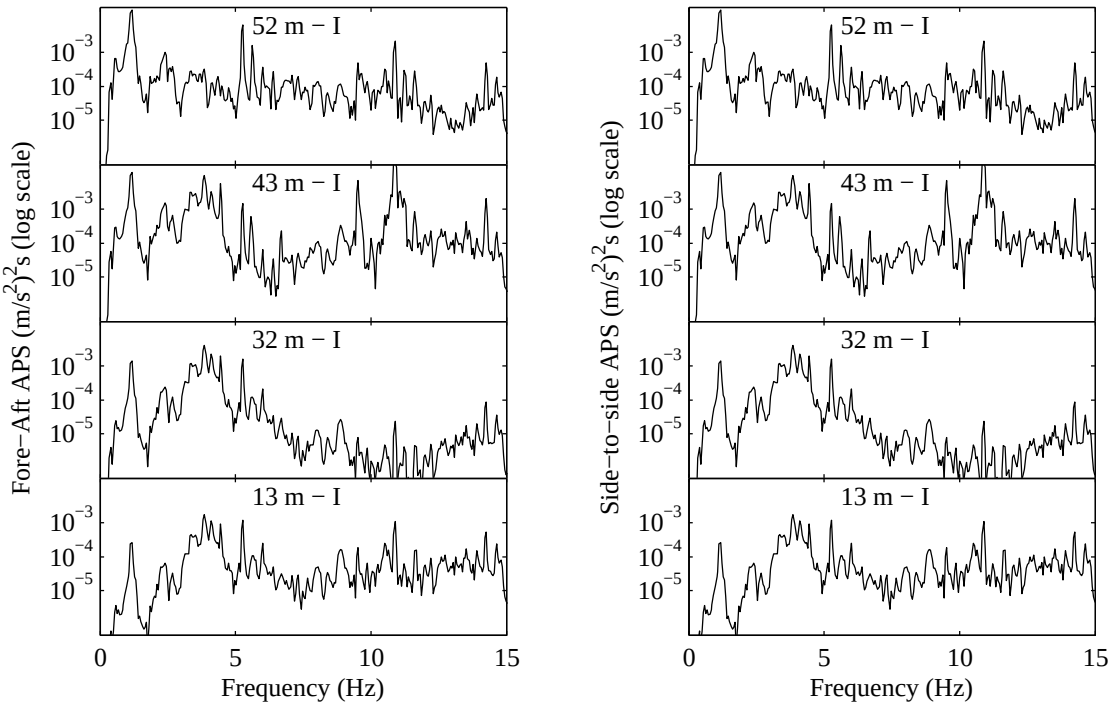

Figure 4.8: Acceleration APS for 900-kW turbine while operating at 22 RPM

4.4 Modal Identification Using MNExT-ERA

The FRF can be calculated for situations where the excitation input is known, such as forced vibration tests. However, for ambient vibration tests with unknown input excitation, output-only system identification procedures prove essential to obtain useful results (James III et al., 1992; Ibrahim and Mikulcik, 1977; Brown et al., 1979; Van Overschee and De Moor, 1996; Peeters and De Roeck, 2001). Instead of comparing the response of the structure to a known input, output-only methods work without specific knowledge of the excitation. By carefully observing the system vibrations, one is able to infer dynamic properties such as natural frequencies and mode shapes. Output-only methods assume broad-band excitation(s) and if used outside this assumption may lead to erroneous results.

The output-only method selected for this analysis, Multiple-Reference Natural Excitation Technique (MNExT) (He et al., 2009) combined with the Eigensystem Realization Algorithm (ERA) (Juang and Pappa, 1985), is an extension of the Natural Excitation Technique (NExT) combined with ERA (James III et al., 1992). The NExT algorithm is based on calculating cross correlation functions of measured response data with a reference channel selected such that the location does not coincide with nodes in the expected mode shapes (James III et al., 1992). To increase the likelihood of identifying additional modes, MNExT-ERA uses cross correlation functions with multiple reference channels to further reduce the possibility that all references coincide with a modal node (He et al., 2009). In the implementation of MNExT-ERA discussed here, Welch's method (Welch, 1967) was first used to estimate cross power

spectra (CPS), which were converted through an inverse discrete Fourier transform to cross correlation functions. In the second step, ERA (Juang and Pappa, 1985) was employed to extract estimates of natural frequencies, damping, and mode shapes from the cross correlation functions.

As part of ERA (Juang and Pappa, 1985), a parameter (system order) was determined to separate actual from spurious modes. The system order, n, must be at least twice the number of modes assumed present in the data. For example, with a system order of 10, the parameters of at most five modes can be estimated. As is standard practice, modal parameters were calculated by increasing the system order in steps of 2 until the results for modes of interest converge according to a defined set of stability criteria (Peeters and De Roeck, 2001; Allemang, 1999), as described below. At the selected system order, only stable estimates (consistently identifiable in lower order systems) are considered reliable.

In applying MNExT-ERA, the recorded dataset was first band pass filtered (0.25 to 20 Hz pass band) then divided into multiple 1 minute segments. Each segment was used to produce an estimate of modal parameters. To reduce duplication and improve frequency resolution (Allemang, 1999; Harris, 1978), the segments were each divided into five overlapping data slices and windowed using a Kaiser-Bessel window. The cross power spectrum of each data channel was then calculated with each of six reference channels (located at 13, 24, and 52 m elevations in the side-to-side and fore-aft directions) and averaged across the data slices. For the parked condition, a sample of cross power spectra from selected channels is shown in Figure 4.9. With all modes of interest in this investigation below 25 Hz, cross correlation functions were

calculated and down sampled to 50 Hz, the required frequency required to resolve 25 Hz signals, to expedite computation of modal parameter estimation using ERA (He et al., 2009; Juang and Pappa, 1985).

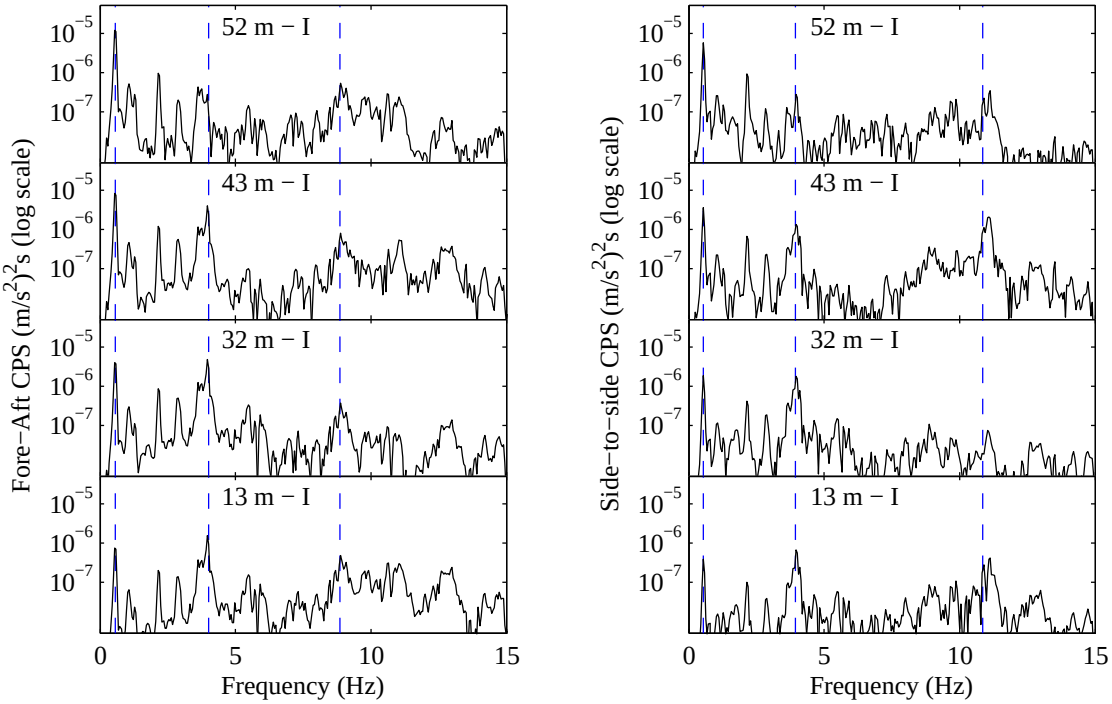

Figure 4.9: Cross power spectra (CPS) with base motion (0 m - I) as input for 900-kW turbine under parked condition

Using stability criteria, an automated procedure was defined to select the system order for each ERA estimate (Fraser et al., 2010). Stability was defined by two rules; stability in natural frequency within 1% and a modal assurance criterion (MAC) exceeding 0.95 between estimates (Allemang and Brown, 1982; Allemang, 2003). Informed by anticipated ranges from previous experimental investigations of wind turbines and other structures (Carne and Nord, 1983; Fraser et al., 2010; Hansen et al., 2006; Murakawa et al., 1996), estimates were considered only if damping values fell between 0% and 50% of critical damping. For this investigation, the minimum

system order that produced highly consistent results, satisfying the above criteria at least 10 consecutive system orders, for identified modes was selected (Peeters and De Roeck, 2001; Allemang, 1999; Fraser et al., 2010). The results that did not satisfy stability criteria at the selected system order were discarded.

In consideration of the previously discussed tendency for turbines to have both fore-aft and side-to-side modes at closely spaced frequencies (Häenler et al., 2006; Molinari et al., 2010; Jonkman et al., 2009; Zhao et al., 2007), the mode shape, in addition to natural frequency was used to sort estimates from each 1 minute segment into similar modes for evaluating statistical properties (mean and standard deviation) of the modal properties. Estimates of modal parameters at each time segment were grouped into 1st, 2nd, and 3rd modes in the fore-aft and side-to-side directions such that: the natural frequency of each estimate matched the average natural frequency within 5% and the mode shape when compared to the average, produced a MAC exceeding 0.95 (Allemang and Brown, 1982; Allemang, 2003). A small number of outlying estimates where the damping deviated by more than 300% from the average were assumed to be erroneous and ignored (approximately 3%).

4.5 Results

4.5.1 900-kW Turbine Parked Condition Identification Results

Using 19 hours of data collected while the turbine was parked, 1,140 estimates of the turbines dynamic properties were performed. A summary of the average frequency, average damping, and standard deviation of the identified properties for the parked turbine is shown in Table 4.2. Resulting frequencies for the modes are visualized as dashed blue lines on the cross power spectra in Figure 4.9. Mode shapes were averaged across estimates and the resulting shapes are shown in Figures 4.10 through 4.12. The first bending modes occurred at a mean frequency of 0.54 Hz in the side-to-side direction (Figure 4.10(a)) and 0.56 Hz in the fore-aft direction (Figure 4.10(b)). The mean frequency of the second bending modes was observed as 3.94 Hz in the side-to-side direction (Figure 4.11(a)) and 4.00 Hz in the fore-aft direction (Figure 4.11(b)). A wider separation between the frequencies of the third bending modes was observed with the fore-aft direction at 8.86 Hz (Figure 4.12(a)) and the side-to-side mode at 10.9 Hz (Figure 4.12(b)). In the mode shape illustrations, the nacelle and rotor are shown for illustration only and are merely translated and rotated as a rigid body to match observed motion of the tower top. All visualized mode shapes include the stations instrumented in the soil, but consistent with the stiff soil at the site, little base translation or rocking is observed. It was found that base rotation contributed 1.8% and 1.6% the peak displacement at the top of the tower in the first bending

modes for fore-aft and side-to-side modes, respectively. Base translation contributed less than 0.2% of the observed peak displacement at the top of the tower for both fore-aft and side-to-side first bending modes. As such, this level of soil-structure interaction (SSI) can be considered to be small (Luco et al., 1988), albeit approximately twice that predicted by a preliminary numerical model of a similar turbine, foundation, and soil system (Prowell et al., 2009). Estimations of natural frequency showed little variation, whereas the modal damping estimates showed a significantly larger variation across all identified modes (Table 4.2). This relatively large variation in the damping is expected as damping estimates are inherently less stable and factors such as the wind speed can influence the results through aerodynamic damping (Riziotis et al., 2004).

Table 4.2: Summary of identified modal properties with 900-kW wind turbine in parked condition

Mode Type	Orientation	Illustration	Mean Freq.	Std. Dev. of Freq.	Mean Damping	Std. Dev of Damping
1st	Side-to-side	Fig. 4.10(a)	0.54 Hz	0.01 Hz	3.4%	1.2%
	Fore-aft	Fig. 4.10(b)	0.56 Hz	0.01 Hz	4.0%	1.4%
2nd	Side-to-side	Fig. 4.11(a)	3.94 Hz	0.03 Hz	1.0%	0.5%
	Fore-aft	Fig. 4.11(b)	4.00 Hz	0.03 Hz	0.9%	0.4%
3rd	Fore-aft	Fig. 4.12(a)	8.86 Hz	0.10 Hz	1.8%	0.7%
	Side-to-side	Fig. 4.12(b)	10.9 Hz	0.04 Hz	0.7%	0.4%

4.5.2 Identification Results for the 900-kW Wind Turbine Operating at 22 RPM

Next, modal parameter estimates were considered for the 1.5 hours when the turbine was operating at a constant 22 RPM with a relatively constant wind speed of

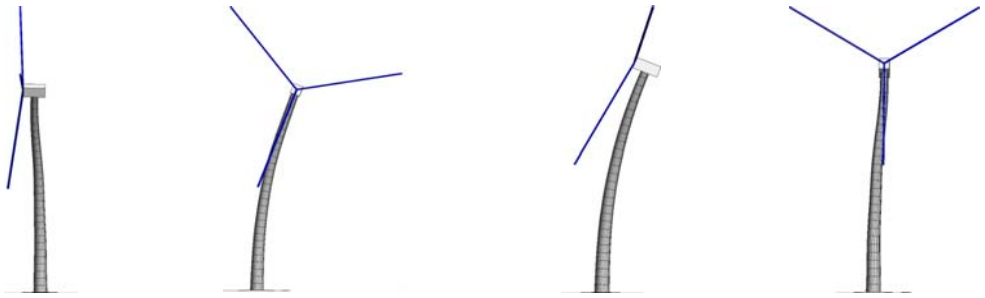

(a) Side-to-side at 0.54 Hz (b) Fore-aft at 0.56 Hz

Figure 4.10: 1st bending modes for 900-kW wind turbine in parked condition

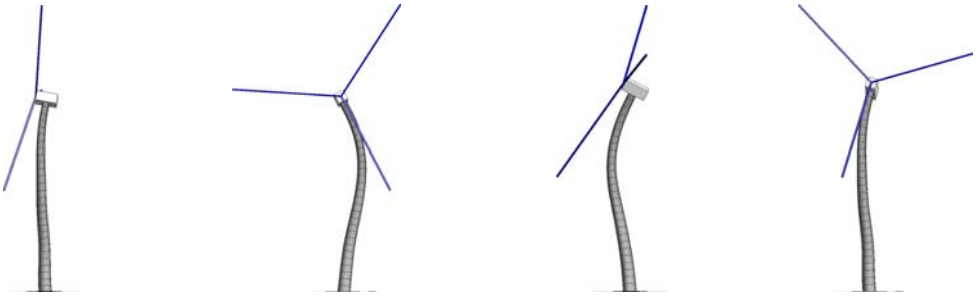

(a) Side-to-side at 3.94 Hz (b) Fore-aft at 4.00 Hz

Figure 4.11: 2nd bending modes for 900-kW wind turbine in parked condition

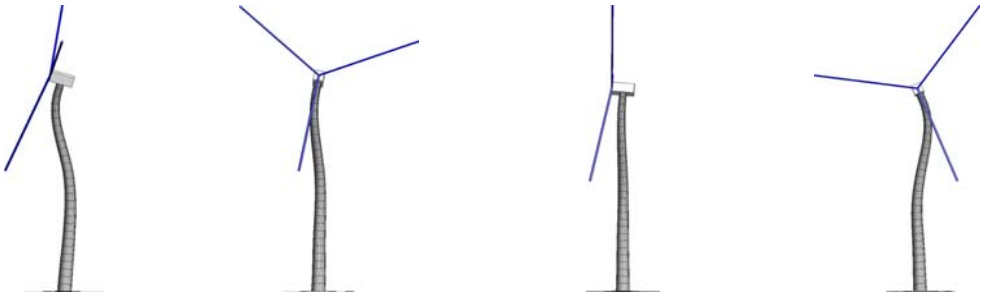

(a) Fore-aft at 8.86 Hz (b) Side-to-side at 10.9 Hz

Figure 4.12: 3rd bending modes for 900-kW wind turbine in parked condition

5.0 m/s with a standard deviation of 2.1 m/s. In the operational period investigated, yaw of the turbine was constrained to ±6 degrees and was assumed to have negligible influence on the reported results since this variation was within the accuracy of alignment of sensors and the rotor.

During this period, the turbine was not only vibrating in response to broad-band excitation such as the wind, but was also continually excited by narrow-band forcing at specific frequencies. In a wind turbine, the frequency of rotation of the rotor, 1P, and the blade passage frequency, 3P, are significant harmonic forcing sources. At a rotor speed of 22 RPM the 1P frequency is 0.37 Hz and the 3P frequency is 1.1 Hz. Visual inspection of the cross power spectra while operating (Figure 4.13) shows peaks at mechanical vibration frequencies and harmonics, indicated by the gray vertical lines. These peaks are consistent with other reported results for operating turbines (Molinari et al., 2010; James III et al., 1992). With no specific consideration of the mechanical forcing, the NExT-ERA algorithm interprets the vibration at these frequencies as a resonance (James III et al., 1992).

Without guidance, the results from the MNExT-ERA algorithm showed a spatial configuration, which represents the forced response of the turbine at 1.1 Hz (Figure 4.14(a) and Table 4.3). Spectral peaks due to the dynamic loading (rotation of the rotor) are interpreted as resonant peaks by MNExT-ERA. Other than the driven response at 1.1 Hz, no modes resembling a first bending mode were possible to identify. This is consistent with the theoretical response of a system to a harmonic excitation at a frequency away from a resonance (Chopra, 2006). Turbine system resonances must be kept separate from forcing frequencies to avoid self excitation

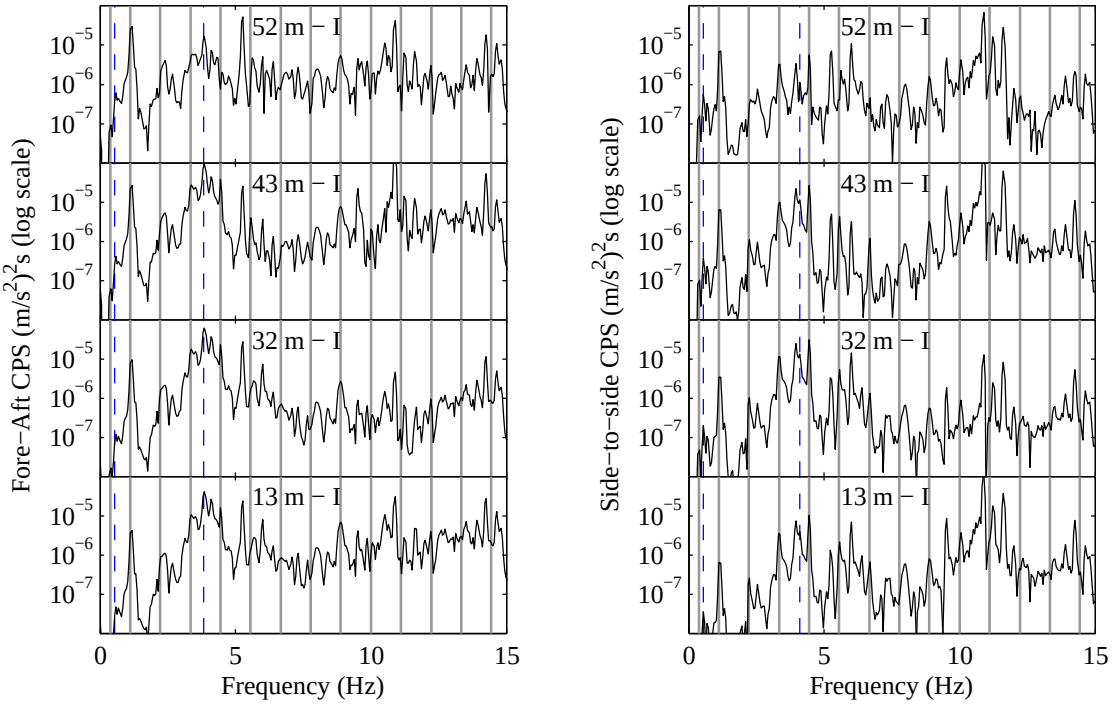

Figure 4.13: CPS with base motion (0 m - I) as input measured from 900-kW while operating at 22 RPM

and the observed behavior is evidence of successful execution of this design goal. A second forced vibration response (Figure 4.14(b) and Table 4.3) was observed at 4.53 Hz, approximately 4 times the blade passage frequency, or 12P.

Table 4.3: Identified response from mechanical excitation for 900-kW turbine

Harmonic of Rotor Speed	Illustration	Mean Freq.	Std. Dev. of Freq.	Mean Damping	Std. Dev. of Damping
3P	Fig. 4.14(a)	1.11 Hz	0.03 Hz	3.6%	1.1%
12P	Fig. 4.14(b)	4.53 Hz	0.01 Hz	0.3%	0.13%

In addition to the forcing from mechanical excitation, the turbine was still being excited by the wind and as such it was still possible to extract structural modes (Table 4.4). As mentioned earlier, in the presence of operational vibration, it was not possible to identify any first bending modes while maintaining the stabilization

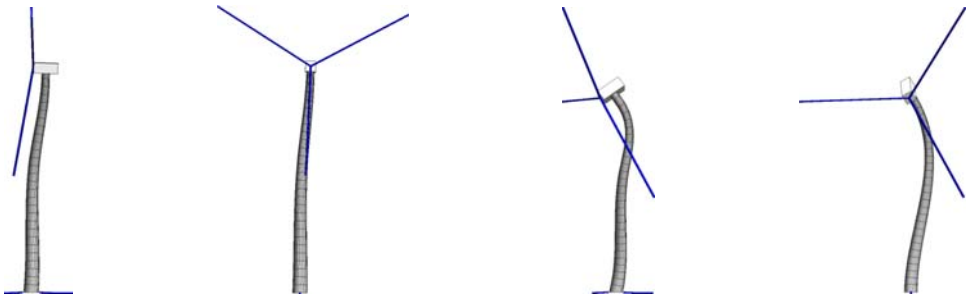

(a) 3P Forced at 1.13 Hz (b) 12P Forced at 4.53 Hz

Figure 4.14: Observed Forced Response of 900-kW Turbine Tower

criteria used for the modal parameter estimates while the turbine was parked. Direct inspection of the data showed that a peak was present near the first mode (Figure 4.13) and prompted more in-depth investigation in this frequency range. By filtering the data with a 0.25 to 0.75 Hz band-pass filter and relaxing the stabilization criteria to only require the modal parameters to be stable across 5 consecutive iterations of system order, a small number of first mode estimates emerged (4 fore-aft and 3 side-to-side). Little change was observed in the frequency (Table 4.4) or mode shape of the first side-to-side mode, but a slight shift in frequency (Table 4.4) and mode shape were observed in the fore-aft mode. Given the limited number of estimates, standard deviation was not meaningful. While higher damping is reported for both first bending modes, the small number of estimates coupled with inherent variability in damping estimates implies a high level of uncertainty. Using a similar approach, a second fore-aft and side-to-side bending mode was observed at 3.82 Hz and 4.09 Hz, respectively (Table 4.4). As with the observed first modes, a slight increase in damping was observed over the parked condition. Inspection of the cross power spectra (Figure 4.13) confirms peaks at each of the estimated frequencies, indicated by dashed blue

lines. Differences in natural frequencies and damping ratios between parked and operating conditions (Tables 4.2 and 4.4) may be due partially to aeroelastic stiffness and damping.

Table 4.4: Summary of identified modal properties with 900-kW wind turbine operating at 22 RPM

Mode Type	Orientation	Mean Freq.	Std. Dev. of Freq.	Mean Damping	Std. Dev of Damping
1st	Fore-aft	0.53 Hz	-	4.7%	-
	Side-to-side	0.54 Hz	-	5.9%	-
2nd	Fore-aft	3.82 Hz	0.07 Hz	1.6%	0.5%
	Side-to-side	4.09 Hz	0.07 Hz	1.5%	0.7%

4.6 Blade Instrumentation

Due to safety and logistical considerations, it was not possible to instrument the turbine rotor (Figure 4.1(b)) during the observations of the global vibrations of the turbine. However, the turbine rotor was later removed and placed on the ground near the turbine. While on the ground, the blade was instrumented using 8 PCB 393A03 accelerometers in 2 orientations to capture both flap (about weak axis) and edge (about strong axis) vibrations. Vibration readings were used to identify the first natural frequencies by peak picking from the power spectra of the readings. The first flap natural frequency was found to be 0.99 Hz and the first edge natural frequency was found to be 1.8 Hz.

4.7 Model Description

Previous work suggests that a beam-column model can provide results that are consistent with more detailed shell FE models for towers (Bazeos et al., 2002) as well as turbine blades (Malcolm and Laird, 2003). This simple configuration represents the predominant approach for numerical modeling of wind turbines for seismic applications (Häenler et al., 2006; Witcher, 2005; Bazeos et al., 2002; Ritschel et al., 2003). As such, a fixed base FE model was developed that represents the turbine tower, nacelle, and rotor (Figure 4.1(b)) using beam-column elements.

The FE model was implemented using the computational platform OpenSees (Mazzoni et al., 2006). The tower (Figure 4.1(b)) was discretized into 51 beam-column elements with a flexural stiffness based on the cross section of the tower at the center of each element. The model used 20 beam-column elements per blade to simulate the inertia and stiffness properties of the rotor (Figure 4.1(b)). Tower element stiffnesses were calculated using the tower diameter and wall thickness from engineering drawings of the turbine. A summary of the tower element properties is presented in Table 4.5.

The blade mass and stiffness distribution were approximated by scaling published values from a similar unit (Jonkman and Buhl Jr., 2005) to match the identified first flap and edge natural frequencies of the tested blades. Unlike the tower where the bending stiffness at the base is only 10 times that at the top, the blade is over 3,000 times stiffer at the root than at the tip (Table 4.5). With a Young's Modulus for the tower steel of 200 GPa and 13 GPa for the blades, the FE model closely matches the

Table 4.5: 900-kW Tower and blade geometric properties

Tower Property	Location		
	Bottom	Middle	Top
Average Outside Diameter	3.24 m	2.66 m	2.05 m
Average Wall Thickness	2.2 cm	1.9 cm	1.25 cm
Average Moment of Inertia	0.26 m^4	0.13 m^4	0.04 m^4
Average Mass Density	1,800 kg/m	1,300 kg/m	650 kg/m
Blade Property	**Location**		
	Root	Middle	Tip
Average Flap Moment of Inertia	0.012 m^4	1.5 x 10^{-3} m^4	1.7 x 10^{-4} m^4
Average Edge Moment of Inertia	0.023 m^4	6.3 x 10^{-3} m^4	1.2 x 10^{-4} m^4
Average Mass Density	900 kg/m	540 kg/m	195 kg/m

first identified natural frequency at 0.57 Hz for both fore-aft and side-to-side mode shapes by uniformly decreasing the reported tower wall thickness by 7% or equivalently reducing by the same percentage the considered Young's Modulus for steel. The predicted second cantilever type mode occurred at 3.90 Hz and 3.88 Hz for the fore-aft and side-to-side mode shapes, respectively. It is observed that the predicted frequencies for the first two tower bending modes (Table 4.6) match the identified frequencies (Table 4.2) very closely. Further, even the numerical estimate of the third side-to-side bending frequency matches the identified frequency within 5%. A relatively greater discrepancy is seen in the third fore-aft bending mode frequency and mode shape. Though not experimentally identified, the predicted first blade flap and edge modes are shown in Figures 4.18 and 4.18, respectively.

4.8 Discussion

To assess the applicability of the current approach of modeling wind turbines using beam-column elements, the experimental results are compared to those cal-

Table 4.6: Summary of predicted and identified resonant frequencies for 900-kW turbine

Mode Type	Orientation	Illustration	Model Freq.	Exp. Parked Freq.
1st Tower Bending	Side-to-side	Fig. 4.15(a)	0.57 Hz	0.54 Hz
	Fore-aft	Fig. 4.15(b)	0.57 Hz	0.56 Hz
Asymmetric 1st Blade Flap	-	Fig. 4.18(a)	0.96 Hz	0.99 Hz
Asymmetric 1st Blade Flap	-	Fig. 4.18(b)	0.99 Hz	0.99 Hz
Collective 1st Blade Flap	-	Fig. 4.18(c)	1.05 Hz	0.99 Hz
Collective 1st Blade Edge	-	Fig. 4.19(a)	1.66 Hz	1.80 Hz
Asymmetric 1st Blade Edge	-	Fig. 4.19(b)	1.78 Hz	1.80 Hz
Asymmetric 1st Blade Edge	-	Fig. 4.19(c)	1.82 Hz	1.80 Hz
2nd Tower Bending	Side-to-side	Fig. 4.16(a)	3.88 Hz	3.94 Hz
	Fore-aft	Fig. 4.16(b)	3.90 Hz	4.00 Hz
3rd Tower Bending	Fore-aft	Fig. 4.17(a)	10.6 Hz	8.86 Hz
	Side-to-side	Fig. 4.17(b)	11.1 Hz	10.9 Hz

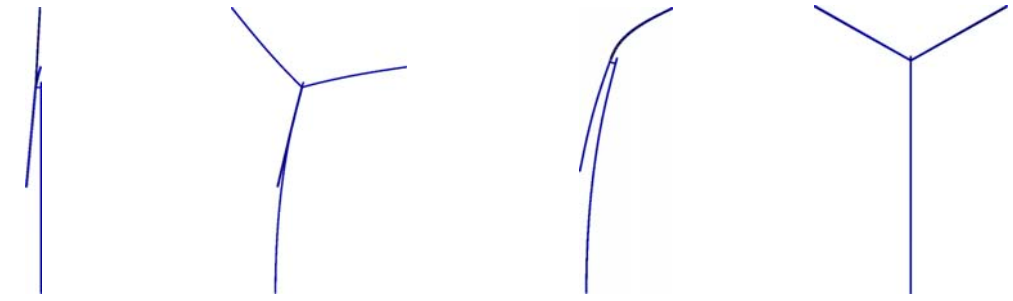

(a) Side-to-side at 0.57 Hz (b) Fore-aft at 0.57 Hz

Figure 4.15: 1st tower bending modes for FE model of 900-kW turbine

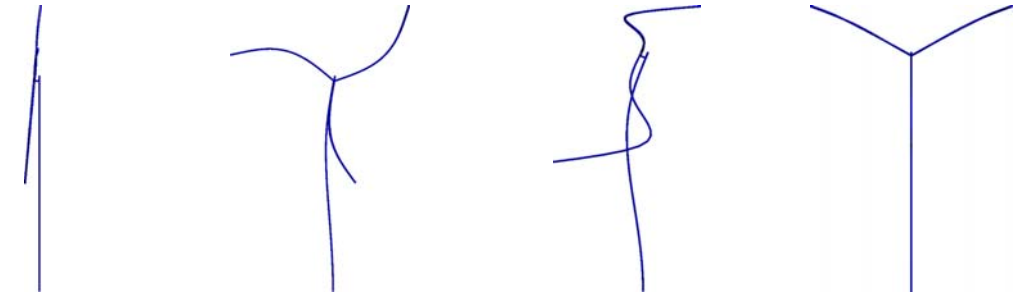

(a) Side-to-side at 3.88 Hz (b) Fore-aft at 3.90 Hz

Figure 4.16: 2nd tower bending modes for FE model of 900-kW turbine

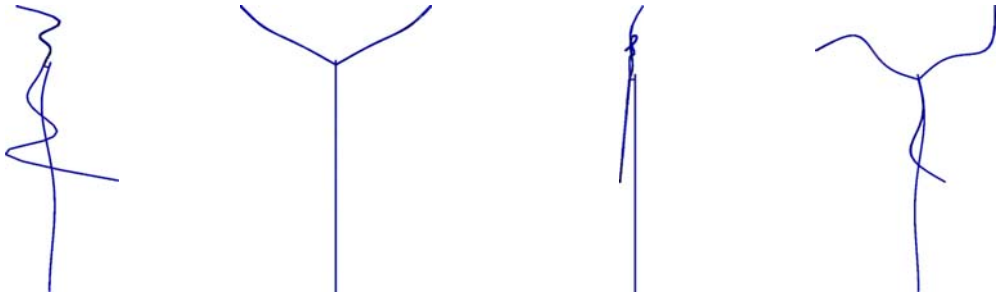

(a) Fore-aft at 10.6 Hz (b) Side-to-side at 11.1 Hz

Figure 4.17: 3rd tower bending modes for FE model of 900-kW turbine

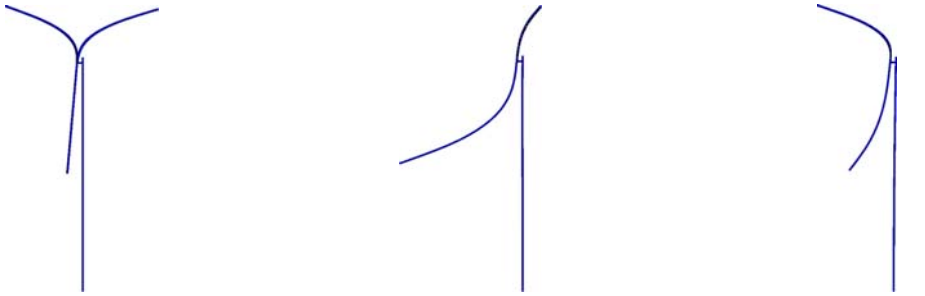

(a) 0.96 Hz (b) 0.99 Hz (c) 1.05 Hz

Figure 4.18: 1st blade flap modes (Side) for FE model of 900-kW turbine

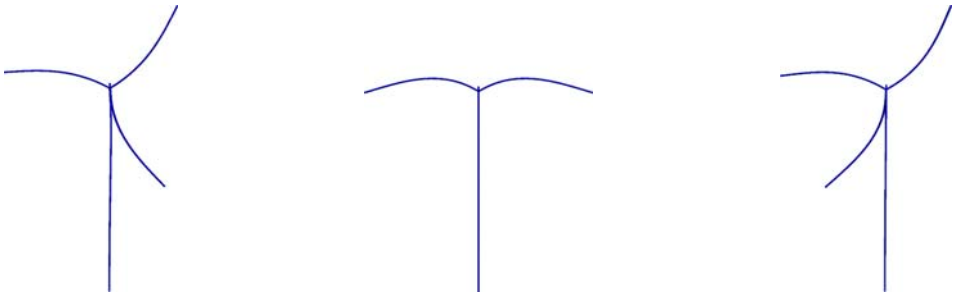

(a) 1.66 Hz (b) 1.78 Hz (c) 1.83 Hz

Figure 4.19: 1st blade edge modes (Front) for FE model of 900-kW turbine

culated using the OpenSees model (Mazzoni et al., 2006). By visual inspection, the experimentally identified mode shapes (Figures 4.10 through 4.12) closely match the predicted tower mode shapes (Figures 4.15 through 4.17). Another method of comparing the experimentally identified modes to those predicted numerically is to compute their MAC values (Allemang and Brown, 1982; Allemang, 2003). Table 4.7 reports the MAC values computed between the average experimentally identified and the numerically predicted mode shapes.

Table 4.7: Computed MAC values between identified and FE model modes for 900-kW turbine

			FE Model Modes					
			Fore-aft			Side-to-side		
			1st	2nd	3rd	1st	2nd	3rd
Exp. Modes	Fore-aft	1st	0.94	0.14	0.16	0.06	0.01	0.01
		2nd	0.12	0.86	0.03	0.02	0.13	0.00
		3rd	0.19	0.15	0.76	0.03	0.00	0.08
	Side-side	1st	0.03	0.01	0.01	0.96	0.15	0.16
		2nd	0.03	0.05	0.00	0.20	0.94	0.00
		3rd	0.00	0.02	0.01	0.16	0.01	0.90

Both methods of deriving mode shapes, experimental identification and numerically predicted, show first and second modes that are essentially constrained to vibration in the fore aft or side-to-side directions. Independence in fore-aft and side-to-side modes is important for turbine specific codes that rely on multi-modal solutions for simulating turbine dynamics (e.g. the FAST code (Jonkman and Buhl Jr., 2005)). In such codes mode shapes are assumed to be independent and specified solely in the fore-aft and side-to-side directions.

In addition to natural frequencies and mode shapes, modal damping ratios are parameters are needed for numerical modeling. The International Electrotechnical

Commission (IEC) recommendations suggest modal damping ratios of 1% of critical damping be used for simulating the seismic response of wind turbines (IEC, 2005). This study revealed modal damping ratios higher than 1%, in the range of 3 to 4%, for primary tower bending modes while the turbine was parked. The identified modal damping ratios for the second and third modes were found close to the recommended 1% value. This difference in damping between primary and higher modes can be addressed in modeling codes by either using the Rayleigh damping model (Chopra, 2006) for FE codes, or by directly specifying modal damping, mode by mode, for multi-modal codes such as FAST (Jonkman and Buhl Jr., 2005). Since previous studies have suggested that aerodynamics contribute significantly to the damping properties of a turbine (James III et al., 1992), it is important that structural damping is appropriately reduced in simulation codes that account explicitly for aerodynamic damping (e.g. the FAST code (Jonkman and Buhl Jr., 2005), GH Bladed (Bossanyi, 2000), and FLEX5 (Hansen et al., 2005)).

The above-described study provides a basis for reducing uncertainty when conducting seismic response predictions for wind turbines (Prowell et al., 2010a). Using the experimental results, the 900-kW turbine was modeled using the FAST code (Prowell et al., 2010b). With this validated model and the advanced capabilities of the FAST code, studies of large turbines can be conducted numerically considering the interaction between wind, earthquake, and operational loads.

4.9 Summary and Conclusion

This chapter presents a set of dynamic ambient vibration field tests performed on a large wind turbine located at Oak Creek Energy Systems in Mojave, California, USA. The tests provided a unique opportunity to obtain the modal properties of a megawatt scale HAWT.

During the vibration tests, the dynamic response of the turbine was measured using an array of up to 48 uni-axial and 11 tri-axial force-balanced accelerometers. These accelerometers were installed simultaneously at selected stations along the tower, covering the whole height. Under parked turbine conditions, a total of 81 channels of acceleration response data were recorded simultaneously. A reduced set of accelerometers, 30 total channels, was used to simultaneously capture vibration while the turbine was operating.

Using the acquired vibration data, the first six modes of the parked turbine and first four vibration modes of the operating turbine (natural frequencies, damping ratios, and mode shapes) were identified using the MNExT-ERA algorithm. On this basis, it is found that: (1) conventional beam-column FE codes can provide mode shapes that agree with experimental results for use in turbine specific multi-modal programs; (2) both first and second tower bending modes in the fore-aft and side-to-side directions show little out of plane deformation, supporting assumed independence between fore-aft and side-to-side motions in multi-modal codes; (3) the identified modal damping ratios are higher than IEC recommended values for seismic response analysis in the first bending modes (in the range of 3% to 4%), but are in line with

recommendations for higher modes while the turbine is parked (approximately 1%); (4) successful identification of modes under operating turbine conditions required guidance from parked condition results due to the presence of harmonic forcing; and (5) an increase in damping, likely due to aerodynamic interaction, was identified while the turbine was operating.

4.10 Acknowledgements

The text below is reproduced verbatim as it appears in the acknowledgments section on page xvii per the UCSD Office of Graduate Studies Formatting Requirements.

Chapter 4 of this dissertation is based on material from a manuscript submitted for publication, tentatively titled "In-situ Ambient Vibration Study of a 900-kW Wind Turbine" with an author list of Ian Prowell, Ahmed Elgamal, J. Enrique Luco, and Joel P. Conte (2011). The dissertation author is the first author of this paper.

Bibliography

Abdel Wahab, M. M. and Roeck, G. D. (1998). "Dynamic testing of prestressed concrete bridges and numerical verification." *Journal of Bridge Engineering*, 3(4), 159–169.

Allemang, R. J. (1999). *Vibrations: Experimental Modal Analysis, Course Notes*. Structural Dynamics Research Laboratory, University of Cincinnati, Cincinnati, Ohio, USA.

Allemang, R. J. (2003). "The modal assurance criteriontwenty years of use and abuse." *SV.Sound and vibration*, 37(8), 14–23.

Allemang, R. J. and Brown, D. L. (1982). "A correlation coefficient for modal vector analysis." *Proceedings of 1st International Modal Analysis Conference*, Bethel, Connecticut, USA. Society of Experimental Mechanics, 110–116.

Bazeos, N., Hatzigeorgiou, G. D., Hondros, I. D., Karamaneas, H., Karabalis, D. L., and Beskos, D. E. (2002). "Static, seismic and stability analyses of a prototype wind turbine steel tower." *Engineering Structures*, 24(8), 1015–1025.

Bossanyi, E. A. (2000). *Bladed for Windows User Manual*. Garrad Hassan and Partners, Bristol, UK.

Brown, D. L., Allemang, R. J., Zimmerman, R., and Mergeay, M. (1979). "Parameters estimation techniques for modal analysis." *Report No. Technique Paper 790221*, Society of Automotive Engineers.

Brownjohn, J. M. W., Moyo, P., Omenzetter, P., and Lu, Y. (2003). "Assessment of highway bridge upgrading by dynamic testing and finite-element model updating." *Journal of Bridge Engineering*, 8(3), 162–172.

Carne, T. G. and Nord, A. R. (1983). "Modal testing of a rotating wind turbine." *Report No. SAND82-0631*, Sandia National Laboratories.

Chopra, A. K. (2006). *Dynamics of Structures: Theory and Application to Earthquake Engineering*. Prentice-Hall, Upper Saddle River, New Jersey, USA.

Doebling, S. W., Farrar, C. R., Prime, M. B., and Shevitz, D. W. (1996). "Damage identification and health monitoring of structural and mechanical systems from changes in their vibration characteristics: A literature review." *Report No. LA-13070-MS*, Los Alamos National Laboratory.

Ewins, D. J. (2000). *Modal testing: theory, practice, and application*. Research Studies Press, Baldock, UK.

Fraser, M., Elgamal, A., He, X., and Conte, J. P. (2010). "Sensor network for structural health monitoring of a highway bridge." *Journal of Computing in Civil Engineering*, 24(1), 11–24.

Häenler, M., Ritschel, U., and Warnke, I. (2006). "Systematic modelling of wind turbine dynamics and earthquake loads on wind turbines." *European Wind Energy Conference and Exhibition*, Athens, Greece. European Wind Energy Association, 1–6.

Halling, M. W., Muhammad, I., and Womack, K. C. (2001). "Dynamic field testing for condition assessment of bridge bents." *Journal of Structural Engineering*, 127(2), 161–167.

Hansen, M. H., Hansen, A., Larsen, T. J., Oye, S., Sorensen, P., and Fuglsang, P. (2005). "Control design for a pitch-regulated, variable speed wind turbine." *Report No. Riso-R-1500(EN)*, Risø National Laboratory.

Hansen, M. H., Thomsen, K., Fuglsang, P., and Knudsen, T. (2006). "Two methods for estimating aeroelastic damping of operational wind turbine modes from experiments." *Wind Energy*, 9(1-2), 171–191.

Harris, F. (1978). "On the use of windows for harmonic analysis with the discrete Fourier transform." *Proceedings of the IEEE*, 66(1), 51–83.

He, X., Moeveni, B., Conte, J. P., Elgamal, A., and Masri, S. F. (2009). "System identification of Alfred Zampa Memorial Bridge using dynamic field test data." *Journal of Structural Engineering*, 135(1), 54–66.

Henderson, A. P. and Patrick, M. B. (1994). "Tensionless pier foundation." U.S. Patent 5586417.

Ibrahim, S. R. and Mikulcik, E. C. (1977). "A method for the direct identification of vibration parameters from the free response.." *The Shock and Vibration Bulletin*, 47(4), 183–198.

IEC (2005). *IEC 61400-1 Ed. 3: Wind Turbines - Part 1: Design Requirements*. International Electrotechnical Commission, Geneva, Switzerland.

James III, G. H., Carne, T. G., and Lauffer, J. P. (1992). "The natural excitation technique (NExT) for modal parameter extraction from operating wind turbines." *Report No. SAND92-1666, UC-261*, Sandia National Laboratories.

Jonkman, J., Butterfield, S., Musial, W., and Scott, G. (2009). "Definition of a 5-MW reference wind turbine for offshore system development." *Report No. NREL/TP-500-38060*, National Renewable Energy Laboratory.

Jonkman, J. M. and Buhl Jr., M. L. (2005). "FAST user's guide." *Report No. NREL/EL-500-38230*, National Renewable Energy Laboratory.

Juang, J. N. and Pappa, R. S. (1985). "An eigensystem realization algorithm for modal parameter identification and model reduction." *Journal of Guidance, Control, and Dynamics*, 8(5), 620–627.

Lauffer, J. P., Carne, T. G., and Ashwill, T. D. (1988). "Modal testing in the design evaluation of wind turbines." *Report No. SAND87-2461*, Sandia National Laboratories.

Lavassas, I., Nikolaidis, G., Zervas, P., Efthimiou, E., Doudoumis, I. N., and Baniotopoulos, C. C. (2003). "Analysis and design of the prototype of a steel 1-MW wind turbine tower." *Engineering Structures*, 25(8), 1097–1106.

Luco, J. E., Trifunac, M. D., and Wong, H. L. (1988). "Isolation of soil-structure interaction effects by full-scale forced vibration tests." *Earthquake Engineering & Structural Dynamics*, 16(1), 1–21.

Malcolm, D. J. and Hansen, A. C. (2006). "WindPACT turbine rotor design study." *Report No. NREL/SR-500-32495*, National Renewable Energy Laborator.

Malcolm, D. J. and Laird, D. L. (2003). "Modeling of blades as equivalent beams for aeroelastic analysis." *2003 ASME Wind Energy Symposium AIAA/ASME*, Reno, Nevada, USA. 293–303.

Mazzoni, S., McKenna, F., and Fenves, G. L. (2006). *Open System for Earthquake Engineering Simulation User Manual*. Pacific Earthquake Engineering Research Center, Berkeley, California, USA.

Molinari, M., Pozzi, M., Zonta, D., and Battisti, L. (2010). "In-field testing of a steel wind turbine tower." *Proceedings of the IMAC-XXVIII*, Bethel, Connecticut, USA. Society for Experimental Mechanics Inc., 1–10.

Murakawa, H., Kato, N., Fujii, K., and Tamura, Y. (1996). "Experimental evaluation of aerodynamic damping of tall buildings." *Journal of Wind Engineering and Industrial Aerodynamics*, 59, 177–190.

Ohta, Y. and Goto, N. (1978). "Empirical shear wave velocity equations in terms of characteristic soil indexes." *Earthquake Engineering and Structural Dynamics*, 6(2), 167–187.

Peeters, B. and De Roeck, G. (2001). "Stochastic system identification for operational modal analysis: A review." *Journal of Dynamic Systems, Measurement, and Control*, 123(4), 659–667.

Prowell, I., Elgamal, A., Jonkman, J., and Uang, C.-M. (2010a). "Estimation of seismic load demand for a wind turbine in the time domain." *Report No. NREL/CP-500-47536*, National Renewable Energy Laboratory.

Prowell, I., Elgamal, A., Lu, J., and Luco, J. E. (2009). "Modal properties of a modern wind turbine including SSI." *17th International Conference on Soil Mechanics & Geotechnical Engineering*, Alexandria, Egypt. International Society for Soil Mechanics and Geotechnical Engineering, 1–4.

Prowell, I., Elgamal, A., Romanowitz, H., Duggan, J. E., and Jonkman, J. (2010b). "Earthquake response modeling for a parked and operating megawatt-scale wind turbine." *Report No. NREL/TP-5000-48242*, National Renewable Energy Laboratory.

Prowell, I. and Veers, P. (2009). "Assessment of wind turbine seismic risk: Existing literature and simple study of tower moment demand." *Report No. SAND2009-1100*, Sandia National Laboratories.

Ritschel, U., Warnke, I., Kirchner, J., and Meussen, B. (2003). "Wind turbines and earthquakes." *2nd World Wind Energy Conference*, Cape Town, South Africa. World Wind Energy Association, 1–8.

Riziotis, V. A., Voutsinas, S. G., Politis, E. S., and Chaviaropoulos, P. K. (2004). "Aeroelastic stability of wind turbines: the problem, the methods and the issues." *Wind Energy*, 7(4), 373–392.

Rolfes, R., Zerbst, S., Haake, G., Reetz, J., and Lynch, J. P. (2007). "Integral shm-system for offshore wind turbines using smart wireless sensors." *The 6th International Workshop on Structural Health Monitoring*, Stanford, California, USA. Standord University, 1–8.

Smyth, A. W., Pei, J.-S., and Masri, S. (2003). "System identification of the vincent thomas suspension bridge using earthquake records." *Earthquake Engineering and Structural Dynamics*, 32(3), 339–367.

Sohn, H., Farrar, C. R., Hemez, F. M., and Czarnecki, J. J. (2002). "A review of structural health review of structural health monitoring literature: 1996-2001." *Report No. LA-UR-02-2095*, Los Alamos National Laboratory.

Van Overschee, P. and De Moor, B. (1996). *Subspace Identification for Linear Systems: Theory-Implementation-Applications*. Kluwer Academic Publishers, Norwell, Massachusetts, USA.

Welch, P. (1967). "The use of fast Fourier transform for the estimation of power spectra: a method based on time averaging over short, modified periodograms." *IEEE transactions on audio and electroacoustics*, 15(2), 70–73.

Wiser, R. and Bolinger, M. (2008). "Annual report on U.S. wind power installation, costs, and performance trends: 2007." *Report No. DOE/GO-102008-2590*, Department of Energy.

Witcher, D. (2005). "Seismic analysis of wind turbines in the time domain." *Wind Energy*, 8(1), 81–91.

Yu, E., Whang, D. H., Conte, J. P., Stewart, J. P., and Wallace, J. W. (2005). "Forced vibration testing of buildings using the linear shaker seismic simulation (lsss) testing method." *Earthquake Engineering and Structural Dynamics*, 34(7), 737–761.

Zhao, X., Maißer, P., and Jingyan, W. (2007). "A new multibody modeling methodology for wind turbine structures using a cardanic joint beam element." *Renewable Energy*, 32(3), 532–546.

Chapter 5

In-situ Ambient Vibration Study of a 1.5-MW Wind Turbine

5.1 Introduction

This chapter complements the work presented in Chapter 4 and describes a set of dynamic tests performed on a 1.5-MW HAWT (Figure 5.1) located at Oak Creek Energy Systems near Mojave, California (Figure 4.2). The tests monitored structural vibrations using an array of 66 force-balanced accelerometer channels from the mobile field laboratory of the George E. Brown, Jr. Network for Earthquake Engineering Simulation (NEES) field testing site at the University of California, Los Angeles (NEES@UCLA). These accelerometers were installed at stations in the turbine tower, on the foundation, and in the surrounding soil. Instead of relocating accelerometers to the different measurement stations with some accelerometers fixed at one or more reference stations (as commonly done for dynamic testing of large structures), ac-

celeration response was recorded simultaneously, including vertical, side-to-side, and fore-aft motion components at each fixed station. For the parked situation, sources of excitation are limited to the wind and vibration transmitted through the ground. In contrast, when the turbine is operating, harmonic narrow band vibration is transmitted throughout the structure from the periodic spinning of the rotor (Figure 4.1(b)) and other rotating components. These dynamic field tests are the first to be presented for such a highly instrumented modern variable pitch HAWT. Therefore, this test series provides a unique opportunity to determine the dynamic properties of the turbine under in-situ conditions for both parked and operating conditions.

Figure 5.1: 1.5-MW wind turbine at Oak Creek Energy Systems

5.2 Description of Turbine

A 1.5-MW turbine (Figure 5.1) installed at Oak Creek Energy Systems (OCES) near Mojave, California, USA, was selected for in-situ measurements. This turbine size (Table 5.1) is characteristic of units installed around the year 2000 (Wiser and Bolinger, 2008). The turbine is a variable pitch machine where the angle of incidence between the blades and the wind is altered to regulate the rotor speed at approximately 17.4 revolutions per minute (RPM). To follow variation in the wind direction, motors yaw the entire rotor and nacelle to face into the wind.

Table 5.1: 1.5-MW Wind Turbine Characteristics

Type	Horizontal axis wind turbine
Nominal power	1.5-MW
Rotor diameter	72.0 m
Tower height	68.4 m
Hub height	70.0 m
Operational speed	17.4 RPM
Mass of nacelle	44,000 kg
Mass of rotor	40,000 kg
Mass of tower	110,000 kg

The tested turbine is installed on a patented foundation, known as the Patrick and Henderson Tensionless Pier (Henderson and Patrick, 1994). The design is a 4.4 m diameter hollow concrete cylinder that extends 9.1 meters below ground surface, capped on each end by a concrete slab with soil filling the central region in between. Anchoring the turbine to the foundation, are post tensioned steel rods that extend through the concrete to the cylinder base. The foundation is installed in a layered stratum where the upper 2 meters are a sandy soil with a drained friction angle of about 40 degrees, underlain by dense silty sands and clayey sands. Using empirical

relations for standard penetrometer test (SPT) results from geotechnical investigations throughout OCES, it is estimated that the shear wave velocity at the site is approximately 300 to 400 m/s near the surface and increases to 400 to 650 m/s at 10 meters below ground surface (Ohta and Goto, 1978).

5.2.1 Additional Damping

Since turbines show little inherent structural damping the tested machine was equipped with devices to provide additional damping in the tower. A series of containers partially filled with fluid, known as sloshing dampers (Fujii et al., 1990), were installed at approximately 2/3 of the tower height. The dampers are tuned such that they dissipate energy at the frequency of interest. Such a strategy is a common and effective means of adding additional energy dissipation capability to a civil structure.

5.3 Instrumentation Layout

The turbine was instrumented with stations at eight distinct elevations along the turbine tower (66 m, 60 m, 54 m, 45 m, 37 m, 27 m, 14 m, and 7 m) at 10 locations (Figure 5.2) with either a single EpiSensor ES-T (tri-axial) or three EpiSensor ES-U (uni-axial, Figure 4.4) to measure vertical, side-to-side, and fore-aft vibrations. Each accelerometer was rigidly clamped to the turbine ensuring satisfactory coupling. An illustrative segment of the acceleration recorded from the tower stations is displayed in Figure 5.3. In addition to the tower stations, four locations on the surface of the foundation were instrumented with a single EpiSensor ES-T accelerometer to capture

translation and rocking of the base of the turbine. Eight stations on the ground, in concentric circles of 6 and 10 meters in diameter, were instrumented with a total of 24 EpiSensor ES-U accelerometers (three uni-axial accelerometers at each of eight stations) to measure the response of the surrounding soil. EpiSensor ES-U units were mounted to a rigid aluminum plate to ensure orthogonality. The soil accelerometers were recessed below the ground surface and covered to reduce extraneous vibration. While readings were captured, the mobile command center was located a suitable distance (approximately 100 m) from the turbine (Figure 5.1) to reduce the influence on recorded results.

The layout and details of the data acquisition equipment are documented in Section 4.3 on page 119. In all 66 channels of acceleration data were recorded simultaneously at a sample rate of 200 Hz. For the operational condition, Figure 5.4 shows a sample of recorded vibration in the turbine tower. The corresponding auto power spectra (APS) for the parked and operating conditions are shown in Figures 5.5 and 5.6, respectively. All data analyzed here will be publically available on the NEES data archive at http://www.nees.org.

5.4 Modal Identification Using MNExT-ERA

Modal identification procedures used to obtain the results reported in this chapter mirror those described in Section 4.4. The cross power spectrum (CPS) of each data channel was then calculated with each of ten reference channels (located at the foundation, 27, 45, 60, and 66 m elevations in the side-to-side and fore-aft

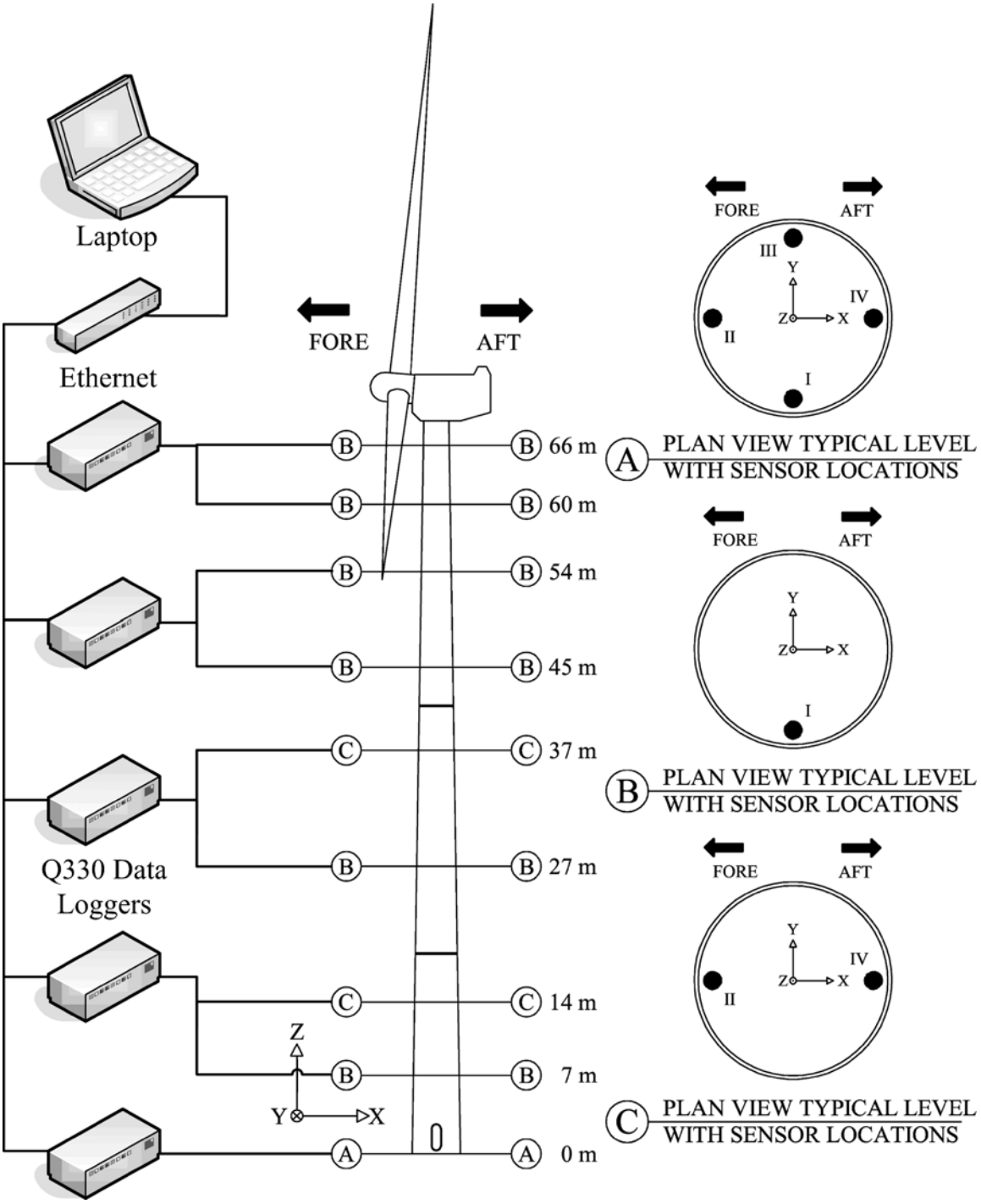

Figure 5.2: Logical diagram of NEES@UCLA data acquisition equipment and layout of accelerometers for 1.5-MW turbine

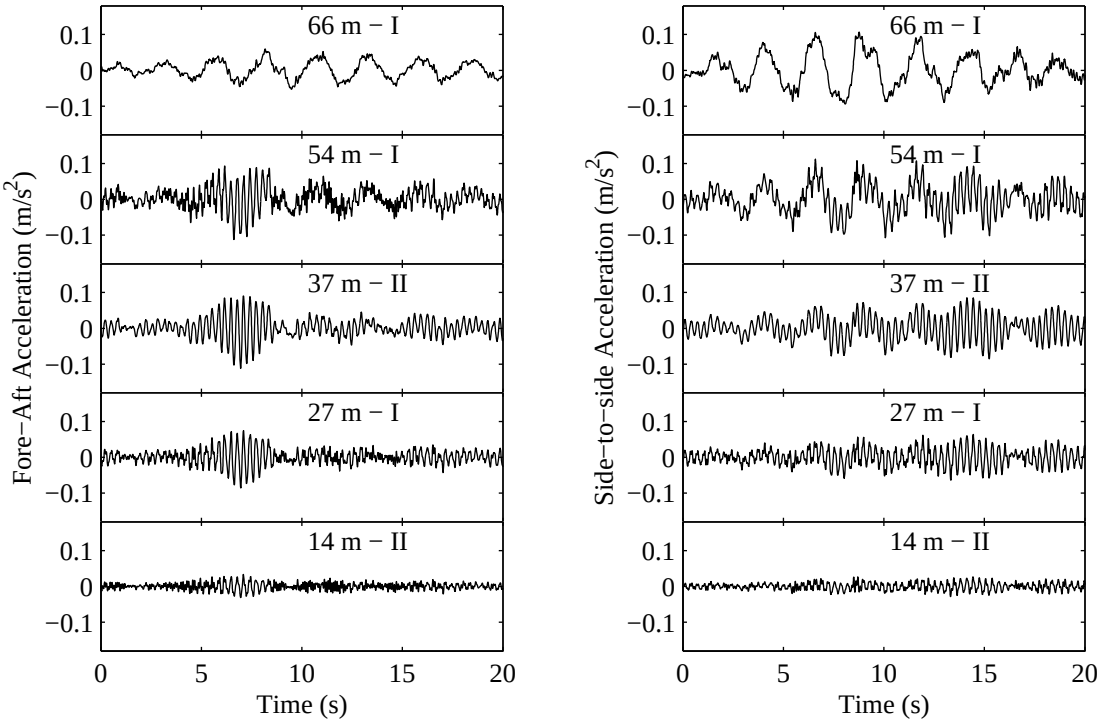

Figure 5.3: Acceleration measured for 1.5-MW turbine while parked

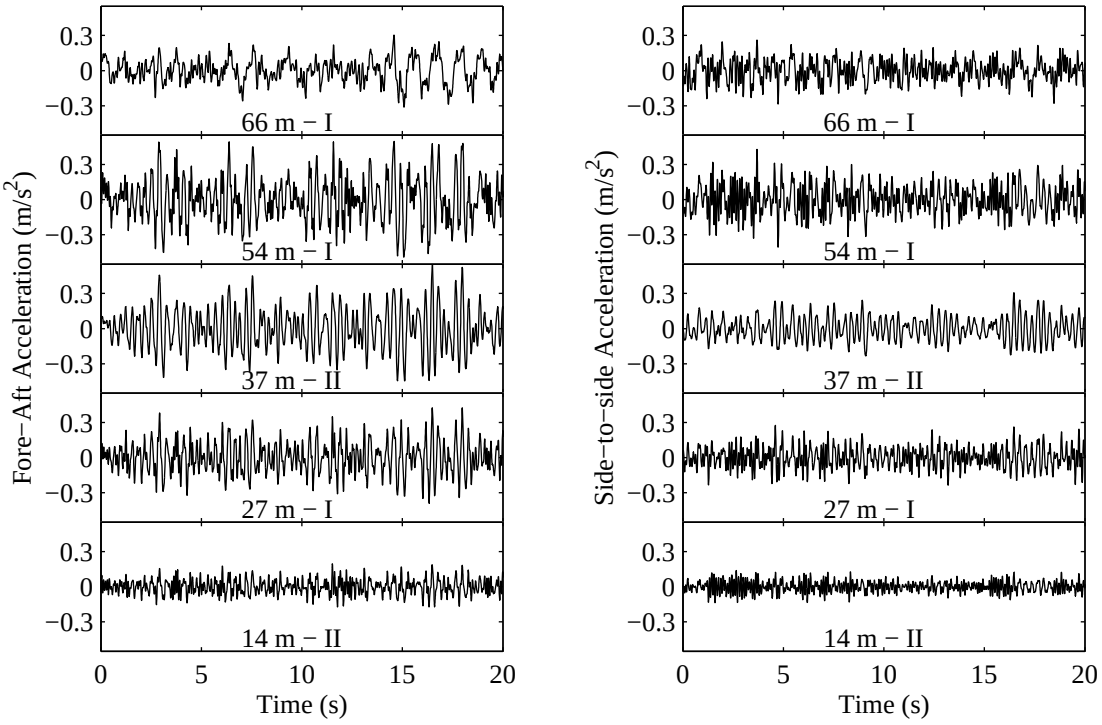

Figure 5.4: Acceleration measured for 1.5-MW turbine while operating at 17.4 RPM

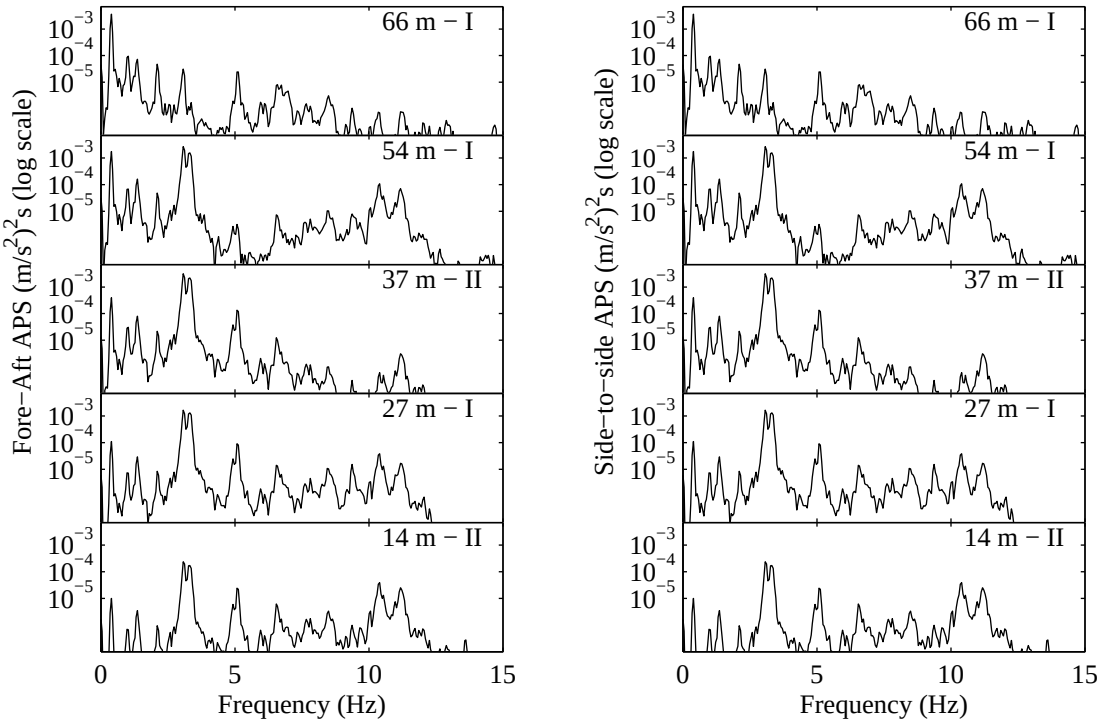

Figure 5.5: Acceleration APS for 1.5-MW turbine while parked

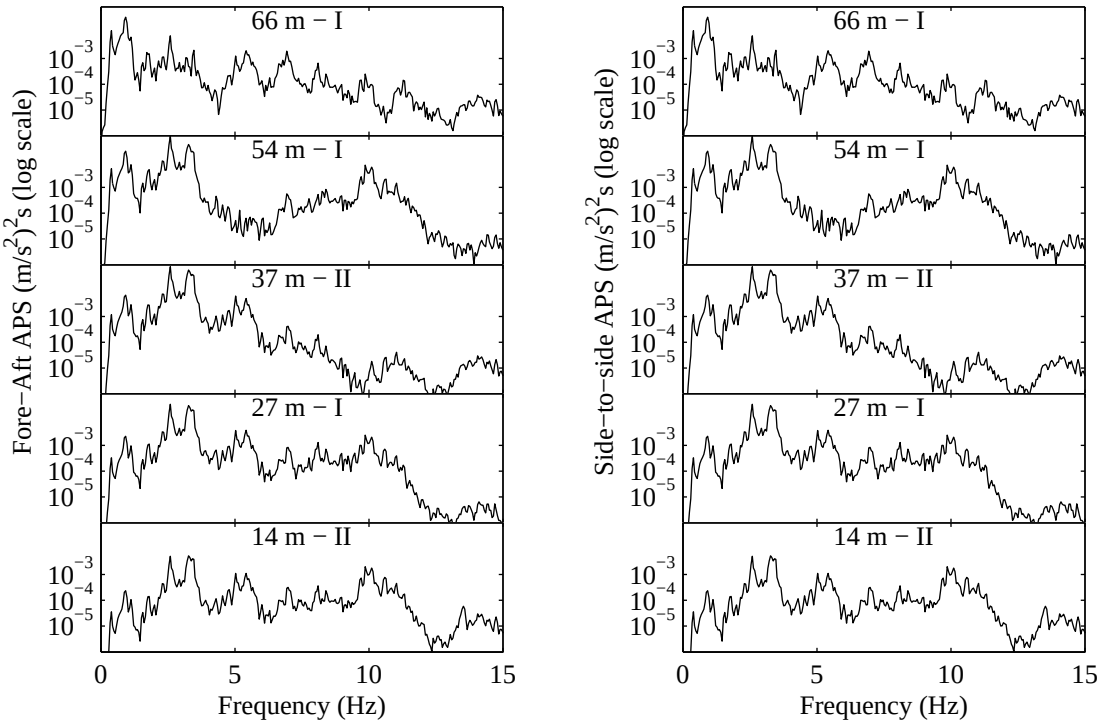

Figure 5.6: Acceleration APS for 1.5-MW turbine while operating at 17.4 RPM

directions) and averaged across the data slices. For the parked condition, a sample of cross power spectra from selected channels is shown in Figure 5.7. The procedure used to calculate cross and auto power spectra was previously described in Section 4.4 on page 125. With all modes of interest in this investigation below 25 Hz, cross correlation functions were calculated and down sampled to 50 Hz, the frequency required to resolve 25 Hz signals, to expedite computation of modal parameter estimation using the Eigenvalue Realization Algorithm (ERA) (He et al., 2009; Juang and Pappa, 1985).

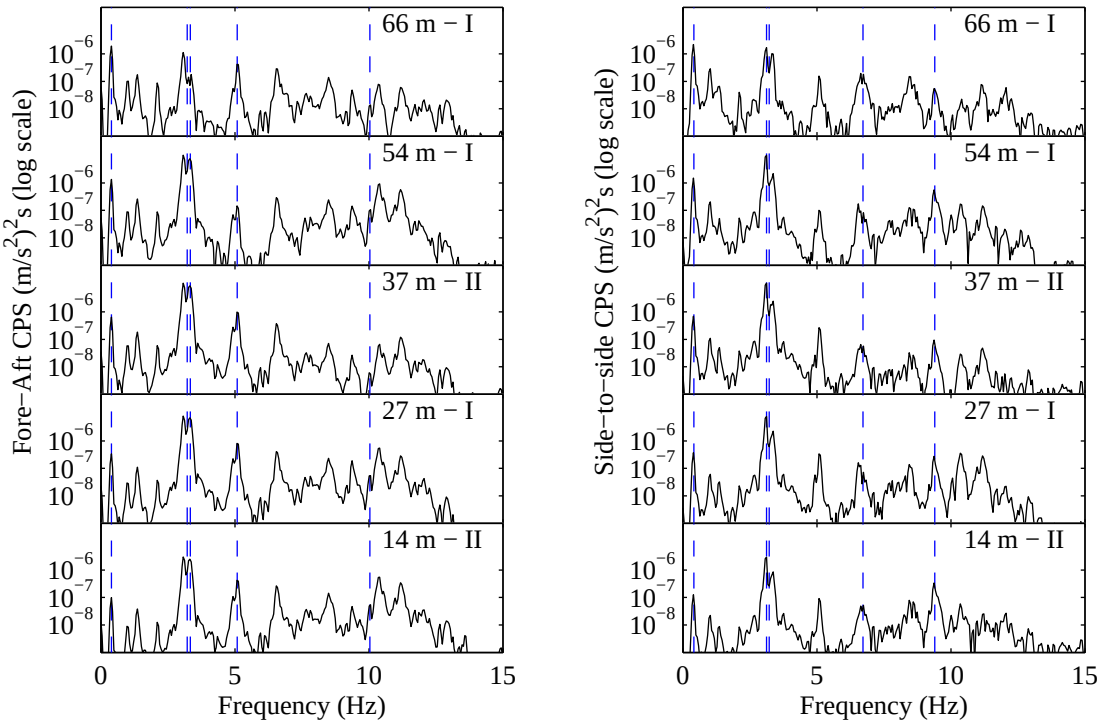

Figure 5.7: Cross power spectra (CPS) with base motion (0 m - I, Figure 5.2) as input for 1.5-MW turbine under parked condition

5.5 Results

5.5.1 Parked Condition Identification Results for 1.5-MW Turbine

Using 80 minutes of data collected while the turbine was parked, 80 estimates of the turbines dynamic properties were performed. During this period the wind speed varied from 8 to 15 m/s. A summary of the average frequency, average damping, and standard deviation of the identified properties for the parked turbine is shown in Table 5.2. Resulting frequencies for the modes are visualized as dashed blue lines on the cross power spectra in Figure 5.7. Mode shapes were averaged across estimates and the resulting shapes are shown in Figures 5.8 through 5.11.

The first bending modes occurred at a mean frequency of 0.39 Hz in the fore-aft direction (Figure 5.8(a)) and 0.41 Hz in the side-to-side direction (Figure 5.8(b)). For what appeared to be a second mode of the tower, three distinct frequencies were observed. The lowest frequency second bending was observed with a mean frequency of 3.12 Hz in the side-to-side direction (Figure 5.9(a)). Two more second bending modes were observed with a mean frequency at 3.22 Hz as a coupled mode (Figure 5.9(b)) and 3.34 Hz in the fore-aft direction (Figure 5.9(c)).

Results show a third mode in both the fore-aft (Figure 5.10(a)) and side-to-side (Figure 5.10(b)) direction at mean frequencies of 5.09 Hz and 6.72 Hz, respectively, that do not resemble the expected third tower modes. These modes may be a result of vibration from sloshing type dampers installed in the turbine tower.

A wider separation between the frequencies of the fourth bending modes was observed with the side-to-side direction at 9.40 Hz (Figure 5.11(a)) and the fore-aft mode at 10.4 Hz (Figure 5.11(a)).

In the mode shape illustrations, the nacelle and rotor are shown for illustration only and are merely translated and rotated as a rigid body to match observed motion of the tower top. All visualized mode shapes include the stations instrumented in the soil, but consistent with the stiff soil at the site, little base translation or rocking is observed.

Estimations of natural frequency showed little variation, whereas the modal damping estimates showed a significantly larger variation across all identified modes (Table 5.2). This relatively large variation in the damping is expected as damping estimates are inherently less stable and factors such as the wind speed can influence the results through aerodynamic damping (Riziotis et al., 2004). High damping present in the first fore-aft and side-to-side mode is likely a direct result of the sloshing dampers installed in the turbine tower.

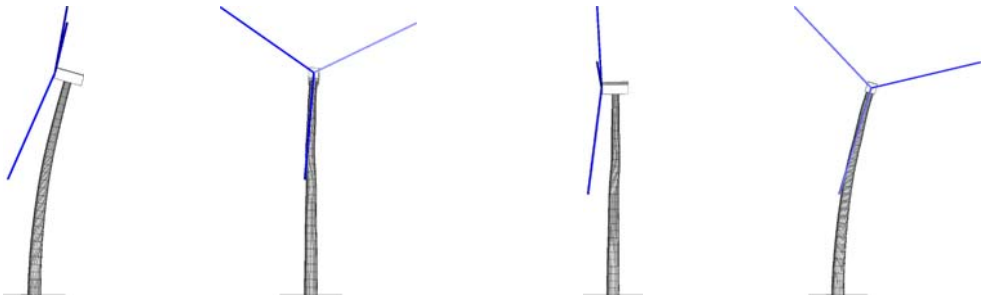

(a) Fore-aft at 0.39 Hz (b) Side-to-side at 0.41 Hz

Figure 5.8: 1st bending modes for 1.5-MW turbine in parked condition

Table 5.2: Summary of identified modal properties for 1.5-MW wind turbine in parked condition

Mode Type	Orientation	Illustration	Mean Freq.	Std. Dev. of Freq.	Mean Damping	Std. Dev of Damping
1st	Fore-aft	Fig. 5.8(a)	0.39 Hz	-[1]	7.3%	-[1]
	Side-to-side	Fig. 5.8(b)	0.41 Hz	0.01 Hz	10.1%	5.2%
2nd	Side-to-side	Fig. 5.9(a)	3.12 Hz	0.04 Hz	1.4%	0.5%
	Coupled	Fig. 5.9(b)	3.22 Hz	0.07 Hz	1.4%	0.4%
	Fore-aft	Fig. 5.9(c)	3.34 Hz	0.02 Hz	1.3%	0.6%
3rd	Fore-aft	Fig. 5.10(a)	5.09 Hz	0.05 Hz	1.1%	0.6%
	Side-to-side	Fig. 5.10(b)	6.72 Hz	0.02 Hz	0.7%	0.3%
4th	Side-to-side	Fig. 5.11(a)	9.40 Hz	-[2]	0.8%	-[2]
	Fore-aft	Fig. 5.11(b)	10.4 Hz	0.05 Hz	1.0%	0.5%

[1]with only 2 estimates statistics are not significant
[2]with only 3 estimates statistics are not significant

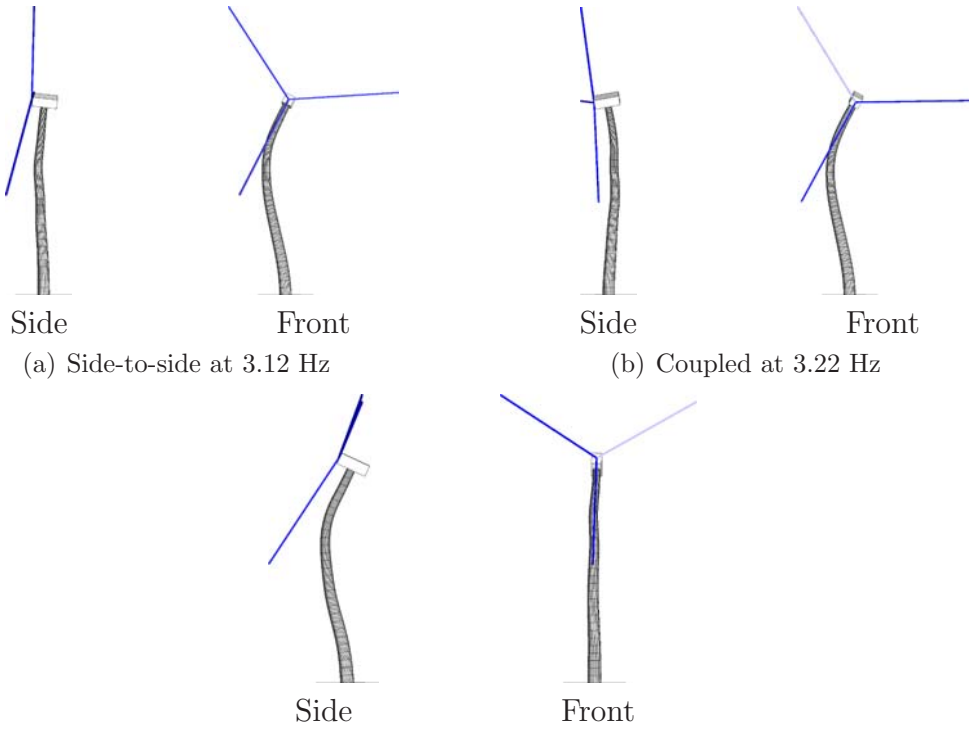

(a) Side-to-side at 3.12 Hz

(b) Coupled at 3.22 Hz

(c) Fore-aft at 3.34 Hz

Figure 5.9: 2nd bending modes for 1.5-MW turbine in parked condition

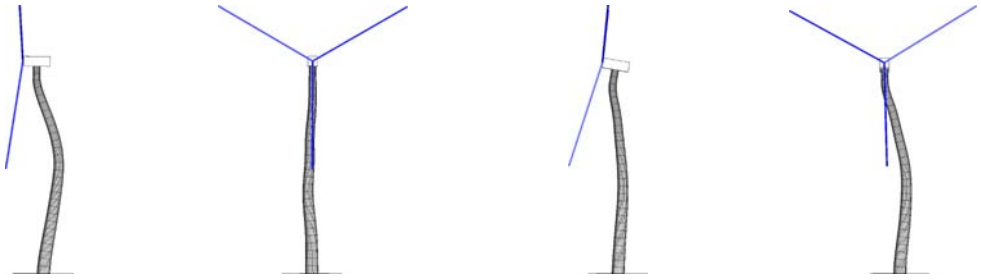

(a) Fore-aft at 5.09 Hz (b) Side-to-side at 6.72 Hz

Figure 5.10: 3rd bending modes for 1.5-MW turbine in parked condition

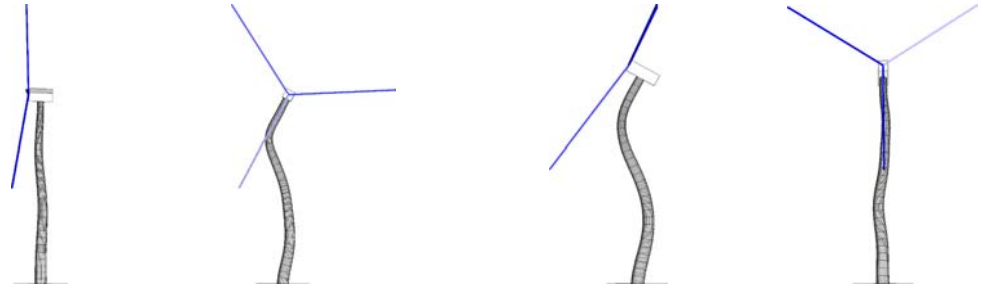

(a) Side-to-side at 9.40 Hz (b) Fore-aft at 10.4 Hz

Figure 5.11: 4th bending modes for 1.5-MW turbine in parked condition

5.5.2 Identification Results for the 1.5-MW Wind Turbine Operating at 17.4 RPM

Next, modal parameter estimates were considered for a 44-hour period where the turbine was primarily operating. Estimates were limited to time periods when the turbine was operating at a constant 17.4 RPM with the nacelle oriented within ±5 degrees of the orientation used for parked estimates, 297 degrees from north. This variability is within the accuracy of alignment of sensors and the rotor. The turbine changed the pitch of the blades to maintain this constant rotational speed despite wind speed ranging from 6.5 m/s to over 16 m/s. A graphical summary of the wind

data is presented in Figure 5.12. In all 1,273 one minute windows (21.2 hours in total) matched the criteria and were used to estimate modal parameters of the operating turbine.

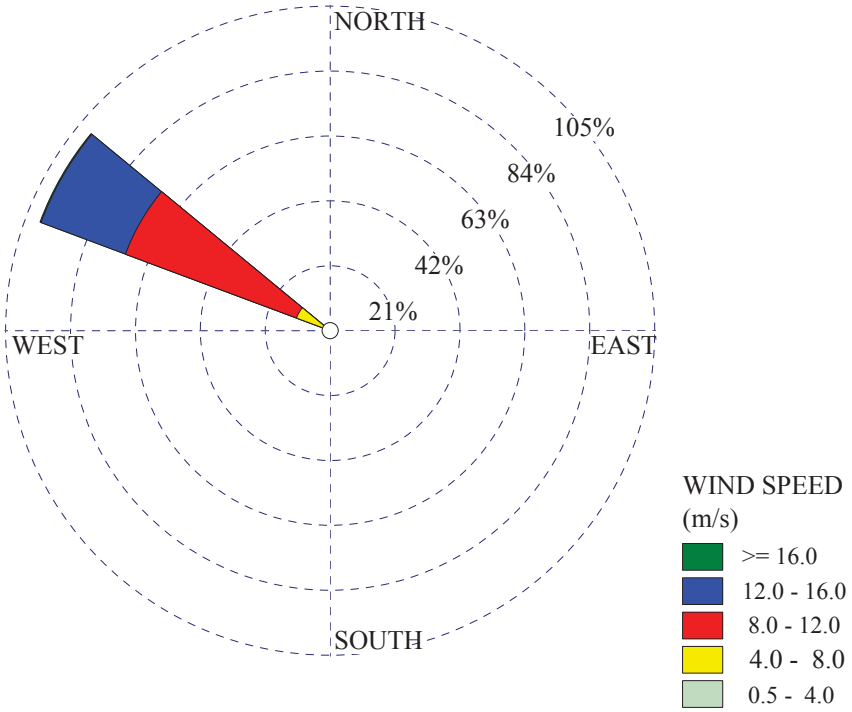

Figure 5.12: Wind rose for operating time period

During this period, the turbine was not only vibrating in response to broad-band excitation such as the wind, but was also continually excited by narrow-band forcing at specific frequencies. In a wind turbine, the frequency of rotation of the rotor, 1P, and the blade passage frequency, 3P, are significant harmonic forcing sources. At a rotor speed of 17.4 RPM the 1P frequency is 0.29 Hz and the 3P frequency is 0.87 Hz. Visual inspection of the cross power spectra while operating (Figure 5.13) shows peaks at mechanical vibration frequencies and harmonics, indicated by the gray vertical lines. These peaks are consistent with other reported results for operating

turbines (Molinari et al., 2010; James III et al., 1992). With no specific consideration of the mechanical forcing, the NExT-ERA algorithm interprets the vibration at these frequencies as a resonance (James III et al., 1992).

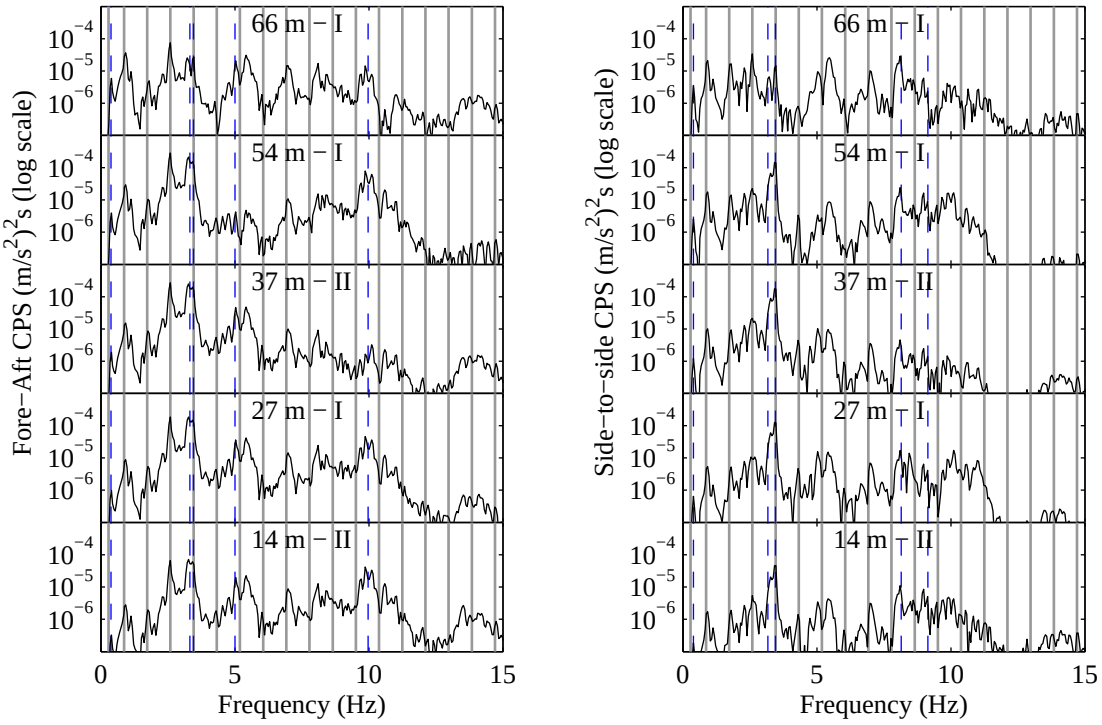

Figure 5.13: CPS with base motion (0 m - I) as input measured for 1.5-MW turbine while operating at 17.4 RPM

In addition to the forcing from mechanical excitation, the turbine was still being excited by the wind and with guidance from the parked condition results it was still possible to extract structural modes (Table 5.3). Little change occurred for the mode shapes of the first modes, but a slight reduction in the frequencies was observed. Again, as in the parked condition, three second tower bending modes were observed. The fore-aft and side-to-side modes both showed a slight increase in frequency. The coupled mode increased more significantly, but was observed at a frequency coincident with a harmonic of the mechanical forcing, which may be contaminating the results

(Figure 5.13). Inspection of the cross power spectra (Figure 5.13) confirms peaks at each of the estimated frequencies, indicated by dashed blue lines. Differences in natural frequencies and damping ratios between parked and operating conditions (Tables 5.2 and 5.3) may be due partially to aeroelastic stiffness and damping.

Table 5.3: Summary of identified modal properties with 1.5-MW wind turbine operating at 17.4 RPM

Mode Type	Orientation	Mean Freq.	Std. Dev. of Freq.	Mean Damping	Std. Dev of Damping
1st	Fore-aft	0.38 Hz	0.01 Hz	7.9%	4.0%
	Side-to-side	0.39 Hz	0.01 Hz	7.6%	2.3%
2nd	Side-to-side	3.17 Hz	0.02 Hz	1.3%	1.1%
	Fore-aft	3.32 Hz	0.06 Hz	2.0%	1.2%
	Coupled	3.45 Hz	0.01 Hz	0.6%	0.2%
3rd	Fore-aft	5.00 Hz	0.09 Hz	1.1%	0.6%
	Side-to-side	8.15 Hz	0.06 Hz	2.0%	1.3%
4th	Side-to-side	9.14 Hz	0.06 Hz	0.9%	0.5%
	Fore-aft	9.97 Hz	0.07 Hz	1.2%	0.6%

5.6 Correlation of Results with Wind Speed

As mentioned above, it was observed that wind speed varied significantly during the time period for which modal estimates of the operating turbine were performed. Wind speeds was measurements from by anemometer installed atop the turbine nacelle, digitized in one minute averages, and recorded as part of the experimental data. Modal estimates were compared to wind speed to assess possible trends in reported results. Figures 5.14 compare the estimated frequency and damping for the first fore-aft mode. From visual inspection little trend was discernible for most modal estimates.

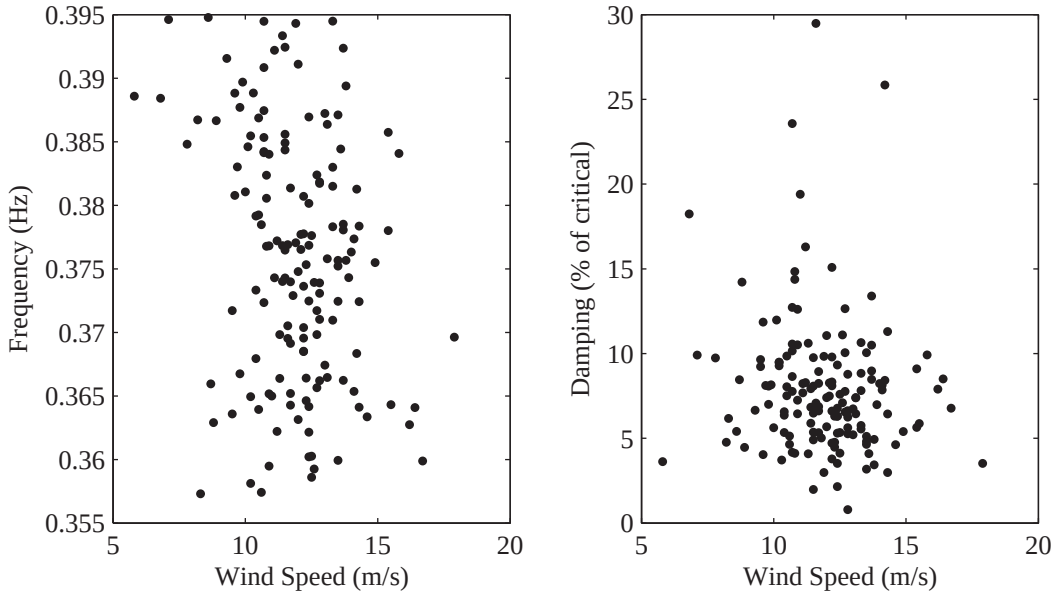

Figure 5.14: Comparison of estimated 1$^{\text{th}}$ fore-aft modal frequency and damping with wind speed

The coefficients of correlation were calculated to more rigorously identify possible dependence of modal estimates on wind speed. Equation 5.1 defines the correlation coefficient (Peeters and De Roeck, 2001).

$$\rho_{xy} = \frac{s_{sy}}{s_x s_y}, \quad s_{xy} = \frac{1}{N-1}\sum_{k=1}^{N}(x_k - \bar{x})(y_k - \bar{y}), \quad \bar{x} = \frac{1}{N}\sum_{k=1}^{N} x_k \tag{5.1}$$

where s_{xy} is the sample covariance; s_x and s_y are simply the standard deviation ($s_m = \sqrt{s_{mm}}$); N is the number of sample points; and k is used to index the sample points. The results are shown in Table 5.4 for all nine identified modes. Most modes show little correlation to either wind speed or nacelle orientation, with some exception. This first side-to-side mode shows a correlation between frequency and wind speed that may be due to the variation in the blade pitch. As the wind speed increases,

the blades re-orient such that the weak axis (flap) instead of the strong axis (edge) of the blade is more closely aligned with side-to-side vibration of the tower. The re-orientation slightly reduces the overall side-to-side stiffness of the coupled tower and blade system, which may also account for the mild negative correlation of the second side-to-side mode frequency and wind speed. The second coupled mode also shows a correlation between frequency and wind speed. Again, it is likely that variation in blade pitch is partially responsible for this correlation. A plot of the modal estimates as a function of wind speed is shown for the second coupled mode in Figure 5.15.

Table 5.4: Coefficient of correlation of modal estimates with wind speed and nacelle orientation

Mode Type	Orientation	ρ_{xy}	
		Freq.	Damping
1st	Fore-aft	-0.25	-0.13
	Side-to-side	-0.40	0.13
2nd	Side-to-side	-0.30	0.24
	Fore-aft	-0.05	0.05
	Coupled	0.66	-0.02
3rd	Fore-aft	-0.04	0.15
	Side-to-side	-0.13	-0.12
4th	Side-to-side	-0.05	-0.03
	Fore-aft	0.03	0.06

5.7 Summary and Conclusion

This chapter presents a set of dynamic ambient vibration field tests performed on a large variable pitch wind turbine located at Oak Creek Energy Systems in Mojave, California, USA. The tests provided a unique opportunity to obtain the modal properties of such a turbine.

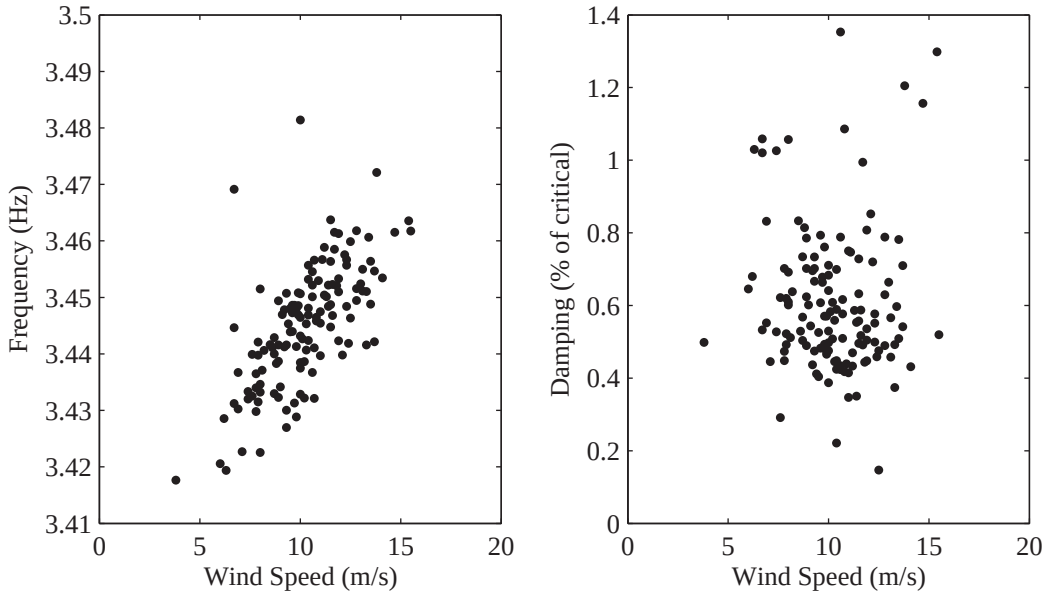

Figure 5.15: Comparison of estimated 2nd coupled modal frequency and damping with wind speed

During the vibration tests, the dynamic response of the turbine was measured using an array 66 channels of force-balanced accelerometer data. These accelerometers were installed simultaneously at selected stations along the tower, covering the whole height.

Using the acquired vibration data, the first nine modes of the parked and operating turbine (natural frequencies, damping ratios, and mode shapes) were identified using the MNExT-ERA algorithm. On this basis, it is found that:

1. Both first and second tower bending modes in the fore-aft and side-to-side directions show little out of plane deformation, which implies they can be considered independent. This orthoganality validates a common assumption of multi-modal codes, such as the FAST code (Witcher, 2005; Jonkman and Buhl Jr., 2005).

2. The identified modal damping ratios are higher than IEC recommended values for seismic response analysis in the first bending modes (in the range of 5% to 10%). On account of the sloshing dampers installed in the turbine tower, it is expected that damping values will be elevated in the frequency range targeted by the devices. For higher modes, where the dampers are less effective, observed levels are in line with the recommended (approximately 1%).

3. Successful identification of modes under operating turbine conditions required guidance from parked condition results due to the presence of harmonic forcing.

4. A strong correlation was not observed between modal estimates and wind speed for most modes.

5.8 Acknowledgements

The text below is reproduced verbatim as it appears in the acknowledgments section on page xvii per the UCSD Office of Graduate Studies Formatting Requirements.

Chapter 5 of this dissertation is based on material from a manuscript under preparation for publication, tentatively titled "In-situ Ambient Vibration Study of a 1.5-MW Wind Turbine" with a preliminary author list of Ian Prowell, Ahmed Elgamal, Joel P. Conte, Hal Romanowitz, and J. Edward Duggan (2011). The dissertation author is the first author of this paper.

Bibliography

Fujii, K., Tamura, Y., Sato, T., and Wakahara, T. (1990). "Wind-induced vibration of tower and practical applications of tuned sloshing damper." *Journal of Wind Engineering and Industrial Aerodynamics*, 33(1-2), 263–272.

He, X., Moeveni, B., Conte, J. P., Elgamal, A., and Masri, S. F. (2009). "System identification of Alfred Zampa Memorial Bridge using dynamic field test data." *Journal of Structural Engineering*, 135(1), 54–66.

Henderson, A. P. and Patrick, M. B. (1994). "Tensionless pier foundation." U.S. Patent 5586417.

James III, G. H., Carne, T. G., and Lauffer, J. P. (1992). "The natural excitation technique (NExT) for modal parameter extraction from operating wind turbines." *Report No. SAND92-1666, UC-261*, Sandia National Laboratories.

Jonkman, J. M. and Buhl Jr., M. L. (2005). "FAST user's guide." *Report No. NREL/EL-500-38230*, National Renewable Energy Laboratory.

Juang, J. N. and Pappa, R. S. (1985). "An eigensystem realization algorithm for modal parameter identification and model reduction." *Journal of Guidance, Control, and Dynamics*, 8(5), 620–627.

Molinari, M., Pozzi, M., Zonta, D., and Battisti, L. (2010). "In-field testing of a steel wind turbine tower." *Proceedings of the IMAC-XXVIII*, Bethel, Connecticut, USA. Society for Experimental Mechanics Inc., 1–10.

Ohta, Y. and Goto, N. (1978). "Empirical shear wave velocity equations in terms of characteristic soil indexes." *Earthquake Engineering and Structural Dynamics*, 6(2), 167–187.

Peeters, B. and De Roeck, G. (2001). "One-year monitoring of the Z24-Bridge: environmental effects versus damage events." *Earthquake Engineering & Structural Dynamics*, 30(2), 149–171.

Riziotis, V. A., Voutsinas, S. G., Politis, E. S., and Chaviaropoulos, P. K. (2004). "Aeroelastic stability of wind turbines: the problem, the methods and the issues." *Wind Energy*, 7(4), 373–392.

Wiser, R. and Bolinger, M. (2008). "Annual report on U.S. wind power installation, costs, and performance trends: 2007." *Report No. DOE/GO-102008-2590*, Department of Energy.

Witcher, D. (2005). "Seismic analysis of wind turbines in the time domain." *Wind Energy*, 8(1), 81–91.

Chapter 6

Assessment of Soil-Structure Interaction of Large Wind Turbines

6.1 Introduction

Expanding on previous investigations, this chapter presents a preliminary investigation into the influence of SSI on the seismic response of the United States National Renewable Energy Laboratory (NREL) 5-MW reference turbine (Jonkman et al., 2009). First, a detailed finite element (FE) model of the turbine is created and validated by comparison with published properties of the NREL 5-MW reference turbine, and extended to include a full three-dimensional soil mesh. The soil-turbine system is then modified to simulate 3 different 15-meter thick soil profiles and subjected to a 1994 Northridge Earthquake record. Using these models simulations are conducted to further assess the influence of SSI on the relative distribution of tower moment and shear demand.

6.2 Turbine and Foundation Description

The National Wind Technology Center (NWTC) located at NREL has published specifications for a reference 5-MW turbine (Table 6.1). This reference model is intended to serve as a standard model for conceptual studies of modern multi-megawatt turbines. Being a slender structure with a hub height of 90 meters, this turbine is similar to structures that might experience significant SSI effects (Luco, 1986).

Table 6.1: Main parameters of 5-MW reference wind turbine

Type	Horizontal axis wind turbine
Power rating	5-MW
Rotor configuration	3 blade upwind
Control	Variable speed, collective pitch
Drivetrain	High speed, multiple-stage gearbox
Cut-in wind speed	3 m/s
Rated wind speed	11.4 m/s
Cut-out wind speed	25 m/s
Rotor speed range	6.9 to 12.1 RPM
Rated tip speed	80 m/s
Rotor diameter	126 m
Tower height	87.6 m
Hub height	90 m
Mass of rotor	111,000 kg
Mass of nacelle	240,000
Mass of tower	347,460 kg

In this study a Patrick and Henderson Tensionless Pier Foundation (Henderson and Patrick, 1994) is considered that consists of a hollow cylindrical concrete shell with a 6.5 meter outer diameter that extends 9-meters below ground surface. Outer and inner corrugated metal shells 0.3 meters apart constitute the hollow cylinder with concrete poured in between. The inner shell is then backfilled with the excavated soil. The turbine tower is attached to the foundation through un-bonded post tensioned

bars that extend to the bottom of the foundation.

6.3 Fixed Base FE Model Description

A simple fixed base FE model was developed that represented the turbine tower, nacelle, and rotor (Figure 4.1(b)) through beam-column elements. Previous work suggests that a beam-column model can provide results that are consistent with more detailed shell models for towers (Bazeos et al., 2002) as well as turbine blades (Malcolm and Laird, 2003). This simple configuration represents the predominant approach for numerical modeling of wind turbines for seismic applications (Bazeos et al., 2002; Ritschel et al., 2003; Jonkman and Buhl Jr., 2005; Witcher, 2005; Häenler et al., 2006).

The FE model was implemented using the computational platform OpenSees (Mazzoni et al., 2006). The tower (Figure 4.1(b)) was divided into 100 beam-column elements with a flexural stiffness based on the cross section of the tower at the center of each element (Jonkman et al., 2009). A total of 48 beam-column elements per blade were used to simulate the mass and stiffness distribution (Jonkman et al., 2009) (Figure 4.1(b)).

With a Young's Modulus for steel of 210 GPa, the above model closely matches the relevant natural frequencies (Table 6.2) reported for the FAST model of the NREL 5-MW reference turbine (Jonkman et al., 2009). The first tower bending mode shapes are shown in Figures 6.1 and 6.2. The 2nd tower bending modes can be observed in Figures 6.3 and 6.4. Though the turbine tower is rotationally symmetric it is

important to consider tower bending modes in both directions because the nacelle and rotor result in different natural frequencies and mode shapes for each direction.

Table 6.2: Fixed base model natural frequencies

Tower Property	Predicted frequency (Hz)	
	FAST	OpenSees
1st Tower Fore-Aft	0.32	0.32
1st Tower Side-to-Side	0.31	0.31
2nd Tower Fore-Aft	2.90	2.75
2nd Tower Side-to-Side	2.93	2.95

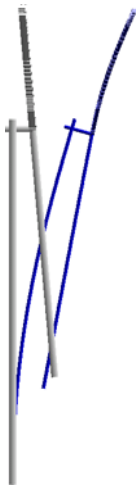

Figure 6.1: 1st fore-aft bending mode for fixed base model

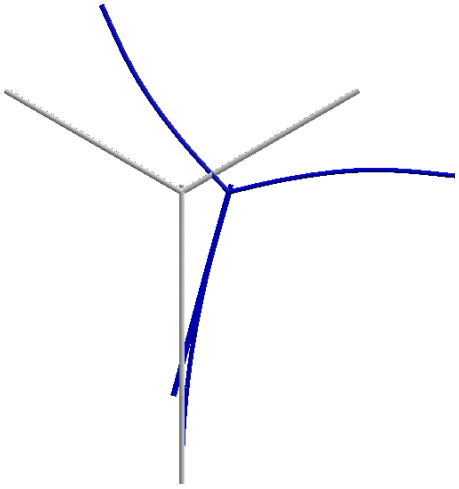

Figure 6.2: 1st side-to-side bending mode for fixed base model

6.4 SSI Model Development

Previous investigations have considered SSI for wind turbines by using equivalent springs and dampers (Jonkman et al., 2009; Zhao and Maißer, 2006). Theory exists to make these springs and dampers independent of the soil and structure system natural frequencies, but large errors may occur in the soil-structure system response at resonance (Ghaffar-Zadeh and Chapel, 1983).

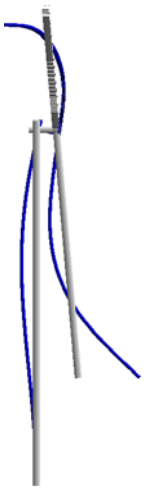

Figure 6.3: 2nd fore-aft bending mode for fixed base model

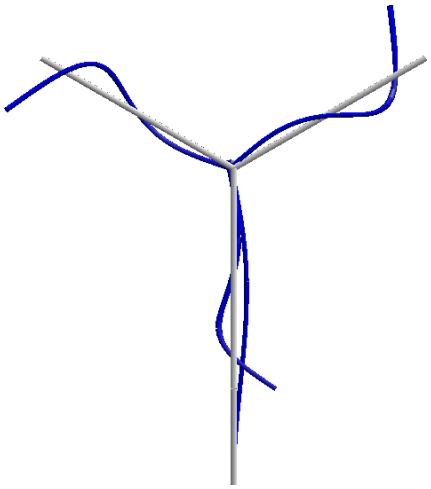

Figure 6.4: 2nd side-to-side bending mode for fixed base model

In this investigation, a full soil mesh is used in order to avoid this source of possible error. Given the continued proliferation of computational power, this approach may prove to be more direct in certain respects. In addition, it is more adaptable to realistic sites where the soil profile is layered.

To numerically consider the impact of SSI for a wind turbine, the fixed base model was extended using OpenSeesPL (Lu et al., 2006) to include a soil domain and a foundation model (Figure 6.5). Linear elastic brick elements with appropriate stiffness and density were used to model the foundation and soil. The soil is modeled first as stiff clay (Table 6.3). The foundation, described earlier, was modeled as a hollow cylinder of elastic material. In this analysis model, the foundation and adjacent soil remain in perfect contact.

Table 6.3: Summary of soil properties (Mazzoni et al., 2007)

Soil type	Soft	Medium	Stiff
Density (ton/m^3)	1.3	1.5	1.8
Shear Modulus (kPa)	1.3 x 10^4	6 x 10^4	15 x 10^4
Bulk Modulus (kPa)	6.5 x 10^4	30 x 10^4	75 x 10^4

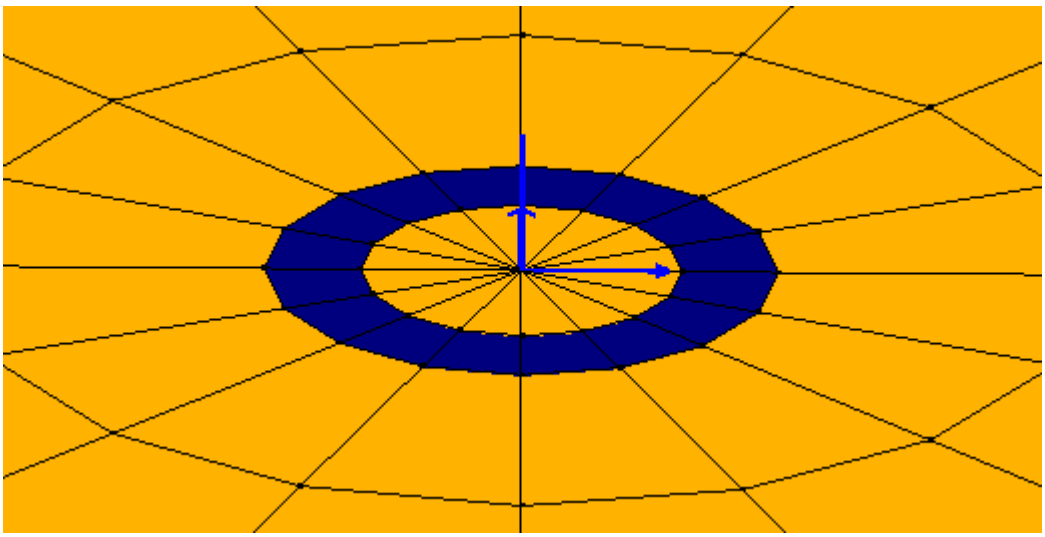

Figure 6.5: Close up of foundation detail in soil mesh

To minimize boundary effects, the soil was modeled to a depth of over 200 meters and a horizontal distance of over 400 meters. The total model consisted of over 1,300 soil elements. Figure 6.6 shows the scale of the mesh in comparison to the size of the turbine. Other meshes were evaluated to verify that the reported results were not influenced by the soil model geometry.

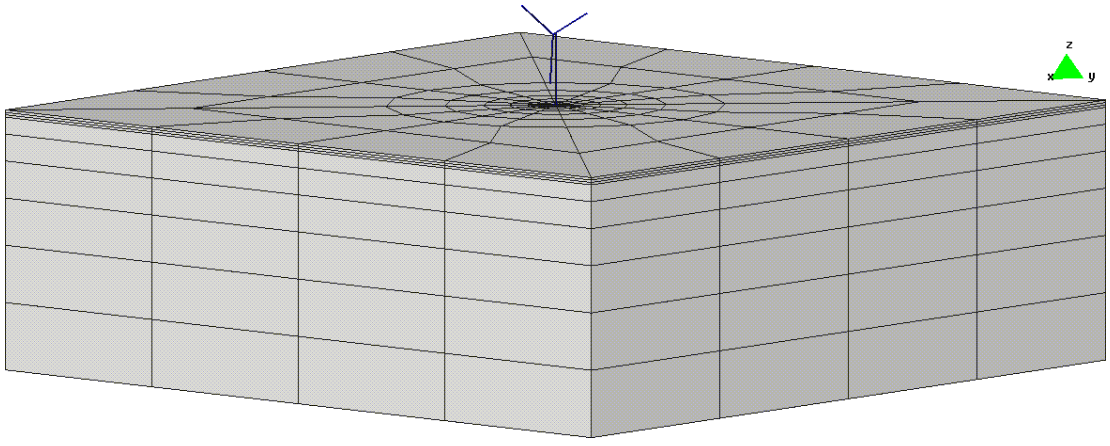

Figure 6.6: Full three-dimensional model of soil and turbine

When modeled with the soil mesh, the first natural frequency occurred at 0.3

Hz for both the fore-aft and side-to-side bending modes. This is close to the fixed base frequency (Table 6.2). Observing the mode shapes (Figures 6.7 and 6.8) shows little influence from the soil mesh on base rotation because of the relative stiffness of the soil and foundation system in comparison to the turbine tower. The second bending mode was predicted at 2.75 Hz for the fore-aft mode and 2.93 Hz side-to-side mode, which closely matches the frequencies of the fixed base model. Again, the mode shapes (Figures 6.9 and 6.10) show little base rotation.

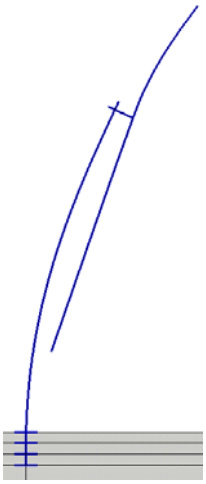

Figure 6.7: 1st fore-aft bending mode for stiff soil model

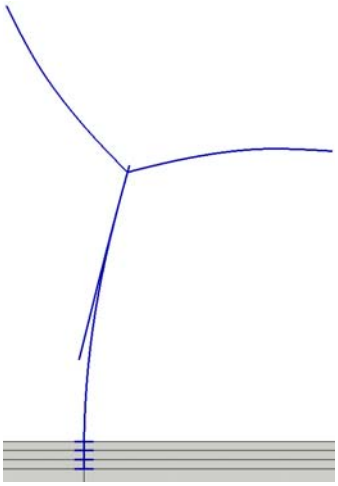

Figure 6.8: 1st side-to-side bending mode for stiff soil model

6.5 SSI Impact for Softer Soil Scenarios

The numerical data presented above shows little SSI effect on the first and second longitudinal bending modes for a turbine founded on stiff clay. To explore the influence of softer soils, the soil properties were modified to create additional medium and soft ground scenarios. A summary of the elastic soil properties is shown in Table 6.3.

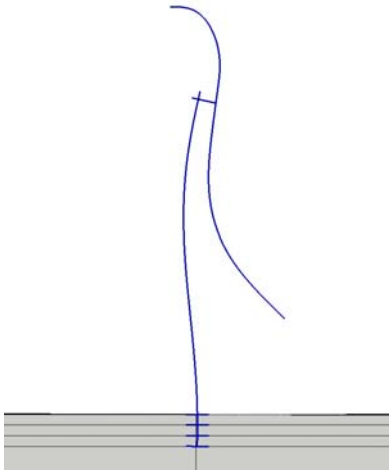

Figure 6.9: 2nd fore-aft bending mode for stiff soil model

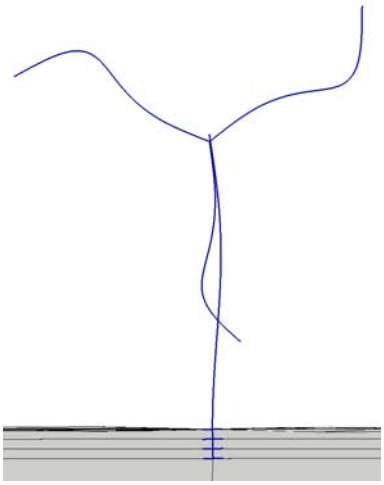

Figure 6.10: 2nd side-to-side bending mode for stiff soil model

The impact of SSI on modal frequencies for the three soil stiffness scenarios is shown in Table 6.4. The resulting mode shapes for the medium stiffness clay were similar to those of the stiff soil model (Figures 6.7, 6.8, 6.9 and 6.10). When the stiffness of the soil mesh was further reduced to the soft scenario, the first natural frequencies were lowered to 0.28 Hz for the fore-aft and side-to-side modes (Figures 6.11 and 6.12). The corresponding second natural frequency for both the second fore-aft and side-to-side modes was found to be 2.68 Hz (Figures 6.13 and 6.14). The second mode in particular shows a pronounced influence from the soil mesh, observable mainly as a rotation of the foundation within the soil (Figures 6.13 and 6.14). The fore-aft second mode (Figure 6.13) further shows a clear influence of added mass from the soil.

Table 6.4: Comparison of natural frequencies for turbine and soil models

Model	Stiff soil	Medium soil	Soft soil
1st Tower Fore-Aft	0.30	0.30	0.28
1st Tower Side-to-Side	0.30	0.30	0.28
2nd Tower Fore-Aft	2.73	2.74	2.68
2nd Tower Side-to-Side	2.93	2.92	2.68

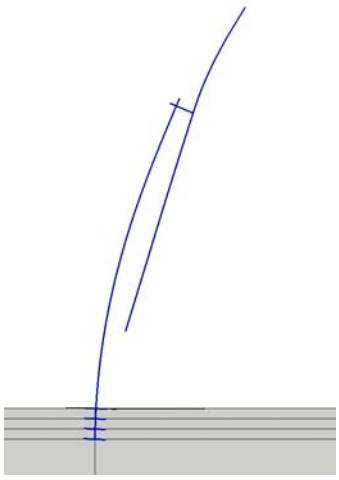

Figure 6.11: 1st fore-aft bending mode for soft soil model

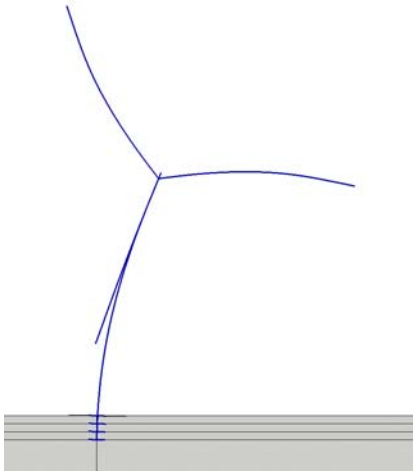

Figure 6.12: 1st side-to-side bending mode for soft soil model

6.6 Earthquake loading for different soils

For simulations of earthquake loading the soil portion of the SSI models was modified to consist of a 15 meter layer of clay underlain by rock. A recording of the 1994 Northridge Earthquake at a granitic rock site was used as the input motion at the base of the clay layer. For this soil profile the same three stiffness values (Table 6.3) previously investigated for influence on modal parameters were simulated. Table 6.5 shows the analytically calculated (Kramer, 1996) and simulated first resonant frequencies of the soil layers. A soil thickness of 15 meters was selected as it is a plausible soil layer. Further consideration was given to ensure the resulting resonances (Table 6.5) did not directly coincide with those of the fixed base turbine (Table 6.2)

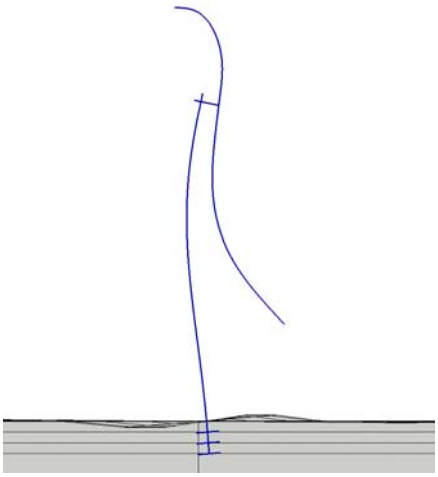

Figure 6.13: 2nd fore-aft bending mode for soft soil model

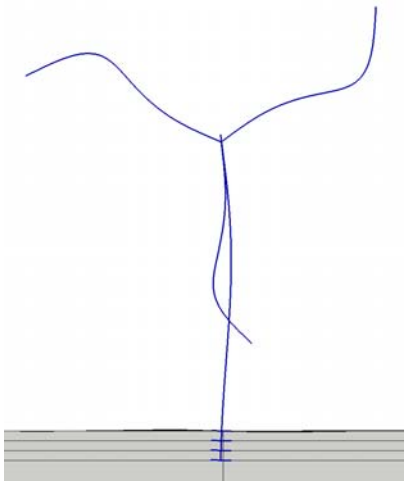

Figure 6.14: 2nd side-to-side bending mode for soft soil model

or those calculated with the influence of the respective soils (Table 6.4).

Table 6.5: First resonant frequencies of 15 meter soil layer

Soil type	Soft	Medium	Stiff
Analytical first resonance	1.7 Hz	3.3 Hz	4.8 Hz
FE Model first resonance	1.7 Hz	3.3 Hz	4.8 Hz

The three SSI models were then subjected to the 1994 Northridge Earthquake record (6.7 moment magnitude) as recorded at the California Strong Motion Instrumentation Program (CSMIP) station 24399, Mt. Wilson. The recording was measured 36.7 km from the source fault and contains a peak ground acceleration of 228.5 cm/s^2, 130.7 cm/s^2, and 87.1 cm/s^2 in the north-south, east-west, and up-down directions, respectively. The north-south component was imparted in line with the turbine drive shaft, the east-west component was applied horizontally perpendicular to the drive shaft, and the up-down component was applied vertically.

6.7 Simulation Results

With a relatively low damping value of 2 percent employed for the soil domain in simulations, the soil layer both amplified and altered the relative amplitude of different frequency components from the input motion (Figure 6.15. The absolute acceleration at the soil surface for the soft soil profile is shown in Figure 6.16. Though soil loads would be driven by relative acceleration, absolute acceleration is shown as it functions as the input to the turbine model. In addition to translation the turbine base is also subjected to rotation as a result of soil compliance. Similar amplification was observed for the other soil profiles. The difference relative amplitude of frequency components results in unique ground motion at the soil surface for each of the simulations.

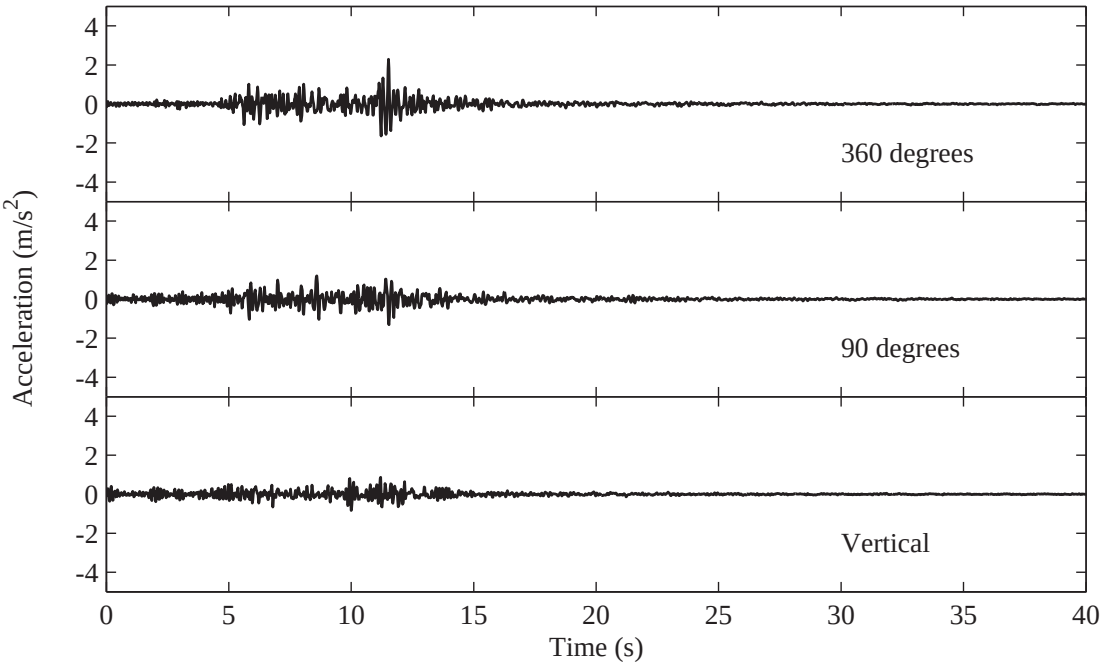

Figure 6.15: Input motion used for simulations from 1994 Northridge Earthquake

To investigate the possible implications of the three scenarios on design, the

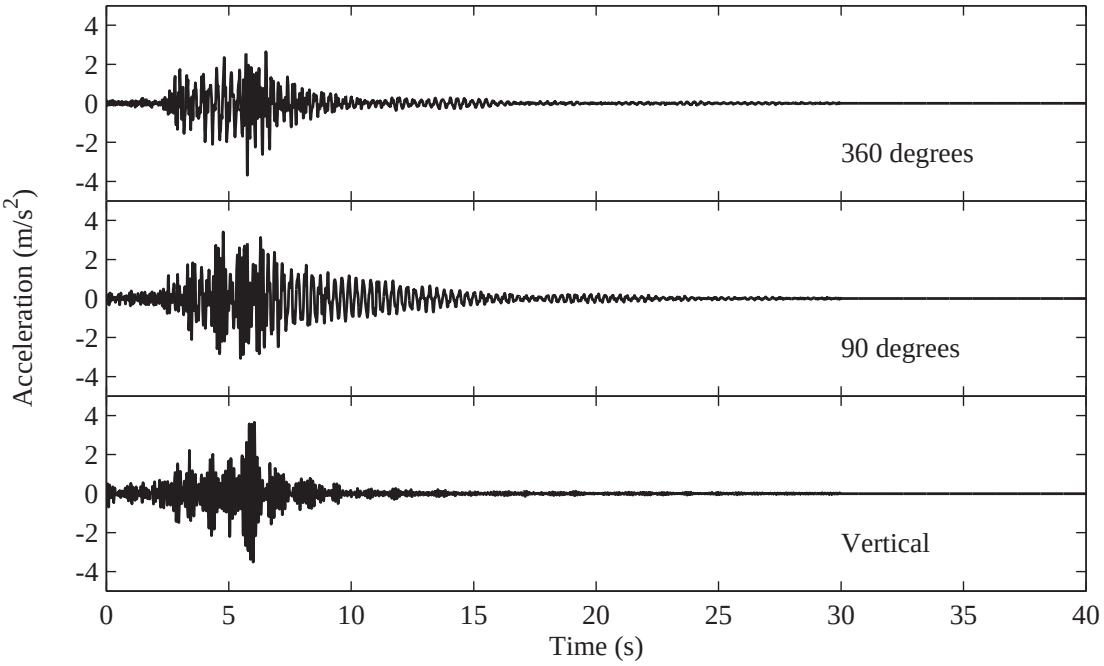

Figure 6.16: Absolute acceleration at soil surface for soft profile

maximum moment and shear demand at the base, 9 locations along the tower, and the top of the tower (Figure 4.1(b)) were calculated. This maximum was taken from the square root of the sum of the squares (SRSS) of the horizontal tower moments at each time step. The resulting moment and shear demand for each of the three soil stiffness scenarios is shown in Figure 6.17 and Figure 6.18, respectively.

As each of the scenarios resulted in different input motions at the turbine base a comparison of moment and shear magnitudes is not instructive. Instead, it is of interest to observe the difference in distribution of maximum moment and shear because this may require redesign of the upper portion of the tower, where it is generally assumed to have considerable lower demand.

All simulation show a second peak in maximum moment demand (Figure 6.17) near the point of maximum displacement in the second tower bending mode (Figures

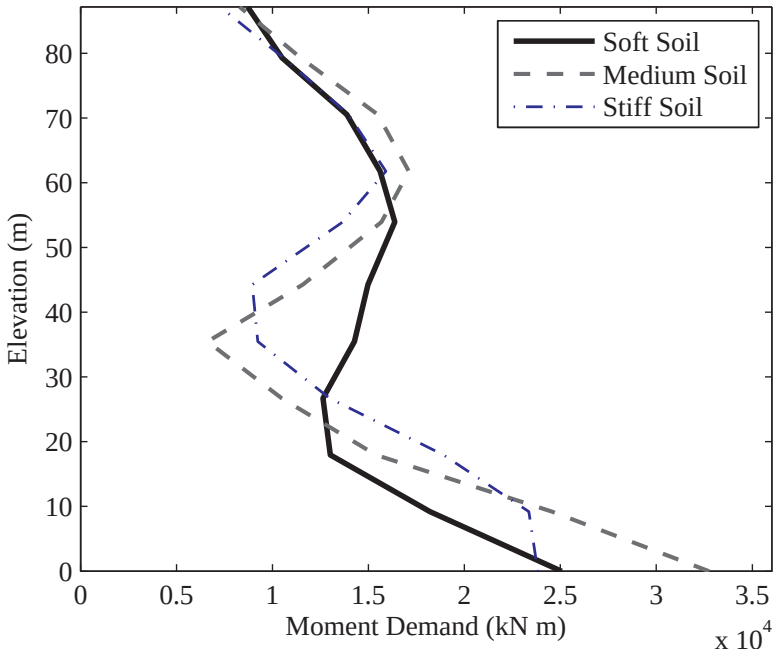

Figure 6.17: Tower moment demand for soil profiles

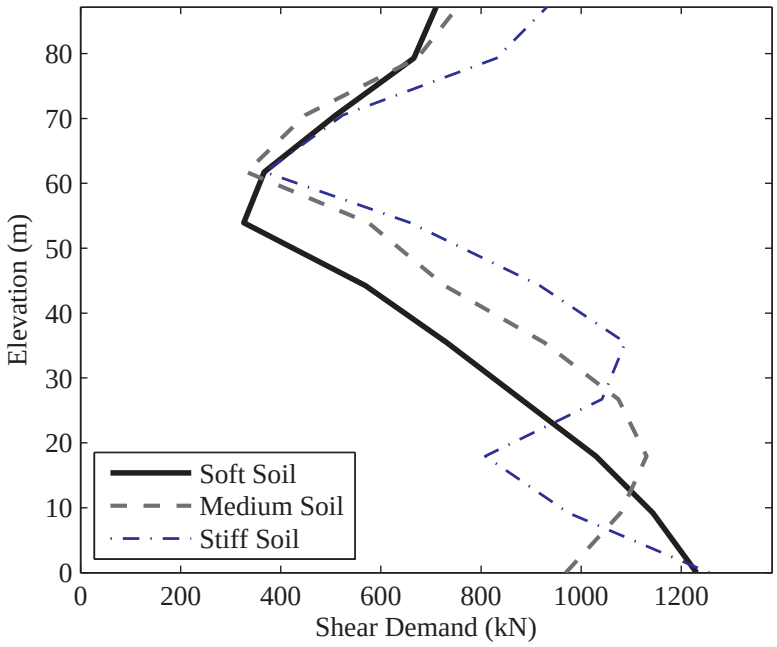

Figure 6.18: Tower shear demand for soil profiles

6.3 and 6.4) not found in fixed base simulations of earthquake loading for smaller turbines (Ritschel et al., 2003; Prowell et al., 2010). In the medium soil simulation, the moment demand shows a higher concentration of moment demand at the base than the other simulations. The soft soil simulation shows a more constant maximum moment demand for the tower in comparison to the two other simulations.

In contrast, the simulations show a minimum in shear demand (Figure 6.18) near the point of maximum displacement in the second tower bending mode (Figures 6.3 and 6.4). The medium soil profile results in a maximum in shear demand around 20 meters up the tower instead of the expected location at the base of the tower.

6.8 Conclusion

A preliminary numerical investigation of the resonant characteristics of a 5-MW wind turbine was presented. Numerical modeling showed the relatively stiff soil produced little SSI influence on the first and second longitudinal modes. In contrast, when softer soils were investigated, a more significant influence was apparent. The second bending mode behavior was clearly impacted, showing a reduction in frequency and increased foundation rotation. However, these changes in dynamic properties (Table 6.4) are small in comparison to safety margins used to space mechanical vibration and resonant frequencies and would are not likely to require redesign of the turbine to account for SSI.

When earthquake like motion was investigated through a simulation of the Northridge (1994) earthquake it was found that the soil stiffness can influence the

maximum moment (Figure 6.17) and shear (Figure 6.18) demand distributions. Unlike the differences in natural frequencies, this shift in demand parameter distribution may influence turbine design. In particular, the increased demand at higher elevations, near maximum displacement in the second mode, may require special consideration of this portion of the tower for large turbines installed in seismically active regions. This conclusion is specific to the ground motion and soil profile considered. It is important for consideration of soil structure interaction that local site conditions and a range of carefully selected ground motions that match the anticipated shaking for the proposed site be selected.

Wind turbines are installed in all soil types throughout the world. This investigation found that for this particular 5-MW turbine, SSI influence on the first and second longitudinal bending modal parameters may be relatively minor, while maximum moment and shear demand distribution may be more significant. This observed influence is specific to the configuration considered here and may be mitigated in actual turbines by appropriate redesign of the tower and foundation to minimize SSI influence. With current trends toward taller and more massive turbines (Wiser and Bolinger, 2008), it is important to conduct further SSI research as an integral component of seismic response studies.

6.9 Acknowledgements

The text below is reproduced verbatim as it appears in the acknowledgments section on page xvii per the UCSD Office of Graduate Studies Formatting Require-

ments.

Chapter 6 of this dissertation is an extended version of the material published in the proceedings of the following two conferences (1) 17th International Conference on Soil Mechanics & Geotechnical Engineering, Alexandria, Egypt, titled "Modal properties of a modern wind turbine including SSI," with authors Ian Prowell, Ahmed Elgamal, Jinchi Lu, and J. Enrique Luco (2009) and (2) 5th International Conference on Recent Advances in Geotechnical Earthquake Engineering and Soil Dynamics in Honor of Professor I.M. Idriss, San Diego, California, USA, titled "Modeling the Influence of Soil Structure Interaction on the Seismic Response of a 5 MW Wind Turbine," authored by Ian Prowell, Ahmed Elgamal, and Jinchi Lu (2010). The dissertation author is the first author of these papers.

Bibliography

Bazeos, N., Hatzigeorgiou, G. D., Hondros, I. D., Karamaneas, H., Karabalis, D. L., and Beskos, D. E. (2002). "Static, seismic and stability analyses of a prototype wind turbine steel tower." *Engineering Structures*, 24(8), 1015–1025.

Ghaffar-Zadeh, M. and Chapel, F. (1983). "Frequency-independent impedances of soil-structure systems in horizontal and rocking modes." *Earthquake Engineering & Structural Dynamics*, 11(4), 523–540.

Häenler, M., Ritschel, U., and Warnke, I. (2006). "Systematic modelling of wind turbine dynamics and earthquake loads on wind turbines." *European Wind Energy Conference and Exhibition*, Athens, Greece. European Wind Energy Association, 1–6.

Henderson, A. P. and Patrick, M. B. (1994). "Tensionless pier foundation." U.S. Patent 5586417.

Jonkman, J., Butterfield, S., Musial, W., and Scott, G. (2009). "Definition of a 5-MW reference wind turbine for offshore system development." *Report No. NREL/TP-500-38060*, National Renewable Energy Laboratory.

Jonkman, J. M. and Buhl Jr., M. L. (2005). "FAST user's guide." *Report No. NREL/EL-500-38230*, National Renewable Energy Laboratory.

Kramer, S. L. (1996). *Geotechnical Earthquake Engineering*. Prentice-Hall, Upper Saddle River, New Jersey, USA.

Lu, J., Elgamal, A., and Yang, Z. (2006). "Openseespl three-dimensional lateral pile-ground interaction version 1.00 user's manual." *Report No. SSRP-06/04*, Department of Structural Engineering, University of California, San Diego.

Luco, J. E. (1986). "Soil-structure interaction effects on the seismic response of tall chimneys." *Soil Dynamics and Earthquake Engineering*, 5(3), 170–177.

Malcolm, D. J. and Laird, D. L. (2003). "Modeling of blades as equivalent beams for aeroelastic analysis." *2003 ASME Wind Energy Symposium AIAA/ASME*, Reno, Nevada, USA. 293–303.

Mazzoni, S., McKenna, F., and Fenves, G. L. (2006). *Open System for Earthquake Engineering Simulation User Manual*. Pacific Earthquake Engineering Research Center, Berkeley, California, USA.

Mazzoni, S., McKenna, F., Scott, M. H., and Fenves, G. L. (2007). *Open System Command Language Manual*. Pacific Earthquake Engineering Research Center, University of California, Berkeley, California, USA.

Prowell, I., Elgamal, A., and Jonkman, J. (2010). "Fast simulation of seismic wind turbine response." *Report No. NREL/CP-500-46225*, National Renewable Energy Laboratory.

Ritschel, U., Warnke, I., Kirchner, J., and Meussen, B. (2003). "Wind turbines and earthquakes." *2nd World Wind Energy Conference*, Cape Town, South Africa. World Wind Energy Association, 1–8.

Wiser, R. and Bolinger, M. (2008). "Annual report on U.S. wind power installation, costs, and performance trends: 2007." *Report No. DOE/GO-102008-2590*, Department of Energy.

Witcher, D. (2005). "Seismic analysis of wind turbines in the time domain." *Wind Energy*, 8(1), 81–91.

Zhao, X. and Maißer, P. (2006). "Seismic response analysis of wind turbine towers including soil-structure interaction." *Proceedings of the Institution of Mechanical Engineers, Part K: Journal of Multi-body Dynamics*, 220(1), 53–61.

Chapter 7

Simulation of Seismic Loads Using the FAST Code

7.1 Introduction

The FAST code is an open source piece of software capable of modeling turbine dynamics (Jonkman and Buhl Jr., 2005). In this chapter modifications to the FAST code are introduced, which enable base shaking time histories to be applied in conjunction with other load sources for wind turbines. First, the FAST code is described with pertinent details of the modifications required for consideration of seismic input. Simulations of a parked turbine subjected to base shaking without consideration of aerodynamics are compared to OpenSees simulations using an experimentally validated turbine model (Prowell et al., 2008). Next, the results presented in Chapter 3 where the turbine was operating while earthquake like input was imparted are used to validate that salient changes in dynamics are numerically reproduced. Lastly, a

FAST model of the 900-kW turbine discussed in Chapter 4 is developed and used to illustrate the importance of considering aerodynamic forces on a turbine when assessing seismic loads.

7.2 Description of the FAST Code

The FAST code is a package that models two- and three-bladed horizontal-axis wind turbines (HAWTs) under various conditions to predict extreme and fatigue loads (Jonkman and Buhl Jr., 2005). For aerodynamic calculations, the FAST code employs the subroutines for HAWTs in the AeroDyn Code (Laino and Hansen, 2002). The FAST code uses a combined modal and multibody dynamics formulation to simulate a turbine's behavior in the time domain. The code solves the equations of motion using a standard multibody dynamics formulation with elements whose flexibility is determined by summing user-defined mode shapes. Wind turbine designers and researchers throughout the world use the FAST code. Germanischer Lloyd Wind Energie evaluated the code and found it suitable for calculating onshore wind turbine loads for design and certification.

Of particular interest to this work are recent updates to the FAST code that allow modeling of an offshore turbine on a movable platform (Jonkman, 2007). These updates are a mechanism to supply a force and moment to be applied at the tower base platform with six degrees of freedom at each time step for a time marching simulation. In earthquake engineering, a base acceleration time history is responsible for the resulting structural loads. The model configuration may prescribe displacement,

velocity, or acceleration time histories for each of the three translational axes. From the prescribed time histories, the corresponding displacement and velocity histories are calculated. At each time step, the forces required to achieve the desired time histories are calculated by simulating a damped oscillator attached at the base of the turbine. By setting the natural frequency of the damped oscillator at twice the highest frequency found in the input motion and using a damping of 65% of critical, a faithful reproduction of the desired time histories can be reproduced. This frequency must also be greater than twice the highest resonance in the turbine model. It is important to note that the simulation time step must be kept sufficiently small to produce stable results. In this investigation, it was found that a time step of 0.002 seconds produced stable results for all simulations.

The current implementation implicitly assumes that the foundation-soil system acts as a rigid block without rocking, but future improvements could remove this limitation. For stiff soil sites, foundation rocking is frequently neglected in earthquake engineering. Site specific conditions should be evaluated to ensure validity for a specific location. In conjunction with the prescribed time histories, all other loading mechanisms in the FAST code are still available. This allows time domain simulation of simultaneous earthquake and wind loads as well as the required simulation of an earthquake-induced emergency shutdown (IEC, 2005). Conducting simulations in the time domain allows a researcher to directly consider nonlinear effects such as structural nonlinearities, aerodynamic hysteresis, control system influence, and transients all of which are important to wind turbine response.

7.3 Comparison to OpenSees Results

7.3.1 OpenSees Model

A finite element (FE) model was developed for OpenSees (Mazzoni et al., 2006) based on the engineering properties of the turbine (Table 2.1) to facilitate dynamic simulation of the turbine while idling. The tower (Figure 3.2) was divided into 30 beam-column elements with a flexural stiffness based on the cross section at the center of each element. Each blade was modeled using 12 beam-column elements to represent the mass and stiffness of the rotor (Figure 3.2). The nacelle was modeled with rigid elements to connect the top of the tower to the rotor. A hinge condition was added to allow for the free rotation of the rotor.

For a parked condition at zero rotational speed, the FE model predicted the first fore-aft (Figure 2.11) and side-to-side (Figure 2.10) bending modes at 1.70 Hz and 1.71 Hz, respectively. The second bending modes were predicted at 11.8 Hz in the fore-aft direction and 12.3 Hz in the side-to-side direction. This model configuration was validated based on full-scale shake table tests of the 65-kW Nordtank turbine and produces good agreement for the predicted and observed mode shapes and frequencies (Prowell et al., 2009). Based on the test results and industry guidelines (IEC, 2005), structural damping was set to 1% for the first mode. Specified in the form of Rayleigh damping, a value of 3.5% was used at 12 Hz to better match the recorded results.

7.3.2 FAST Model

As described earlier, the FAST code is a combined multi-body and modal dynamics formulation. In a FAST model there are five flexible bodies: the tower; three blades; and the drive shaft. As in the OpenSees model described above, the nacelle (Figure 3.2) is considered a rigid body. The mass and stiffness distribution used for the FAST model was derived to match that used in the OpenSees model as closely as possible. The FAST code relies on external calculation of mode shapes and requires that mode shapes be described by a five coefficient polynomial of the form: $\phi(x) = a_2x^2 + a_3x^3 + a_4x^4 + a_5x^5 + a_6x^6$. The coefficients must sum to a value of 1. As the tower is assumed to have a cantilevered base, the constant and linear coefficients are neglected. Coefficients used for the model described here were calculated by selecting polynomial coefficients that best approximated the first side-to-side and fore-aft modes (Figures 2.10 and 2.11) as well as the second side-to-side and fore-aft modes developed from the OpenSees model.

Using engineering properties in conjunction with both the tower and blade dynamic characterization identification results, a model of the turbine was constructed for the FAST code. The resulting FAST model was tuned to predict the first and second side-to-side and fore-aft bending modes for the parked turbine at the same frequencies as experimentally identified (Table 3.5). In addition, blade stiffness was adjusted to match the first flap and edge modes identified experimentally (Table 3.7). The resulting mode types and frequencies for the turbine model are presented and compared to experimental estimates in Table 7.1. Observed and predicted properties

agreed well, with the exception of the observed coupled bending mode and the second blade flap modes.

Table 7.1: Predicted and identified natural frequencies while parked for 65-kW Nordtank turbine

Mode Type	Orientation	OpenSees Model Freq. (Hz)	FAST Model Freq. (Hz)	Exp. Estimate Freq. (Hz)
1st Bending	Fore-aft	1.70	1.70	1.70
	Side-to-side	1.71	1.71	1.71
Asymmetric 1st Blade Flap	-	3.35	3.41	3.47
Collective 1st Blade Flap	-	3.40	3.43	3.47
Asymmetric 1st Blade Flap	-	3.51	3.51	3.47
Asymmetric 1st Blade Edge	-	5.51	5.60	5.79
Asymmetric 1st Blade Edge	-	5.70	5.72	5.79
Collective 1st Blade Edge	-	5.78	5.81	5.79
Collective 2nd Blade Flap	-	7.96	9.17	11.0
Asymmetric 2nd Blade Flap	-	8.11	9.35	11.0
Asymmetric 2nd Blade Flap	-	8.32	9.48	11.0
2nd Bending	Fore-aft	11.8	11.9	11.9
	Side-to-side	12.3	12.4	12.4

7.3.3 Comparison of Seismic Response While Parked

The two turbine models were used to conduct base shaking simulations for three earthquakes recorded in California (Table 7.2). Since OpenSees cannot address aerodynamics and other operational loads for a turbine, both models were developed so that the wind turbine was parked with the high speed shaft brake engaged without aerodynamics during the simulations to accommodate direct comparison. Both horizontal components of the time histories were used to simulate the response of a turbine for a fixed base condition. This assumption is suitable for the stiff soils found at many wind farms. Further consideration of soil structure interaction would be

warranted for locations with soft soils (Bazeos et al., 2002; Zhao and Maißer, 2006). Figure 7.1 shows a comparison for the calculated acceleration from OpenSees and the FAST code at the top of the nacelle for 1981 Westmorland Earthquake acceleration time history recorded at the fire station. The results for the other earthquake simulations also show the same high level of agreement observed for the Westmorland Earthquake simulation.

Table 7.2: Earthquake data

Earthquake	Moment Mag. (M_w)	Station	PGA (g)	Source Dist. (km)
1981 Westmorland	5.9	Fire Station	0.50	7.2
2000 Yountville	5.0	Fire Station No. 3	0.41	13.7
1940 El Centro	6.9	Array Station 9	0.35	12.2

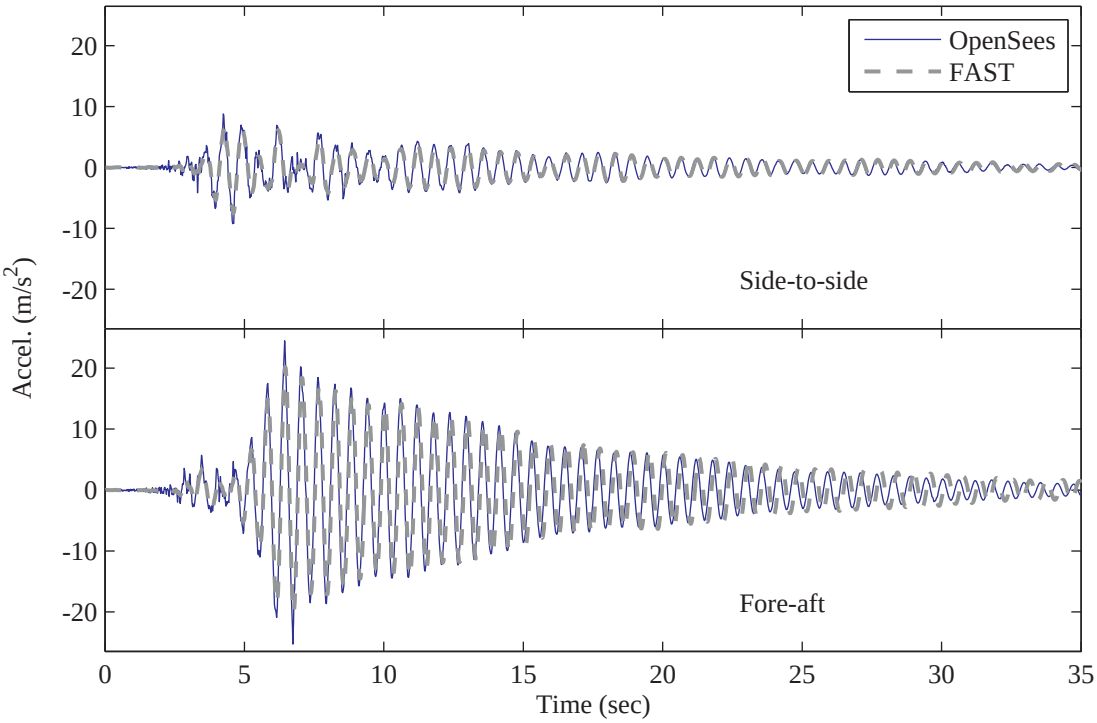

Figure 7.1: Comparison of acceleration time histories of 65-kW models for the 1981 Westmorland earthquake

To investigate the possible implications of the two models on design loads, the maximum moment demand at the base, the lower joint, the upper joint, and the top of the tower (Figure 3.2) was calculated. This maximum was taken from the square root of the sum of the squares (SRSS) of the horizontal tower moments at each time step. As with the acceleration time history, the moment demands calculated by the FAST and the OpenSees models show good agreement (Figure 7.2).

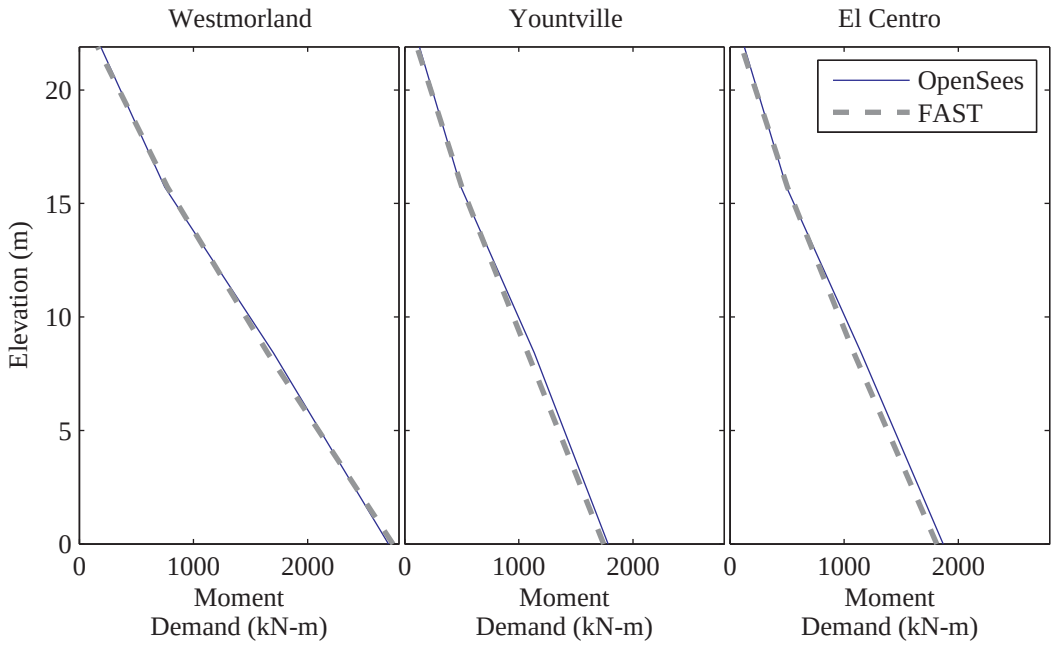

Figure 7.2: Comparison of moment demand for of 65-kW models

7.4 Simulations Including Aerodynamic and Operational Effects

Showing good agreement with OpenSees results, the FAST model was employed in simulations of seismic excitation of the 65-kW turbine discussed in Chapter

3. The recorded velocity time history from the corresponding experimental test was used as the earthquake input for each simulation. By using the recorded velocity instead of acceleration, the need to correct for residual velocity was eliminated thus reducing the amount of numerical manipulation required for simulations. The resulting acceleration from the simulations was compared to that recorded and found to agree.

For wind input in the simulations, a simple non-turbulent wind field with the estimated hub height wind speed and direction was used (Table 3.4). For operational simulations, the rotor angular velocity was kept at a constant 55 RPM, while the parked simulations were conducted with the high speed shaft brake engaged to prevent rotation, mirroring experimental conditions.

It is important to note that the simulation time step must be kept sufficiently small to produce stable results. In this investigation it was found that a time step of 0.001 seconds produced stable results for all simulations. Further, to allow dissipation of initial transient behavior, 300 seconds were simulated prior to initiation of the earthquake motions. In the results reported here, this initial period was discarded.

7.4.1 Simulation Results

To compare results from the simulations to those recorded experimentally, corresponding plots of tower top acceleration for EQ1, EQ2, and EQ3 (Figures 7.3 through 7.5), moment envelope (Figure 7.6), and acceleration envelope (Figure 7.7) were prepared. Inspection of these plots shows good agreement with general trends observed in the experimental results (Figures 3.31 through 3.34).

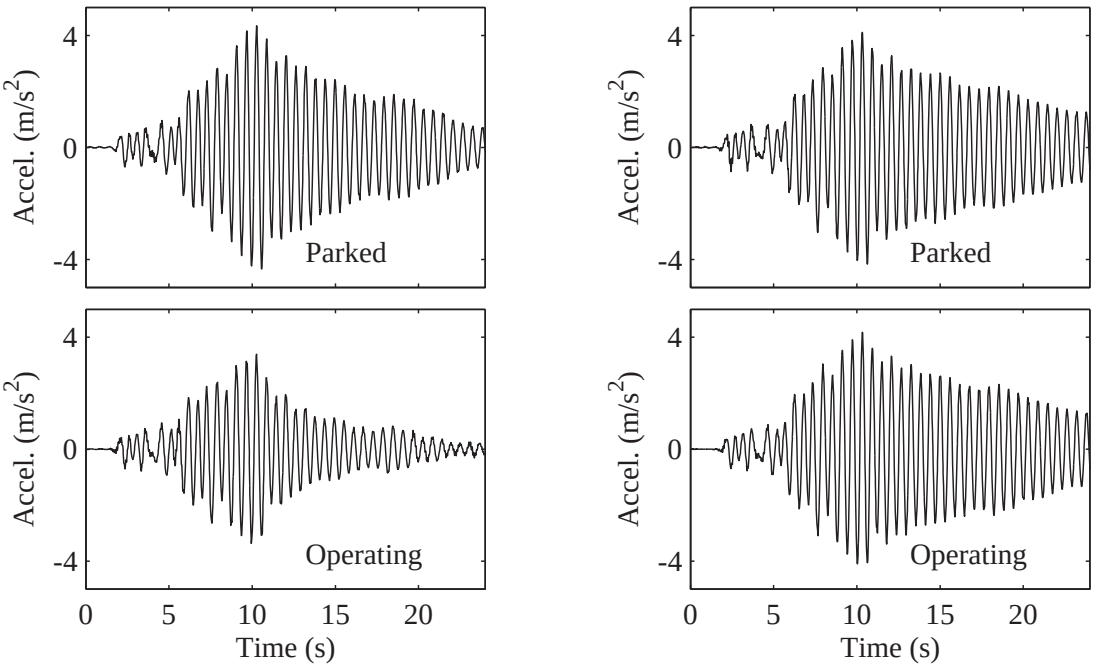

(a) Configuration 1 (b) Configuration 2

Figure 7.3: Simulated tower top in-plane absolute acceleration for EQ1

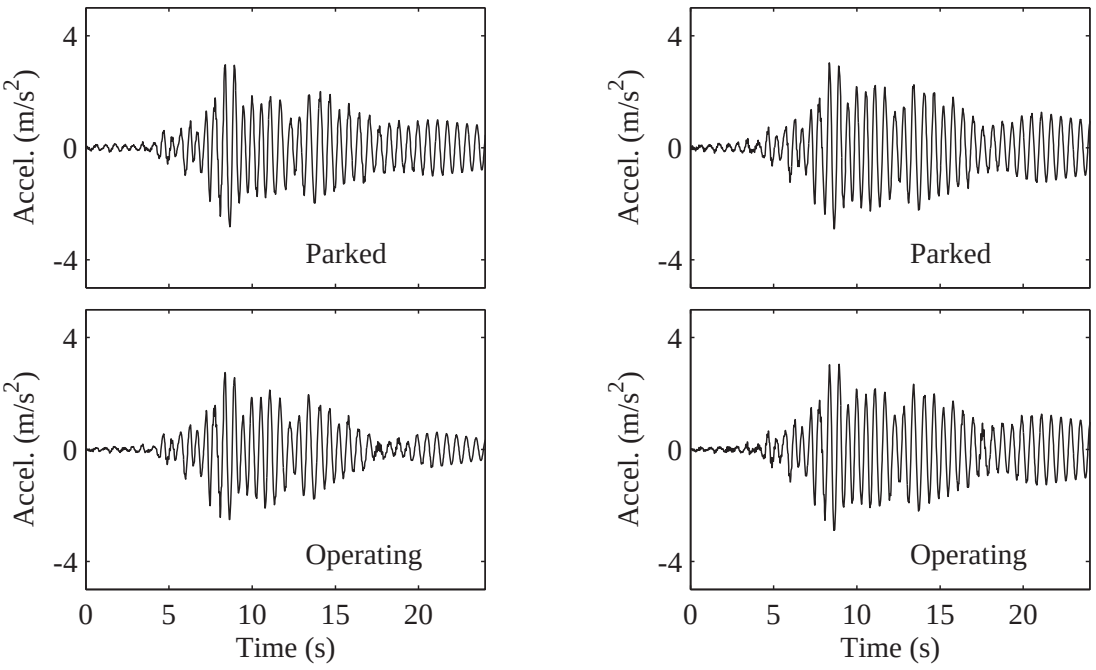

(a) Configuration 1 (b) Configuration 2

Figure 7.4: Simulated tower top in-plane absolute acceleration for EQ2

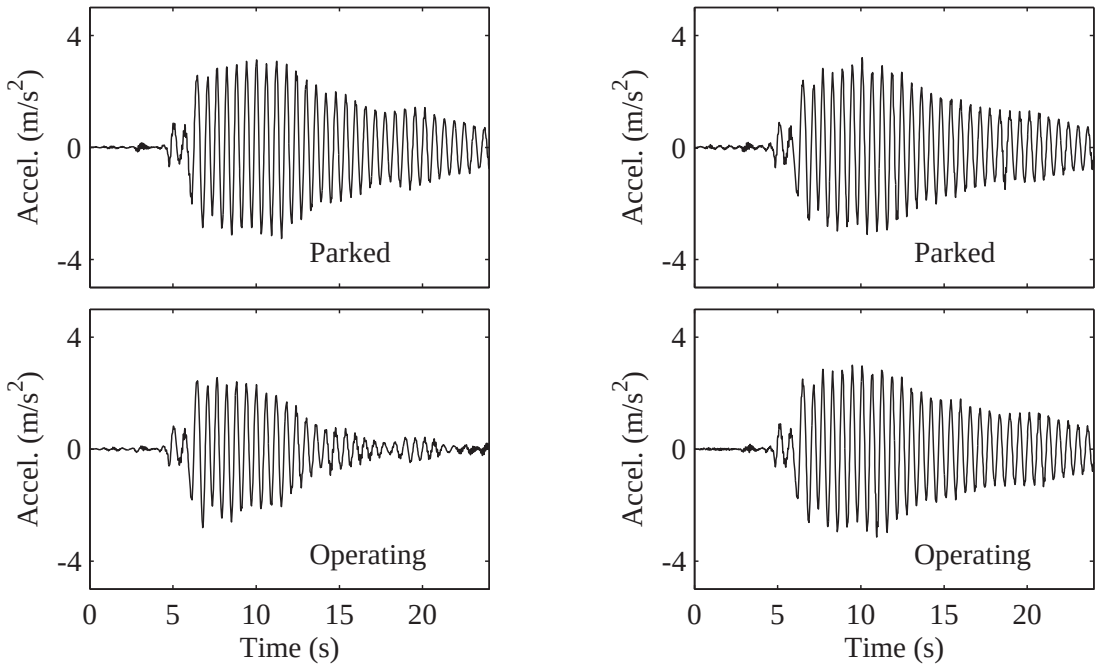

(a) Configuration 1 (b) Configuration 2

Figure 7.5: Simulated tower top in-plane absolute acceleration for EQ3

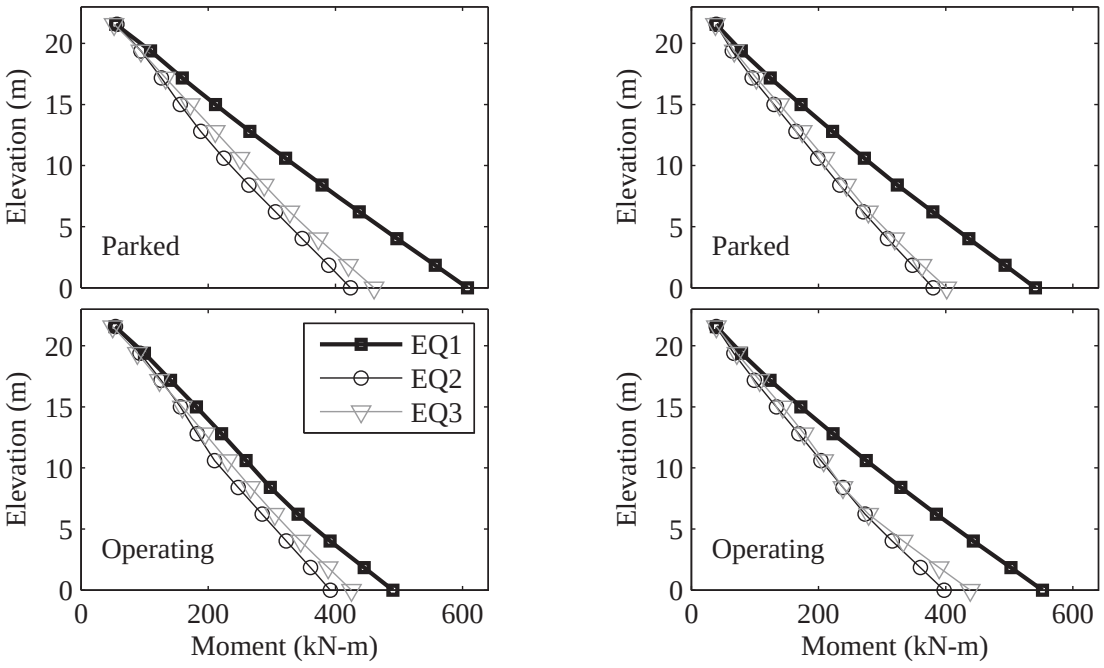

(a) Configuration 1 (b) Configuration 2

Figure 7.6: Simulated moment envelope

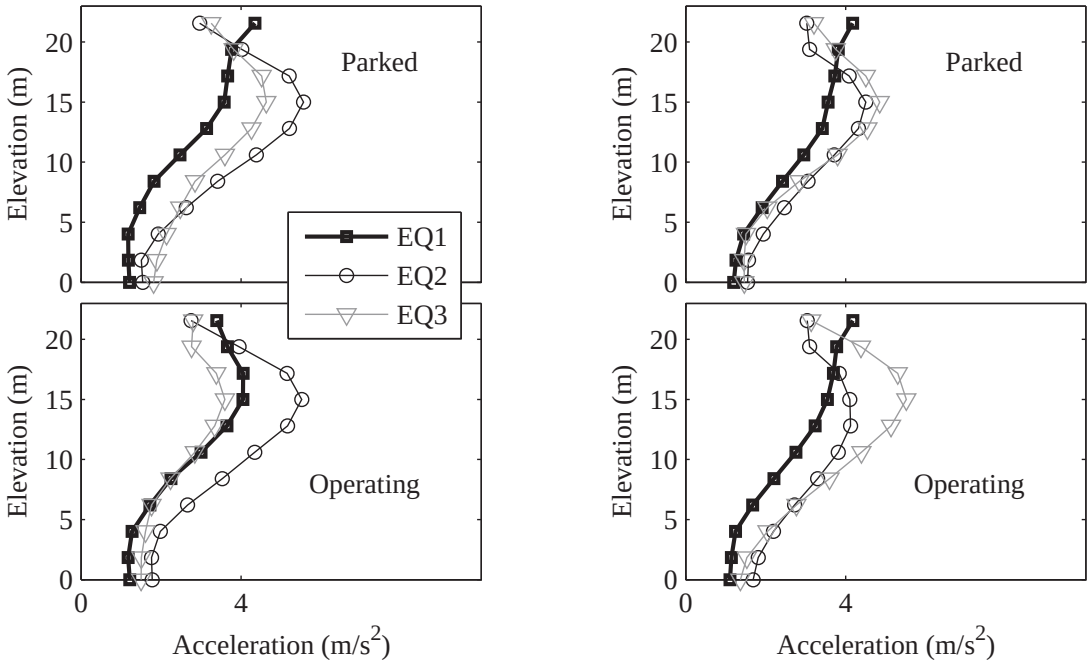

(a) Configuration 1 (b) Configuration 2

Figure 7.7: Observed acceleration envelope

For all scenarios, the tower top acceleration response shows similarity in maximum amplitude and envelope, between simulated results (Figures 7.3 through 7.5) and experimental results (Figures 3.31 through 3.33). As observed earlier, the only scenario to show a clear reduction in maximum acceleration and a more rapid decay was the operational state in configuration 1. The simulation is able to capture this behavior by properly modeling coupled blade flapping and appropriate consideration of aerodynamic damping in the AeroDyn Code (Laino and Hansen, 2002).

Likewise, trends in the simulated moment demand (Figure 7.6) agree closely with the experimental results (Figure 3.34), showing that operational state influenced demand for configuration 1, but did not significantly influence demand for configuration 2. The simulated demand slightly exceeds that measured experimentally for all

scenarios, but given experimental measurement uncertainty shows good agreement.

Similar to the experimental observations (Figure 3.35), simulated acceleration envelope profiles (Figure 7.7) show second mode activity for all scenarios. The simulated acceleration envelope also shows the reduction in first mode response in configuration 1 when operating as seen experimentally.

Trends in the PSD for of the tower moment demand for the simulations show in Figure 7.8 resemble those observed experimentally (Figure 3.36). Again, there is a marked reduction in the contribution of the first mode to the demand while the turbine in operating in configuration on, but little change in the contribution of higher modes. Since the model did not predict a mode 11.3 Hz, as observed experimentally, the moment demand is missing this contribution.

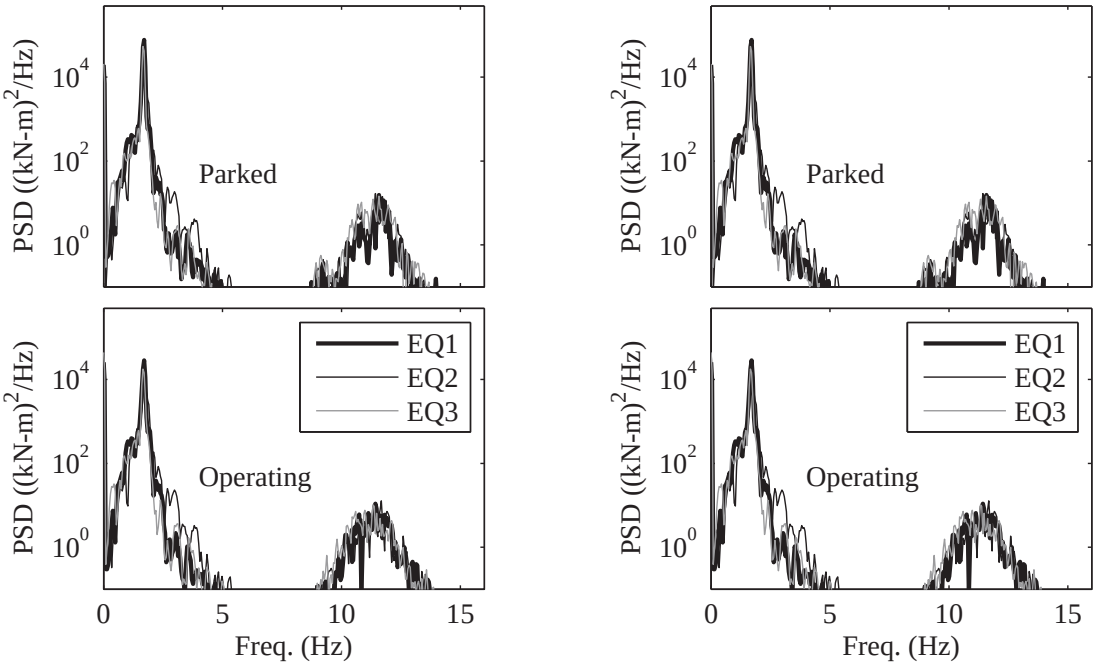

(a) Configuration 1

(b) Configuration 2

Figure 7.8: Simulated PSD of in-plane moment demand (log scale)

7.5 Implication of Aerodynamics for Seismic Response

7.5.1 FAST Turbine Model Description

Field measurements and analysis of the 900-kW NEG Micon turbine discussed in chapter 4 served as a basis for the development of a beam-column finite element model that using the OpenSees code (Mazzoni et al., 2006) and the FAST code (Jonkman and Buhl Jr., 2005) to predict structural loads. Properties for equivalent beam elements were developed for the tower using engineering drawings and specifications (Table 4.1). Blade properties were arrived at by scaling reported values of stiffness and mass for the blades of the 1.5-MW turbine presented in the "WindPACT Turbine Rotor Design Study" (Malcolm and Hansen, 2006) to create a blade whose first flap and edge resonances matched those measured in the field (Table 4.6). Using this OpenSees model, mode shapes were calculated as a basis for the FAST model. Because the second side-to-side and fore-aft tower modes contained a node near the top of the turbine, it was necessary to use a 7^{th} order polynomial to describe mode shapes instead of the standard 6^{th} order polynomial used by default in the FAST code (Jonkman and Buhl Jr., 2005). Following minor adjustments, it was found that the final FAST model produced natural frequency estimates that closely matched those observed experimentally (Table 7.3).

Table 7.3: Summary of predicted and identified resonant frequencies

Mode Type	Orientation	Illustration	Model Freq.	Exp. Parked Freq.
1st Tower Bending	Side-to-side	Fig. 4.15(a)	0.57 Hz	0.54 Hz
	Fore-aft	Fig. 4.15(b)	0.57 Hz	0.56 Hz
Asymmetric 1st Blade Flap	-	Fig. 4.18(a)	1.00 Hz	0.99 Hz
Asymmetric 1st Blade Flap	-	Fig. 4.18(b)	1.01 Hz	0.99 Hz
Collective 1st Blade Flap	-	Fig. 4.18(c)	1.05 Hz	0.99 Hz
Collective 1st Blade Edge	-	Fig. 4.19(a)	1.69 Hz	1.80 Hz
Asymmetric 1st Blade Edge	-	Fig. 4.19(b)	1.79 Hz	1.80 Hz
Asymmetric 1st Blade Edge	-	Fig. 4.19(c)	1.83 Hz	1.80 Hz
2nd Tower Bending	Side-to-side	Fig. 4.16(a)	3.97 Hz	3.94 Hz
	Fore-aft	Fig. 4.16(b)	3.96 Hz	4.00 Hz

7.5.2 Numerical Simulations

To understand the implications of this approach to modeling a turbine subjected to an earthquake, simulations were conducted using the model described above. For all simulations a 10-minute-long wind field, with a mean speed of 12 m/s, was generated using TurbSim (Jonkman, 2009) with level A IEC turbulence intensity. The simulations fall into two categories: independent simulations, in which only wind or earthquake loads are present and coupled simulations, in which the two load sources were simulated simultaneously. The first 200 seconds of all results were discarded to eliminate the influence of initial transients. For simulations in which earthquake loads were present, the recorded ground motions of the 1940 El Centro earthquake (Figure 2) were used. The 1940 El Centro earthquake measured 6.9 according to the moment magnitude scale. For the two selected horizontal components recorded at Array Station 9 in El Centro, California, the peak ground acceleration was 3.4 m/s^2 in the north-south direction. The north-south component was aligned with the wind and the east-west component was imparted horizontally, perpendicular to the wind.

In all earthquake simulations, the ground motion (Figure 7.9) started 400 seconds into the simulation and lasted approximately 55 seconds.

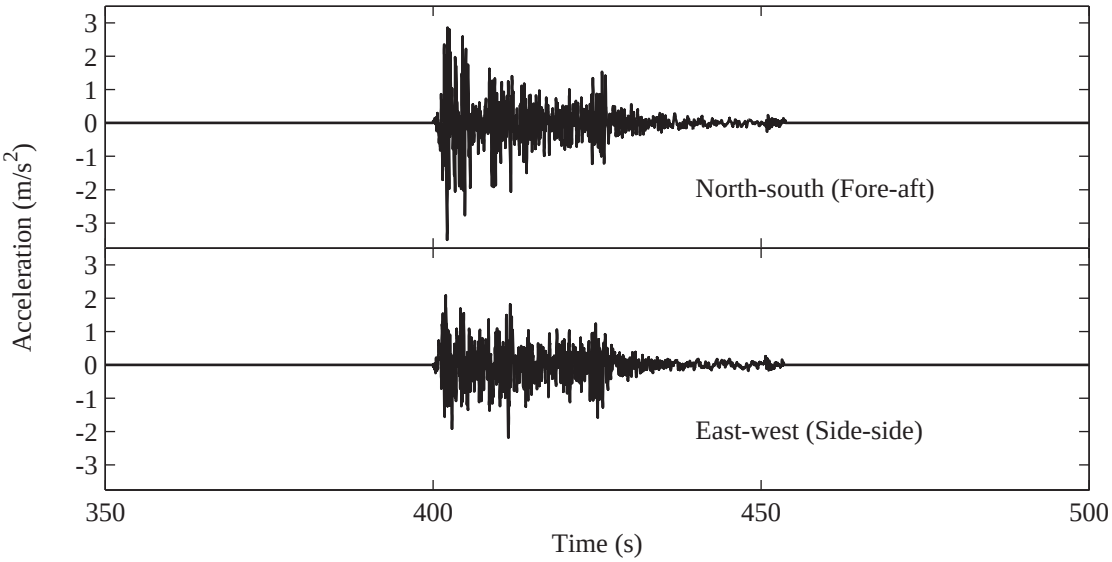

Figure 7.9: Acceleration time history for 1940 El Centro earthquake

Initial efforts have approached earthquake loading of wind turbines by simulating wind and earthquake loads independently and superimposing the results. This approach is advantageous because it allows the use of existing tools and techniques for both simulation sets. In most cases, these simulations are simple to conduct because of their familiarity.

In this analysis, a total of four independent simulations were conducted using the FAST code for the 900-kW turbine already introduced. These were conducted on the turbine in cases of parked, operating, emergency shutdown, and with an earthquake simulation. In the parked simulation, the turbine was parked with the high-speed shaft brake engaged and the blade tip brakes deployed. In the operating and emergency shutdown simulations, a simple generator model was used in the FAST

code to regulate the rotor speed at approximately 22 RPM. The emergency shutdown was initiated by deploying the tip brakes 401.28 seconds into the simulation followed 4 seconds later by the engagement of the high-speed shaft brake to bring the rotor to a full stop. For the uncoupled earthquake simulation, wind and operational loads were not considered to emulate a conventional finite element simulation that does not consider the aerodynamic interaction. In addition to the four independent simulations, a set of three coupled simulations were conducted looking at the parked, operating, and emergency shutdown cases in conjunction with the occurrence of the 1940 El Centro earthquake. Other simulation parameters were consistent with the independent simulations to allow direct comparison of the results.

7.5.3 Results of 900-kW NEG Micon Simulations

By conducting the analysis using a turbine specific code, the FAST code, many parameters can be evaluated to assist in understanding the response of the turbine to possible load combinations. This section focuses on bending moment demand at the base of the turbine tower for the simulations discussed. The predominant bending moment at the tower base is due to fore-aft bending of the tower for wind loading. In the earthquake loading simulation, there were bending moments in both directions due to the two horizontal components of the input motion (Figure 7.9). To allow direct comparison of demand in the various scenarios, a single moment value is equal to the square root of the sum of the squares (SRSS) of the two horizontal moments. Table 7.4 shows a comparison of the maximum moment demand for the simulations.

The maximum demand was 12.5 MN-m for both the operating and earthquake

Table 7.4: Base moment demand for simulations of coupled wind and earthquake loading

Load Case	Earthquake	Aerodynamics	Demand (MN-m)
Parked turbine	No	Yes	2.3
Operating turbine	No	Yes	10.1
Emergency shutdown	No	Yes	10.1
Parked turbine	Yes	No	12.5
Parked turbine	Yes	Yes	9.8
Operating turbine	Yes	Yes	12.5
Emergency shutdown	Yes	Yes	10.2

simulations. This maximum resulted in the operating simulation when considering both aerodynamic and earthquake loading and in the earthquake simulation considering earthquake loading only. A partial safety factor of 1.0 was applied to all demand parameters when independent simulations were combined for the earthquake simulation (IEC, 2005). For the operating turbine this led to a resulting moment demand of 22.6 MN-m in comparison to the 12.5 MN-m found in the coupled simulation. Such a difference in an estimate of demand would likely have design implications on the turbine. This raises questions about the accuracy and level of conservatism when conducting independent simulations.

A direct comparison of the moment demand in the simulations conducted for the parked turbine, when subjected to the El Centro earthquake, considered with and without aerodynamics shows the source of this difference (Figures 7.10 through 7.12). Little difference is seen in the side-side moment demand (Figure 7.10), but the fore-aft moment demand (Figure 7.11) clearly shows the influence of aerodynamic damping. When aerodynamics were not considered, the amplitude of the fore-aft moment demand continued to grow 20 seconds into the earthquake, whereas when

aerodynamics were considered, the demand stopped growing 10 seconds after the onset of shaking. The combined demand (Figure 7.12) clearly shows that the increase in damping in consideration of aerodynamic loads resulted in a lower overall demand.

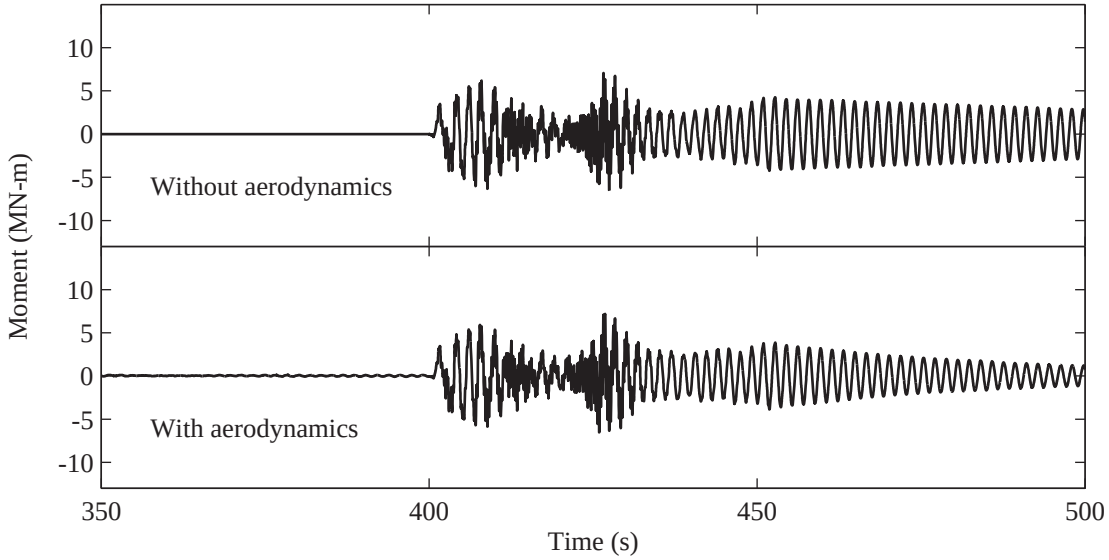

Figure 7.10: Side-side moment demand at tower base for parked case

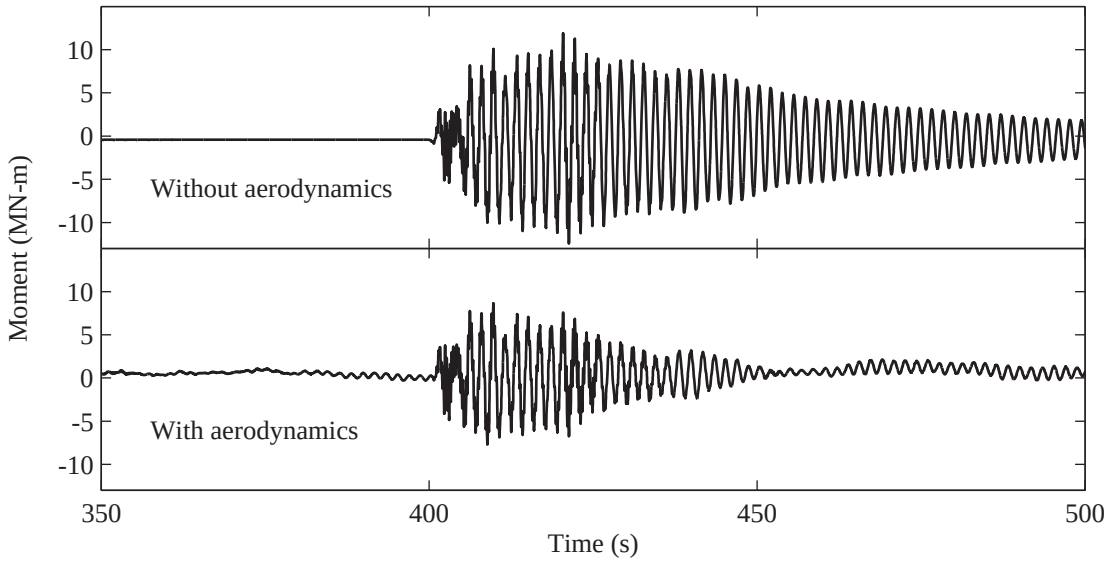

Figure 7.11: Fore-aft moment demand at tower base for parked case

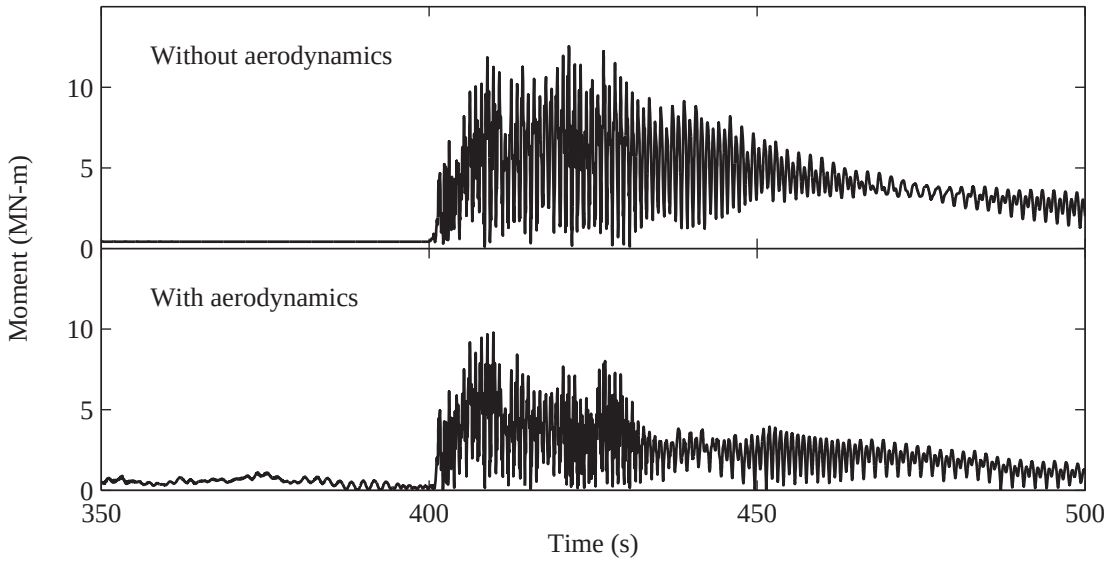

Figure 7.12: SRSS moment demand at tower base for parked case

7.6 Discussion of 900-kW NEG Micon Simulations

A model of a 900-kW turbine that matched field measurements for natural frequencies and mode shapes was built. Using this model and the FAST code, a set of simulations were conducted to investigate the differences between predictions of tower moment demands using uncoupled and coupled simulations. The results show a significant difference in demand depending on modeling approach. In the example show, the supporting tower may have insufficient capacity based on independent simulations, but be suitable according coupled simulation. Such implications could clearly affect the economic viability of wind energy in regions with a high seismic hazard. For an actual site-specific assessment of design loads for turbines, many more simulations must be considered. Typically, many different wind fields must be simulated to achieve an appropriate level of confidence in derived design loads (Fogle et al., 2008). In a similar manner, a site-specific assessment should be conducted for

earthquake loads to consider site characteristics in deriving a suite of selected ground motions (Conte and Zhang, 2007). Simulations that consider these ground motions must be conducted to assess the implications relative orientation of shaking and wind.

7.7 Conclusion

The modifications to the FAST code (Jonkman and Buhl Jr., 2005) introduced in this chapter, enable base shaking time histories to be applied in conjunction with other load sources for wind turbines. Simulations of a parked turbine subjected to base shaking without consideration of aerodynamics, are compared to conventional FE simulations using OpenSees and show favorable agreement for both tower top acceleration time history and tower moment demand. The OpenSees model was based on Model II discussed in Chapter 2 with appropriate updates considering findings from Chapter 3. The FAST model was then used to simulate experimental conditions for tests where the turbine was operating. These simulations faithfully reproduced the experimentally observed dynamics of the turbine, discussed in Chapter 3. Further, trends in tower moment demand showed good agreement between both simulations and experimental data. A FAST model of a 900-kW NEG Micon turbine demonstrates that ignoring aerodynamic forces on a turbine when assessing seismic loads may result in inaccurate predictions of extreme loads. This supports the use of the FAST code and others that appropriately model rotor aerodynamics to provide useful insight into turbine dynamic response and structural demand for load cases involving combined wind and earthquake loads.

7.8 Acknowledgements

The text below is reproduced verbatim as it appears in the acknowledgments section on page xvii per the UCSD Office of Graduate Studies Formatting Requirements.

Chapter 7 of this dissertation is an extended version of material published in the following three National Renewable Energy Laboratory reports and a manuscript under preparation for publication as a journal article: (1) "FAST Simulation of Wind Turbine Seismic Response," authored by Ian Prowell, Ahmed Elgamal, and Jason Jonkman (2010), (2) "Estimation of Seismic Load Demand for a Wind Turbine in the Time Domain," with authors Ian Prowell, Ahmed Elgamal, Jason Jonkman, and Chia-Ming Uang (2010), (3) "Earthquake Response Modeling for a Parked and Operating Megawatt-Scale Wind Turbine" with authors Ian Prowell, Ahmed Elgamal, Harold Romanowitz, J. Edward Duggan, and Jason Jonkman (2010), and (4) tentatively titled "Shake Table Testing of a Utility Scale Wind Turbine Including Operational Effects" with a preliminary author list of Ian Prowell, Ahmed Elgamal, Chia-Ming Uang, J. Enrique Luco, Hal Romanowitz, and Ed Duggan (2011). The dissertation author is the first author of these papers.

Bibliography

Bazeos, N., Hatzigeorgiou, G. D., Hondros, I. D., Karamaneas, H., Karabalis, D. L., and Beskos, D. E. (2002). "Static, seismic and stability analyses of a prototype wind turbine steel tower." *Engineering Structures*, 24(8), 1015–1025.

Conte, J. P. and Zhang, Y. (2007). "Performance based earthquake engineering: Application to an actual bridge-foundation-ground system." *12th Italian National Conference on Earthquake Engineering*, Pisa, Italy. 1–18.

Fogle, J., Agarwal, P., and Manuel, L. (2008). "Towards an improved understanding of statistical extrapolation for wind turbine extreme loads." *46th AIAA Aerospace Sciences Meeting and Exhibit*, Reno, Nevada, USA. American Institute of Aeronautics and Astronautics.

IEC (2005). *IEC 61400-1 Ed. 3: Wind Turbines - Part 1: Design Requirements*. International Electrotechnical Commission, Geneva, Switzerland.

Jonkman, B. J. (2009). "TurbSim user's guide: Version 1.50." *Report No. NREL/TP-500-46198*, National Renewable Energy Laboratory.

Jonkman, J. M. (2007). "Dynamics modeling and loads analysis of an offshore floating wind turbine." *Report No. NREL/TP-500-41958*, National Renewable Energy Laboratory.

Jonkman, J. M. and Buhl Jr., M. L. (2005). "FAST user's guide." *Report No. NREL/EL-500-38230*, National Renewable Energy Laboratory.

Laino, D. J. and Hansen, A. C. (2002). *User's Guide to the Wind Turbine Dynamics Computer Software AeroDyn*. Windward Engineering, LC, Salt Lake City, Utah, USA.

Malcolm, D. J. and Hansen, A. C. (2006). "WindPACT turbine rotor design study." *Report No. NREL/SR-500-32495*, National Renewable Energy Laborator.

Mazzoni, S., McKenna, F., and Fenves, G. L. (2006). *Open System for Earthquake Engineering Simulation User Manual*. Pacific Earthquake Engineering Research Center, Berkeley, California, USA.

Prowell, I., Elgamal, A., Veletsos, M., and Restrepo, J. (2008). "Shake table test of a 65kW wind turbine and computational simulation." *Proceedings of the 14th World Conference on Earthquake Engineering*, Beijing, China. 1–8.

Prowell, I., Veletzos, M., Elgamal, A., and Restrepo, J. (2009). "Experimental and numerical seismic response of a 65kW wind turbine." *Journal of Earthquake Engineering*, 13(8), 1172–1190.

Zhao, X. and Maißer, P. (2006). "Seismic response analysis of wind turbine towers including soil-structure interaction." *Proceedings of the Institution of Mechanical Engineers, Part K: Journal of Multi-body Dynamics*, 220(1), 53–61.

Chapter 8

General Trends in Seismic Load for Wind Turbines

8.1 Introduction

As with any civil structure, earthquake loading is a consideration for turbines installed in seismically active regions. To understand these loads, early numerical investigations (Bazeos et al., 2002; Lavassas et al., 2003) focused on tower loading using models that lump the nacelle and rotor as a point mass when determining the seismic component of the response. This approach works well for estimating seismic loads of smaller turbines while not operating (Prowell et al., 2009).

New technologies for modern large turbines, such as variable pitch and active control, sometimes change the design-driving considerations, with fatigue and turbulence becoming important considerations along with extreme events (Malcolm and Hansen, 2006). Through these techniques and careful design, modern turbines

can be optimized to be lighter and more cost effective. For these lighter turbines, simulating earthquake and wind loads simultaneously in the time domain is required to reduce the uncertainty of the results (Ritschel et al., 2003; Witcher, 2005; Häenler et al., 2006; Zhao and Maißer, 2006) and becomes desirable to account for load cases required by certification guidelines (IEC, 2005; GL, 2003). Typical load cases include the non-operating case, continued operation through the earthquake, and an emergency shutdown in response to earthquake induced vibrations.

With support of the Network for Earthquake Engineering Simulation (NEES) and funding from the National Science Foundation (NSF), systematic work led by researchers at University of California San Diego (UCSD) has been conducted to improve experimental understanding and simulation capabilities for seismic response of turbines. In partnership with the National Renewable Energy Laboratory (NREL), the FAST code (Jonkman and Buhl Jr., 2005), a free and open tool for simulating turbine dynamics, was modified to include base shaking as a load source. Through field testing, in-situ characteristics of modern turbines were experimentally assessed to aid in calibration of models presented here (Prowell et al., 2011a). Shake table tests were conducted on an actual, full-scale 65-kW wind turbine, to validate combined earthquake and operational simulations conducted in the FAST code (Prowell et al., 2011b).

This chapter assesses the implications of seismic hazard for a range of turbine models, with a rated power from 65-kW to 5-MW (Jonkman et al., 2009; Prowell et al., 2011a, 2009; Malcolm and Hansen, 2006). Using the FAST code, time domain simulations were conducted, including both wind and seismic input for the

non-operational, operational, and emergency shutdown load cases. To investigate the implications of earthquake characteristics on turbine response, a large suite of earthquake motions were considered. The influence of operational state, not traditionally considered for civil structures, on the reliability of simplified relations between intensity measures (IMs) and engineering demand parameters (EDPs), is assessed (Mackie and Stojadinovic, 2005).

Using these simulation results, simplified methods of combining earthquake and operational loads are assessed for accuracy. It is found that high quality estimation of the parked condition seismic demand for the turbine is essential for these methods to produce reliable results. Alternatives to the traditional linear load combination are considered for predicting the load envelope as well as the median.

Finally the results are compared to extreme loads from high wind and turbulent conditions for the 5-MW NREL reference turbine (Jonkman et al., 2009). Many of the considered earthquakes produced tower demand above other extreme loads. In extreme cases, earthquake demand exceeds twice that from other sources for the turbine. This finding clearly shows that earthquake loading can be design driving for large turbines and is important to consider for region with seismic hazard.

8.2 Numerical Simulations

To obtain a better understanding of the influence of earthquake loads, simulations are conducted using the FAST code that subject the turbine to a turbulent wind field while imposing acceleration time histories for non-operational, operational,

and emergency shutdown scenarios.

8.2.1 Description of the FAST Code

The FAST code (Jonkman and Buhl Jr., 2005) is a package capable of modeling two- and three-bladed horizontal-axis wind turbines (HAWTs) under various conditions for prediction of extreme and fatigue loads. For aerodynamic calculations, the FAST code employs the subroutines for HAWTs found in the AeroDyn Code (Laino and Hansen, 2002). Using a combined modal and multi-body dynamics formulation, the FAST code simulates the dynamic behavior of a turbine in the time domain. The equations of motion are solved using a standard multi-body dynamics approach with elements whose flexibility is determined by the summation of mode shapes provided by the user. The FAST code is widely used in research throughout the world. Germainsher Lloyd (GL) WindEnergie evaluated the combination of the FAST code and the AeroDyn Code and found it to be suitable for calculation of onshore wind turbine loads for design and certification. For the purpose of simulating earthquake loads for operating turbines, the FAST code was modified to incorporate base shaking as a load source (Prowell et al., 2010a).

8.2.2 Turbine Models

For this investigation a total of four distinct turbine models were considered, ranging in rated power from 65-kW to 5-MW (Table 8.1). This range represents turbines from the early 1980s when production of electricity from the wind began on a utility scale to very large modern turbines (Hau, 2006). The 65-kW Nordtank model

was developed at UCSD using data collected from shake table testing (Prowell et al., 2011b). As the outcome of ambient vibration field testing (Prowell et al., 2011a), the 900-kW NEG Micon model was developed. The other two models considered were developed for studies by NREL. The 1.5-MW WP turbine was developed for the "WindPACT Turbine Rotor Design Study" (Malcolm and Hansen, 2006) and the model used here is the model included as part of the certification tests for the FAST code (Jonkman and Buhl Jr., 2005). The 5-MW NREL Baseline turbine was developed as a common model for researchers considering large next generation turbines (Jonkman et al., 2009). With rotor diameters ranging from 16 to 90 meters, this selection accounts for a wide range of turbine designs covering relatively short period designs (0.59 sec) to long period structures (3.22 sec). This range is well suited to develop an understanding of trends in seismic demand that correlate with turbine size.

Table 8.1: Wind turbine parameters

Power rating	65-kW	900-kW	1.5-MW	5-MW
Manufacturer	Nordtank	NEG Micon	WindPACT model	NREL model
Rotor configuration	3 bladed upwind	3 bladed upwind	3 bladed upwind	3 bladed upwind
Speed regulation	Passive stall	Passive stall	Variable pitch	Variable pitch
Operational speed (rpm)	45 - 55	14 - 22	18	7 - 12
Hub height (m)	22.6	55	84	90
Rotor diameter (m)	16	53.6	70	90
Mass of rotor (kg)	1,600	18,300	32,000	111,000
Mass of nacelle (kg)	2,700	23,000	51,000	240,000
Mass of tower (kg)	6,100	68,700	122,000	350,000
First period (s)	0.59	1.75	2.48	3.22

For the two models based on existing physical turbines, engineering properties

for the tower and blades were used to construct models for the FAST code (Table 8.1). The resulting models were tuned to predict the first and second side-to-side and fore-aft bending modes for the parked turbine near the experimentally identified frequencies. Blade properties were adjusted to match experimentally identified first flap and edge modes. The resulting mode types and frequencies for the turbine model agreed well with identified estimates as shown in (Table 8.2).

Table 8.2: Wind dynamic characteristics

Mode type	65-kW Nordtank		900-kW NEG Micon	
	Model freq. (Hz)	Exp. parked freq. (Hz)	Model freq. (Hz)	Exp. parked freq. (Hz)
1st Fore-aft tower	1.70	1.70	0.57	0.56
1st Side-to-side tower	1.71	1.71	0.57	0.54
1st Blade flap 1	3.41	3.47	1.00	0.99
1st Blade flap 2	3.43	3.47	1.01	0.99
1st Blade flap 3	3.51	3.47	1.05	0.99
1st Blade edge 1	5.60	5.79	1.69	1.80
1st Blade edge 2	5.72	5.79	1.79	1.80
1st Blade edge 3	5.81	5.79	1.83	1.80
2nd Fore-aft tower	11.9	11.9	3.96	4.00
2nd Side-to-side tower	12.4	12.4	3.97	3.94

8.2.3 Description of Turbulent Wind Fields

To simulate realistic and consistent wind loads for the range of turbines studied, a wind speed of 7.35 m/s at an elevation of 10 m (U_{10}) was scaled to wind speed at each hub height using 8.1.

$$U_z = \frac{U_{10}}{(10/z)^{1/5}} \tag{8.1}$$

The resulting hub height mean wind speeds are summarized in (Table 8.3). A

single 600-second long wind field was generated for each of the four hub heights with the specified mean wind speed and a level B International Electrotechnical Commission (IEC) turbulence intensity using TurbSim (Jonkman, 2009). The wind condition and turbulence intensity considered is a typical scenario experienced by production machines and does not represent an extreme event.

Table 8.3: Hub height wind speeds

Power rating (kW)	Hub height (m)	Mean wind speed (m/s)
65	22.6	8.6
900	55	9.5
1,500	84	10.0
5,000	90	11.4

8.2.4 Descriptions of Ground Motions

To simulate earthquake loading, 99 ground motions were considered, each having three components, two horizontal and one vertical (Mackie and Stojadinovic, 2005). The motions are binned into a total of 5 groups based on event magnitude and source to recording distance. Four of the bins come from the Pacific Earthquake Engineering Research Center (PEER) Strong Motion Database. Motions with a magnitude (M_w) less than 6.5 were considered small magnitude (SM), and were considered large magnitude (LM) if M_w is greater than 6.5. Motions only included non-near fault motions ($R > 15$ km), so the small distance (SR) bin included motions with a closest distance (R) ranging from 15 to 30 km. Motions with a closest distance greater than 30 km were in the large distance bin. The fifth bin of near-field motions includes high-magnitude earthquakes measured at a distance of less than 15 km, come from

Luco's near field data set (Luco, 2001). Existing attenuation relationships rely on magnitude and distance parameters to describe local ground motion at a site, which facilitates probabilistic seismic hazard analysis by allowing statistical descriptions of site specific shaking (Power et al., 2008; Conte and Zhang, 2007).

The ground motion set considered represents a wide range of shaking intensities. The 5% damped square root of the sum of the squares (SRSS) acceleration response spectrum for the horizontal components was calculated for each motion and is shown in light grey on Figure 8.1(a), with the thicker black line showing the mean for the entire motion set. Vertical lines indicate the first period of each of the turbines considered. Distinct intensity bands of the total ensemble from each of the five groups are apparent when the mean of each is compared 8.1(b).

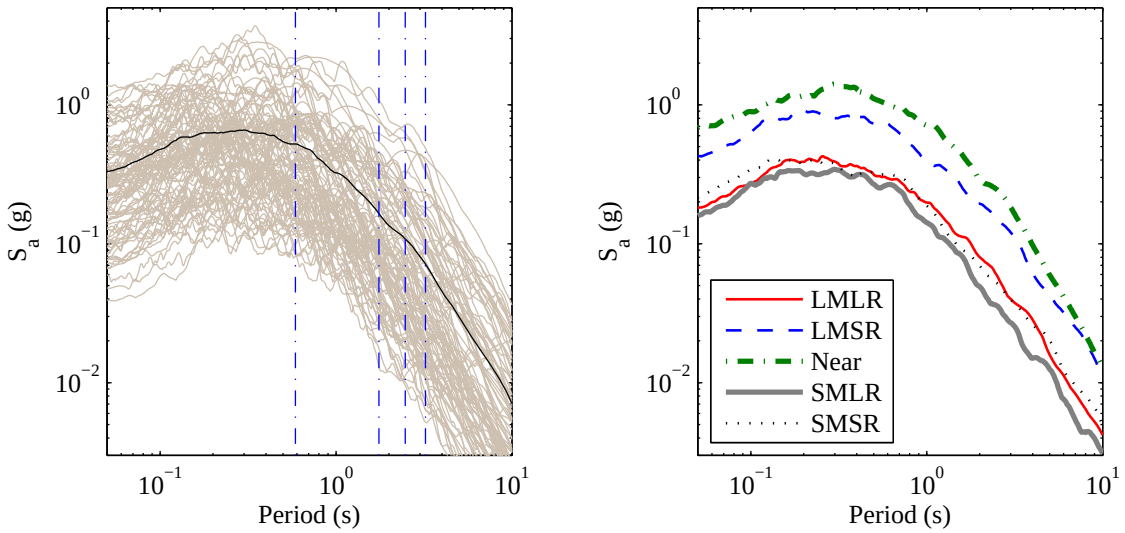

(a) Ensemble mean

(b) Mean of each group

Figure 8.1: 5% damped SRSS response spectrum (Note: S_a is spectral acceleration and not pseudo spectral acceleration)

8.2.5 Load Cases

Three load cases were considered: non-operational, operating, and emergency shutdown.

1. The non-operational simulations were divided into two states, parked and idling. For the fixed pitch turbines (65-kW and 900-kW models) a brake located on the high speed drive shaft (HSS) is used to park the rotor, preventing it from spinning in the wind. Instead of applying the HSS brake, the active pitch turbines (1.5-MW and 5-MW models) idled by rotating the blades such that they did not generate sufficient torque to spin the rotor.

2. In the operational case, the turbine continued to rotate with the control system acting as expected under normal conditions.

3. For the fixed pitch turbines (65-kW and 900-kW models), shutdown was initiated by deployment of aerodynamic brakes located at the tip of each blade, followed by application of HSS brake four seconds later. For the active pitch turbines (1.5-MW and 5-MW models), the emergency shutdown was achieved by feathering the turbine blades at a rate of eight degrees per second. Following the emergency shutdown, the larger turbines were left idling, without application of the HSS brake.

8.2.6 Simulation Details

For the operational and non-operational load cases, simulations were run for each of the 4 turbines with the appropriate turbulent wind field. For each of the 99

earthquake events, 2 simulations were considered, which interchanged the horizontal earthquake components to reduce bias due to relative orientation with wind direction. If the operational simulation resulted in acceleration in the nacelle exceeding 1 m/s^2, an additional run was conducted with an emergency shutdown initiated when the threshold was exceeded. For all simulations, this threshold was not reached before initiation of earthquake excitation, but was shortly thereafter for many simulations. In total, more than 2,000 simulations were run.

The total time for each simulation was 600 seconds with a time step of 0.001 seconds. Wind loads were the sole source of loading during the first 400 seconds, allowing complete attenuation of initial transient behavior. Earthquake shaking initiated immediately following this period. Simulations where the turbine is subjected to the same operational conditions and wind state, without earthquake induced base shaking provide control for comparison. Reported results discard the first 200 seconds of the simulation to allow dissipation of initial transient behavior.

8.3 Input Intensity and Resulting Demand

The PEER decision making framework for seismic performance assessment relies on an efficient model of the expected demand conditioned on an earthquake IM (Cornell and Krawinkler, 2000). To understand the efficiency of different IMs for resulting demand in wind turbines, two EDPs are considered for the simulations presented here, the square root of the sum of the squares (SRSS) bending moment demand at the base of the turbine tower as well as the SRSS moment demand at the root

of the turbine blades. The following IMs are considered: (1) peak ground displacement (PGD), (2) peak ground velocity (PGV), (3) peak ground acceleration (PGA), (4) cumulative absolute velocity (CAV), (5) arias intensity, (6) spectral displacement (S_d), (7) average S_d, (8) pseudo-spectral velocity (PSV), (9) average spectral velocity, (10) pseudo-spectral acceleration (PSA), and (11) average spectral acceleration. Averaged values are calculated at the period of the first and second tower fore-aft and side-to-side bending modes. Mackie and Stojadinovic (2005) present a clear definition of each of the considered intensity measures.

An exponential relation is assumed for mapping the IM to the median EDP ($\widehat{EDP}$) as shown in equation 8.2. Equivalently, this relation can be expressed as a linear mapping by equation 8.3 where $A = \ln(a)$ and $B = b$.

$$\widehat{EDP} = a \cdot (IM)^b \tag{8.2}$$

$$ln(\widehat{EDP}) = A + B \cdot ln(IM) \tag{8.3}$$

A least-squares regressions is performed to determine coefficient values of a and b for each of the EDP/IM relationships. The resulting standard deviation (dispersion) can be expressed by equation 8.4 where df is the number of parameters being estimated (Mackie and Stojadinovic, 2005).

$$\sigma = \sqrt{\frac{\sum_{i=1}^{n}(ln(EDP_i) - ln(\widehat{EDP}))^2}{n - df}} \tag{8.4}$$

In many cases, it is appropriate to consider the EDP/IM relationship as bilinear with two values of A and B for different regions, in the linear space representation, equation 8.3. Figure 8.2 shows the EDP/IM relationship for PSA and the SRSS tower base moment demand for the four turbines considered. The increasing trend in demand for increasing earthquake intensity is typical and expected. Using linear, or bilinear fits where needed to reduce dispersion, for each of the investigated IMs it is found that for all turbines and load cases, S_d, PSV, and PSA produce the best predictor (lowest dispersion) for tower base demand.

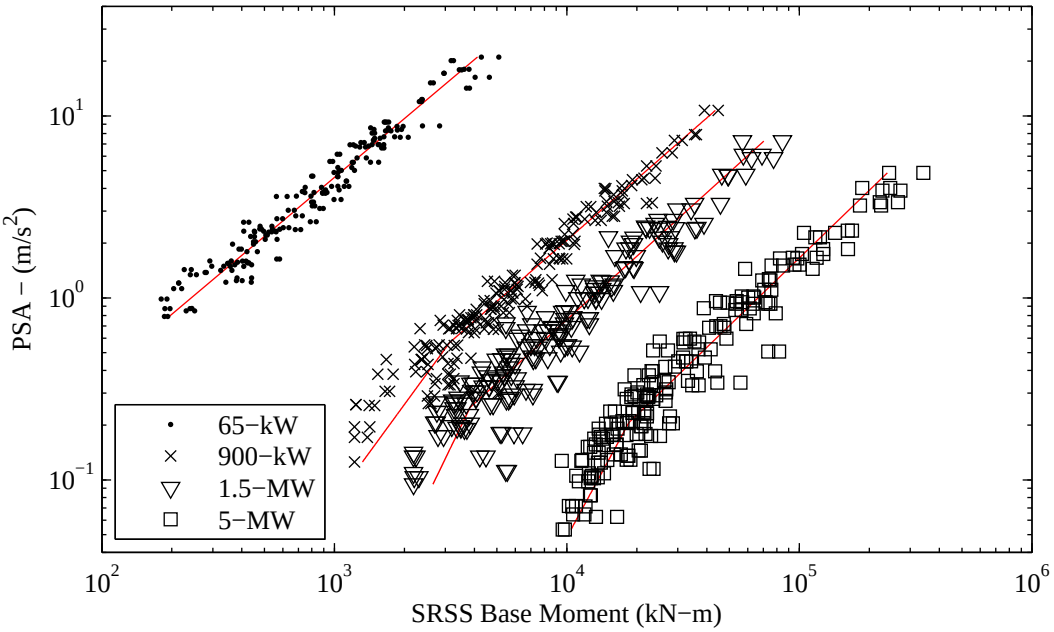

Figure 8.2: IM to tower EDP relationship for parked load case

8.4 Simulation Results

The presented results for the parked load case match expected EDP/IM relationship trends of increasing demand for increasing intensity (Figure 8.2), but in

the operating and emergency shutdown case the larger turbines, 900-kW or greater rated power, all exhibit a vertical region where demand shows little to no dependency on earthquake intensity (Figure 8.3 and Figure 8.4). This region is a direct result of simultaneous wind load on the turbines. For comparison, control simulations were conducted that only subjected the turbine to the considered wind field for each of the load cases. Resulting demand for the tower and blades is presented in Table 8.4. Inspection of the results shows that baseline demand, without earthquake excitation, accurately predicts the demand in this vertical region. Clearly, for these larger turbines, small intensity earthquakes exert almost no influence on tower moment demand.

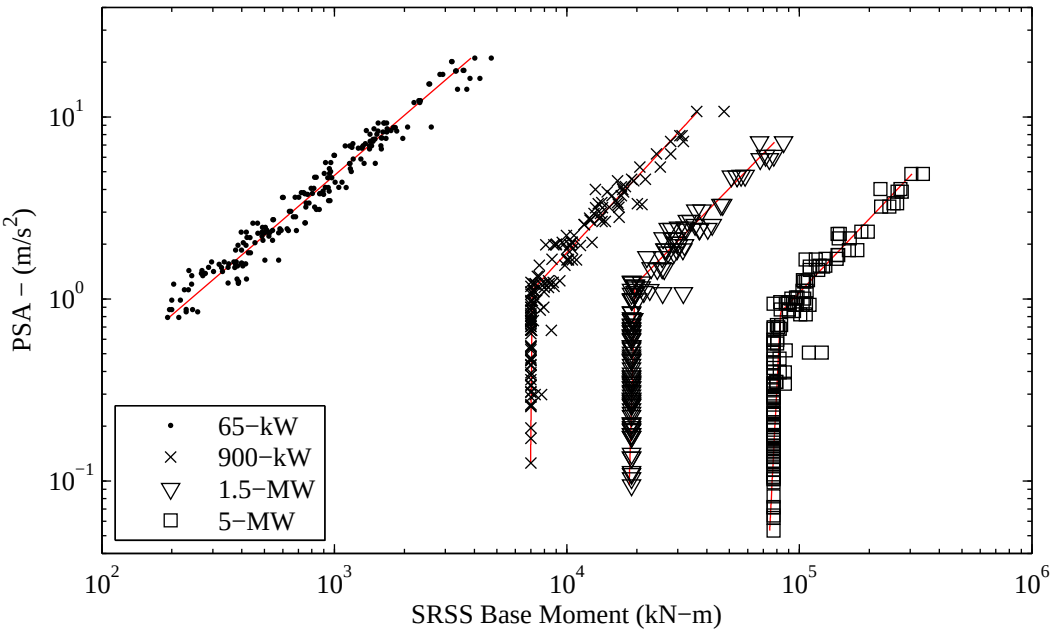

Figure 8.3: IM to tower EDP relationship for operating load case

This same behavior is more extreme when considering demand at the blade root, where even high intensity earthquake events appear to exert no influence on

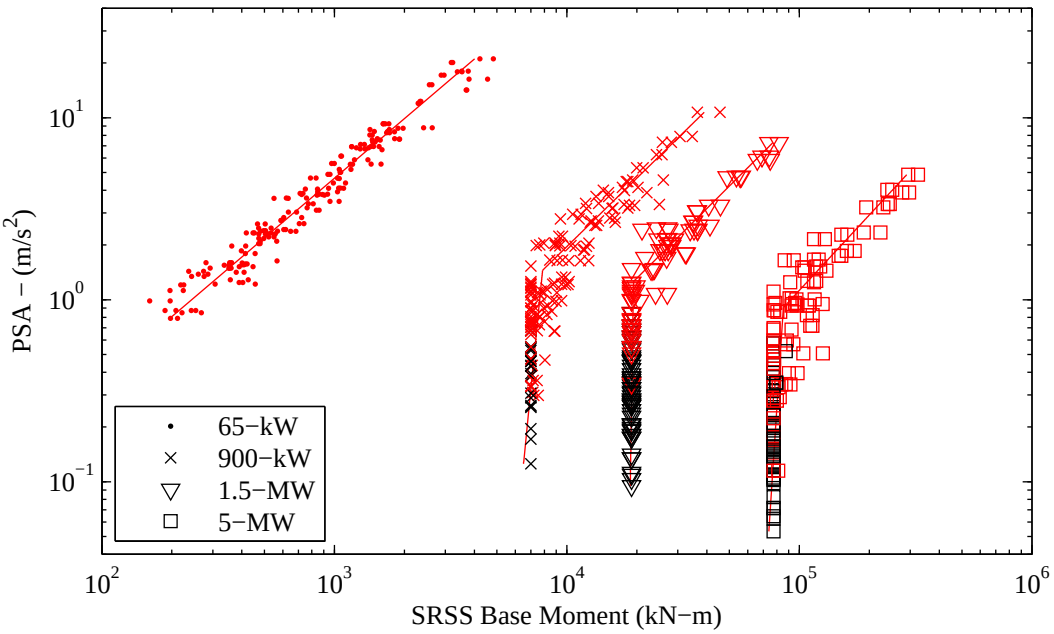

Figure 8.4: IM to tower EDP relationship for emergency shutdown load case (results in black did not result in an emergency shutdown)

Table 8.4: Baseline engineering demand parameters

Power rating (kW)	Tower base moment (kN-m)			Blade one root moment (kN-m)		
	Non-operating	Operating	Emergency shutdown	Non-operating	Operating	Emergency shutdown
65	35	124	124	6	15	17
900	1,200	7,000	7,000	154	770	770
1,500	1,000	19,000	19,000	440	1,800	1,800
5,000	9,200	78,000	78,000	4,600	13,400	13,400

the resulting maximum (Figure 8.5 and Figure 8.6). Again, the baseline simulations predict the demand at which this vertical region occurs (Table 8.4). For the parked case, some influence of earthquake intensity is observed, but resulting demand falls well below the operational and emergency shutdown simulations (Figure 8.7).

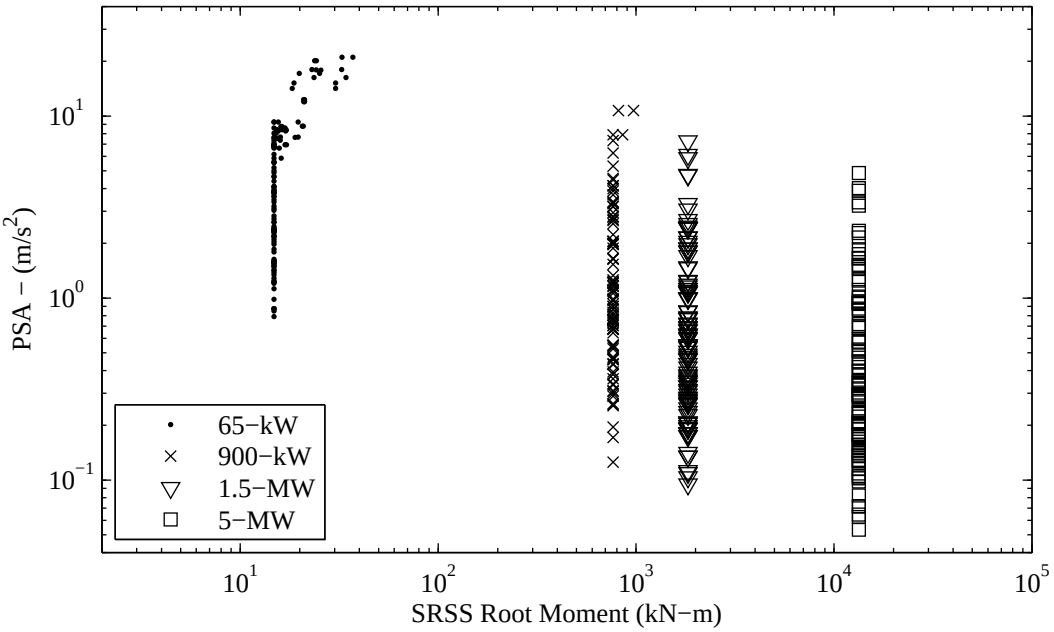

Figure 8.5: IM to blade EDP relationship for operating load case

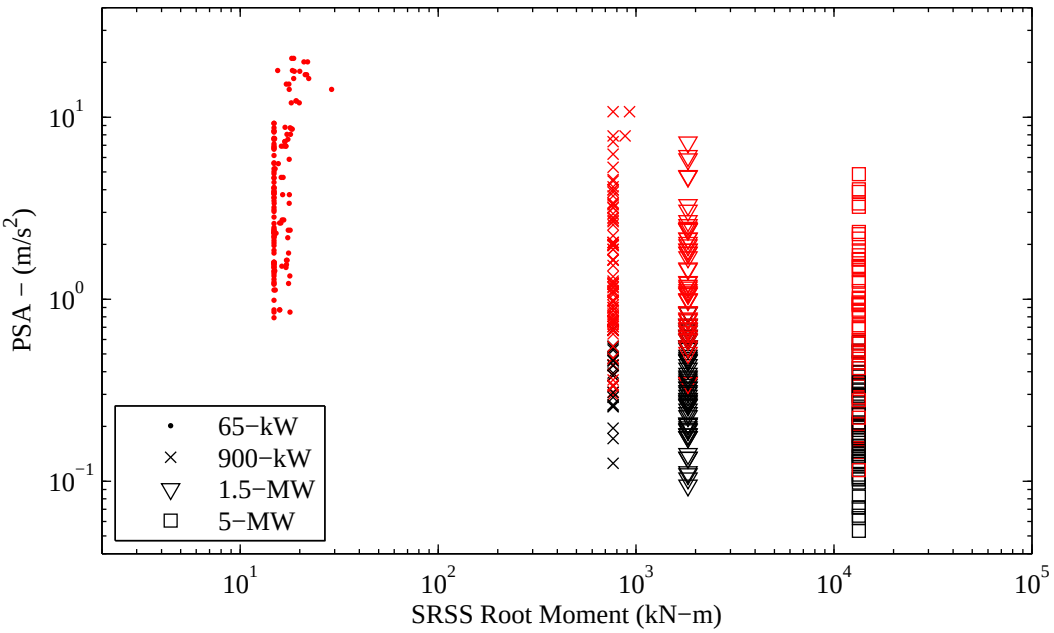

Figure 8.6: IM to blade EDP relationship for emergency shutdown load case (results in black did not result in an emergency shutdown)

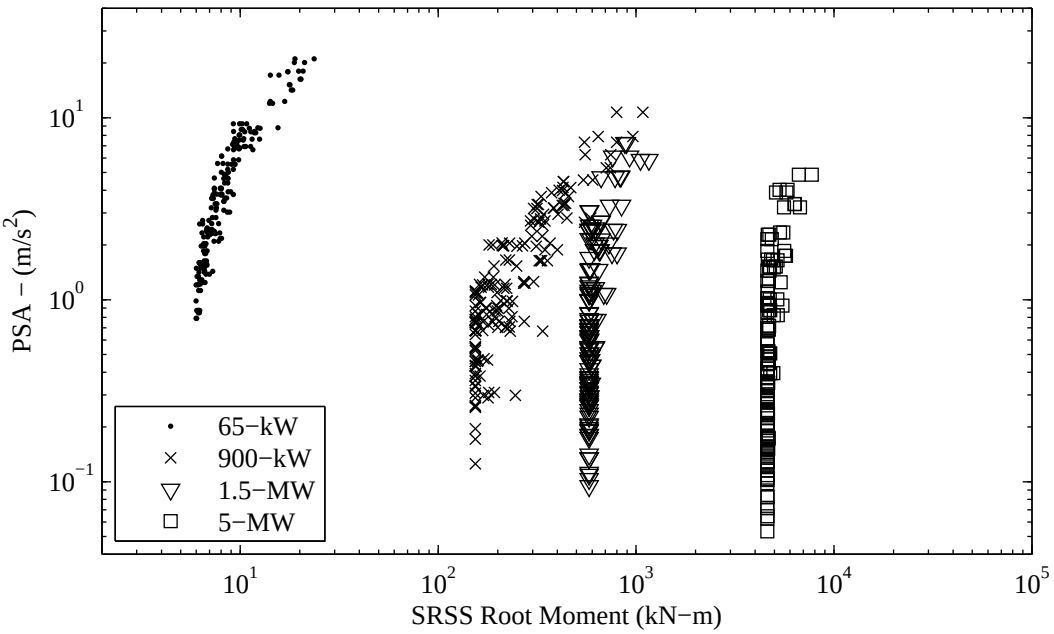

Figure 8.7: IM to blade EDP relationship for parked load case

8.5 Discussion

8.5.1 Estimation of Seismic and Wind Load Combinations

The combined load cases simulated here are plausible scenarios and also required by certification guidelines as possible sources of design driving loads (IEC, 2005). Various suggestions exist for a simplified procedure to estimate these combined loads without direct time simulation. Most take the form of linear addition as shown in Equation 8.5.

$$u = \phi_e \cdot Q_e + \phi_o \cdot Q_o \tag{8.5}$$

Where ϕ_e and ϕ_o are safety factors modifying the earthquake demand, Q_e, and the operational demand, Q_o. Generally a value of 1.0 is suggested for both

load factors, ϕ_e and ϕ_o (IEC, 2005). For illustration, here Q_o will be taken as the demand resulting from an emergency shutdown under the simulated wind conditions (Table 8.4). The earthquake bending moment for the tower, Q_e, will be estimated by equation 8.6, as suggested in IEC (2005) Annex C.

$$Q_e = h_t \cdot M_{eff} \cdot A \tag{8.6}$$

Where h_t is the height at the head of the tower, M_{eff} is the effective mass, and A is the design acceleration. M_{eff} is simply taken as the total mass of the rotor and nacelle plus half of the tower mass (IEC, 2005). As required, the design acceleration (A) will be modified from the typical value assuming 5% damping to a value of 1% using a factor of 1.4 (ASCE, 2007; ICC, 2006). This allows the tower moment to be expressed (eq. 8.7) similarly to the assumed relation for the EDP/IM relationship.

$$Q_e = 1.4 \cdot h_t \cdot M_{eff} \cdot (PSA(\zeta = 5\%))^1 \tag{8.7}$$

Where the coefficients describing the curve are $a = 1.4 \cdot h_t \cdot M_{eff}$ and $b = 1$. Values of a and b obtained from least square fits for the simulations with higher earthquake intensity are compared to the simplified estimates in Table 8.5. Figures 8.8 through 8.11 show Q_e and U from the linear combination using equation 8.5 along with simulation results for each of the four turbines. For the large turbines, over 900-kW rated power, equation 8.5 bounds almost all simulation results. For the 65-kW turbine the contribution of the operational load is almost negligible. As this turbine is a fixed pitch turbine designed to survive wind speeds in excess of 53 m/s, well

above the considered 8.6 m/s, it is likely that the extreme wind demand may exceed that of the seismic load case.

Table 8.5: Fit parameters for tower base bending moment

Power rating (kW)	Simulation least squares (parked)		Simplified estimate	
	a	b	a	b
65	242	0.93	226	1
900	5,200	0.89	5,260	1
1,500	12,680	0.86	16,610	1
5,000	66,400	0.81	64,510	1

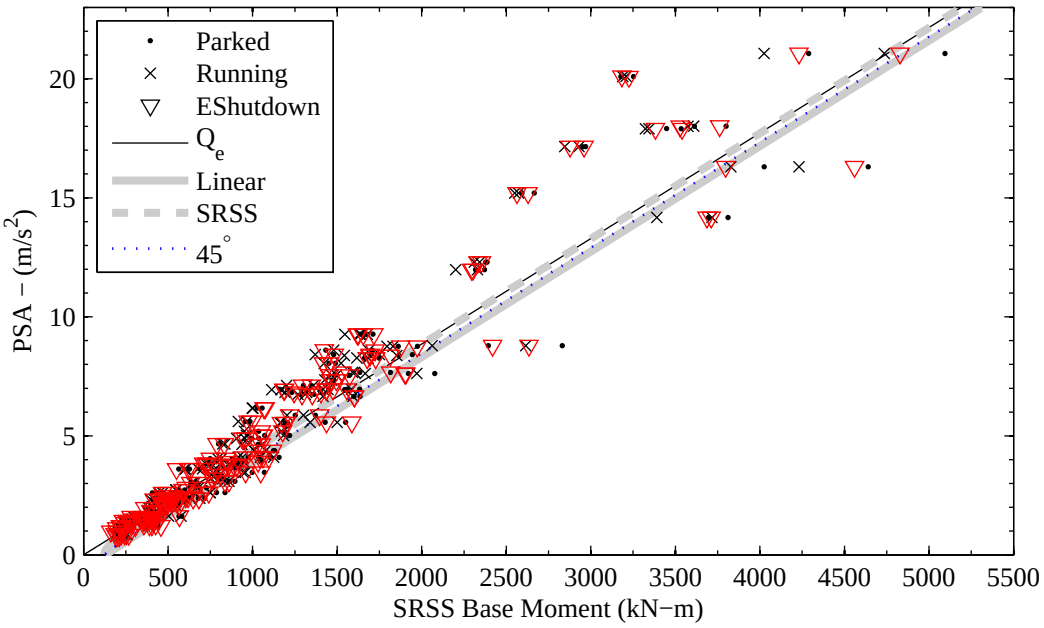

Figure 8.8: Comparison of simulation and simplified load combinations for 65-kW Nordtank

Though it is suggested that equation 8.5 is an upper bound, the overestimation for the resulting demand of the 900-kW and 1.5-MW turbines is excessive and undermines the usefulness of a simplified method. Inspection of the results shows that the primary source of error is the estimate of the seismic demand, Q_e. For the 65-kW

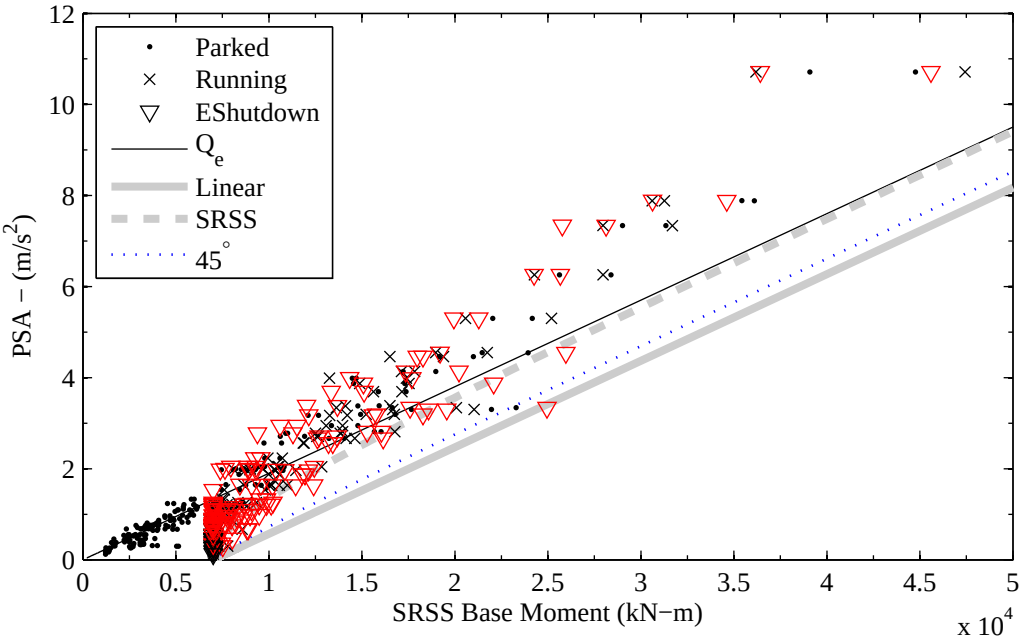

Figure 8.9: Comparison of simulation and simplified load combinations for 900-kW NEG Micon

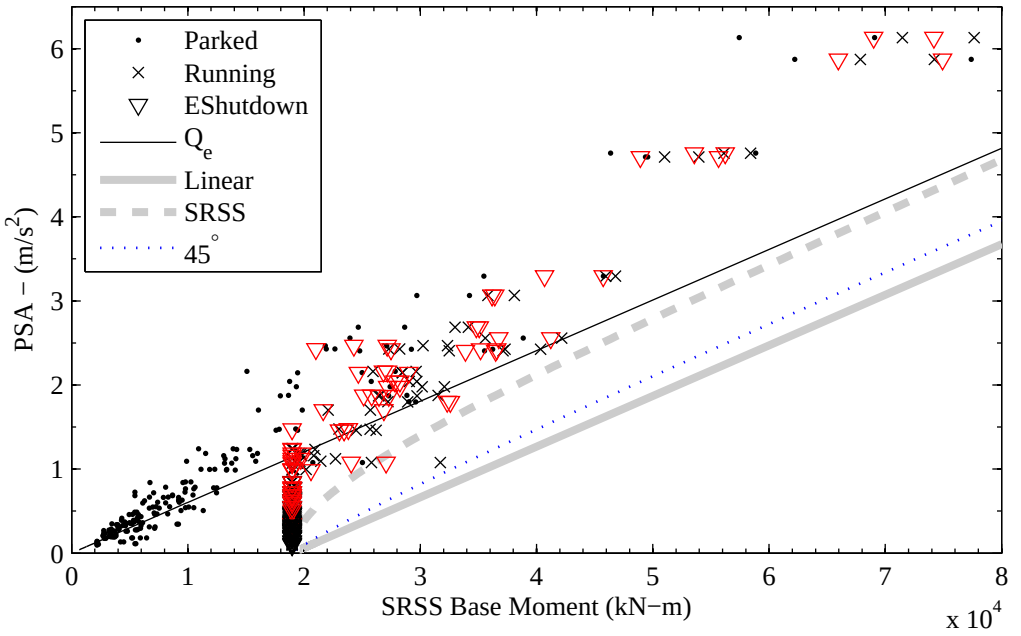

Figure 8.10: Comparison of simulation and simplified load combinations for 1.5-MW WindPACT

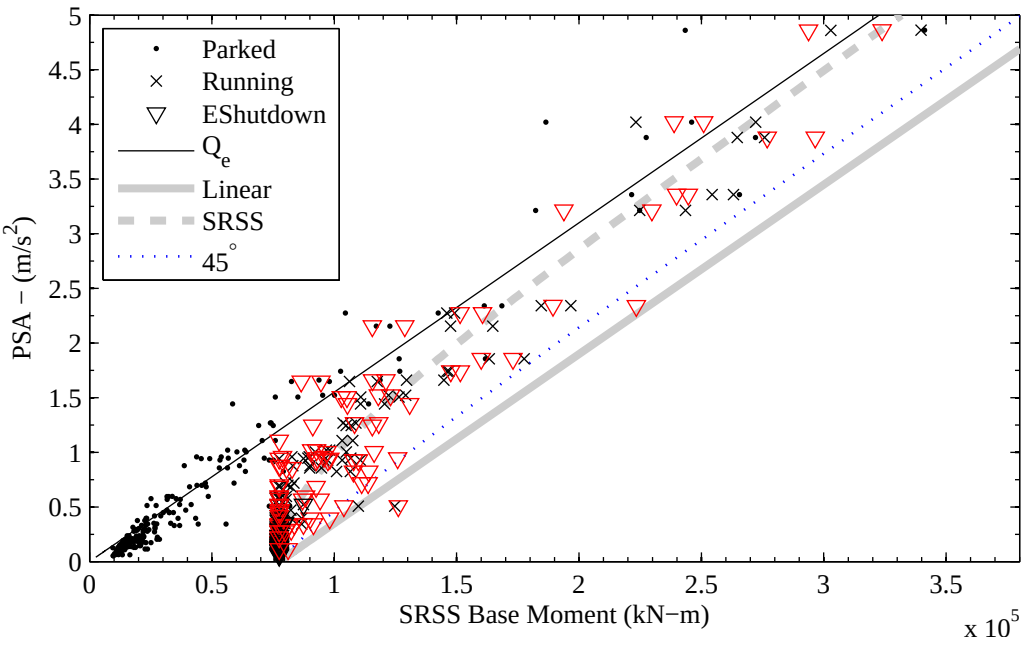

Figure 8.11: Comparison of simulation and simplified load combinations for 5-MW NREL

and 5-MW where the slope of Q_e follows more closely with the mean of simulation results, the linear load combination produces a much more reasonable envelope.

To further reduce the degree of conservatism in combining seismic and wind loads it has been suggested that the loads be combined as the SRSS, equation 8.8. By considering the two loads as vector quantities with a relative orientation, θ, equation 8.9 can be used to combine the two loads. At the two extremes for θ, 0 and 90 degrees, equation 8.9 simplifies to equation 8.5 and equation 8.8, respectively.

$$U = \sqrt{Q_e^2 + Q_o^2} \tag{8.8}$$

$$U = \sqrt{(Q_e + cos(\theta)Q_o)^2 + (sin(\theta)Q_o)^2} \tag{8.9}$$

Figures 8.8 through 8.11 show a comparison of these additional methods of combining loads. As before, for the 900-kW and 1.5-MW, inaccuracy in predicting Q_e results in a poor estimate of the combined loads. However for the 5-MW turbine it becomes apparent that a SRSS approach provides a good estimate of the median combined load and a value of $\theta = 45$ degrees may provide a tighter upper bound for the combined load, which can be approximated by equation 8.10.

$$U = \sqrt{(Q_e + cos(45°)Q_o)^2 + (sin(45°)Q_o)^2} \approx \sqrt{Q_e^2 + 1.4 \cdot Q_e \cdot Q_o + Q_o^2} \qquad (8.10)$$

8.5.2 Extreme Loads

Definition of extreme wind loads for a wind turbine is beyond the scope of this investigation. As the 5-MW turbine is a reference model studied by multiple investigators, external publications document extreme wind demand for this turbine (Fogle et al., 2008; Jonkman et al., 2009).

Based on extensive simulations, Fogle et al. (2008) show the distribution of maximum loads as a function of wind speed for the 5-MW NREL turbine. As the turbine uses active pitch to minimize structural loads, it is found that, counter to intuition, high levels of tower moment demand may occur at the rated wind speed of 11.4 m/s. The study found that the maximum fore-aft tower-base bending moment was approximately 98 MN-m for normal operation of the NREL 5-MW turbine. In another study (Jonkman et al., 2009), a maximum moment of approximately 85

MN-m was observed. Using a load factor of 1.25 for normal operation and 1.2 for extrapolation to extreme loads, resulting in a total factor of 1.5, a range of 128 MN-m to 147 MN-m is required of the tower. For extreme turbulence simulations with a load factor of 1.35, it was found that the maximum moment demand was 153 MN-m (Jonkman et al., 2009).

Many of the parked, operating, and emergency shutdown simulations presented here resulted in demand above this level. Maximum tower base moment demand for the 5-MW machine from simulations here are 341 MN-m, 340 MN-m, and 324 MN-m for the parked, operating, and emergency shutdown simulations respectively, which is considerably above that from extreme wind events (Fogle et al., 2008; Jonkman et al., 2009). In contrast it is found that blade root bending demand is unlikely to be driven by the occurrence of even an extremely rare, high intensity earthquake.

The analysis presented here assumes linear material response of the turbine tower even in extreme events. This assumption is enforced by industry requirements that the turbine tower remain elastic (IEC, 2005). In light of this requirement, an analysis similar to that presented here will produce appropriate ultimate loads for design of a turbine. When non-linear material behavior occurs, it is anticipated that softening and other structural changes will occur, which results in a divergence from linear results. Recent work shows that modern turbine towers may be capable of non-linear response to seismic events without collapse (Nuta, 2010). Since current non-linear modeling tools are not readily capable of considering aerodynamic and operational effects these were not considered by Nuta (2010), but may be important when considering seismic loads for turbines (Prowell et al., 2010b). As illustrated here,

accurate prediction of the seismic contribution, Q_e, is essential for reliable estimation of the combined load case. Further advances in simulation are needed to fully consider non-linear damage and collapse of wind turbines in response to seismic loading.

8.6 Conclusions

The work presented here shows that it is now possible and practical to conduct time domain simulations considering combined wind and earthquake loads for multiple scenarios using the FAST code. It is found that PSA or equivalent spectral quantities (PSV and S_d) are efficient estimators of tower base moment demand. For low intensity earthquakes, tower base moment demand of the larger turbines is driven almost exclusively by wind loads.

Results are compared to simple methods for estimating combined wind and earthquake loads. For this combination, accurate estimation of the earthquake contribution is shown to be essential for reliable superposition of the two loads. It is proposed that adding the seismic and wind loads as vector quantities with appropriate relative orientations can produce reliable estimates of the median and an approximate envelope of the combination.

For the 5-MW turbine, demand from strong earthquake events is shown to be well above that anticipated from extreme wind events. This suggests that for large turbines in regions of high seismic hazard, seismic events are important to consider when developing extreme loads and may be design driving. In contrast, results show that it is unlikely that even strong shaking will result in design driving loads for the

turbine blades.

8.7 Acknowledgements

The text below is reproduced verbatim as it appears in the acknowledgments section on page xvii per the UCSD Office of Graduate Studies Formatting Requirements.

Chapter 8 of this dissertation is an extended version of a manuscript in preparation for publication tentatively titled "Understanding Trends in Seismic Demand for the Current Inventory of Wind Turbines," with a preliminary author list of Ian Prowell, Ahmed Elgamal, Chia-Ming Uang, and Jason Jonkman (2011). The dissertation author is the first author of this paper.

Bibliography

ASCE (2007). *Seismic Rehabilitation of Existing Buildings ASCE/SEI 41/06*. American Society of Civil Engineers, Reston, Virginia, USA.

Bazeos, N., Hatzigeorgiou, G. D., Hondros, I. D., Karamaneas, H., Karabalis, D. L., and Beskos, D. E. (2002). "Static, seismic and stability analyses of a prototype wind turbine steel tower." *Engineering Structures*, 24(8), 1015–1025.

Conte, J. P. and Zhang, Y. (2007). "Performance based earthquake engineering: Application to an actual bridge-foundation-ground system." *12th Italian National Conference on Earthquake Engineering*, Pisa, Italy. 1–18.

Cornell, C. A. and Krawinkler, H. (2000). "Progress and challenges in seismic performance assessment." *PEER Center News*, 3(2), 1–4.

Fogle, J., Agarwal, P., and Manuel, L. (2008). "Towards an improved understanding of statistical extrapolation for wind turbine extreme loads." *Wind Energy*, 11(6), 613–635.

GL (2003). *Guidelines for the Certification of Wind Turbines*. Germanischer Lloyd, Hamburg, Germany.

Häenler, M., Ritschel, U., and Warnke, I. (2006). "Systematic modelling of wind turbine dynamics and earthquake loads on wind turbines." *European Wind Energy Conference and Exhibition*, Athens, Greece. European Wind Energy Association, 1–6.

Hau, E. (2006). *Wind Turbines*. Springer, Berlin, Germany.

ICC (2006). *International Building Code 2006*. International Code Council, Country Club Hills, Illinois, USA.

IEC (2005). *IEC 61400-1 Ed. 3: Wind Turbines - Part 1: Design Requirements*. International Electrotechnical Commission, Geneva, Switzerland.

Jonkman, B. J. (2009). "TurbSim user's guide: Version 1.50." *Report No. NREL/TP-500-46198*, National Renewable Energy Laboratory.

Jonkman, J., Butterfield, S., Musial, W., and Scott, G. (2009). "Definition of a 5-MW reference wind turbine for offshore system development." *Report No. NREL/TP-500-38060*, National Renewable Energy Laboratory.

Jonkman, J. M. and Buhl Jr., M. L. (2005). "FAST user's guide." *Report No. NREL/EL-500-38230*, National Renewable Energy Laboratory.

Laino, D. J. and Hansen, A. C. (2002). *User's Guide to the Wind Turbine Dynamics Computer Software AeroDyn*. Windward Engineering, LC, Salt Lake City, Utah, USA.

Lavassas, I., Nikolaidis, G., Zervas, P., Efthimiou, E., Doudoumis, I. N., and Baniotopoulos, C. C. (2003). "Analysis and design of the prototype of a steel 1-MW wind turbine tower." *Engineering Structures*, 25(8), 1097–1106.

Luco, N. (2001). "Probabilistic seismic demand analysis, smrf connection fractures, and near source effects," PhD thesis, Stanford University.

Mackie, K. and Stojadinovic, B. (2005). "Fragility basis for california highway overpass bridge seismic decision making." *Report No. 2005/02*, Pacific Earthquake Engineering Research Center.

Malcolm, D. J. and Hansen, A. C. (2006). "WindPACT turbine rotor design study." *Report No. NREL/SR-500-32495*, National Renewable Energy Laborator.

Nuta, E. (2010). "Seismic analysis of steel wind turbine towers in the canadian environment. Master's thesis, University of Toronto, Toronto, Ontario, Canada.

Power, M., Chiou, B., Abrahamson, N., Bozorgnia, Y., Shantz, T., and Roblee, C. (2008). "An overview of the NGA project." *Earthquake Spectra*, 24(1), 3–21.

Prowell, I., Elgamal, A., Jonkman, J., and Uang, C.-M. (2010a). "Estimation of seismic load demand for a wind turbine in the time domain." *Report No. NREL/CP-500-47536*, National Renewable Energy Laboratory.

Prowell, I., Elgamal, A., Luco, J. E., and Conte, J. P. (2011a). "In-situ ambient vibration study of a 900-kW wind turbine." *Journal of Earthquake Engineering and Structural Dyamics*, (Under review).

Prowell, I., Elgamal, A., Romanowitz, H., Duggan, J. E., and Jonkman, J. (2010b). "Earthquake response modeling for a parked and operating megawatt-scale wind turbine." *Report No. NREL/TP-5000-48242*, National Renewable Energy Laboratory.

Prowell, I., Uang, C.-M., Elgamal, A., Luco, J. E., and Jonkman, J. (2011b). "Shake table testing of a utility-scale wind turbine including operational effects." *Under Preparation*.

Prowell, I., Veletzos, M., Elgamal, A., and Restrepo, J. (2009). "Experimental and numerical seismic response of a 65kW wind turbine." *Journal of Earthquake Engineering*, 13(8), 1172–1190.

Ritschel, U., Warnke, I., Kirchner, J., and Meussen, B. (2003). "Wind turbines and earthquakes." *2nd World Wind Energy Conference*, Cape Town, South Africa. World Wind Energy Association, 1–8.

Witcher, D. (2005). "Seismic analysis of wind turbines in the time domain." *Wind Energy*, 8(1), 81–91.

Zhao, X. and Maißer, P. (2006). "Seismic response analysis of wind turbine towers including soil-structure interaction." *Proceedings of the Institution of Mechanical Engineers, Part K: Journal of Multi-body Dynamics*, 220(1), 53–61.

Chapter 9

Concluding Remarks

9.1 Summary of Contributions and Highlight of Findings

The contributions to the field of seismic response of wind turbines presented in this dissertation can be split into two broad categories: i) experimental results improving scientific understanding of dynamics for actual full-scale turbines (available for re-use from the NEEShub Project Warehouse at http://nees.org/warehouse) and ii) numerical contributions enabling seismic simulation in the FAST code, performing preliminary validation for the code updates, and analyzing trends in earthquake shaking combined with other load sources for wind turbines. The experimental work provides data, which was previously unavailable and serves as a basis for calibration of numerical work. The numerical contributions provide a common platform, which has been shown to reproduce observed experimental results that practitioners and re-

searchers can use for future studies of combined loading scenarios for wind turbines. As a whole this work provides a cohesive body of knowledge, which advances the field of earthquake engineering as it applies to wind turbines.

9.1.1 Experimental Contributions

1. Experimental results from the first full-scale shake table test of a wind turbine were presented and support the following conclusions:

   (a) The salient resonant response characteristics were identified with first mode damping estimated to be below 1% for the tested parked-turbine configuration.

   (b) Beam-column computational models were calibrated and found to be a valuable tool for assessment of seismic response.

   (c) For small utility scale turbines, a first mode response was shown to provide a reasonable approximation. As such, the response spectrum approach may provide a convenient approach for estimating the seismically induced peak shear force and moment.

   (d) For larger modern turbines, higher modes may play a prominent role in the overall seismic response. Higher fidelity modeling may be necessary for such situations (Häenler et al., 2006). Additional experimental data related to damping and soil structure interaction effects would be also most worthwhile.

2. Experimental results from a second, more detailed, full-scale test of a 65-kW

turbine are presented and analyzed. The test protocol was designed to augment the results from a previous test and from a calibrated FE model. Key additions were: multiple test motions at multiple levels of shaking, more extensive in-plane and additional out-of-plane instrumentation, and multiple test configurations. The results from this set of tests reinforce past experimental and numerical findings. The experimental results were analyzed and supporting findings as described below:

(a) Additional damping appears to only be significant for first mode response to fore-aft shaking (configuration 1).

(b) For turbines similar to the tested unit, a simple procedure is suggested to estimate tower top displacement and, with knowledge of lateral stiffness, base shear demand.

(c) Degradation of the connection between the tower and foundation was identified as a possible and undesirable damage mechanism.

(d) Higher mode response, important for seismic loading of larger turbines and not successfully captured in the initial shake table test, was illustrated.

(e) For consideration of combined wind and earthquake loads, it is shown that relative orientation influences the dynamic response of a turbine.

3. A set of dynamic ambient vibration field tests performed on two large wind turbines located at Oak Creek Energy Systems in Mojave, California, USA. The tests provided a unique opportunity to obtain the modal properties of megawatt scale HAWTs. During the vibration tests, the dynamic response of

the turbines was measured using a dense array of force-balanced accelerometers for both the parked and operational states. These accelerometers were installed simultaneously at selected stations along the tower, covering the whole height. Using the acquired vibration data, the first six modes of the parked turbine and first four vibration modes of the operating turbine (natural frequencies, damping ratios, and mode shapes) were identified using the MNExT-ERA algorithm for the 900-kW turbine. For the 1.5-MW turbine, a total of nine modes were identified for both the parked and operating conditions. On this basis, the following observations are presented.

(a) In agreement with findings for the 65-kW turbine, conventional beam-column FE codes can provide mode shapes that agree with experimental results for use in turbine specific multi-modal programs.

(b) Both first and second tower bending modes in the fore-aft and side-to-side directions show little out of plane deformation, supporting assumed independence between fore-aft and side-to-side motions in multi-modal codes.

(c) In contrast to the findings for the 65-kW turbine, the identified modal damping ratios are higher than IEC recommended values for seismic response analysis in the first bending modes (in the range of 3% to 10%), but are in line with recommendations for higher modes while the turbine is parked (approximately 1%).

(d) Successful identification of modes under operating turbine conditions required guidance from parked condition results due to the presence of har-

monic forcing.

(e) An increase in damping, likely due to aerodynamic interaction, was identified while the 900-kW turbine was operating. Unlike the 65-kW turbine where damping increased only for fore-aft vibration, it was found that for the 900-kW damping increased for both fore-aft and side-to-side modes.

(f) Variation in damping for the 1.5-MW turbine was more complicated, showing an increase for some modes and a decrease for others. This behavior is likely due to changes in blade pitch depending on wind speed and operational state.

9.1.2 Numerical Contributions

1. A numerical investigation of the resonant characteristics of a 5-MW wind turbine was presented. Additionally, the a recording of the 1994 Northridge Earthquake from a rock site is used to consider implications of soil stiffness on the resulting tower moment and shear demand. Findings support the following conclusions.

   (a) The relatively stiff soil produced little SSI influence on the first and second longitudinal modes. In contrast, when softer soils were investigated, a more significant influence was apparent. The second bending mode behavior was clearly impacted, showing a reduction in frequency and increased foundation rotation. However, these changes in dynamic properties (Table 6.4) are small in comparison to safety margins used to space mechani-

cal vibration and resonant frequencies and would are not likely to require redesign of the turbine to account for SSI.

(b) For earthquake like motion, it was found that the soil stiffness can influence the maximum moment (Figure 6.17) and shear (Figure 6.18) demand distributions. Unlike the differences in natural frequencies, this shift in demand parameter distribution may influence turbine design. In particular, the increased demand at higher elevations, near maximum displacement in the second mode, may require special consideration of this portion of the tower for large turbines installed in seismically active regions.

(c) With current trends toward taller and more massive turbines (Wiser and Bolinger, 2008), it is important to conduct further SSI research as an integral component of seismic response studies.

2. The modifications to the FAST code (Jonkman and Buhl Jr., 2005) introduced in this dissertation, enable base shaking time histories to be applied in conjunction with other load sources for wind turbines. Below is a list summarizing major findings.

(a) Simulations of a parked turbine subjected to base shaking without consideration of aerodynamics, are compared to conventional FE simulations using OpenSees and show favorable agreement for both tower top acceleration time history and tower moment demand.

(b) These simulations faithfully reproduced the experimentally observed dynamics of the turbine, discussed in Chapter 3. Further, trends in tower

moment demand showed good agreement between both simulations and experimental data.

(c) A FAST model of a 900-kW NEG Micon turbine demonstrates that ignoring aerodynamic forces on a turbine when assessing seismic loads may result in inaccurate predictions of extreme loads. This supports the use of the FAST code and others that appropriately model rotor aerodynamics to provide useful insight into turbine dynamic response and structural demand for load cases involving combined wind and earthquake loads.

3. It is now possible and practical to conduct time domain simulations considering combined wind and earthquake loads for multiple scenarios using the FAST code. Extensive simulations to a wide range of earthquake motions for four different turbines lead to the following conclusions.

(a) PSA or equivalent spectral quantities (PSV and S_d) are efficient estimators of tower base moment demand. For low intensity earthquakes, tower base moment demand of the larger turbines is driven almost exclusively by wind loads.

(b) For simplified combination of opperational and earthquake loads, accurate estimation of the earthquake contribution is shown to be essential for reliable superposition. It is proposed that adding the seismic and wind loads as vector quantities with appropriate relative orientations can produce reliable estimates of the median and an approximate envelope of the combination.

(c) For the 5-MW turbine, demand from strong earthquake events is shown to be well above that anticipated from extreme wind events. This suggests that for large turbines in regions of high seismic hazard, seismic events are important to consider when developing extreme loads and may be design driving.

(d) In contrast to the possibility of tower moment demand being driven by seismic demand, results show that it is unlikely that even strong shaking will result in design driving loads for the turbine blades.

9.2 Recommendations for Future Research

To extend the work presented in this dissertation, additional research to further investigate the effects of seismic loads for wind turbines is needed. The following is a list of topics that are likely to further advance the field.

1. This dissertation presents results for in-situ characterization of large modern wind turbines. The industry could significantly benefit from further publicly available results characterizing turbines. In particular there are many soil conditions, foundation types, and turbine models where dynamic characteristics have not been assessed. Further, studies similar to those presented by He (2008) exploring the implications of wind speed, temperature, and other factors would assist in developing a more complete understanding of the variability of assumed dynamic properties.

2. Ongoing monitoring of operational turbines in seismically active regions is also

a promising research effort. Such an effort could provide the data needed for better characterization. In addition, data from an instrumented turbine subjected to an actual earthquake would be extremely valuable. Due to the cost of large turbines and logistical constraints of shake table testing facilities it is difficult to capture real field conditions of an operating turbine. Instead, ongoing monitoring of a large turbine could cost effectively provide these results.

3. Currently there is limited information regarding non-linear response of wind turbines. At the University of California, San Diego a recent test was completed looking at buckling of a turbine tower under monotonically increasing lateral load. This investigation and possible follow-on work will prove to be of great value in predicting ultimate loads of wind turbine towers.

4. As shown here and investigated by others (Bazeos et al., 2002; Kiyomiya et al., 2002; Zhao and Maißer, 2006) soil-structure interaction is an important phenomena for wind turbines, especially large modern machines. Tools capable of modeling an operational turbine, foundation, and soil system subjected to a turbulent wind field are needed to fully understand the implications of possible soil-structure interaction.

5. The work presented by Nuta (2010) is of great value in understanding non-linear behavior of a wind turbine in response to earthquake excitation. As suggested by results here, consideration of aerodynamics and operational loads is important to accurately estimate resulting structural demand. Development of tools capable of modeling non-linear material behavior in conjunction with

turbine dynamics has the potential to clarify collapse mechanisms. Additionally, such tools will provide value to designers so that designs can account for and capitalize on possible ductility in the turbine structure.

6. The AeroDyne code used in this dissertation and by many researchers is currently limited in its ability to generate a wind field at an arbitrary heading (Jonkman, 2009). This limitation introduces difficulties in exploring implications of relative orientation of seismic and wind loads. The work presented here simply rotates the input motion by 90 degrees, but a more systematic analysis would change this angle in smaller increments to create a more complete understanding of the influence.

7. The current United States Department of Energy (DOE) goal to modularize the FAST code is directly in line with many of the recommendations listed above. Such a modularization would allow best of breed tools to be used for consideration of boundary conditions. This would facilitate the cross disciplinary research needed to fully understand seismic loads for wind turbines by allowing domain experts to conduct appropriate portions of simulations using tools that they are already familiar with.

Bibliography

Bazeos, N., Hatzigeorgiou, G. D., Hondros, I. D., Karamaneas, H., Karabalis, D. L., and Beskos, D. E. (2002). "Static, seismic and stability analyses of a prototype wind turbine steel tower." *Engineering Structures*, 24(8), 1015–1025.

Häenler, M., Ritschel, U., and Warnke, I. (2006). "Systematic modelling of wind turbine dynamics and earthquake loads on wind turbines." *European Wind Energy*

Conference and Exhibition, Athens, Greece. European Wind Energy Association, 1–6.

He, X. (2008). "Vibration-based damage identification and health monitoring of civil structures," PhD thesis, University of California, San Diego.

Jonkman, B. J. (2009). "TurbSim user's guide: Version 1.50." *Report No. NREL/TP-500-46198*, National Renewable Energy Laboratory.

Jonkman, J. M. and Buhl Jr., M. L. (2005). "FAST user's guide." *Report No. NREL/EL-500-38230*, National Renewable Energy Laboratory.

Kiyomiya, O., Rikiji, T., and van Gelder, P. H. A. J. M. (2002). "Dynamic response analysis of onshore wind energy power units during earthquakes and wind." *Proceedings of The Twelfth (2002) International Offshore and Polar Engineering Conference*, Kitakyushu, Japan. The International Society of Offshore and Polar Engineers, 520–526.

Nuta, E. (2010). "Seismic analysis of steel wind turbine towers in the canadian environment. Master's thesis, University of Toronto, Toronto, Ontario, Canada.

Wiser, R. and Bolinger, M. (2008). "Annual report on U.S. wind power installation, costs, and performance trends: 2007." *Report No. DOE/GO-102008-2590*, Department of Energy.

Zhao, X. and Maißer, P. (2006). "Seismic response analysis of wind turbine towers including soil-structure interaction." *Proceedings of the Institution of Mechanical Engineers, Part K: Journal of Multi-body Dynamics*, 220(1), 53–61.

Appendix A

Additional Data from 2004 Shake Table Test

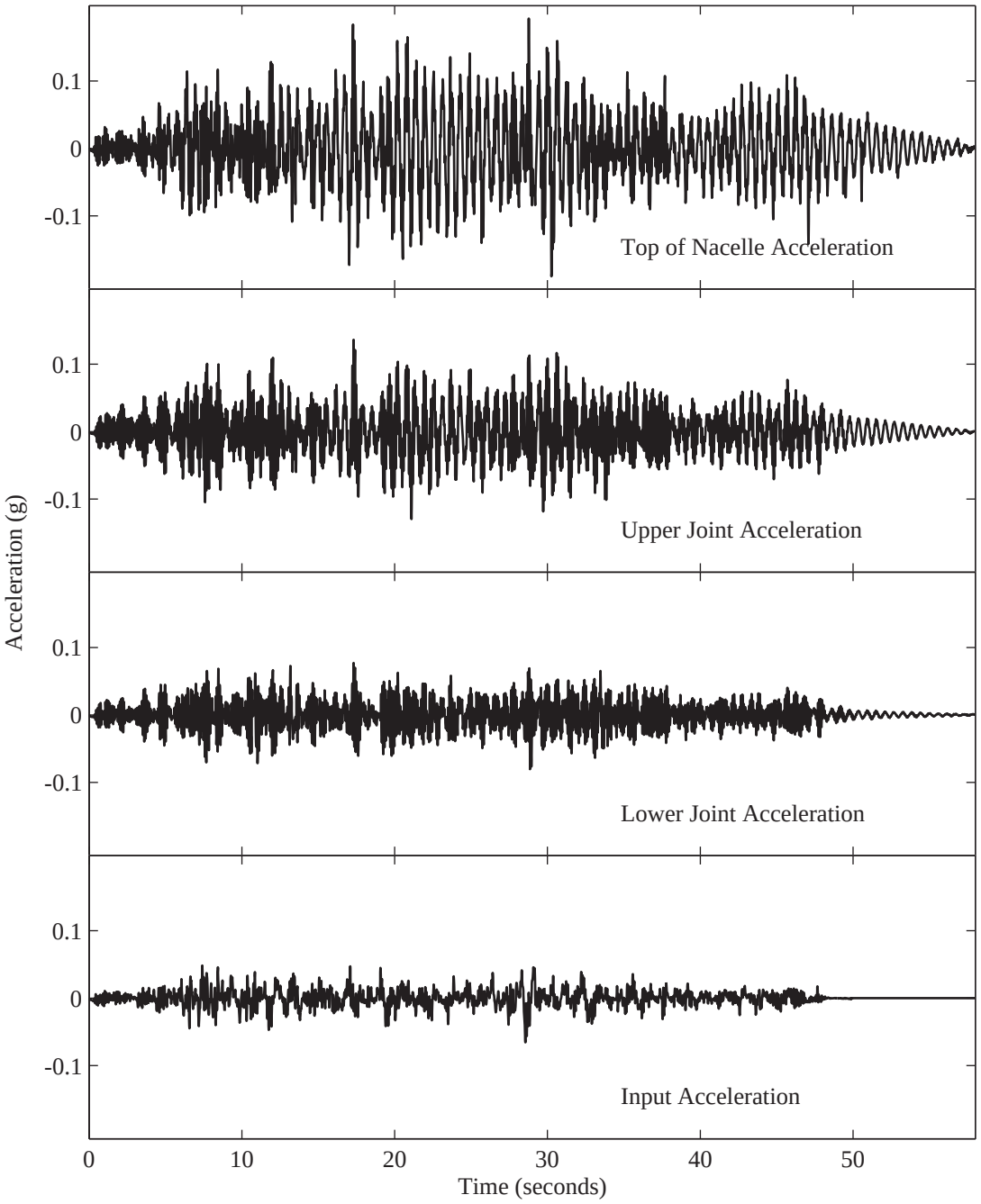

Figure A.1: Recorded acceleration for Landers 50% level test

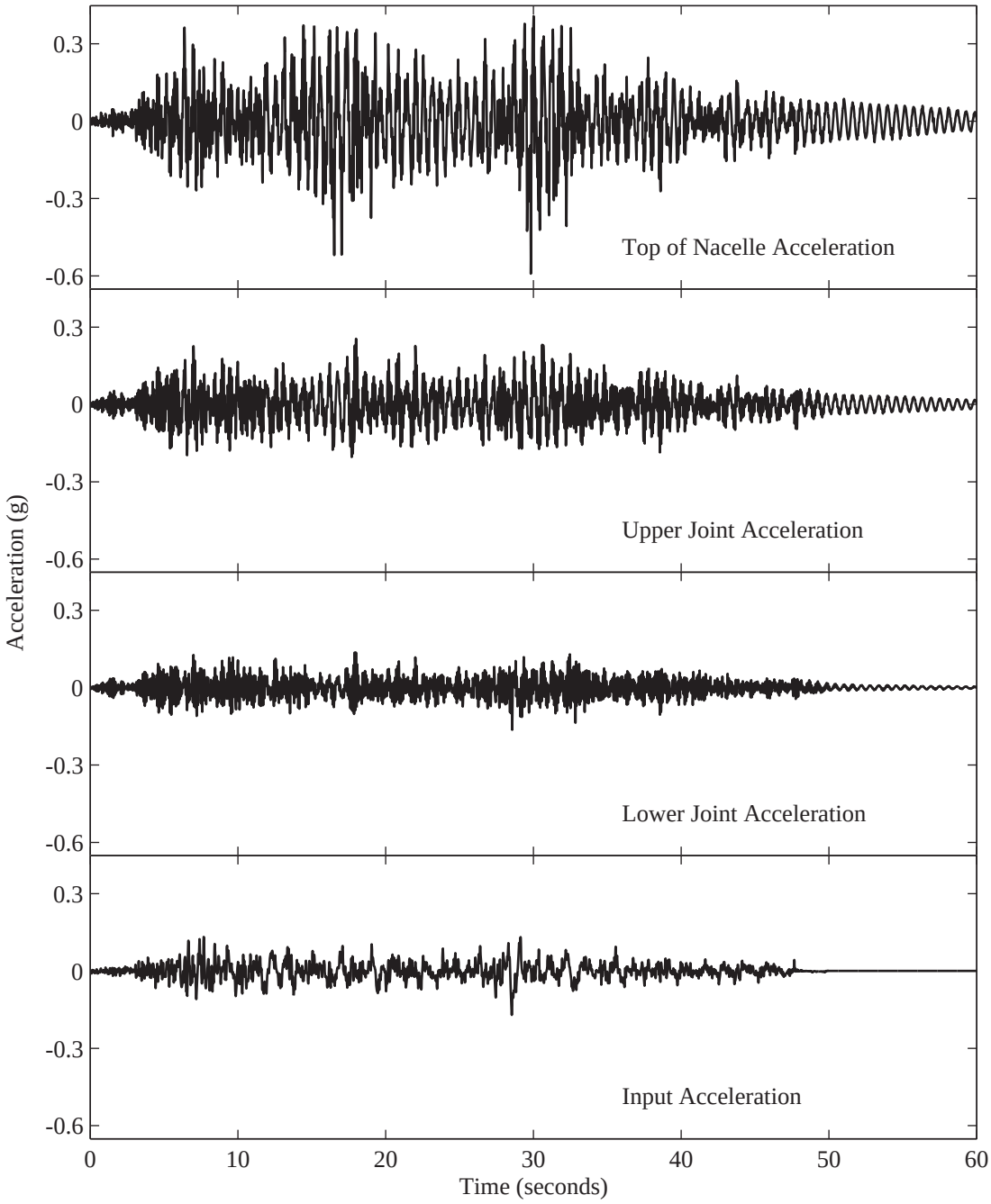

Figure A.2: Recorded acceleration for Landers 143% level test

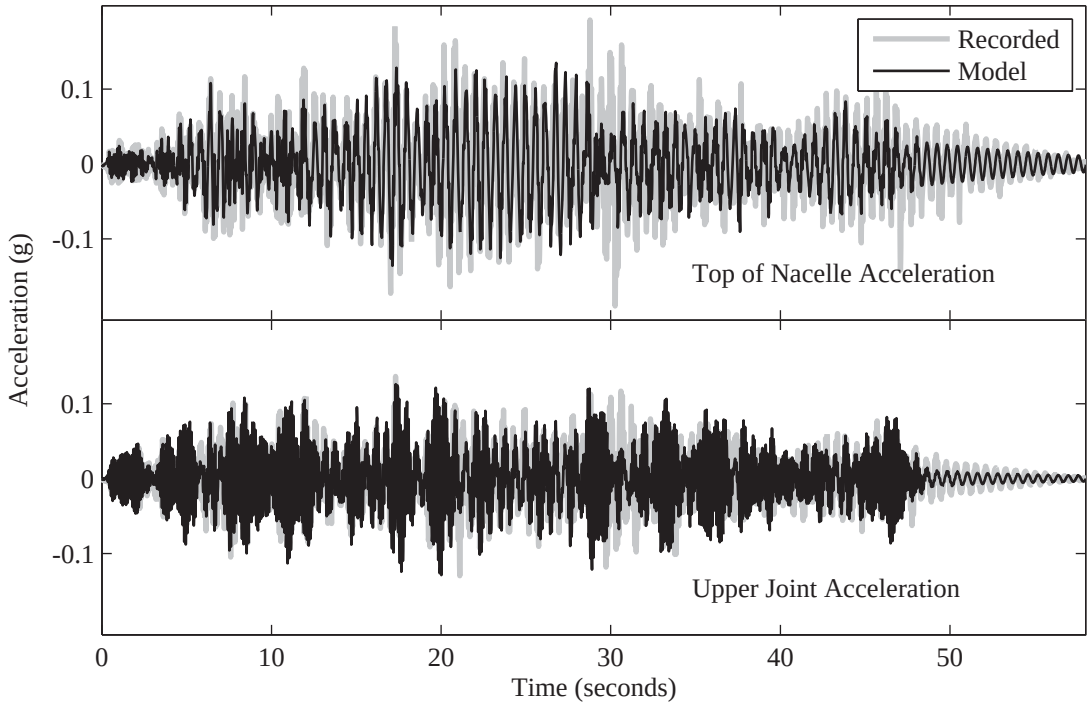

Figure A.3: Model II acceleration for Landers 50% level simulation

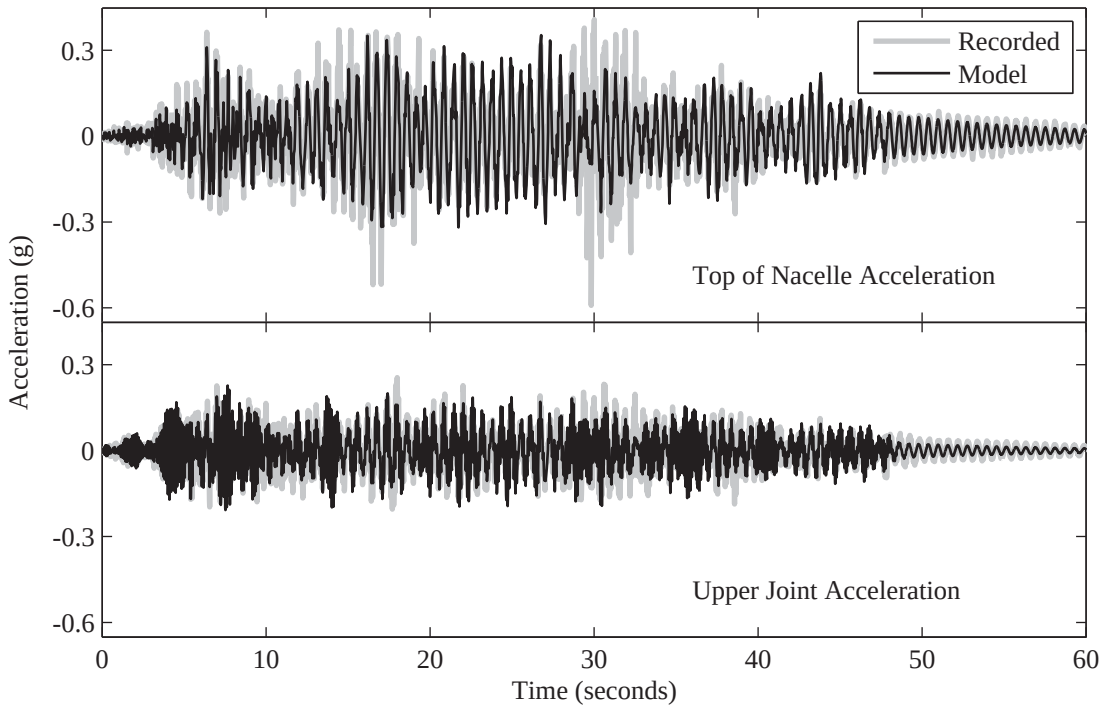

Figure A.4: Model II acceleration for Landers 143% level simulation

Appendix B

Code Based Estimate of Fundamental Period

For the 2006 IBC (ICC, 2006), the turbines fundamental period T (in seconds) is estimated by the equation $T = C_t(h_n)^x$, in which h_n is height, and C_t and x are constants with the defaults values of 0.0488 and 0.75 (metric units), respectively. In order to match the observed period T of 0.59 s, an effective turbine height $h_n = 27.8$ m is needed, approximately equal to the turbine hub height of 22.6 m plus two thirds of the blade length. This effective height implicitly accounts for the geometric configuration of the rotor blades extending above the turbines tower (Figures 2.1 and 2.2).

Bibliography

ICC (2006). *International Building Code 2006*. International Code Council, Country Club Hills, Illinois, USA.

Appendix C

Details of In-Situ Test Data

This appendix presents pertinent details of the data collected from Oak Creek Energy Systems using equipment provided by the NEES equipment site located at UCLA. This data set will be publicly available on the NEES data repository.

C.1 Data File Name Convention

Each data file is a tab delimited text file named to indicate the time at which data collection started in UTC time. The file name format is:

YYYYMMDDHHMMSS<extension>

This format is broken down into the following parts: YYYY is the year; MM is the month; DD is the day; HH is the hour MM is the minute; SS is the second; and <extension> is a user defined extension with no significant meaning.

C.2 Conversion of Data to Engineering Units

The collected data files contain two main classifications of data, time and acceleration. The time is stored in seconds from from January 1, 1970. The the data is stored in the UTC time zone. Conventional time processing utilities may be used to convert the recorded time to the desired time zone. Equation C.1 is used to convert the recorded acceleration into units of g.

$$R \cdot \frac{8}{2^{24}} \cdot \frac{5}{\text{Scale Factor}} = A \tag{C.1}$$

Where R is the recorded value in the data file and the resulting value of A is acceleration in units of g. For tests where the eccentric mass shaker was used, data files also contain an estimate of the shaker rotational frequency and a single pulse per shaker revolution. Equation C.2 is used to convert the recorded shaker frequency into units of Hz.

$$R \cdot \frac{40}{2^{24}} \cdot 2 = f \tag{C.2}$$

Where R is the recorded value in the data file and the resulting value of f is the shaker frequency in units of Hz. The one pulse per revolution may simply be taken as a high or low value.

C.3 Data File Column Information

The following tables define the various data files collected from in-situ testing.

Table C.1: Format for 900-kW turbine data files recorded on 1/27/2009

Col.	Name	Units	Location (m)			Orientation	Scale
			X	Y	Z		Factor
1	Time	sec	-	-	-	-	-
2	52-I-Z	g	0.20	-0.48	52.37	Z	5.00
3	52-I-Y	g	0.20	-0.48	52.37	Y	5.00
4	52-I-X	g	0.20	-0.48	52.37	X	5.01
5	43-I-Z	g	0.25	-0.58	43.15	Z	5.00
6	43-I-Y	g	0.25	-0.58	43.15	Y	4.99
7	43-I-X	g	0.25	-0.58	43.15	X	5.00
8	32-I-Z	g	-0.30	0.94	31.52	Z	4.98
9	32-I-Y	g	-0.30	0.94	31.52	Y	4.99
10	32-I-X	g	-0.30	0.94	31.52	X	9.99
11	32-II-Z	g	0.30	-0.69	31.52	Z	5.01
12	32-II-Y	g	0.30	-0.69	31.52	Y	4.99
13	32-II-X	g	0.30	-0.69	31.52	X	5.00
14	13-I-Z	g	0.33	-0.81	13.43	Z	5.00
15	13-I-Y	g	0.33	-0.81	13.43	Y	5.00
16	13-I-X	g	0.33	-0.81	13.43	X	5.00
17	0-I-Z	g	1.93	0.00	0.00	Z	4.99
18	0-I-Y	g	1.93	0.00	0.00	Y	4.99
19	0-I-X	g	1.93	0.00	0.00	X	5.01
20	0-II-Z	g	-1.93	0.00	0.00	Z	5.03
21	0-II-Y	g	-1.93	0.00	0.00	Y	5.00
22	0-II-X	g	-1.93	0.00	0.00	X	5.00
23	G-I-Z	g	6.22	0.00	-0.20	Z	5.00
24	G-I-Y	g	6.22	0.00	-0.20	Y	4.99
25	G-I-X	g	6.22	0.00	-0.20	X	5.00
26	G-II-Z	g	10.00	0.00	-0.20	Z	5.00
27	G-II-Y	g	10.00	0.00	-0.20	Y	4.99
28	G-II-X	g	10.00	0.00	-0.20	X	5.00
29	G-III-Z	g	-6.38	0.00	-0.20	Z	5.00
30	G-III-Z	g	-6.38	0.00	-0.20	Y	5.00
31	G-III-Z	g	-6.38	0.00	-0.20	X	5.00

Table C.2: Format for 900-kW turbine data files recorded between 3/17/2009 and 3/19/2009

Col.	Name	Units	Location (m)			Orientation	Scale
			X	Y	Z		Factor
1	Time	sec	-	-	-	-	-
2	52-IV-Z	g	0.76	0.00	52.37	Z	5.00
3	52-IV-Y	g	0.76	0.00	52.37	Y	4.99
4	52-IV-X	g	0.76	0.00	52.37	X	5.00
5	52-I-Z	g	-0.43	-0.64	52.37	Z	5.01
6	52-I-Y	g	-0.43	-0.64	52.37	Y	4.99
7	52-I-X	g	-0.43	-0.64	52.37	X	5.01
8	52-II-Z	g	-0.76	0.00	52.37	Z	5.00
9	52-II-Y	g	-0.76	0.00	52.37	Y	4.99
10	52-II-X	g	-0.76	0.00	52.37	X	4.99
11	52-III-Z	g	-0.43	0.64	52.37	Z	4.98
12	52-III-Y	g	-0.43	0.64	52.37	Y	5.00
13	52-III-X	g	-0.43	0.64	52.37	X	4.99
14	43-I-Z	g	0.41	-0.97	43.15	Z	5.00
15	43-I-Y	g	0.41	-0.97	43.15	Y	4.99
16	43-I-X	g	0.41	-0.97	43.15	X	5.00
17	32-IV-Z	g	1.07	0.00	31.52	Z	4.99
18	32-IV-Y	g	1.07	0.00	31.52	Y	5.00
19	32-IV-X	g	1.07	0.00	31.52	X	5.00
20	32-I-Z	g	-0.48	-0.66	31.52	Z	5.01
21	32-I-Y	g	-0.48	-0.66	31.52	Y	4.99
22	32-I-X	g	-0.48	-0.66	31.52	X	5.00
23	32-II-Z	g	-1.07	0.00	31.52	Z	4.99
24	32-II-Y	g	-1.07	0.00	31.52	Y	4.99
25	32-II-X	g	-1.07	0.00	31.52	X	5.01
26	32-III-Z	g	-0.48	0.66	31.52	Z	5.00
27	32-III-Y	g	-0.48	0.66	31.52	Y	5.00
28	32-III-X	g	-0.48	0.66	31.52	X	5.00
29	22-I-Z	g	0.43	-1.22	22.48	Z	5.02
30	22-I-Y	g	0.43	-1.22	22.48	Y	4.99
31	22-I-X	g	0.43	-1.22	22.48	X	5.03
32	13-IV-Z	g	1.30	0.00	13.44	Z	5.00
33	13-IV-Y	g	1.30	0.00	13.44	Y	5.00
34	13-IV-X	g	1.30	0.00	13.44	X	5.00
35	13-I-Z	g	-0.48	-1.27	13.44	Z	4.98
36	13-I-Y	g	-0.48	-1.27	13.44	Y	4.99
37	13-I-X	g	-0.48	-1.27	13.44	X	5.00

Continued on next page

Table C.2: – continued from previous page

Col.	Name	Units	Location (m)			Orientation	Scale
			X	Y	Z		Factor
38	13-II-Z	g	-1.30	0.00	13.44	Z	5.00
39	13-II-Y	g	-1.30	0.00	13.44	Y	4.99
40	13-II-X	g	-1.30	0.00	13.44	X	5.00
41	13-III-Z	g	-0.43	1.27	13.44	Z	4.99
42	13-III-Y	g	-0.43	1.27	13.44	Y	4.99
43	13-III-X	g	-0.43	1.27	13.44	X	5.00
44	7-I-Z	g	0.41	-1.40	6.71	Z	4.98
45	7-I-Y	g	0.41	-1.40	6.71	Y	4.99
46	7-I-X	g	0.41	-1.40	6.71	X	5.00
47	0-IV-Z	g	1.45	0.00	0.00	Z	5.00
48	0-IV-Y	g	1.45	0.00	0.00	Y	5.00
49	0-IV-X	g	1.45	0.00	0.00	X	5.00
50	0-I-Z	g	0.00	-1.88	0.00	Z	5.01
51	0-I-Y	g	0.00	-1.88	0.00	Y	5.00
52	0-I-X	g	0.00	-1.88	0.00	X	5.02
53	0-II-Z	g	-1.88	0.00	0.00	Z	4.98
54	0-II-Y	g	-1.88	0.00	0.00	Y	4.99
55	0-II-X	g	-1.88	0.00	0.00	X	5.00
56	0-III-Z	g	0.00	1.88	0.00	Z	5.00
57	0-III-Y	g	0.00	1.88	0.00	Y	5.00
58	0-III-X	g	0.00	1.88	0.00	X	4.99
59	G-IV-Z	g	6.27	0.00	-0.20	Z	4.99
60	G-IV-Y	g	6.27	0.00	-0.20	Y	5.00
61	G-IV-X	g	6.27	0.00	-0.20	X	4.99
62	G-I-Z	g	0.00	-6.35	-0.20	Z	5.00
63	G-I-Y	g	0.00	-6.35	-0.20	Y	5.00
64	G-I-X	g	0.00	-6.35	-0.20	X	5.01
65	G-II-Z	g	-6.86	0.00	-0.20	Z	5.00
66	G-II-Y	g	-6.86	0.00	-0.20	Y	5.00
67	G-II-X	g	-6.86	0.00	-0.20	X	5.00
68	G-III-Z	g	0.00	6.55	-0.20	Z	4.98
69	G-III-Y	g	0.00	6.55	-0.20	Y	4.99
70	G-III-X	g	0.00	6.55	-0.20	X	4.99
71	G-VIII-Z	g	10.03	0.00	-0.20	Z	5.01
72	G-VIII-Y	g	10.03	0.00	-0.20	Y	5.00
73	G-VIII-X	g	10.03	0.00	-0.20	X	5.00
74	G-V-Z	g	0.00	-9.19	-0.10	Z	5.00
75	G-V-Y	g	0.00	-9.19	-0.10	Y	5.00
76	G-V-X	g	0.00	-9.19	-0.10	X	5.00
77	G-VI-Z	g	-9.70	0.00	-0.20	Z	4.99

Continued on next page

Table C.2: – continued from previous page

Col.	Name	Units	Location (m)			Orientation	Scale
			X	Y	Z		Factor
78	G-VI-Y	g	-9.70	0.00	-0.20	Y	4.99
79	G-VI-X	g	-9.70	0.00	-0.20	X	4.99
80	G-VII-Z	g	0.00	9.22	-0.20	Z	5.00
81	G-VII-Y	g	0.00	9.22	-0.20	Y	5.00
82	G-VII-X	g	0.00	9.22	-0.20	X	-5.01
83	Shaker Pulse	-	-	-	-	-	-
84	Shaker Freq.	Hz	-	-	-	-	1

Table C.3: Format for 900-kW turbine data files recorded between 3/24/2009 and 3/28/2009

Col.	Name	Units	Location (m)			Orientation	Scale
			X	Y	Z		Factor
1	52-IV-Z	g	0.76	0.00	52.37	Z	5.00
2	52-IV-Y	g	0.76	0.00	52.37	Y	4.99
3	52-IV-X	g	0.76	0.00	52.37	X	5.00
4	52-I-Z	g	-0.43	-0.64	52.37	Z	5.01
5	52-I-Y	g	-0.43	-0.64	52.37	Y	4.99
6	52-I-X	g	-0.43	-0.64	52.37	X	5.01
7	52-II-Z	g	-0.76	0.00	52.37	Z	5.00
8	52-II-Y	g	-0.76	0.00	52.37	Y	4.99
9	52-II-X	g	-0.76	0.00	52.37	X	4.99
10	52-III-Z	g	-0.43	0.64	52.37	Z	4.98
11	52-III-Y	g	-0.43	0.64	52.37	Y	5.00
12	52-III-X	g	-0.43	0.64	52.37	X	4.99
13	43-I-Z	g	0.41	-0.97	43.15	Z	5.00
14	43-I-Y	g	0.41	-0.97	43.15	Y	4.99
15	43-I-X	g	0.41	-0.97	43.15	X	5.00
16	32-IV-Z	g	1.07	0.00	31.52	Z	4.99
17	32-IV-Y	g	1.07	0.00	31.52	Y	5.00
18	32-IV-X	g	1.07	0.00	31.52	X	5.00
19	32-I-Z	g	-0.48	-0.66	31.52	Z	5.01
20	32-I-Y	g	-0.48	-0.66	31.52	Y	4.99
21	32-I-X	g	-0.48	-0.66	31.52	X	5.00
22	32-II-Z	g	-1.07	0.00	31.52	Z	4.99
23	32-II-Y	g	-1.07	0.00	31.52	Y	4.99
24	32-II-X	g	-1.07	0.00	31.52	X	5.01
25	32-III-Z	g	-0.48	0.66	31.52	Z	5.00
26	32-III-Y	g	-0.48	0.66	31.52	Y	5.00
27	32-III-X	g	-0.48	0.66	31.52	X	5.00
28	22-I-Z	g	0.43	-1.22	22.48	Z	5.02
29	22-I-Y	g	0.43	-1.22	22.48	Y	4.99
30	22-I-X	g	0.43	-1.22	22.48	X	5.03
31	13-IV-Z	g	1.30	0.00	13.44	Z	5.00
32	13-IV-Y	g	1.30	0.00	13.44	Y	5.00
33	13-IV-X	g	1.30	0.00	13.44	X	5.00
34	13-I-Z	g	-0.48	-1.27	13.44	Z	4.98
35	13-I-Y	g	-0.48	-1.27	13.44	Y	4.99
36	13-I-X	g	-0.48	-1.27	13.44	X	5.00
37	13-II-Z	g	-1.30	0.00	13.44	Z	5.00

Continued on next page

Table C.3: – continued from previous page

Col.	Name	Units	Location (m)			Orientation	Scale Factor
			X	Y	Z		
38	13-II-Y	g	-1.30	0.00	13.44	Y	4.99
39	13-II-X	g	-1.30	0.00	13.44	X	5.00
40	13-III-Z	g	-0.43	1.27	13.44	Z	4.99
41	13-III-Y	g	-0.43	1.27	13.44	Y	4.99
42	13-III-X	g	-0.43	1.27	13.44	X	5.00
43	7-I-Z	g	0.41	-1.40	6.71	Z	4.98
44	7-I-Y	g	0.41	-1.40	6.71	Y	4.99
45	7-I-X	g	0.41	-1.40	6.71	X	5.00
46	0-IV-Z	g	1.45	0.00	0.00	Z	5.00
47	0-IV-Y	g	1.45	0.00	0.00	Y	5.00
48	0-IV-X	g	1.45	0.00	0.00	X	5.00
49	0-III-Z	g	0.00	1.45	0.00	Z	5.01
50	0-III-Y	g	0.00	1.45	0.00	Y	5.00
51	0-III-X	g	0.00	1.45	0.00	X	5.02
52	0-II-Z	g	-1.45	0.00	0.00	Z	4.98
53	0-II-Y	g	-1.45	0.00	0.00	Y	4.99
54	0-II-X	g	-1.45	0.00	0.00	X	5.00

Table C.4: Format for 1.5-MW turbine data files recorded between 6/17/2009 and 6/19/2009

Col.	Name	Units	Location (m)			Orientation	Scale
			X	Y	Z		Factor
1	Time	sec	-	-	-	-	-
2	66-I-Z	g	0.84	0.00	66.07	Z	5.00
3	66-I-Y	g	0.84	0.00	66.07	Y	5.00
4	66-I-X	g	0.84	0.00	66.07	X	5.00
5	61-I-Z	g	0.86	0.00	60.58	Z	5.00
6	61-I-Y	g	0.86	0.00	60.58	Y	5.00
7	61-I-X	g	0.86	0.00	60.58	X	5.00
8	54-I-X	g	0.51	-1.19	54.28	X	5.00
9	54-I-Z	g	0.51	-1.19	54.28	Z	5.00
10	54-I-Y	g	0.51	-1.19	54.28	Y	5.00
11	45-I-X	g	0.53	-1.26	45.44	X	5.00
12	45-I-Z	g	0.53	-1.26	45.44	Z	5.00
13	45-I-Y	g	0.53	-1.26	45.44	Y	5.00
14	37-IV-Z	g	1.02	0.00	37.36	Z	5.00
15	37-IV-Y	g	1.02	0.00	37.36	Y	5.00
16	37-IV-X	g	1.02	0.00	37.36	X	5.00
17	37-II-Z	g	-1.02	0.00	37.36	Z	5.00
18	37-II-Y	g	-1.02	0.00	37.36	Y	5.00
19	37-II-X	g	-1.02	0.00	37.36	X	5.00
20	27-I-X	g	0.53	-1.68	26.82	X	5.00
21	27-I-Z	g	0.53	-1.68	26.82	Z	5.00
22	27-I-Y	g	0.53	-1.68	26.82	Y	5.00
23	14-IV-Z	g	1.19	0.00	14.17	Z	5.00
24	14-IV-Y	g	1.19	0.00	14.17	Y	5.00
25	14-IV-X	g	1.19	0.00	14.17	X	5.00
26	14-II-Z	g	-1.19	0.00	14.17	Z	5.00
27	14-II-Y	g	-1.19	0.00	14.17	Y	5.00
28	14-II-X	g	-1.19	0.00	14.17	X	5.00
29	7-I-X	g	0.53	-2.26	7.34	X	5.00
30	7-I-Z	g	0.53	-2.26	7.34	Z	5.00
31	7-I-Y	g	0.53	-2.26	7.34	Y	5.00
32	0-IV-Z	g	2.16	0.00	0.00	Z	5.00
33	0-IV-Y	g	2.16	0.00	0.00	Y	5.00
34	0-IV-X	g	2.16	0.00	0.00	X	5.00
35	0-I-Z	g	0.00	-2.16	0.00	Z	5.00
36	0-I-Y	g	0.00	-2.16	0.00	Y	5.00
37	0-I-X	g	0.00	-2.16	0.00	X	5.00

Continued on next page

Table C.4: – continued from previous page

Col.	Name	Units	Location (m)			Orientation	Scale Factor
			X	Y	Z		
38	0-II-Z	g	-2.16	0.00	0.00	Z	5.00
39	0-II-Y	g	-2.16	0.00	0.00	Y	5.00
40	0-II-X	g	-2.16	0.00	0.00	X	5.00
41	0-III-Z	g	0.00	2.16	0.00	Z	10.00
42	0-III-Y	g	0.00	2.16	0.00	Y	10.00
43	0-III-X	g	0.00	2.16	0.00	X	10.00
44	G-IV-Z	g	5.94	0.00	0.00	Z	5.00
45	G-IV-Y	g	5.94	0.00	0.00	Y	5.00
46	G-IV-X	g	5.94	0.00	0.00	X	5.00
47	G-I-Z	g	0.00	-5.94	0.00	Z	5.00
48	G-I-Y	g	0.00	-5.94	0.00	Y	5.00
49	G-I-X	g	0.00	-5.94	0.00	X	5.00
50	G-II-Z	g	-5.94	0.00	0.00	Z	5.00
51	G-II-Y	g	-5.94	0.00	0.00	Y	5.00
52	G-II-X	g	-5.94	0.00	0.00	X	5.00
53	G-III-Z	g	0.00	5.94	0.00	Z	5.00
54	G-III-Y	g	0.00	5.94	0.00	Y	5.00
55	G-III-X	g	0.00	5.94	0.00	X	5.00
56	G-VIII-Z	g	9.91	0.00	0.00	Z	5.00
57	G-VIII-Y	g	9.91	0.00	0.00	Y	5.00
58	G-VIII-X	g	9.91	0.00	0.00	X	5.00
59	G-V-Z	g	0.00	-9.91	0.00	Z	5.00
60	G-V-Y	g	0.00	-9.91	0.00	Y	5.00
61	G-V-X	g	0.00	-9.91	0.00	X	5.00
62	G-VI-Z	g	-9.91	0.00	0.00	Z	5.00
63	G-VI-Y	g	-9.91	0.00	0.00	Y	5.00
64	G-VI-X	g	-9.91	0.00	0.00	X	5.00
65	G-VII-Z	g	0.00	9.91	0.00	Z	5.00
66	G-VII-Y	g	0.00	9.91	0.00	Y	5.00
67	G-VII-X	g	0.00	9.91	0.00	X	5.00

Appendix D

Details of 2010 Shake Table Test Data

This appendix presents pertinent details of the data collected from shake table tests conducted using the LHPOST maintained and operated by the NEES equipment site located at UCSD. This data set will be publicly available on the NEES data repository.

D.1 Test Program and Instrument Layout

The shake table testing conducted using the NEES LHPOST consisted of a series of earthquake simulations, simulated wave, and white noise motions. The testing matrix describing the sequence of each test run is presented in Table D.1. Table D.3 describes each of the input motions (earthquake, simulated wave, and white noise). Estimates of wind speed and direction (see Section 3.6 on page 75 for

details) are presented in Table D.2. The layout of the sensors is provided in Table D.4.

Table D.1: Test Matrix

Test No.	Trial No.	Date	Time	Input Mot.	Scale Fact.	Conf.	State	DAQ Samp. Freq. (Hz)	MTS Samp. Freq. (Hz).
1	1	2/9	-	NA	NA	2	Parked	240	256
1	2	2/9	-	WN-01	1.00	2	Parked	240	256
2	1	2/9	-	WN-01	1.00	2	Parked	2000	256
3	1	2/10	11:02	WN-02	1.00	2	Parked	2000	256
3	2	2/10	11:11	FF-03	0.67	2	Parked	2000	256
3	3	2/10	11:25	WN-02	1.00	2	Parked	2000	256
3	4	2/10	11:32	FF-03	0.67	2	Operating	2000	256
4	1	2/11	10:53	WN-02	1.00	2	Parked	2000	256
4	2	2/11	11:08	WN-02	1.00	2	Operating	2000	256
4	3A	2/11	11:58	MS-01	1.00	2	Parked	2000	256
4	3B	2/11	12:05	MS-01	1.00	2	Parked	2000	256
4	4	2/11	12:13	WN-02	1.00	2	Parked	2000	256
4	5	2/11	12:24	MS-01	1.00	2	Operating	2000	256
4	6	2/11	12:32	WN-02	1.00	2	Parked	2000	256
4	7	2/11	12:42	NF-01	0.67	2	Parked	2000	256
4	8	2/11	12:46	WN-02	1.00	2	Parked	2000	256
4	9	2/11	12:57	NF-01	0.67	2	Operating	2000	256
5	1	2/11	13:05	WN-02	1.00	2	Parked	2000	256
5	2A	2/11	13:11	FF-01	1.00	2	Parked	2000	256
5	2B	2/11	13:15	FF-01	0.67	2	Parked	2000	256
5	3	2/11	13:20	WN-02	1.00	2	Parked	2000	256
5	4	2/11	13:23	FF-01	0.67	2	Operating	2000	256
5	5	2/11	13:33	WN-02	1.00	2	Parked	2000	256
5	6	2/11	13:40	NF-02	0.67	2	Parked	2000	256
5	7	2/11	13:43	WN-02	1.00	2	Parked	2000	256
5	8	2/11	13:51	NF-02	0.67	2	Operating	2000	256
5	9	2/11	13:56	WN-02	1.00	2	Parked	2000	256
6	1	2/11	14:03	MS-01	1.00	2	Parked	2000	256
6	2A	2/11	14:10	WN-02	1.00	2	Parked	2000	256
6	2B	2/11	-	WN-02	1	2	Parked	2000	256
6	2C	2/11	14:36	WN-02	1.00	2	Parked	2000	256
7	1	2/12	12:30	FT-02	1.00	2	Parked	2000	256
7	2	2/12	12:45	FT-01	1.00	2	Parked	2000	256

Continued on next page

Table D.1: – continued from previous page

Test No.	Trial No.	Date	Time	Input Motion	Scale Fact.	Conf.	State	DAQ Samp. Freq. (Hz)	MTS Samp. Freq. (Hz).
7	3	2/12	12:54	FT-01	1.00	2	Operating	2000	256
8	1	2/12	13:17	WN-02	1.00	2	Parked	2000	256
8	2	2/12	13:25	FF-02	0.67	2	Parked	2000	256
8	3	2/12	13:29	WN-02	1.00	2	Parked	2000	256
8	4	2/12	13:38	FF-02	0.67	2	Operating	2000	256
8	5	2/12	13:43	WN-02	1.00	2	Parked	2000	256
8	6	2/12	13:50	FF-03	0.67	2	Parked	2000	256
8	7	2/12	13:53	WN-02	1.00	2	Parked	2000	256
8	8	2/12	13:59	WN-02	1.00	2	Parked	1024	1024
9	1	2/16	-	NA	NA	2	Parked	1024	1024
9	2	2/16	-	NA	NA	2	Parked	1024	1024
9	3	2/16	-	NA	NA	2	Parked	1024	1024
9	4	2/16	-	NA	NA	2	Parked	1024	1024
9	5	2/16	-	NA	NA	2	Parked	1024	1024
10	1	2/17	10:49	WN-04	1.00	2	Parked	1024	1024
10	2	2/17	11:00	FF-01	0.67	2	Parked	1024	1024
10	3	2/17	11:04	WN-04	1.00	2	Parked	1024	1024
10	4	2/17	-	FF-01	0.67	2	Operating	1024	1024
10	5	2/17	13:55	WN-04	0.67	2	Parked	1024	1024
11	1	2/17	14:02	FF-03	0.67	2	Parked	1024	1024
11	2	2/17	14:07	WN-04	0.80	2	Parked	1024	1024
11	3	2/17	14:15	FF-03	0.67	2	Operating	1024	1024
11	4	2/17	14:27	WN-04	1.00	2	Parked	1024	1024
11	5	2/17	14:38	WN-04	1.00	2	Operating	1024	1024
11	6A	2/17	15:05	FF-01	1.00	2	Parked	1024	1024
11	6B	2/17	15:06	FF-01	0.67	2	Parked	1024	1024
11	7	2/17	15:10	WN-04	1.00	2	Parked	1024	1024
11	8	2/17	15:18	FF-01	0.67	2	Operating	1024	1024
11	9	2/17	15:25	WN-04	1.00	2	Parked	1024	1024
12	1	2/19	10:05	WN-04	1.00	1	Parked	1024	1024
12	2	2/19	10:27	FF-01	0.67	1	Parked	1024	1024
12	3	2/19	10:31	WN-04	1.00	1	Parked	1024	1024
12	4	2/19	10:42	FF-01	0.67	1	Operating	1024	1024
13	1	2/19	14:04	WN-04	0.80	1	Parked	1024	1024
13	2	2/19	14:15	FF-01	0.67	1	Parked	1024	1024
13	3	2/19	14:19	WN-04	0.80	1	Parked	1024	1024
13	4	2/19	14:28	FF-01	0.67	1	Operating	1024	1024
13	5	2/19	14:32	WN-04	0.80	1	Parked	1024	1024

Continued on next page

Table D.1: – continued from previous page

Test No.	Trial No.	Date	Time	Input Motion	Scale Fact.	Conf.	State	DAQ Samp. Freq. (Hz)	MTS Samp. Freq. (Hz).
14	1	2/19	14:41	FF-03	0.67	1	Parked	1024	1024
14	2	2/19	14:44	WN-04	0.80	1	Parked	1024	1024
14	3	2/19	14:52	FF-03	0.67	1	Operating	1024	1024
14	4	2/19	14:56	WN-04	0.80	1	Parked	1024	1024
15	1	2/19	15:04	WN-04	0.80	1	Operating	1024	1024
15	2A	2/19	15:13	NF-01	0.80	1	Parked	1024	1024
15	2B	2/19	15:18	NF-01	0.67	1	Parked	1024	1024
15	3	2/19	15:23	WN-04	0.80	1	Parked	1024	1024
15	4	2/19	15:31	NF-01	0.67	1	Operating	1024	1024
15	5	2/19	15:35	WN-04	0.80	1	Parked	1024	1024
16	1	2/22	12:17	WN-04	0.80	1	Parked	1024	1024
16	2	2/22	12:28	FF-01	0.67	1	Parked	1024	1024
16	3	2/22	12:34	WN-04	0.80	1	Parked	1024	1024
16	4	2/22	12:58	FF-01	0.67	1	Parked	1024	1024
16	5	2/22	14:43	WN-04	0.80	1	Parked	1024	1024
16	6	2/22	14:58	FF-01	1.00	1	Parked	1024	1024
17	1	2/22	15:02	WN-04	0.80	1	Parked	1024	1024
17	2	2/22	15:15	FF-01	0.89	1	Parked	1024	1024
17	3	2/22	15:19	WN-04	0.80	1	Parked	1024	1024
17	4	2/22	15:37	FF-01	0.94	1	Parked	1024	1024
17	5	2/22	15:41	WN-04	0.80	1	Parked	1024	1024
17	6	2/22	16:09	FF-01	0.94	1	Parked	1024	1024
17	7	2/22	16:12	WN-04	0.80	1	Parked	1024	1024

Table D.2: Estimated wind speed and direction

Test No.	Trial No.	Wind Speed (m/s)	Wind Direction (deg)
1	1	-	-
1	2	-	-
2	1	-	-
3	1	2.5	307
3	2	2.5	315
3	3	2.2	288
3	4	2.2	310
4	1	0.8	181

Continued on next page

Table D.2: – continued from previous page

Test No.	Trial No.	Wind Speed (m/s)	Wind Direction (deg)
4	2	1.2	198
4	3A	1.9	225
4	3B	1.6	206
4	4	1.9	216
4	5	2.2	209
4	6	3.1	201
4	7	2.5	209
4	8	2.5	212
4	9	2.7	195
5	1	2.2	200
5	2A	2.5	197
5	2B	2.4	203
5	3	2.1	209
5	4	2.0	211
5	5	3.3	201
5	6	2.5	203
5	7	2.1	204
5	8	2.5	206
5	9	2.6	206
6	1	2.5	199
6	2A	2.7	211
6	2B	-	-
6	2C	2.8	218
7	1	3.3	299
7	2	3.6	294
7	3	3.6	293
8	1	3.9	293
8	2	4.0	293
8	3	4.0	293
8	4	4.1	291
8	5	4.1	291
8	6	4.1	291
8	7	4.1	290
8	8	4.1	290
9	1	-	-
9	2	-	-
9	3	-	-
9	4	-	-
9	5	-	-
10	1	0.5	181

Continued on next page

Table D.2: – continued from previous page

Test No.	Trial No.	Wind Speed (m/s)	Wind Direction (deg)
10	2	0.7	187
10	3	0.7	196
10	4	-	-
10	5	3.1	261
11	1	3.3	265
11	2	3.3	262
11	3	3.1	268
11	4	2.9	266
11	5	3.8	264
11	6A	2.8	260
11	6B	2.8	261
11	7	2.8	261
11	8	2.8	271
11	9	2.7	260
12	1	1.1	175
12	2	1.3	174
12	3	1.3	173
12	4	1.4	170
13	1	3.6	195
13	2	3.5	197
13	3	3.6	198
13	4	3.9	198
13	5	4.0	198
14	1	4.5	203
14	2	4.4	202
14	3	4.5	203
14	4	4.0	182
15	1	4.9	203
15	2A	4.9	197
15	2B	5.1	207
15	3	5.5	206
15	4	4.5	204
15	5	4.5	206
16	1	4.1	274
16	2	3.8	284
16	3	3.5	285
16	4	3.9	265
16	5	2.2	257
16	6	2.0	256
17	1	2.2	246

Continued on next page

Table D.2: – continued from previous page

Test No.	Trial No.	Wind Speed (m/s)	Wind Direction (deg)
17	2	2.4	259
17	3	2.5	253
17	4	3.2	255
17	5	3.6	255
17	6	3.2	255
17	7	3.2	249

Table D.3: Input motion information

Input Motion	Name	Station and Component	MCE Scale Factor	Units
FF-01	1994 Northridge	14145 Mulholland Dr. - 009	1.39	g
FF-02	1999 Kocaeli	Duzce - 180	1.90	g
FF-03	1992 Landers	Coolwater - LN	3.28	g
FT-01	Wave like motion	Synthetic wave motion	*	in
FT-02	Wave like motion	Synthetic wave motion	*	in
MS-01	1988 Saguenay	Dickey - 90	2*	g
NF-01	1976 Imperial Valley	El Centro Array No. 7 - 140	2.66	g
NF-02	1999 Chi-Chi	TCU065 - N	1.10	g
WN-01	White noise	0.03 RMS white noise	*	g
WN-02	White noise	0.05 RMS white noise	*	g
WN-04	White noise	0.05 RMS white noise	*	g

* Resultant amplitude not related to MCE

Table D.4: Sensor table

Channel Name	Instrument	Units	Location (m)			Orientation
			X	Y	Z	
A1-1	Accelerometer	g	-0.91	-0.91	-0.05	X
A2-1	Accelerometer	g	-0.91	0.91	-0.05	X
A3-1	Accelerometer	g	0.30	-0.91	-0.05	Y
A1-2	Accelerometer	g	0.00	1.02	0.15	X
A2-2	Accelerometer	g	0.00	1.02	0.15	Y
A3-2	Accelerometer	g	0.00	-1.02	0.15	X
A4-2	Accelerometer	g	1.02	0.00	0.15	Z
A5-2	Accelerometer	g	0.00	1.02	0.15	Z
A6-2	Accelerometer	g	-1.02	0.00	0.15	Z
A7-2	Accelerometer	g	0.00	-1.02	0.15	Z
A1-3	Accelerometer	g	0.00	1.02	2.06	X
A2-3	Accelerometer	g	0.00	1.02	2.06	Y
A1-4	Accelerometer	g	0.00	1.02	3.96	X
A2-4	Accelerometer	g	0.00	1.02	3.96	Y
A1-5	Accelerometer	g	0.00	1.02	5.88	X
A2-5	Accelerometer	g	0.00	1.02	5.88	Y
A1-6	Accelerometer	g	0.00	0.79	8.11	X
A2-6	Accelerometer	g	0.00	0.79	8.11	Y
A1-7	Accelerometer	g	0.00	0.79	10.01	X
A2-7	Accelerometer	g	0.00	0.79	10.01	Y
A3-7	Accelerometer	g	0.00	-0.79	10.01	X
A1-8	Accelerometer	g	0.00	0.79	11.92	X
A2-8	Accelerometer	g	0.00	0.79	11.92	Y
A1-9	Accelerometer	g	0.00	0.79	13.82	X
A2-9	Accelerometer	g	0.00	0.79	13.82	Y
A1-10	Accelerometer	g	0.00	0.59	16.04	X
A2-10	Accelerometer	g	0.00	0.59	16.04	Y
A1-11	Accelerometer	g	0.00	0.59	17.46	X
A2-11	Accelerometer	g	0.00	0.59	17.46	Y
A1-12	Accelerometer	g	0.00	0.59	18.91	X
A2-12	Accelerometer	g	0.00	0.59	18.91	Y
A1-13	Accelerometer	g	0.00	0.59	20.33	X
A2-13	Accelerometer	g	0.00	0.59	20.33	Y
A1-14	Accelerometer	g	0.00	0.59	21.78	X
A2-14	Accelerometer	g	0.00	0.59	21.78	Y
A3-14	Accelerometer	g	0.00	-0.55	21.78	X
A1-N	Accelerometer	g	-0.66	-1.09	0.00	X*
A2-N	Accelerometer	g	-0.66	-1.09	0.00	X*
A3-N	Accelerometer	g	-0.66	-1.09	0.00	Y*

Continued on next page

Table D.4: – continued from previous page

Channel Name	Instrument	Units	Location (m)			Orientation
			X	Y	Z	
ATNX	Accelerometer	g	15.34	0.00	9.17	X
ATNY	Accelerometer	g	15.34	0.00	9.17	Y
ATEX	Accelerometer	g	0.00	10.16	9.17	X
ATEY	Accelerometer	g	0.00	10.16	9.17	Y
LD1-1	LVDT	in	-1.30	-0.91	0.00	X
LD2-1	LVDT	in	-1.30	0.91	0.00	X
LD3-1	LVDT	in	-0.91	1.30	0.00	Y
LD4-1	LVDT	in	0.91	1.30	0.00	Y
LD5-1	LVDT	in	0.00	-1.03	0.00	Z
LD6-1	LVDT	in	-1.03	0.00	0.00	Z
LD7-1	LVDT	in	0.00	1.03	0.00	Z
LD8-1	LVDT	in	1.03	0.00	0.00	Z
LD9-1	LVDT	in	0.00	-1.03	0.00	Y
LD10-1	LVDT	in	-1.03	0.00	0.00	X
LD11-1	LVDT	in	0.00	1.03	0.00	Y
LD12-1	LVDT	in	1.03	0.00	0.00	X
LD13-1	LVDT	in	0.00	-1.03	0.00	X
LD14-1	LVDT	in	0.00	1.03	0.00	X
Long Acc. fbk	Accelerometer	g	-	-	-	X
Long Disp.fbk	Displacement	in	-	-	-	X
Long Force fbk	Force	kips	-	-	-	X
Long Reference	Reference units	-	-	-	-	X
Long Vel. fbk	Velocity	in/s	-	-	-	X
1-2-1D	Strain gauge	in/in	0.95	0.31	0.33	Diag.
1-2-1H	Strain gauge	in/in	0.95	0.31	0.33	Y
1-2-1V	Strain gauge	in/in	0.95	0.31	0.33	Z
S1-3-1	Strain gauge	in/in	1.02	0.00	3.00	Y
1-3-1D	Strain gauge	in/in	0.00	1.02	3.00	Diag.
1-3-1H	Strain gauge	in/in	0.00	1.02	3.00	X
1-3-1V	Strain gauge	in/in	0.00	1.02	3.00	Z
S2-3-1	Strain gauge	in/in	-1.02	0.00	3.00	Y
2-3-1D	Strain gauge	in/in	0.00	-1.02	3.00	Diag.
2-3-1H	Strain gauge	in/in	0.00	-1.02	3.00	X
2-3-1V	Strain gauge	in/in	0.00	-1.02	3.00	Z
S1-6-1	Strain gauge	in/in	0.00	0.79	8.25	X
1-6-1D	Strain gauge	in/in	0.79	0.00	8.25	Diag.
1-6-1H	Strain gauge	in/in	0.79	0.00	8.25	Y
1-6-1V	Strain gauge	in/in	0.79	0.00	8.25	Z
S2-6-1	Strain gauge	in/in	0.00	-0.79	8.25	X
2-6-1D	Strain gauge	in/in	-0.79	0.00	8.25	Diag.

Continued on next page

Table D.4: – continued from previous page

Channel Name	Instrument	Units	Location (m)			Orientation
			X	Y	Z	
2-6-1H	Strain gauge	in/in	-0.79	0.00	8.25	Y
2-6-1V	Strain gauge	in/in	-0.79	0.00	8.25	Z
S1-8	Strain gauge	in/in	0.79	0.00	11.91	Y
S2-8	Strain gauge	in/in	-0.79	0.00	11.91	Y
1-10-1D	Strain gauge	in/in	0.59	0.00	16.19	Diag.
1-10-1H	Strain gauge	in/in	0.59	0.00	16.19	Y
1-10-1V	Strain gauge	in/in	0.59	0.00	16.19	Z
2-10-1D	Strain gauge	in/in	-0.59	0.00	16.19	Diag.
2-10-1H	Strain gauge	in/in	-0.59	0.00	16.19	Y
2-10-1V	Strain gauge	in/in	-0.59	0.00	16.19	Z
S1-12	Strain gauge	in/in	0.59	0.00	18.91	Y
S2-12	Strain gauge	in/in	-0.59	0.00	18.91	Y
SP1	String Pot.	in	0.80	0.00	21.9	X
SP2	String Pot.	in	0.60	0.00	15.9	X
SP3	String Pot.	in	0.60	0.00	8.0	X
SP4	String Pot.	in	0.00	0.80	21.9	Y
SP5	String Pot.	in	0.00	0.60	15.9	Y
SP6	String Pot.	in	0.00	0.60	8.0	Y

*For configuration 1. X and Y coordinates and orientation change as the nacelle is rotated for configuration 2. Elevation, Z is taken to be 0 at mid-height of the nacelle.

D.2 Data File Format

All original data are stored in MTS binary format. Three seperate DAQs were uesed to collect data, and data from each DAQ (or node) are stored in a seperate files. A Matlab function to load the MTS binary data files, loadbin.m, is provided below. Original MTS data files were upsampled to the highest sample rate and synchronized for each test. The processed results were then stored in a single HDF5 format file for each run. Resulting file names is of the format Test_X_Trial_Y.h5, where X and

Y are the test and trial number, respectively, as listed in Table D.1. The Matlab function, loadhdf5.m, listed below may be used to load the data. As column number is not consistent in either the MTS binary files or the HDF5 files, the sensor name listed in Table D.4 should be used to locate the sensor in the data matrix.

Below is a listing of code for Matlab to load data stored using the MTS binary format and HDF5.

Listing D.1: Function to load MTS binary data files (loadbin.m)

```
function [x,deltaT,desc,units,fileInfo,...
    fileDate,header,isText] = ...
    loadbin(fileName,silent)
% Load MTS time series data file.
% [x,deltaT,desc,units,fileInfo,...
%   fileDate,header,isText] = ...
%   loadbin(fileName,silent)
%
%    fileName :  File name text.
%    silent     :  Silent error messages flag (optional)
%                (if nonzero, an error returns error
%                message in "fileInfo" with all
%                other fields empty, otherwise error
%                message is returned to command window.
%    x        :  Time series data (one column per
%                channel).
%    deltaT   :  Sample interval.
%    desc     :  Channel descriptors text array (one
%                row per channel).
%    units    :  Channel units text array (one row per
%                channel).
%    fileInfo :  File information text.
%    fileDate :  File creation date text.
%    header   :  Header text (returned as string matrix:
%                 ['key1'; 'value1'; 'key2';
%               'value2'; ...]).
%    isText   :  File was written as text instead
%                of binary.
%
%    size(x, 1) returns the number of data points
%                per channel.
%    size(x, 2) returns the number of channels.
%
```

```
%    See also "savebin".

%    Brad Thoen 28-Jun-00.
%    Copyright (c) 2000 by MTS Systems Corporation.

x     = [];
deltaT     = [];
desc  = [];
units      = [];
fileInfo = [];
fileDate = [];
header   = [];
message    = [];
isText     = [];
if ~exist('silent','var')
     silent = [];
end
if ~exist('fileName','var')
     fileName = [];
end
if isempty(fileName)
     silent = 0;
end
if isempty(fileName)
     message = ...
       'File name is a mandatory input to loadbin.';
     if silent
          fileInfo = message;
     else
          error(message);
     end
     return
end

% open file
[f, message] = fopen(fileName, 'r');
if f < 3
     if silent
          fileInfo = message;
     else
          error(message);
     end
     return
end

% read and interpret fixed header record #1
```

```
% to determine
% if file is valid MTS series file
hdr = fread(f, 129, 'char');
key = 'FILE_TYPE';
val = 'TIME_SERIES';
if ~strcmp(char(hdr(1:1+length(key)-1)'), key)
     message = 'File is not an MTS series file.';
else
     val1 = 'TIME_SERIES_WITH_EXTENDED_HEADER';
     val2 = 'TIME_SERIES';
     if strcmp(char(hdr(33:33+length(val1)-1)'),...
        val1)
          extHdr = 1;
     elseif strcmp(char(hdr(33:33+length(val2)-1)'),...
        val2)
          extHdr = 0;
     else
          message = 'File is not an MTS series file.';
     end
end
if ~isempty(message)
     if silent
          fileInfo = message;
     else
          error(message);
     end
     return
end

% determine whether file is text or binary format
% by looking for carriage return/line feed character
crlf = 10;
if isempty(find(hdr == crlf))
     isText = 0;     % binary
else
     isText = 1;     % text
end

% start over, now that we know whether to read the
% file as binary or as text
frewind(f);                % go back to beginning of file
hdr = freadHdr(f, isText);     % advance over fixed
                             % header record #1
header = char(char(hdr(1:32))', char(hdr(33:128))');

% read and interpret fixed header records #2 - #5
```

```
channels = 0;
key1 = 'FILE_DATE';
key2 = 'FILE_INFO';
key3 = 'DELTA_T';
key4 = 'CHANNELS';
for i = 2:5
     hdr = freadHdr(f, isText);
     header = char(header, char(hdr(1:32))', ...
       char(hdr(33:128))');
     if strcmp(char(hdr(1:1+length(key1)-1)'), key1)
          fileDate = char(hdr(33:128))';
     elseif strcmp(char(hdr(1:1+length(key2)-1)'), key2)
          fileInfo = char(hdr(33:128))';
     elseif strcmp(char(hdr(1:1+length(key3)-1)'), key3)
          deltaT = str2num(char(hdr(33:128))');
     elseif strcmp(char(hdr(1:1+length(key4)-1)'), key4)
          channels = str2num(char(hdr(33:128))');
     end
end

% read and interpret channel descriptor and units
% header records (must follow fixed header section;
% can be in any order within)
desc  = zeros(channels, 96);
units = zeros(channels, 96);
for i = 1:2*channels
     hdr  = freadHdr(f, isText);
     header = char(header, char(hdr(1:32))', ...
       char(hdr(33:128))');
     key1 = 'DESC.CHAN_';
     len1 = length(key1);
     key2 = 'UNITS.CHAN_';
     len2 = length(key2);
     if strcmp(char(hdr(1:1+len1-1)'), key1)
          chanNum = str2num(char(hdr((len1+1):32)'));
          if ~isempty(chanNum)
               desc(chanNum,:) = hdr(33:128)';
          end
     elseif strcmp(char(hdr(1:1+len2-1)'), key2)
          chanNum = str2num(char(hdr((len2+1):32)'));
          if ~isempty(chanNum)
               units(chanNum,:) = hdr(33:128)';
          end
     end
end
desc  = char(desc);
```

```
units = char(units);

% read extended header records
% (must follow channel descriptor and units
% header section)
if (extHdr)

     % read number of extended header records
     hdr = freadHdr(f, isText);
     header = char(header, char(hdr(1:32))', ...
       char(hdr(33:128))');
     key = 'EXTENDED_HEADER_RECORDS';
     if strcmp(char(hdr(1:1+length(key)-1)'), key)
          extHdrRecs = str2num(char(hdr(33:128))');
     else
          extHdrRecs = 0;
     end

     % read extended header records
     for i = 1:extHdrRecs
          hdr = freadHdr(f, isText);
          header = char(header, char(hdr(1:32))', ...
             char(hdr(33:128))');
     end
end

% read multiplexed data
[data, filePoints] = freadData(f, isText);

% Figure out the number of time steps that we
% have data for all the channels.
numTimeSamples = floor(filePoints/channels);
% Update the number of points that we will
% read out of the file.  This will effectively
% discard the last data point for some channels, but
% at least this will allow reading most of the data.
newFilePoints = numTimeSamples*channels;
% pre-allocate memory to save time
x = zeros(numTimeSamples,channels);
% demultiplex channel data into columns
for i = 1:channels
     x(:,i) = data(i:channels:newFilePoints);
end

% close file
fclose(f);
```

```
function hdr = freadHdr(f, isText)
     if isText
          hdr = fgetl(f);
          len = length(hdr);
          if len < 128
               hdr = [char(hdr), blanks(128-len)];
               % pad to 128 chars
          else
               hdr = hdr(1:128);
               % clip to 128 chars
          end
          hdr = hdr(:);
     else
          hdr = fread(f, 128, 'char');
     end

function [data, npts] = freadData(f, isText)
     if isText
          [data, npts] = fscanf(f, '%f', inf);
     else
          [data, npts] = fread(f, inf, 'float32');
     end
```

Listing D.2: Function to load HDF5 data files (loadhdf5.m)

```
function [dataMatrix, sampleFreq, desc, units, ...
    metaData ] = ...
    loadhdf5(fileName, location)
% Load data to hdf5 time series data file.
% [dataMatrix, sampleFreq, desc, units, ...
%   metaData ] = ...
%   loadhdf5(fileName)
%
%    fileName :  File name text.
%    dataMatrix :  N x M time series data matrix
%                  (M channels of N data points)
%    sampleFreq :  Sample interval (optional;
%                  default = 0.0).
%    desc       :  Channel descriptors text cell.
%    units      :  Channel units text cell
%   metaData    :  Extra information about the data
%   location    :  The path to the data in the hdf5
%                  file (default is /)
```

```
20
sampleFreq=1;


% input argument checking
25 if ~exist('fileName','var')
    error('File name is a mandatory input to loadhdf5.')
end

if ~exist('location','var')
30     location = '/';
end
hinfo  = hdf5info(fileName);

if strcmp(location,'/')
35     dataSet = hinfo.GroupHierarchy.Datasets;
else
    error('Currently only / is supported as a location.')
end


40
numChannels = length(hinfo.GroupHierarchy.Datasets);
if numChannels == 1
    dataMatrix = hdf5read(dataSet);

45     numChannels = size(dataMatrix,2);
    fullName = dataSet.Name;

    numAttribures =...
        length(dataSet(1).Attributes);
50     numExtraAtters = 0;
    extraAtterIndexes=zeros(1,numAttribures);
    for iAttribute = 1:numAttribures
        atterName = dataSet.Attributes(1,iAttribute).Name;
        if strcmp([fullName '/Units'],atterName)
55             unitsh5=...
                hdf5read(...
                dataSet.Attributes(1,iAttribute));
        elseif strcmp(...
                [fullName '/Sample Rate'],atterName)
60             sampleFreq =...
                dataSet.Attributes(1,iAttribute).Value;
        elseif strcmp(...
                [fullName '/Channel Name'],atterName)
            desch5 =...
65              hdf5read(...
```

```
                dataSet.Attributes(1,iAttribute));
        else
            numExtraAtters = numExtraAtters+1;
            extraAtterIndexes(numExtraAtters)=iAttribute;
        end
    end
    units = cell(1,numChannels);
    desc = cell(1,numChannels);
    for iChannel = 1:numChannels
        units{iChannel}=unitsh5(iChannel).Data;
        desc{iChannel}=desch5(iChannel).Data;
    end
    metaData = cell(numExtraAtters,numChannels+1);
    for iExtraAtter = 1:numExtraAtters
        iAttribute = extraAtterIndexes(iExtraAtter);
        tempName = dataSet.Attributes(1,iAttribute).Name;
        splitExtraAtterName = tab_split(tempName, '/');
        extraAtterName = splitExtraAtterName{end};
        if length(extraAtterName) >= 11 && ...
                strcmp('Bad Segment',extraAtterName(1:11))
            extraAtterName = 'Bad Segment';
        end
        metaData{iExtraAtter,1}=extraAtterName;
        curData = ...
            hdf5read(dataSet.Attributes(1,iAttribute));

        for iChannel = 1:numChannels
            try
                metaData{iExtraAtter,iChannel+1} = ...
                    curData(iChannel).Data;
            catch ME
                metaData{iExtraAtter,iChannel+1} = ...
                    curData(iChannel);
            end

        end
    end
else
    % Deal with old format file with a data series for
    % each channel
    desc = cell(1,numChannels);
    units = cell(1,numChannels);

    for iChannel = 1:numChannels
        fullName = dataSet(1,iChannel).Name;
        desc{iChannel} = fullName(2:end);
```

```
        numAttributes =...
            length(dataSet(1,iChannel).Attributes);
        for iAttribute = 1:numAttributes
            atterName = ...
                dataSet(1,iChannel).Attributes(...
                1,iAttribute).Name;
            if strcmp([fullName '/Units'],atterName)
                units{iChannel}=...
                    dataSet(1,iChannel).Attributes(...
                    1,iAttribute).Value.Data;
            elseif strcmp([fullName '/Sample Rate'],...
                    atterName)
                curSampRate =...
                    dataSet(1,iChannel).Attributes(...
                    1,iAttribute).Value;
                if iChannel ==1
                    sampleFreq =curSampRate;
                else
                    if sampleFreq ~= curSampRate
                        error('%s%s%i%s%i%s',...
                            'File has multipe ',...
                            'sample rates',...
                            sampleFreq, ' and ',...
                            curSampRate,'.');
                    end
                end
            end
        end

        curDat = hdf5read(dataSet(iChannel));
        if iChannel ==1
            dataMatrix= zeros(length(curDat),...
                numChannels);
        end
        dataMatrix(:,iChannel)=curDat;


    end
end
```

Listing D.3: Custom code to split a string required for loadhdf5.m (tab_split.m)

```
function result = tab_split(string, delimiter)

% Setup a cell to store the results
result = {};
while (isempty(string) == 0)
```

```
    if ~exist('delimiter','var')
        % Split up the string based on a tab (ASCII 9)
        [token,string] = strtok(string,9);
    else
        [token,string] = strtok(string,delimiter);
    end
    % Append the next token to the result cell
    % Make sure to trim leading and trailing white space
    result = {result{:}, strtrim(token)};
end
```